INTERNATIONAL DOCTORAL
SCHOOL OF THE USC

Rubén
Varela Fernández

PhD Thesis

Research and development of advanced controlled drug delivery systems: application in Keratoconus and Leber's Hereditary Optic Neuropathy

Santiago de Compostela, 2022

Doctoral Programme in Drug Research and Development

TESE DE DOUTORAMENTO

RESEARCH AND DEVELOPMENT OF ADVANCED CONTROLLED DRUG DELIVERY SYSTEMS: APPLICATION IN KERATOCONUS AND LEBER'S HEREDITARY OPTIC NEUROPATHY

Rubén Varela Fernández

ESCOLA DE DOUTORAMENTO INTERNACIONAL DA UNIVERSIDADE DE SANTIAGO DE COMPOSTELA

PROGRAMA DE DOUTORAMENTO EN INVESTIGACIÓN E DESENVOLVEMENTO DE MEDICAMENTOS

SANTIAGO DE COMPOSTELA

2022

USC
UNIVERSIDADE
DE SANTIAGO
DE COMPOSTELA

DECLARACIÓN DO AUTOR DA TESE

Research and development of advanced controlled drug delivery systems: application in keratoconus and Leber's Hereditary Optic Neuropathy

D. Rubén Varela Fernández,

Presento a miña tese seguindo o procedemento axeitado ao Regulamento e declaro que:

1) A miña tese abarca os resultados da elaboración do meu traballo.
2) De selo caso, na tese faise referencia ás colarboracións que tivo este traballo.
3) A tese é a versión definitiva presentada para a súa defensa e coincide coa versión enviada en formato electrónico.
4) Confirmo que a tese non incorre en ningún tipo de plaxio doutros autores nin de traballos presentados por mín para a obtención doutros títulos.

En Santiago de Compostela, a 15 de abril de 2022

Asdo. Rubén Varela Fernández

USC
UNIVERSIDADE
DE SANTIAGO
DE COMPOSTELA

AUTORIZACIÓN DOS DIRECTORES DA TESE

Research and development of advanced controlled drug delivery systems: application in keratoconus and Leber's Hereditary Optic Neuropathy

Dna. María Isabel Lema Gesto

D. Francisco Javier Otero Espinar

D. Miguel González Barcia

INFORMAN:

Que a presente tese, correspóndese co traballo realizado por D. Rubén Varela Fernández, baixo a nosa dirección, e autorizamos a súa presentación, considerando que reúne os requisitos esixidos no Regulamento de Estudos de Doutoramento da USC, e que como directores desta non incorre nas causas de abstención establecidas na Lei 40/2015.

De acordo co indicado no Regulamento de Estudos de Doutoramento, declara tamén que a presente tese de doutoramento é idónea para ser defendida en base á modalidade de *Monográfica con reprodución de publicacións*, nos que a participación do/a doutorando/a foi decisiva para a súa elaboración e as publicacións se axustan ao Plan de Investigación.

En Santiago de Compostela, a 15 de abril de 2022

Asdo. M. Isabel Lema Gesto Asdo. Francisco J. Otero Espinar Asdo. Miguel González Barcia

USC
UNIVERSIDADE
DE SANTIAGO
DE COMPOSTELA

A mi Familia

"El éxito no es la victoria, sino todo lo que has peleado por ganar"

Rafael Nadal.

USC
UNIVERSIDADE
DE SANTIAGO
DE COMPOSTELA

USC
UNIVERSIDADE
DE SANTIAGO
DE COMPOSTELA

AGRADECIMIENTOS

La realización de la presente Tesis Doctoral es el resultado del esfuerzo conjunto de muchas personas que me han apoyado y ayudado durante este largo y, en ocasiones, arduo camino de dedicación, esfuerzo y trabajo. Por ello, aprovecho estas líneas para expresarles mi más profundo y sincero agradecimiento.

En primer lugar, me gustaría darles las gracias a mis tres directores de tesis, María Isabel Lema Gesto, Francisco J Otero Espinar y Miguel González Barcia, por brindarme la oportunidad de formar parte de sus grupos de investigación, permitirme trabajar con ellos y proporcionarme la formación científica adecuada para desarrollar esta tesis.

A **M. Isabel Lema Gesto**, por su valioso apoyo científico y personal, así como la excelente orientación. Le agradezco además que siempre haya estado disponible para el seguimiento directo de todas las propuestas de investigación. Gracias por su conocimiento y enseñanzas, su gran cariño y el apoyo que siempre me ha brindado desde el primer momento.

A **Francisco J. Otero Espinar**, por guiarme en todas las fases del programa de doctorado con su excelente y continua aportación científica, así como con sus consejos personales. Le estaré eternamente agradecido por haber creído en mí desde el primer minuto y por permitirme adentrarme en el bonito mundo de la ciencia. El éxito de esta tesis está estrechamente relacionado con su persona.

A **Miguel González Barcia**, por apoyar mi desarrollo científico y personal. Gracias por su preocupación, consejos y motivación para la realización de todos estos proyectos y, sobre todo, por brindarme la oportunidad de conocer dos aspectos muy importantes y que admiro profundamente: el primero, su gran capacidad de compartir su conocimiento y el segundo, su gran calidad humana.

Quisiera agradecer también a **Anxo Fernández Ferreiro** y **Pablo Aguiar Fernández**, cuya colaboración me ha permitido llevar a cabo aquellos ensayos relacionados con la Medicina Nuclear. A pesar de no estar directamente relacionados con mi proyecto, les agradezco la ayuda y los servicios prestados para el desarrollo de la tesis.

A todos los miembros del Departamento de Farmacia, Farmacología y Tecnología Farmacéutica de la Facultad de Farmacia de la Universidad de Santiago de Compostela, así

como del Laboratorio de Investigación en Neurociencias Clínicas del Instituto de Investigación Sanitaria de Santiago de Compostela, por todo el apoyo proporcionado durante el desarrollo de la presente tesis. Mención especial merecen:

A mis compañeros/as de laboratorio de la Facultad de Farmacia, **Andrea Conde**, **Andrea Luaces**, **Carlos**, **Guillermo**, **Iria**, **Victor**, **Victoria** y **Xurxo**, quienes, más que compañeros, son familia. Creo que no habría suficientes palabras para expresar el eterno agradecimiento, amor y admiración que siento hacia ellos. Gracias por apoyarme y ayudarnos mutuamente en este largo camino, pero, sobre todo, por hacerme valorar la palabra amistad. Por esas mañanas perezosas, por las pausas para el café, por quedarnos hasta tarde montando y desmontando ensayos, por las risas y bromas del día a día, por los congresos, los viajes a Lugo y los planes improvisados. En definitiva, gracias por el día a día, el cual siempre ha sido maravilloso a vuestro lado.

A mis compañeros/as de Medicina Nuclear, **David**, **Manuel** y **Noemí**, por haberme ayudado siempre que lo necesitaba, así como por la amistad, motivación y apoyo que siempre me han dado fuera del laboratorio.

A mis compañeros/as del Departamento de Farmacia, Farmacología y Tecnología Farmacéutica de la Facultad de Farmacia, **Iván**, **Miriam**, **Clara**, **Victor Santos**, **Ana Iglesias**, **Sonia**, **Rebeca**, **Helena**, **Lorena**, **María Vivero**, **Xian**, **Andrea López**, **Patricia**, **Iago**, **Alejandro**, **Fernando**, **Ángela**, **Ana Filipa**, **Axel** y **Thoa**, por haber estado siempre dispuestos a ayudarme en todo momento, así como compartir el día a día del Departamento.

A mis compañeros/as del Laboratorio de Neurociencias Clínicas, especialmente a **Uxía** y **Maite**, por su conocimiento y enseñanzas, así como por el cariño, apoyo y ayuda que siempre me han brindado desde el primer minuto y a lo largo de la realización de este proyecto.

A mis compañeros/as de la Farmacia de Luou, **Pili**, **Inés**, **Victoria**, **Tania**, **Javier**, **Antonio** e **Iria**, por ponerme siempre las cosas fáciles para poder compaginar el trabajo entre la farmacia y el laboratorio, por apoyarme desde el primer momento y durante todo el camino para llegar hasta aquí. Por aportarme su conocimiento, enseñanzas y su gran cariño, pero también por las anécdotas del día a día, las risas desde primera hora de la mañana y el buen ambiente constante.

Al resto de integrantes del Departamento de Farmacia, Farmacología y Tecnología Farmacéutica de la Facultad de Farmacia, así como del Laboratorio de Investigación en Neurociencias Clínicas, por la ayuda y los servicios prestados.

USC UNIVERSIDADE DE SANTIAGO

Ya fuera del ámbito profesional, me gustaría expresar mi profundo agradecimiento a todas las personas que han pasado por mi vida en los últimos años y han contribuido, con su apoyo y presencia, a alcanzar esta meta.

A toda mi familia, por la dedicación, el sacrificio, la paciencia y el amor incondicional. Gracias por enseñarme a afrontar las dificultades del día a día y por darme impulso siempre que lo necesitaba.

A mis padres, **Josefa** y **Jesús**, por haber sacrificado su vida para darme una mejor a mí. Gracias por enseñarme los valores más importantes de la vida, así como por su apoyo incondicional y su paciencia infinita. Gracias por estar ahí siempre, en cualquier momento y en cualquier circunstancia.

A mi hermana, **Tamara**, por ser el mayor regalo que me ha podido dar la vida. Gracias por ser mi mayor apoyo en todo momento, por cuidarme, por comprender mis inquietudes, mis miedos y mis deseos, por enseñarme a ver el lado positivo de las cosas y por hacer de hermana mayor en los momentos en los que no podía tirar del carro. Gracias por creer en mí aun cuando yo no lo hacía.

A todos, muchas gracias.

USC
UNIVERSIDADE DE SANTIAGO DE COMPOSTELA

USC
UNIVERSIDADE
DE SANTIAGO
DE COMPOSTELA

RESUMO

Na actualidade, máis de 250 millóns de persoas loitan contra a discapacidade visual en todo o mundo por causas potencialmente previbles ou corrixibles e estímase que os trastornos oculares aumenten nas próximas dúas décadas, podendo describirse xeralmente como trastornos do segmento anterior e do segmento posterior. A calidade de vida, unha medida importante do benestar físico, emocional e social, parece estar asociada negativamente coa discapacidade visual, e cada vez máis avalíanse as intervencións oftálmicas pola súa asociación coa calidade de vida. O deseño dun sistema eficiente de administración de fármacos que permita a súa vehiculización a un tecido concreto do ollo converteuse nun gran reto para os científicos do sector farmacéutico. En comparación con outras vías de administración, a administración de fármacos por vía ocular enfrentouse a importantes retos plantexados pola gran eficiencia das diversas barreiras oculares. Moitas destas barreiras son inherentes e exclusivas da anatomía e da fisioloxía ocular, o que supón un reto para os científicos especializados na administración de fármacos.

Nas últimas dúas décadas, as tecnoloxías de administración de fármacos oculares avanzaron de forma dinámica, dando lugar a novas intervencións terapéuticas para os trastornos oculares crónicos. Os obxectivos principais de calquera **sistema de administración de fármacos por vía ocular** fundaméntanse en manter as concentracións terapéuticas do fármaco no lugar de destino, reducir a frecuencia de dosificación e atravesar as diferentes barreiras oculares, tanto estáticas como dinámicas. Estas inimitables barreiras non solo exclúen a entrada de xenobióticos, senon que tamén aminoran a absorción activa de axentes terapéuticos. Así, o deseño dun esquema de administración ideal debe ir dirixido a obter una maior biodisponibilidade do fármaco, un incremento na permanenza e unha liberación controlada do mesmo no lugar de administración ou de acción, que poida superar as distintas barreiras oculares.

Os sistemas convencionais de administración de fármacos adoecen dunha escasa biodisponibilidade e de fluctuacións no nivel plasmático do fármaco, sendo incapaces de lograr unha liberación sostida. Sen un mecanismo de administración eficaz, todo o proceso terapéutico

USC UNIVERSIDADE DE SANTIAGO DE COMPOSTELA

pode resultar inútil. Unha liberación lenta, prolongada e/ou sostida do fármaco adoita ser o obxectivo máis desexado, aínda que os métodos para definir unha taxa de liberación óptima para a mellora da resposta terapéutica ou biolóxica seguen sendo escasos. Polo xeral, a dinámica de liberación do fármaco depende da cantidade de fármaco cargado na matriz do portador, das solubilidades do fármaco na matriz e no medio de liberación, e das propiedades da matriz que afectan á cinética de difusión do fármaco. A cantidade de carga segue sendo, na súa maior parte, un factor empírico no desenvolvemento de sistemas portadores de fármacos, aínda que se dispón de métodos experimentais para anticipar as cargas mínimas efectivas, polo que a preferencia común diríxese á obtención de grandes capacidades de carga, capaces de manter altas concentracións en sangue ou tecidos. Con todo, nalgúns casos demostrouse que os gradentes temporais das moléculas bioactivas poden ser máis eficaces que unha concentración constante á hora de inducir a resposta biolóxica desexada.

Os papeis crave da concentración e o tempo están recoñecidos en farmacoloxía, pero o estudo sistemático da interrelación entre dose, farmaco/toxicocinética e farmaco/toxicodinámica segue supoñendo un reto importante. Neste contexto, os sistemas de administración de fármacos son unha valiosa ferramenta para xerar gradentes temporais e espaciais de fármacos nos tecidos diana e poderían explorarse en profundidade para investigar como estes factores determinan as accións terapéuticas.

Nos últimos anos, estase a observar un aumento dos enfoques novidosos para a administración invasiva de potentes axentes terapéuticos co fin de lograr un cumplimento terapéutico óptimo. A **instilación tópica oftálmica** é a ruta de administración máis desexable, considerando que é fácil de manexar e rentable a nivel económico, sendo especialmente útil para o tratamento de trastornos que afectan ao segmento anterior do ollo.

Con todo, a principal desvantaxe das formulacións oftálmicas convencionais de aplicación tópica é a relativamente baixa biodisponibilidad ocular. Isto pode atribuírse ás altas taxas de renovación do líquido lagrimal e á elevada drenaxe nasolacrimal. No entanto, a administración controlada de fármacos mediante o uso de nanoformulacións mucoadhesivas, como as nanopartículas ou os sistemas lipídicos nanoestructurados, pódese lograr unha alta biodisponibilidade dos fármacos nos tecidos anteriores, como a conxuntiva e a córnea.

USC UNIVERSIDADE DE SANTIAGO

Pola súa banda, a administración directa de fármacos mediante **inxección intravítrea ou implantes intravítreos** presenta moitas vantaxes no tratamento de enfermidades do segmento posterior do ollo. A diferenza da administración de fármacos por vía sistémica, a administración

local de fármacos por vía intravítrea elude as barreiras hemato-oculares, permitindo alcanzar niveis intraoculares de fármaco máis elevados con menor número de efectos secundarios.

O **queratocono** é unha ectasia corneal dexenerativa e progresiva que afecta a nenos e adultos xóvenes, xerando unha gran incapacidade visual, de calidade de vida e con gran impacto sociosanitario. A incidencia establecida de 1/2000 na poboación xeral viuse aumentada debido á maior precisión e sensibilidade das técnicas tomográficas corneales actuais. É esencial unha actuación médica nos distintos estadíos da ectasia para previr a súa progresión e así evitar o transplante corneal. Na actualidade, non se dispón de ningún tratamento eficaz que permita frear e/ou atrasar a evolución do QC. Estudos previos demostraron a implicación da inmunidade innata nesta enfermidade. Os receptores Toll-Like 2 (TLR2) en células epiteliais corneais poden usarse como biomarcadores específicos de diagnóstico e progresión do queratocono. Por outra banda, tamén se demostrou que a lactoferrina (Lf), proteina inmnuomoduladora e antiinflamatoria, está diminuída na devandita patoloxía. Baseándonos nestas evidencias previas, sería interesante levar a cabo o deseño e desenvolvemento de sistemas novidosos de liberación prolongada cargados con lactoferrina para administración tópica oftálmica dirixidas a TLR2 a modo dunha potencial aproximación terapéutica do queratocono.

Do mesmo xeito, a **Neuropatía Óptica Hereditaria de Leber (LHON)** é unha enfermidade xenética mitocondrial caracterizada por provocar unha perda bilateral da visión central como consecuencia da dexeneración das células ganglionares da retina (RGCs) e o nervio óptico, debido a mutacións puntuais no xenoma mitocondrial que xeran alteracións na cadea respiratoria. Cabe sinalar que a LHON ten unha prevalencia estimada de 1/30.000, afectando predominantemente a adultos xóvenes (entre 15-30 anos) de todos os grupos étnicos, cunha preponderancia masculina (80%). En consonancia con esta hipótese, a perda selectiva de RGCs observada como adelgazamento do RNFL só se produce na fase atrófica tardía da enfermidade, imposibilitando a recuperación visual. Polo tanto, o período entre a disfunción celular e a perda de células podería ser considerado como unha xanela terapéutica a través da cal se podería restaurar a visión mediante a normalización da función mitocondrial. Debe terse en conta que a orixe mitocondrial de moitas enfermidades oculares poderían usarse como obxectivo farmacolóxico e ser considerada unha alternativa de tratamento para as neuropatías ópticas. Na actualidade, as opcións de tratamento da LHON seguen sendo limitadas e unha das estratexias terapéuticas que presenta maior interese está constituída por un análogo da coenzima Q10 (CoQ10), a idebenona, unha benzoquinona de cadea curta dotada dunha potente acción

USC UNIVERSIDADE DE SANTIAGO

antioxidante e inhibidora da peroxidación lipídica, ademais de interactuar coa cadea de transporte electrónico, modulando o fluxo de electróns. En base a iso, un dos enfoques máis interesantes estaría fundamentado no deseño, desenvolvemento e caracterización de formas farmacéuticas de liberación prolongada contendo idebenona, formuladas mediante a utilización de polímeros biodegradables e biocompatibles, ben de poliésteres derivados do petróleo (PCL) ou procedentes de recursos agrarios (PLGA).

A presente tese doutoral divídese en dúas seccións principais en concordancia coas dúas enfermidades oculares previamente descritas. A primeira sección céntrase no deseño, desenvolvemento e caracterización de diferentes tipos de sistemas nanoparticulares cargados con lactoferrina para administración tópica oftálmica, como alternativa farmacolóxica para o tratamento do queratocono, e consta de tres capítulos. Pola súa banda, a segunda sección céntrase no deseño, desenvolvemento e caracterización de dúas formas farmacéuticas de liberación prolongada, microsferas e implantes, destinadas a administración intravítrea para o tratamento da neuropatía óptica hereditaria de Leber, incluíndo os dous capítulos restantes.

O **capítulo 1** comprende e describe o deseño, optimización e caracterización de dous tipos diferentes de nanopartículas baseadas en quitosano como sistemas novos de administración de lactoferrina. O obxectivo deste capítulo está baseado no deseño, desenvolvemento e caracterización de nanopartículas de CS/ TPP e CS/ SBE-β-CD cargadas con lactoferrina como sistemas de administración tópica de fármacos e como alternativa farmacolóxica para o tratamento do queratocono. Realizouse unha comparación entre as nanopartículas CS/TPP tradicionais e as nanopartículas CS/ SBE-β-CD para levar a cabo a inmobilización de proteínas de alto peso molecular destinadas á administración tópica oftálmica. Tamén se levaron a cabo diversos análises para demostrar a idoneidade de ambas as formulacións en relación á liberación sostida de lactoferrina e á mellora da permeabilidade corneal, obtendo unha base preclínica sólida, non só mediante ensaios *in vitro*, senón tamén con ensaios *ex vivo* e *in vivo*. Ademais diso, desenvolveuse un novo estudo de biopermanencia ocular de nanopartículas poliméricas baseado nunha técnica de radiomarcaxe con diferentes radiotrazadores para avaliar a bioadhesión das partículas destinadas á administración tópica oftálmica. Obtívose unha base preclínica consistente para ambos os nanosistemas, podendo ser considerado como un potencial primeiro tratamento farmacolóxico para o queratocono, alternativo aos actuais métodos clínicos invasivos. Ambos os dous tipos de nanopartículas obtivéronse mediante a técnica de xelificación ionotrópica. Estudouse o tamaño e a morfoloxía das nanopartículas en función das

USC UNIVERSIDADE DE SANTIAGO DE COMPOSTELA

condicións de preparación. Ditas nanopartículas mostraban un tamaño medio de 180,73 ± 40,67 nm, cunha polidispersión (PDI) de 0,170 ± 0,067 e valores de potencial ζ positivo, que oscilaban entre 17,13 e 19,89 mV. A lactoferrina incorporouse con éxito a ambos os tipos de nanotransportadores. Os perfís de liberación *in vitro* mostraron unha liberación mellorada, prolongada e controlada de lactoferrina desde a matriz polimérica. Estas formulacións tamén demostraron non ter problemas de estabilidade nin de citotoxicidade, así como propiedades mucoadhesivas axeitadas, cun elevado tempo de permanencia na superficie ocular. Así pois, ambos os tipos de nanopartículas poderían considerarse sistemas de administración de fármacos oftálmicos tópicos de liberación controlada.

A novidade deste traballo radica en poñer a proba a idoneidade das formulacións baseadas en quitosano para mellorar a permanencia e a penetración do fármaco na córnea, ademais de avaliar a capacidade de manter e controlar a liberación do fármaco. Estes novos sistemas de liberación non son irritantes para o ollo e producen un maior tempo de retención ocular, proporcionando así unha maior eficacia e biodisponibilidade. Outras vantaxes son a alta biocompatibilidade, a facilidade de preparación, a alta eficiencia de encapsulación e carga, a maior estabilidade física tras o almacenamento, así como a mellor permeabilidade do fármaco.

O **capítulo 2** baseouse no deseño, desenvolvemento e caracterización fisicoquímica de NLCs cargados con lactoferrina como nova alternativa terapéutica para o tratamento do queratocono. O obxectivo central deste enfoque de liberación controlada e específica no lugar de acción céntrase predominantemente na comprensión das propiedades farmacocinéticas e farmacodinámicas do fármaco, xunto cunha mellor inmunoxenicidade para mellorar o resultado terapéutico. Tamén se estudou a idoneidade dos NLCs para controlar a liberación de lactoferrina e mellorar a súa permeabilidade corneal, adquirindo unha base sólida desde o punto de vista preclínico. De feito, realizouse un novo ensaio de biopermeabilidade ocular baseado nun método de radiomarcaxe para avaliar a bioadhesión dos NLCs destinados a instilación tópica oftálmica. Os NLCs cargados con lactoferrina preparáronse con éxito mediante un método de dobre emulsión/evaporación de disolventes. Os NLCs resultantes foron avaliados en termos de tamaño de partícula, distribución de tamaño (PDI), carga superficial, morfoloxía, eficiencia de encapsulación (EE), capacidade de carga (LC), estabilidade, citotoxicidade, liberación *in vitro* e retención na superficie ocular. Os datos resultantes mostraron un tamaño de 119,45 ± 11,44 nm, un valor de PDI de 0,151 ± 0,045 e unha carga superficial de -17,50 ± 2,53 mV. Ademais, obtivéronse valores elevados de EE e LC (ata o 75%). O estudo de liberación *in vitro* demostrou

USC UNIVERSIDADE DE SANTIAGO DE COMPOSTELA

un patrón de liberación controlado para a lactoferrina. Os NLCs tamén resultaron ser estables, non tóxicos e mostraron propiedades mucoadhesivas. Por tanto, obtívose unha base preclínica consistente, polo que os NLC poderían ser considerados como un potencial sistema novo de liberación controlada de lactoferrina para o tratamento do queratocono.

O **capítulo 3** describe o deseño, a optimización e a caracterización de oito tipos diferentes de nanopartículas baseadas en PLGA (nanoesferas e nanocápsulas) como sistemas novos de administración dunha proteína, a lactoferrina, co fin de obter unha base preclínica sólida como tratamento farmacolóxico alternativo aos actuais métodos clínicos invasivos para o queratocono. As diferentes nanopartículas preparáronse mediante dúas técnicas de nanoprecipitación modificadas, utilizando unha mestura de tres compoñentes de fármaco/ polímero/ surfactante (Lf/ PLGA/ Poloxamer), como forma de superar as limitacións inherentes ás NPs de PLGA convencionais. Estes nanotransportadores poliméricos modificados, destinados á administración oftálmica tópica, foron sometidos a caracterización *in vitro*, modificación da superficie e avaliacións *ex vivo* e *in vivo*. Obtívose un rango de tamaño adecuado, unha distribución de tamaño uniforme e valores de potencial ζ negativos para todos os tipos de formulacións. A lactoferrina incorporouse con éxito a todos os tipos de nanotransportadores con valores axeitados de eficiencia de encapsulación e capacidade de carga. Os perfís de liberación *in vitro* mostraron unha liberación prolongada e controlada de lactoferrina desde a matriz polimérica. Estas formulacións tampouco demostraron problemas de inestabilidade ou citotoxicidade. Así pois, todos os tipos de nanopartículas poderían considerarse como novos nanotransportadores para a liberación controlada de lactoferrina por vía tópica oftálmica. Esta mellora logrouse mediante un aumento da permanencia de Lf na superficie ocular ou mellorando a permeabilidade corneal de Lf.

O **capítulo 4** describe o deseño, o desenvolvemento e a caracterización de microesferas (MSs) de PLGA cargadas con idebenona mediante un método de emulsión/evaporación de solvente, así como a caracterización fisicoquímica, co obxectivo de investigar novos enfoques intravítreos para unha liberación controlada e sostida de idebenona como nova alternativa de tratamento da LHON. Con iso búscase diminuír a necesidade da administración sistémica do fármaco e minimizar a frecuencia das inxeccións oculares requiridas. A idoneidade das formulacións de MSs de PLGA cargadas con idebenona para controlar e manter a liberación de idebenona levouse a cabo coa finalidade de adquirir unha base preclínica fiable a través de ensaios *in vitro* e *ex vivo*.

USC UNIVERSIDADE DE SANTIAGO DE COMPOSTELA

Obtivéronse de valores adecuados de rendemento de produción, eficacia de encapsulación e capacidade de carga. As MSs mostraron unha forma esférica, cun rango de tamaño de 10 - 25 μm e unha superficie lisa e non porosa. Os espectros FTIR demostraron que non había interaccións químicas entre a idebenona e os diferentes polímeros. As análises de RMN en estado sólido, difractometría de raios X, DSC e TGA indicaron que a microencapsulación conduciu á amorfización do fármaco. Os perfís de liberación *in vitro* axustáronse a un perfil cinético biexponencial. Ademais, as MSs de PLGA cargadas con idebenona non mostraron efectos citotóxicos nun modelo de tecido organotípico. Os resultados suxiren, por tanto, que as MSs de PLGA poderían ser unha alternativa para a administración intraocular de idebenona a longo prazo, mostrando potenciais vantaxes terapéuticas como un novo enfoque terapéutico para o tratamento da Neuropatía Óptica Hereditaria de Leber (LHON).

O **capítulo 5** inclúe un estudo piloto destinado á avaliación da viabilidade e as características da liberación prolongada e controlada de idebenona a partir dun implante intravítreo de PCL. O deseño, desenvolvemento e caracterización dos implantes de PCL cargados con idebenona, preparados mediante un método de homoxeneización/extrusión/evaporación de disolventes, permitiu a obtención de altos valores de rendemento de produción, eficacia de encapsulación e capacidade de carga. A caracterización *in vitro* completouse coa avaliación das propiedades mecánicas e instrumentais. Avaliouse a liberación *in vitro* de idebenona desde os implantes de PCL, ademais de controlar a erosión do implante mediante o estudo da perda de masa e os cambios na morfoloxía da superficie. Utilizáronse técnicas de DSC, TGA, FTIR e raios X para estimar a estabilidade e a interacción entre os compoñentes do implante. Estableceuse unha base preclínica consistente, apoiando a idea dos implantes de PCL cargados de idebenona como unha nova estratexia de liberación intraocular sostida a longo prazo para o tratamento da LHON.

En conclusión, nesta tese doutoral detállanse os procesos de deseño, desenvolvemento e caracterización de diferentes formulacións destinadas á obtención dunha liberación controlada e prolongada de diferentes fármacos. Na primeira parte desta tese doutoral, deseñáronse e desenvolvéronse con éxito tres tipos diferentes de nanopartículas. Todas estas formulacións cargáronse con lactoferrina como fármaco diana e propuxéronse como alternativas farmacolóxicas para o tratamento do queratocono. Obtivéronse nanopartículas estables e de tamaño axustable mediante diferentes métodos de preparación. Así mesmo, todas elas mostraron propiedades fisicoquímicas apropiadas para a súa administración por vía tópica

USC UNIVERSIDADE DE SANTIAGO

oftálmica, apoiando a idea de que quedaban retidas a nivel corneal, prolongando o tempo de liberación do fármaco desde o propio tecido, además de mostrar unha axeitada estabilidade ao almacenamento, ao pH e á forza iónica. Tamén se obtivo unha liberación controlada de lactoferrina, corroborando o seu uso como posibles sistemas de liberación de fármacos hidrofílicos. Todos os datos obtidos confirmaron as súas propiedades mucoadhesivas, sen evidencia de citotoxicidade tisular.

Na segunda parte desta tese doutoral, deseñáronse e desenvolvéronse con éxito dous sistemas diferentes de administración de fármacos como novas alternativas para o tratamento da LHON, cargados con idebenona, destinados á administración intravítrea. Ambas as formulacións caracterizáronse fisicoquímicamente para crear unha base preclínica sólida a partir da cal realizar estudos *in vivo*. Así mesmo, logrouse unha liberación controlada e sostida de idebenona a partir de ambas as formulacións, o que confirma o seu uso como potenciais sistemas de liberación de fármacos para a administración intravítrea a longo prazo. Ambos os sistemas mostraron propiedades fisicoquímicas axeitadas, así como unha estabilidade apropiada en relación co almacenamento, o pH e os cambios de forza iónica. Os datos resultantes mostraron que todas as formulacións poderían considerarse potenciais sistemas para a liberación controlada de fármacos.

Como conclusión xeral, propuxéronse, por vez primeira, diferentes formulacións biodegradables de liberación prolongada para a administración de diferentes fármacos para o tratamento de patoloxías oculares, tanto do segmento anterior como posterior do ollo, apoiado en amplos estudos preclínicos co fin de obter unha base preclínica sólida como potenciais tratamentos farmacolóxicos para o queratocono e a Neuropatía Óptica Hereditaria de Leber (LHON). Isto viuse apoiado por numerosos estudos de caracterización *in vitro*, *ex vivo* e *in vivo*. Con todo, debe explorarse en profundidade unha mellor correlación cos datos *in vivo* para comprender o verdadeiro potencial destes nanotransportadores.

USC
UNIVERSIDADE DE SANTIAGO DE COMPOSTELA

RESUMEN

En la actualidad, más de 250 millones de personas luchan contra la discapacidad visual en todo el mundo por causas potencialmente prevenibles o corregibles y se prevé que los trastornos oculares aumenten en las próximas dos décadas, pudiendo describirse generalmente como trastornos del segmento anterior y del segmento posterior. La calidad de vida, una medida importante del bienestar físico, emocional y social parece estar asociada negativamente con la discapacidad visual, y cada vez más se evalúan las intervenciones oftálmicas por su asociación con la calidad de vida. El diseño de un sistema eficiente de administración de fármacos que permita su vehiculización a un tejido concreto del ojo se ha convertido en un gran reto para los científicos del sector farmacéutico. En comparación con otras vías de administración, la administración de fármacos por vía ocular se ha enfrentado a importantes retos planteados por la gran eficiencia de las diversas barreras oculares. Muchas de estas barreras son inherentes y exclusivas de la anatomía y la fisiología ocular, lo que supone un reto para los científicos especializados en la administración de fármacos.

En las dos últimas décadas, las tecnologías de administración de fármacos oculares han avanzado de forma dinámica, dando lugar a nuevas intervenciones terapéuticas para los trastornos oculares crónicos. Los objetivos principales de cualquier **sistema de administración de fármacos por vía ocular** están fundamentados en mantener las concentraciones terapéuticas del fármaco en el lugar de destino, reducir la frecuencia de dosificación y atravesar las diferentes barreras oculares, tanto estáticas como dinámicas. Estas inimitables barreras no sólo excluyen la entrada de xenobióticos, sino que también desalientan la absorción activa de agentes terapéuticos. Así, el diseño de un esquema de administración ideal debe ir dirigido a obtener una mayor biodisponibilidad del fármaco, un incremento en la permanencia y una liberación controlada del mismo en el lugar de administración o de acción, que pueda superar las distintas barreras oculares.

Los sistemas convencionales de administración de fármacos adolecen de una escasa biodisponibilidad y de fluctuaciones en el nivel plasmático del fármaco, siendo incapaces de lograr una liberación sostenida. Sin un mecanismo de administración eficaz, todo el proceso terapéutico puede resultar inútil. Una liberación lenta, prolongada y/o sostenida del fármaco

suele ser el objetivo más deseado, aunque los métodos para definir una tasa de liberación óptima para la mejora de la respuesta terapéutica o biológica son escasos. La dinámica de liberación del fármaco depende de la cantidad de fármaco cargado en la matriz del portador, de las solubilidades del fármaco en la matriz y en el medio de liberación, y de las propiedades de la matriz que afectan a la cinética de difusión del fármaco. La cantidad de carga sigue siendo, en su mayor parte, un factor empírico en el desarrollo de sistemas portadores de fármacos, aunque se dispone de métodos experimentales para anticipar al menos las cargas mínimas efectivas, por lo que la preferencia común se dirige a la obtención de grandes capacidades de carga, capaces de mantener altas concentraciones en sangre o tejidos. Sin embargo, en algunos casos se ha demostrado que los gradientes temporales de las moléculas bioactivas pueden ser más eficaces que una concentración constante para inducir la respuesta biológica deseada.

Los papeles clave de la concentración y el tiempo están reconocidos en farmacología, pero el estudio sistemático de la interrelación entre dosis, farmaco/toxicocinética y farmaco/toxicodinámica sigue suponiendo un reto importante. En este contexto, los sistemas de administración de fármacos son una valiosa herramienta para generar gradientes temporales y espaciales de fármacos en los tejidos diana y podrían explorarse en profundidad para investigar cómo estos factores determinan las acciones terapéuticas.

En los últimos años, se está observando un aumento de los enfoques novedosos para la administración no invasiva de potentes agentes terapéuticos con el fin de lograr un cumplimiento terapéutico óptimo. La **instilación tópica oftálmica** es la ruta de administración más deseable, considerando que es fácil de manejar y rentable a nivel económico, siendo especialmente útil para el tratamiento de trastornos que afectan al segmento anterior del ojo. No obstante, la principal desventaja de las formulaciones oftálmicas convencionales de aplicación tópica es la relativamente baja biodisponibilidad ocular. Esto puede atribuirse a las altas tasas de renovación del líquido lagrimal y al elevado drenaje nasolacrimal. No obstante, la administración controlada de fármacos mediante el uso de nanoformulaciones mucoadhesivas, como las nanopartículas o los sistemas lipídicos nanoestructurados, se puede lograr una alta biodisponibilidad de los fármacos en los tejidos anteriores, como la conjuntiva y la córnea.

USC UNIVERSIDADE DE SANTIAGO

Por su parte, la administración directa de fármacos mediante **inyecciones intravítreas o implantes intravítreos** presenta muchas ventajas en el tratamiento de enfermedades del segmento posterior del ojo. A diferencia de la administración de fármacos por vía sistémica, la

administración local de fármacos por vía intravítrea elude las barreras hemato-oculares, permitiendo alcanzar niveles de fármacos intraoculares más elevados con menor número de efectos secundarios.

El **queratocono** es una ectasia corneal degenerativa y progresiva que afecta a niños y adultos jóvenes, generando una gran incapacidad visual, de calidad de vida y con gran impacto sociosanitario. La incidencia establecida de 1/2000 en la población general se ha visto aumentada debido a la mayor precisión y sensibilidad de las técnicas tomográficas corneales actuales. Es esencial una actuación médica en los distintos estadios de la ectasia para prevenir su progresión y así evitar el trasplante corneal. En la actualidad, no se dispone de ningún tratamiento eficaz que permita frenar y/o retrasar la evolución del QC. Estudios previos han demostrado la implicación de la inmunidad innata en esta enfermedad. Los receptores Toll-Like 2 (TLR2) en células epiteliales corneales pueden usarse como biomarcadores específicos de diagnóstico y progresión de queratocono. Por otra parte, también se ha demostrado que la lactoferrina (Lf), proteína inmnuomoduladora y antiinflamatoria, está disminuida en dicha patología. Basándonos en estas evidencias previas, sería interesante llevar a cabo el diseño y desarrollo de sistemas novedosos de liberación prolongada cargados con lactoferrina para administración tópica oftálmica dirigidas a TLR2 a modo de una potencial aproximación terapéutica del queratocono.

De igual modo, la **neuropatía óptica hereditaria de Leber (LHON)** es una enfermedad genética mitocondrial caracterizada por provocar una pérdida bilateral de la visión central como consecuencia de la degeneración de las células ganglionares de la retina (RGCs) y el nervio óptico, debido a mutaciones puntuales en el genoma mitocondrial que generan alteraciones en la cadena respiratoria. Cabe señalar que la LHON tiene una prevalencia estimada de 1/30.000, afectando predominantemente a adultos jóvenes (entre 15-30 años) de todos los grupos étnicos, con una preponderancia masculina (80%). En consonancia con esta hipótesis, la pérdida selectiva de RGCs observada como adelgazamiento del RNFL sólo se produce en la fase atrófica tardía de la enfermedad, imposibilitando la recuperación visual. Por lo tanto, el periodo entre la disfunción celular y la pérdida de células podría ser considerado como una ventana terapéutica a través de la cual se podría restaurar la visión mediante la normalización de la función mitocondrial. Teniendo en cuenta el origen mitocondrial de muchas enfermedades oculares, las mitocondrias como objetivo farmacológico podrían ser consideradas una alternativa de tratamiento para las neuropatías ópticas. En la actualidad, las opciones de

USC UNIVERSIDADE DE SANTIAGO

tratamiento de la LHON siguen siendo limitadas y una de las estrategias terapéuticas que presenta mayor interés está constituida por un análogo de la coenzima Q10 (CoQ10), la idebenona, una benzoquinona de cadena corta dotada de una potente acción antioxidante e inhibidora de la peroxidación lipídica, además de interactuar con la cadena de transporte electrónico, modulando el flujo de electrones. En base a ello, uno de los enfoques más interesantes estaría fundamentado en el diseño, desarrollo y caracterización de formas farmacéuticas de liberación prolongada conteniendo idebenona, formuladas mediante la utilización de polímeros biodegradables y biocompatibles, bien de poliésteres derivados del petróleo (PCL) o procedentes de recursos agrarios (PLGA).

La presente tesis doctoral se divide en dos secciones principales en concordancia con las dos enfermedades oculares previamente descritas. La primera sección se centra en el diseño, desarrollo y caracterización de diferentes tipos de sistemas nanoparticulares cargados con lactoferrina para administración tópica oftálmica, como alternativa farmacológica para el tratamiento del queratocono, y consta de tres capítulos. Por su parte, la segunda sección se centra en el diseño, desarrollo y caracterización de dos formas farmacéuticas de liberación prolongada, microsferas e implantes, destinadas a administración intravítrea para el tratamiento de la neuropatía óptica hereditaria de Leber, incluyendo los dos capítulos restantes.

El **capítulo 1** comprende y describe el diseño, optimización y caracterización de dos tipos diferentes de nanopartículas basadas en quitosano como sistemas novedosos de administración de lactoferrina. El objetivo de este capítulo está basado en el diseño, desarrollo y caracterización de nanopartículas de CS/TPP y CS/SBE-β-CD cargadas con lactoferrina como sistemas de administración tópica de fármacos como alternativa farmacológica para el tratamiento del queratocono. Se ha realizado una comparación entre las nanopartículas CS/TPP tradicionales y las nanopartículas CS/SBE-β-CD para llevar a cabo la inmovilización de proteínas de alto peso molecular destinadas a la administración oftálmica tópica. También se han llevado a cabo diversos análisis para demostrar la idoneidad de ambas formulaciones en relación con la liberación sostenida de lactoferrina y a la mejora de la permeabilidad corneal, obteniendo una base preclínica sólida, no sólo mediante ensayos *in vitro*, sino también con ensayos *ex vivo* e *in vivo*. Además de ello, se ha desarrollado un novedoso estudio de biopermanencia ocular de nanopartículas poliméricas basado en una técnica de radiomarcaje con diferentes radiotrazadores para evaluar la bioadhesión de las partículas destinadas a la administración tópica oftálmica.

USC UNIVERSIDADE DE SANTIAGO DE COMPOSTELA

Se ha obtenido una base preclínica consistente para ambos nanosistemas, pudiendo ser considerado como un potencial primer tratamiento farmacológico para el queratocono, alternativo a los actuales métodos clínicos invasivos. Ambos tipos de nanopartículas se han obtenido mediante la técnica de gelificación ionotrópica. Se ha estudiado el tamaño y la morfología de las nanopartículas en función de las condiciones de preparación. Dichas nanopartículas mostraban un tamaño medio de 180,73 ± 40,67 nm, con una polidispersión (PDI) de 0,170 ± 0,067 y valores de potencial ζ positivo, que oscilaban entre 17,13 y 19,89 mV. La lactoferrina se incorporó con éxito a ambos tipos de nanotransportadores. Los perfiles de liberación *in vitro* mostraron una entrega mejorada, prolongada y controlada de lactoferrina desde la matriz polimérica. Estas formulaciones también demostraron no tener problemas de estabilidad ni de citotoxicidad, así como propiedades mucoadhesivas adecuadas, con un elevado tiempo de permanencia en la superficie ocular. Así pues, ambos tipos de nanopartículas podrían considerarse sistemas de administración de fármacos oftálmicos tópicos de liberación controlada.

La novedad de este trabajo radica en poner a prueba la idoneidad de las formulaciones basadas en quitosano para mejorar la permanencia y la penetración del fármaco en la córnea, además de evaluar la capacidad de mantener y controlar la liberación del fármaco. Estos novedosos sistemas de liberación no son irritantes para el ojo y producen un mayor tiempo de retención ocular, proporcionando así una mayor eficacia y biodisponibilidad. Otras ventajas son la alta biocompatibilidad, la facilidad de preparación, la no necesidad de grandes restricciones durante el procedimiento de preparación, la alta eficiencia de encapsulación y carga, la mayor estabilidad física tras el almacenamiento y la mejor permeabilidad del fármaco.

El **capítulo 2** se ha basado en el diseño, desarrollo y caracterización fisicoquímica de NLCs cargados de lactoferrina como nueva alternativa terapéutica para el tratamiento del queratocono. El objetivo central de este enfoque de liberación controlada y específica en el lugar de acción se centra predominantemente en la comprensión de las propiedades farmacocinéticas y farmacodinámicas del fármaco, junto con una mejor inmunogenicidad para mejorar el resultado terapéutico. También se ha estudiado la idoneidad de la NLC para controlar la liberación de Lf y mejorar su permeabilidad corneal, adquiriendo una sólida base desde el punto de vista preclínico. De hecho, se ha realizado un novedoso ensayo de biopermeabilidad ocular basado en un método de radiomarcaje para evaluar la bioadhesión de la NLC para instilación tópica. Los NLCs cargados de lactoferrina se prepararon con éxito mediante un método de doble

USC UNIVERSIDADE DE SANTIAGO

emulsión/evaporación de disolventes. Los NLCs resultantes han sido evaluados en términos de tamaño de partícula, distribución de tamaño (PDI), carga superficial, morfología, eficiencia de encapsulación (EE), capacidad de carga (LC), estabilidad, citotoxicidad, liberación in vitro y retención en la superficie ocular. Los datos resultantes mostraron un tamaño de 119,45 ± 11,44 nm, un valor de PDI de 0,151 ± 0,045 y una carga superficial de -17,50 ± 2,53 mV. Además, se obtuvieron valores elevados de EE y LC (hasta el 75%). El estudio de liberación in vitro demostró un patrón de liberación controlado para la lactoferrina. Los NLCs también resultaron ser estables, no tóxicos y mostraron propiedades mucoadhesivas. Por lo tanto, se obtuvo una base preclínica consistente, por lo que los NLC podrían ser considerados como un potencial sistema novedoso de liberación controlada de lactoferrina para el tratamiento del queratocono.

El **capítulo 3** describe el diseño, la optimización y la caracterización de ocho tipos diferentes de nanopartículas basadas en PLGA (nanoesferas y nanocápsulas) como sistemas novedosos de administración de una proteína, la lactoferrina, con el fin de obtener una base preclínica sólida como tratamiento farmacológico alternativo a los actuales métodos clínicos invasivos para el queratocono. Las diferentes nanopartículas se prepararon mediante dos técnicas de nanoprecipitación modificadas, utilizando una mezcla de tres componentes de fármaco/polímero/surfactante (Lf/PLGA/Poloxamer), como forma de superar las limitaciones inherentes a las NPs de PLGA convencionales. Estos nanotransportadores poliméricos modificados, destinados a la administración oftálmica tópica, fueron sometidos a caracterización *in vitro*, modificación de la superficie y evaluaciones *ex vivo* e *in vivo*. Se obtuvo un rango de tamaño adecuado, una distribución de tamaño uniforme y valores de potencial ζ negativos para todos los tipos de formulaciones. La lactoferrina se incorporó con éxito a todos los tipos de nanotransportadores con valores adecuados de eficiencia de encapsulación y capacidad de carga. Los perfiles de liberación *in vitro* mostraron una liberación prolongada y controlada de lactoferrina desde la matriz polimérica. Estas formulaciones tampoco demostraron problemas de inestabilidad o citotoxicidad. Así pues, todos los tipos de nanopartículas podrían considerarse como nuevos nanotransportadores para la liberación controlada de lactoferrina por vía tópica oftálmica. Esta mejora se ha logrado mediante un aumento de la permanencia de Lf en la superficie ocular o mejorando la permeabilidad corneal de Lf.

USC UNIVERSIDADE DE SANTIAGO DE COMPOSTELA

El **capítulo 4** describe el diseño, el desarrollo y la caracterización de microesferas (MSs) de PLGA cargadas con idebenona mediante un método de emulsión/evaporación de solvente, así

como la caracterización fisicoquímica, con el objetivo de investigar nuevos enfoques intravítreos para una liberación controlada y sostenida de idebenona como nueva alternativa de tratamiento de la LHON. Con ello se busca disminuir la necesidad de la administración sistémica del fármaco o minimizar la frecuencia de las inyecciones oculares requeridas. La idoneidad de las formulaciones de las MSs de PLGA cargadas con idebenona para controlar y mantener la liberación de idebenona también se llevó a cabo mediante la adquisición de una base preclínica fiable a través de ensayos *in vitro* y *ex vivo*.

Se han obtenido de valores adecuados de rendimiento de producción, eficacia de encapsulación y capacidad de carga. Las MSs mostraron una forma esférica, con un rango de tamaño de 10 - 25 µm y una superficie lisa y no porosa. Los espectros FTIR demostraron que no había interacciones químicas entre la idebenona y los diferentes polímeros. Los análisis de RMN en estado sólido, difractometría de rayos X, DSC y TGA indicaron que la microencapsulación condujo a la amorfización del fármaco. Los perfiles de liberación *in vitro* se ajustaron a un perfil cinético biexponencial. Además, las MSs de PLGA cargadas con idebenona no mostraron efectos citotóxicos en un modelo de tejido organotípico. Los resultados sugieren, por tanto, que las MSs de PLGA podrían ser una alternativa para la administración intraocular de idebenona a largo plazo, mostrando potenciales ventajas terapéuticas como un nuevo enfoque terapéutico para el tratamiento de la Neuropatía Óptica Hereditaria de Leber (LHON).

El **capítulo 5** incluye un estudio piloto destinado a la evaluación de la viabilidad y las características de la liberación prolongada y controlada de idebenona a partir de un implante intravítreo de PCL. El diseño, desarrollo y caracterización de los implantes de PCL cargados con idebenona, preparados mediante un método de homogeneización/extrusión/evaporación de disolventes, ha permitido la obtención de altos valores de rendimiento de producción, eficacia de encapsulación y capacidad de carga. La caracterización *in vitro* se completó con la evaluación de las propiedades mecánicas e instrumentales. Se ha evaluado la liberación *in vitro* de idebenona desde los implantes de PCL, además de controlar la erosión del implante mediante el estudio de la pérdida de masa y los cambios en la morfología de la superficie. Se utilizaron técnicas de DSC, TGA, FTIR y rayos X para estimar la estabilidad y la interacción entre los componentes del implante. Se estableció una base preclínica consistente, apoyando la idea de los implantes de PCL cargados de idebenona como una nueva estrategia de liberación intraocular sostenida a largo plazo para el tratamiento de la LHON.

USC UNIVERSIDADE DE SANTIAGO

En **conclusión**, en esta tesis doctoral se detallan los procesos de diseño, desarrollo y caracterización de diferentes formulaciones destinadas a la obtención de una liberación controlada y prolongada de diferentes fármacos. En la primera parte de esta tesis doctoral, se diseñaron y desarrollaron con éxito tres tipos diferentes de nanopartículas. Todas estas formulaciones se cargaron con lactoferrina como fármaco diana y se propusieron como alternativas farmacológicas para el tratamiento del queratocono. Se obtuvieron nanopartículas estables y de tamaño ajustable mediante diferentes métodos de preparación. Asimismo, mostraron propiedades fisicoquímicas apropiadas para su administración por vía tópica oftálmica, apoyando la idea de que quedaban retenidas en la capa corneal, prolongando el tiempo de liberación del fármaco desde el propio tejido, así como una buena estabilidad al almacenamiento, al pH y a la fuerza iónica. También se obtuvo una liberación controlada de Lf, corroborando su uso como posibles sistemas de liberación de fármacos hidrofílicos. Todos los datos obtenidos confirmaron sus propiedades mucoadhesivas, sin evidencia de citotoxicidad tisular.

En la segunda parte de esta tesis doctoral, se diseñaron y desarrollaron con éxito dos sistemas diferentes de administración de fármacos como nuevas alternativas para el tratamiento del LHON, cargados con idebenona, ambos destinados a la administración intravítrea. Ambas formulaciones se caracterizaron fisicoquímicamente para crear una base preclínica sólida a partir de la cual realizar estudios *in vivo*. Asimismo, se ha logrado una liberación controlada y sostenida de idebenona a partir de ambas formulaciones, lo que confirma su uso como potenciales sistemas de liberación de fármacos para la administración intravítrea a largo plazo. Ambos sistemas han mostrado propiedades fisicoquímicas adecuadas, así como una estabilidad adecuada en relación con el almacenamiento, el pH y los cambios de fuerza iónica. Los datos resultantes mostraron que todas las formulaciones podrían considerarse como potenciales sistemas para la liberación controlada de fármacos.

Como conclusión general, se ha propuesto, por primera vez, diferentes formulaciones biodegradables de liberación prolongada para la administración de diferentes fármacos para el tratamiento de patologías oculares, tanto del segmento anterior como posterior del ojo, apoyado en amplios estudios preclínicos con el fin de obtener una base preclínica sólida como potenciales tratamientos farmacológicos del queratocono y de la Neuropatía Óptica Hereditaria de Leber (LHON). Esto se ha visto apoyado por numerosos estudios de caracterización *in vitro*,

USC UNIVERSIDADE DE SANTIAGO

ex vivo e *in vivo*. No obstante, debe explorarse en profundidad una mejor correlación con los datos *in vivo* para comprender el verdadero potencial de estos nanotransportadores.

USC
UNIVERSIDADE
DE SANTIAGO
DE COMPOSTELA

USC
UNIVERSIDADE
DE SANTIAGO
DE COMPOSTELA

INDEX

Statement of the problem **49**

Objectives **50**

Organization **51**

INTRODUCTION

DRUG DELIVERY AND RELEASE INTO THE EYE **57**

1. Drug delivery to the anterior segment of the eye 58
2. Drug delivery to the posterior segment of the eye 58

CORNEA AND ECSTATIC CORNEAL DISORDERS **59**

1. Introduction 59
2. Signs of corneal disease 60
   - 2.1. Superficial signs of corneal disease 60
   - 2.2. Deep-seated signs of corneal disease 62
3. Ecstatic corneal disorders 63
   - 3.1. Post-laser-assisted in situ keratomileusis corneal ectasia (post-LASIK corneal ectasia) 64
   - 3.2. Keratotorus or Pellucid Marginal Degeneration (PMD) 65
   - 3.3. Keratoglobus 67
   - 3.4. Keratoconus 68

OPTIC NEUROPATHIES: THERAPEUTIC ARSENAL IN LHON **72**

1. Introduction 72
2. Optic neuropathies 73

USC UNIVERSIDADE DE SANTIAGO DE COMPOSTELA

2.1. Optic neuritis 73
2.2. Devic's disease 74
2.3. Neurretinitis 74
2.4. Ischemic optic neuropathy 74
2.5. Traumatic optic neuropathy 74
2.6. Compressive optic neuropathy 75
2.7. Toxic optic neuropathy 75
2.8. Nutritional optic neuropathy 75
2.9. Hereditary optic neuropathies 76
3. Impact of genetics on hereditary retinal diseases 76
4. Leber's Hereditary Optic Neuropathy (LHON) 76
5. Therapeutic arsenal in the LHON treatment 80
5.1. Classical therapy: physical methods 80
5.2. Classical therapy: pharmacological methods 81
5.3. Gene therapy 84
5.4. Advanced therapy: stem cells 84
5.5. Preventive therapy: prevention of germline transmission 85
References 85

CHAPTER 1

Introduction 115

Materials 118

Experimental methods 119
1. Screening study: CS/TPP and CS/SBE-β-CD nanoparticles formation 119
2. Preparation of blank CS/TPP nanoparticles 119
2.1. Preparation of blank CS/SBE-β-CD nanoparticles 120
2.2. Preparation of lactoferrin-loaded CS/TPP nanoparticles 120
2.3. Preparation of lactoferrin-loaded CS/SBE-β-CD nanoparticles 121

USC UNIVERSIDADE DE SANTIAGO DE COMPOSTELA

3. Physicochemical characterization of chitosan-based nanoparticles 121
3.1. Particle size, size distribution and ζ potential 121
3.2. Morphological evaluation 121
3.3. Production yield (PY) of nanoparticles 122
3.4. Encapsulation efficiency (EE) and loading capacity (LC) of nanoparticles 122
4. Stability studies 123
4.1. Stability to storage 123
4.2. Stability to pH 123
4.3. Stability to ionic strength 124
5. *In vitro* release study 124
6. Cytotoxicity analysis 125
6.1. Bovine Corneal Opacity and Permeability test (BCOP) 126
6.2. Hen's egg test on the chorioallantoic membrane (HET-CAM) 127
7. Mucoadhesion study 128
7.1. *In vitro* ocular mucoadhesion study 129
7.2. *Ex vivo* ocular mucoadhesion study 129
7.3. *In vivo* mucoadhesion study 130
8. Data analysis 132
Results and discussion 132
1. Screening study: CS/TPP and CS/SBE-β-CD nanoparticles formation 132
1.1. Preparation of CS/TPP nanoparticles 132
1.2. Preparation of CS/SBE-β-CD nanoparticles 133
2. Physicochemical characterization of nanoparticles 135
2.1. Particle size, size distribution and ζ potential 135
2.2. Morphological evaluation 136
2.3. Production yield, encapsulation efficiency, and loading capacity of nanoparticles 137
2.4. Effect of protein loading on size, surface charge, EE (%) and LC (%) 138
3. Stability studies 139

USC UNIVERSIDADE DE SANTIAGO DE COMPOSTELA

3.1. Stability to storage 139
3.2. Stability to pH 140
3.3. Stability to ionic strength 141
4. *In vitro* release study 142
5. Cytotoxicity analysis 143
5.1. Bovine Corneal Opacity and Permeability test (BCOP) 143
5.2. Hen's egg test on the chorioallantoic membrane (HET-CAM) 144
6. Ocular surface mucoadhesion study 145
6.1. *In vitro* mucoadhesion study 145
6.2. *Ex vivo* corneal mucoadhesion study 146
6.3. *In vivo* ocular surface permanence study 146

Conclusion 149

References 151

Supplementary information 157

1. Experimental methods 157
1.1. Mucoadhesion study 157
2. Results and discussion 157
2.1. Screening study: CS/TPP and CS/SBE-β-CD nano-particles formation 157
2.2. Morphological evaluation 158
2.3. Stability studies 158
2.4. Cytotoxicity analysis 159
2.5. *In vivo* ocular surface permanence study 160

CHAPTER 2

INTRODUCTION 163

Materials 165

Experimental methods 166

USC UNIVERSIDADE DE SANTIAGO DE COMPOSTELA

1. Preparation of lactoferrin-loaded NLC 166
2. Physicochemical characterization of lactoferrin-loaded NLC 167
2.1. Particle size, size distribution and z potential 167
2.2. Morphology evaluation 167
2.3. Determination of production yield, encapsulation efficiency, and loading capacity 167
3. Stability studies 168
3.1. Stability to storage 168
3.2. Stability to pH 169
3.3. Stability to ionic strength 169
4. *In vitro* release study 169
5. Ophthalmic toxicity analysis 170
5.1. Bovine Corneal Opacity and Permeability test (BCOP) 170
5.2. Hen's egg test on the chorioallantoic membrane (HET-CAM) 171
6. Ocular surface retention study 171
6.1. *Ex vivo* ocular surface retention study 171
6.2. *In vivo* ocular surface retention study 172
7. Data analysis 173

Results and discussion 173

1. Preparation of lactoferrin-loaded NLC 173
2. Physicochemical characterization of NLC 174
2.1. Particle size, size distribution, and surface charge 174
2.2. Morphological evaluation 175
2.3. Production yield, encapsulation efficiency, and loading capacity of NLC 176
2.4. Effect of protein loading on size, EE, and LC 177
3. Stability studies 178
3.1. Stability to storage 178
3.2. Stability to pH 179
3.3. Stability to ionic strength 179

USC UNIVERSIDADE DE SANTIAGO DE COMPOSTELA

4. *In vitro* release study 181

5. Ophthalmic toxicity analysis 182

5.1. Bovine Corneal Opacity and Permeability test (BCOP) 182

5.2. Hen's egg test on the chorioallantoic membrane (HET-CAM) 183

6. Ocular surface retention study 183

6.1. *Ex vivo* ocular surface retention study 183

6.2. *In vivo* ocular surface retention study 184

Conclusion 187

References 188

CHAPTER 3

Introduction 200

Materials 203

Experimental methods 203

1. Preparation of PLGA nanoparticles 203

1.1. One-step nanoprecipitation method: nanospheres 203

1.2. Two-step nanoprecipitation method: nanocapsules 204

2. Physicochemical characterization of nanoparticles 204

2.1. Particle size, size distribution, and z potential 204

2.2. Morphological evaluation 204

2.3. Production yield (PY) of nanoparticles 205

2.4. Encapsulation efficiency (EE) and loading capacity (LC) of nanoparticles 205

3. Stability studies 205

3.1. Stability to storage 205

3.2. Stability to pH 206

3.3. Stability to ionic strength 206

4. *In vitro* release study 206

USC UNIVERSIDADE DE SANTIAGO DE COMPOSTELA

5. Cytotoxicity analysis 207
5.1. Bovine Corneal Opacity and Permeability test (BCOP) 207
5.2. Hen's egg test on the chorioallantoic membrane (HET-CAM) 207
6. Ocular surface retention study 208
6.1. *Ex vivo* corneal surface retention study 208
6.2. *In vivo* corneal surface retention study 208
7. Data analysis 210
Results and discussion 210
1. Preparation of lactoferrin-loaded PLGA nanoparticles 210
1.1. One-step nanoprecipitation method: lactoferrin-loaded PLGA nanospheres 210
1.2. Two-step nanoprecipitation method: lactoferrin-loaded PLGA nanocapsules 210
2. Physicochemical characterization of nanoparticles 211
2.1. Particle size, size distribution, and □ potential 211
2.2. Effect of protein loading on size and surface charge 212
2.3. Morphological evaluation 214
2.4. Production yield (PY), encapsulation efficiency (EE), and loading capacity (LC) of nanoparticles 215
3. Stability studies 215
3.1. Stability study during storage 215
3.2. Stability to pH 217
3.3. Stability study to ionic strength 218
4. *In vitro* release study 220
5. Cytotoxicity analysis 222
5.1. Bovine Corneal Opacity and Permeability test (BCOP) 222
5.2. Hen's egg test on the chorioallantoic membrane (HET-CAM) 223
6. Ocular surface retention study 224
6.1. *Ex vivo* corneal surface model 224
6.2. *In vivo* corneal biopermanence study 225
Conclusion 229

USC UNIVERSIDADE DE SANTIAGO DE COMPOSTELA

References **230**

CHAPTER 4

Introduction **243**

Materials **246**

Experimental methods **246**

1. Idebenone-loaded PLGA microspheres: preparation procedure 246
2. Microspheres physicochemical characterization 247
   - 2.1. Mean particle size, particle size distribution, and surface charge 247
   - 2.2. Morphological evaluation 248
   - 2.3. Production yield (PY) 248
   - 2.4. Encapsulation Efficiency (EE) and Loading Capacity (LC) 249
   - 2.5. Optimization of microspheres preparation procedure 250
   - 2.6. Effect of the polymer characteristics 250
   - 2.7. Effect of the drug:polymer ratio and PVA concentration 251
3. *In vitro* release study 252
4. Stability studies 252
   - 4.1. Stability to storage 253
   - 4.2. Stability to pH 253
   - 4.3. Stability to ionic strength 253
5. Moisture content 254
6. Solid State Nuclear Magnetic Resonance (ss-NMR) 254
7. Differential Scanning Calorimetry (DSC) and thermogravimetry analysis (TGA) 255
8. Fourier-transformed infrared spectroscopy (FTIR) analysis 255
9. X-Ray diffractometry analysis 256
10. Mercury intrusion porosimetry (MIP) assay 257
11. Syringeability and injectability studies 258

USC

12. Ocular irritancy and toxicity analysis of microspheres 259
12.1. Hen`s egg test on the chorioallantoic membrane (HET-CAM) 259
13. Statistical analysis 260
Results and discussion 260
1. Microsphere's preparation 260
2. Microsphere's optimization procedure 261
3. Microspheres physicochemical characterization 264
3.1. Mean particle size, particle size distribution, and surface charge 264
3.2. Morphology evaluation 266
3.3. Production yield (PY), Encapsulation Efficiency (EE), and Loading Capacity (LC) 267
4. *In vitro* release study 268
5. Stability studies 270
5.1. Stability to storage 270
5.2. Stability to pH 272
5.3. Stability to ionic strength 273
6. Moisture content 274
7. Solid-State Nuclear Magnetic Resonance (ss-NMR) 275
8. Differential Scanning Calorimetry (DSC) and Thermogravimetry analysis (TGA) 278
9. Fourier-transformed infrared spectroscopy (FTIR) 279
10. X-Ray diffractometry analysis 280
11. Mercury intrusion porosimetry 282
12. Ocular irritancy and toxicity analysis 284
Conclusion 284
References 286
Supplementary information 292

USC UNIVERSIDADE DE SANTIAGO DE COMPOSTELA

1. Supplementary figures ss-NMR 292
2. Supplementary figures MSs stability 293

CHAPTER 5

Introduction 297

Materials 299

Experimental methods 300

1. Preparation of idebenone-loaded PCL implants 300
2. Physicochemical characterization of implants 300
   2.1. Size, size distribution, and weight uniformity 300
   2.2. Morphology evaluation 301
   2.3. Production yield (PY, %) 301
   2.4. Encapsulation Efficiency (EE, %) 301
   2.5. Loading Capacity (LC, %) 302
3. Mechanical properties: tensile and elongation at break studies 302
4. Friability test 303
5. Differential Scanning Calorimetry (DSC) and Thermogravimetry analysis (TGA) 303
6. Fourier-Transformed Infrared Spectroscopy (FTIR) 304
7. X-Ray diffractometry analysis 304
8. *In vitro* release study 305
9. Water uptake, mass loss, and mass remaining studies 306
10. Stability studies 307
    10.1. Stability to storage 307
    10.2. Stability under physiological conditions 307
11. Injectability of implants 308
12. Cytotoxicity analysis 309
    12.1. Hen's egg test on the chorioallantoic membrane (HET-CAM) 309

USC UNIVERSIDADE DE SANTIAGO DE COMPOSTELA

13. Statistical analysis....310

Results and discussion....311

1. Preparation and optimization of idebenone-loaded PCL implants....311
2. Implant characterization....311
   2.1. Mean size, size distribution, and weight uniformity....311
   2.2. Morphological evaluation....312
   2.3. Production yield (PY), encapsulation efficiency (EE), and loading capacity (LC) 313
3. Mechanical properties: tensile strength and elongation at break....314
4. Friability test....315
5. Differential scanning calorimetry (DSC) and thermogravimetry analysis (TGA)....315
6. FTIR analysis....316
7. X-Ray diffractometry analysis....317
8. Stability studies....318
   8.1. Stability to storage....318
   8.2. Stability to pH....318
   8.3. Stability to ionic strength....319
9. *In vitro* release study....320
10. Implant's erosion study: water uptake, mass loss, and mass remaining....322
11. Injectability of implants....324
12. Cytotoxicity analysis....325
    12.1. Hen's egg test on the chorioallantoic membrane (HET-CAM)....325

Conclusion....326

References....327

Conclusions....335

Appendix....343

USC UNIVERSIDADE DE SANTIAGO DE COMPOSTELA

Conflict of interests.....343

Animal experiments.....343

Funding.....343

Articles derived from this thesis.....344

USC
UNIVERSIDADE
DE SANTIAGO
DE COMPOSTELA

List of abbreviations

AMP	Adenosine Monophosphate
AMPK	AMP Activated Protein Kinase
ANOVA	Analysis of the Variance
ARVO	Association for Research in Vision and Ophthalmology
ATP	Adenosine Triphosphate
AUC	Area Under the Curve
BBB	Blood-Brain Barrier
BCOP	Bovine Corneal Opacity and Permeability test
BSS	Balanced Salt Solution
CAM	Choroallantoic Membrane
CD	Cyclodextrin
CDVA	Corrected Distance Visual Acuity
CHUS	University Hospital Complex of Santiago de Compostela
CLMI	Cone Location and Magnitude Index
CON	Compressive Optic Neuropathy
CS/SBE-β-CD	Chitosan/ Sulfobutylether-β-cyclodextrin
CS/TPP	Chitosan/ Tripolyphosphate
CT	Computed Tomography
CXL	Corneal Collagen Crosslinking
DAPK	Deep Anterior Lamellar Keratoplasty
DCM	Dichloromethane
DDS	Drug Delivery System
DE/SE	Double Emulsion/Solvent Evaporation
DLS	Dynamic Light Scattering
DLS-NIBS	Dynamic Light Scattering with Non-Invasive Back Scattering
DLVO	Derjaguin, Landau, Verwey, and Overbeek
DMSO	Dimethyl sulfoxide
DNA	Deoxyribonucleic Acid
DOTA	1, 4, 7, 10-tetraazacyclododecane-1, 4, 7, 10-tetraacetic acid
DSC	Differential Scanning Calorimetry
ECHM	European Committee for Hyperbaric Medicine
EE	Encapsulation Efficiency
ERR	Estrogen Related Receptors
FDA	Food Drug Administration
F-FDG	2-[^{18}F]- fluoro-2-Deoxy-D-glucose
FTIR	Fourier-transformed Infrared Spectroscopy
GMP	Guanosine Monophosphate
HBOT	Hyperbaric Oxygen Therapy
HET-CAM	Hen's Egg Test on the Choroallantoic Membrane
ICH	International Council for Harmonization of Technical Requirements for Pharmaceuticals for Human Use

USC UNIVERSIDADE DE SANTIAGO DE COMPOSTELA

ICR	Intracorneal Ring
IL	Interleukin
ION	Ischemic Optic Neuropathy
IR	Infrared Absorption Spectroscopy
IS	Irritation Score
IVIS	*In vitro* Irritation Score
KC	Keratoconus
KCI	Keratoconus Classification Index
KPI	Keratoconus Prediction Index
KSI	Keratoconus Severity Index
LC	Loading Capacity
LED	Light Emitting Diodes
Lf	Lactoferrin
LHON	Leber's Hereditary Optic Neuropathy
LMWCS	Low Molecular Weight Chitosan
LOD	Limit of Detection
LOQ	Limit of Quantification
MIP	Mercury Intrusion Porosimetry
MLEM	Maximum Likelihood Expectation Maximization
MMP	Matrix Metalloprotease
MP	Microparticle
MRT	Medium Residence Time
MS	Microsphere
MTP	Mitochondrial Transition Pore
NADH	Nicotinamide Adenine Dinucleotide
NC	Nanocapsule
NIR	Near-Infrared Light Therapy
NLC	Nanostructured Lipid Carrier
NMO	Neuromyelitis Optica
NMR	Nuclear Magnetic Resonance
NS	Nanosphere
OD	Optical Density
OXPHOS	Oxidative Phosphorylation System
O/W	Oil-in-Water
PBS	Phosphate Buffered Saline
PCL	Poly-ε-caprolactone
PDI	Polydispersity Index
PEE	Punctuate Epithelial Erosions
PET	Positron Emission Tomography
PGD	Preimplantation Genetic Diagnosis
PK	Penetrating Keratoplasty
PLGA	Poly(lactic-co-glycolic) Acid
PMD	Pellucid Marginal Degeneration
PNT	Pronuclear Transfer
Post-LASIK	Post-Laser Assisted *in situ* Keratomileusis
PPAR	Peroxisome Proliferator Activated Receptor
PVA	Polyvinyl Alcohol
PVDF	Polyvinylidene Fluoride

USC UNIVERSIDADE DE SANTIAGO DE COMPOSTELA

PY	Production Yield
RGC	Retinal Ganglion Cell
RH	Relative Humidity
RNFL	Retinal Nerve Fiber Layer
ROI	Region of Interest
ROS	Reactive Oxygen Species
RSD	Relative Standard Deviation
SBE-β-CD	Sulfobutylether-β-cyclodextrin
SEM	Scanning Electron Microscopy
SOD	Superoxide Dismutase
ST	Spindle Transfer
TEM	Transition Electron Microscopy
TGA	Thermogravimetry analysis
TLR	Toll-Like Receptor
TNF	Tumor Necrosis Factor
TON	Toxic Optic Neuropathy
TPP	Tripolyphosphate
UDVA	Uncorrected Distance Visual Acuity
UVA	Ultraviolet A
VAD	Visual Acuity Decrease
VH	Vitreous Humor
WAX	Wide-Angle X ray

USC
UNIVERSIDADE DE SANTIAGO DE COMPOSTELA

USC
UNIVERSIDADE
DE SANTIAGO
DE COMPOSTELA

Objectives and organization

USC
UNIVERSIDADE
DE SANTIAGO
DE COMPOSTELA

USC
UNIVERSIDADE
DE SANTIAGO
DE COMPOSTELA

OBJECTIVES AND ORGANIZATION

STATEMENT OF THE PROBLEM

An effective treatment of ocular diseases involves the achievement of effective drug concentrations at the target site for an enough period. Nevertheless, conventional ocular drug delivery systems might not be sufficient to effectively treat ocular diseases due to the unique anatomy and physiology of the eye that contribute to its great protection by restricting the access at of exogenous substances to the target site of action.

In the past decades, new revolutionary therapy strategies have emerged for treatment of eye diseases due to the new innovations in material science, and an improvement of the pharmaceutical technology and biopharmaceutics approaches, where a variety of systems were designed and developed to promote the drug delivery to the different parts of the eye, with some advantages compared to the conventional drug delivery systems.

The recent advances made in ocular drug delivery for these site-specific and controlled release strategies were focused on the bioavailability enhancement by prolonging the drug retention time, and an improvement of the pharmacokinetic and pharmacodynamic drug profiles, as well as a better immunogenicity and the system recognition for an enhanced therapeutic efficacy, as a way to have a substantial impact on the treatment of ocular diseases. These advances were applied to the design and development of newer approaches in combination with novel therapeutic agents to create versatile delivery systems with a high therapeutic efficacy at the target site for the treatment of two different ocular diseases, one from the anterior segment of the eye, keratoconus (KC), and the other one from the posterior segment, Leber's Hereditary Optic Neuronopathy (LHON).

There is no available medical or pharmacological treatment to prevent the development or decrease the progression of keratoconus, where only optical treatment for visual rehabilitation (glasses or contact lenses) and surgical conservative treatments have shown as the therapeutic strategies. Nevertheless, the new advances in the design and development of delivery systems should postulate as a pharmacological alternative for the effective instillation of drugs through

USC
DE SANTIAGO
DE COMPOSTELA

the topical ophthalmic administration. Ophthalmic formulation requires a higher precorneal residence time and an enhanced drug penetration in order to improve the drug bioavailability. Therefore, a drug-delivery system offering longer retention and a sustained release of the drug to pass through these barriers would be essential. Novel drug-delivery technologies employing cyclodextrins and colloidal systems would be a good treatment strategy. An effort to demonstrate the suitability of different nanoparticulate formulations to control and sustain the drug release, in addition to improve the corneal permeability should be also considered.

On the other hand, retinal diseases such as LHON are challenging to treat due to the complex anatomy, physiology, and biochemistry of the eye that hinders the drug access to the target site. Besides, it is a rare disease whose etiology and treatment options remain unclear. An appropriate administration route is needed to achieve therapeutic drug levels in the target site, being the intravitreal injection the most promising option. Efficient intravitreal drug delivery systems should be designed aiming to overcome these drawbacks with negligible tissue damage in order to subsequently improve patient compliance and adherence to treatment, as well as reducing the treatment costs.

OBJECTIVES

The main objective of this work was based on the research, design, and preclinical development of controlled release pharmaceutical forms intended for ocular administration, these being: (I) lactoferrin-loaded nanoparticles for the treatment of keratoconus, based on blocking TLR2 expression and enhanced with the pharmacological effect of the protein itself, (II) solid and biodegradable idebenone microspheres for the treatment of LHON, and (III) biodegradable intravitreal idebenone implants for the treatment of LHON. In order to fulfill these purposes, a series of specific objectives linked to this project were set, including:

- Regarding Keratoconus:

  I. Design and development of controlled-release chitosan-based nanoparticles loaded with lactoferrin for topical ophthalmic administration.

  II. Design and development of controlled-release nanostructured lipid systems (NLCs) loaded with lactoferrin for topical ophthalmic administration.

USC

III. Design and development of controlled-release PLGA nanoparticles loaded with lactoferrin for topical ophthalmic administration.

IV. Physicochemical characterization of all lactoferrin-loaded nanoparticles for the obtention of a consistent preclinical basis.

V. *In vivo* study of the biodistribution of lactoferrin-loaded nanoparticles in an animal model.

- Regarding LHON:

I. Selection of the delivery systems with the greatest potential for intravitreal administration of idebenone, taking into account previous studies with biodegradable polymers at ocular level, the most widely studied pharmaceutical forms being intravitreal injections and implants.

II. Design and development of intravitreal implants formulated with polycaprolactone (PCL) as structural polymer, containing idebenone.

III. Design of biodegradable polymer microparticles containing idebenone intended for intravitreal administration.

IV. Characterization and *in vitro* evaluation of the different pharmaceutical forms elaborated, through:

a) Determination of the basic composition of the systems created.

b) Physicochemical and technological characterization of the different formulations.

c) Characterization studies of the systems by carrying out *in vitro* studies based on previously developed studies.

USC UNIVERSIDADE DE SANTIAGO DE COMPOSTELA

ORGANIZATION

Based on the formulated objectives, this doctoral thesis is presented as a compendium of five original research works and one review article. This doctoral thesis has been organized to comply with the regulation of the International Doctorate School at the University of Santiago

de Compostela (Spain) regarding thesis structure, languages, and ethical and intellectual properties.

The present doctoral thesis is divided in two main sections in correspondence with the two ocular diseases addressed. The first section focuses on the design, development, and characterization of lactoferrin-loaded nanoparticles for the treatment of keratoconus. It is divided in three chapters, from Chapter 1 to 3.

Chapter 1 was based on the design, preparation, and characterization of lactoferrin-loaded CS/TPP and CS/SBE-β-CD nanoparticles as topical ophthalmic drug delivery systems as a pharmacological alternative for keratoconus treatment. A comparison between the traditional CS/TPP nanoparticles and CS/SBE-β-CD nanoparticles in order to carry out the immobilization of high molecular weight proteins intended for topical ophthalmic administration was made. An effort to demonstrate the suitability and robustness of both chitosan-based formulations to sustain the lactoferrin release and improve the corneal permeability was also carried out by obtaining a consistent preclinical base, not just through *in vitro* tests, but also with *ex vivo* and *in vivo* assays. Certainly, a novel corneal surface permanence study of polymeric nanoparticles based on a radiolabeling technique with different radiotracers were carried out to assess the bioadhesion of particles intended for ophthalmic topical administration.

Chapter 2 was grounded on the design, development, and characterization of Lf-loaded NLCs as nanosized systems intended for the topical ophthalmic treatment of KC. Similarly, the central commitment of this site-specific and controlled-delivery approach is predominantly centered on the understanding of enhanced pharmacokinetics and pharmacodynamics drug properties, together with better immunogenicity to improve the therapeutic effect. An effort to prove the appropriateness of NLC to control the Lf release and improve its corneal permeability was also studied by acquiring a strong preclinical foundation. Indeed, a new ocular biopermanence assay based on a radiolabeling method was performed to evaluate the NLC bioadhesion proposed for topical instillation.

Chapter 3 comprises the design, development, and characterization of Lf-loaded PLGA nanoparticles, which were prepared by two different modified nanoprecipitation techniques, using a three-component mixture of drug/polymer/surfactant (Lf/PLGA/Poloxamer), as a way to overcome conventional PLGA NPs inherent limitations. These modified polymeric nanocarriers, intended for topical ophthalmic administration, were subjected to *in vitro* characterization, surface-modification, and *in vitro* and *in vivo* assessments.

USC UNIVERSIDADE DE SANTIAGO DE COMPOSTELA

The second section of the present thesis comprises the studies related to the design, development and characterization of idebenone-loaded microspheres and implants for the treatment of the LHON. It consists of two chapters, from Chapter 4 to 5.

Chapter 4 was aimed to investigate novel intravitreal approaches for an idebenone controlled and sustained release as a new alternative LHON treatment to diminish the need for systemic drug administration or minimize the frequency of required ocular injections. The present work describes the design and development of idebenone-loaded PLGA MSs by the oil-in-water emulsion/evaporation technique, as well as the physicochemical characterization. The appropriateness of idebenone-loaded PLGA MSs formulations to control and maintain the idebenone release was also performed by acquiring a reliable preclinical basis through *in vitro* and *ex vivo* assays.

Chapter 5 was based on the design, development, and physicochemical characterization of a biodegradable drug-loaded poly-ε-caprolactone implant that may provide flexibility in the choice of the active substance and controlled release for a long period; for this purpose, idebenone was employed as a model drug. A preclinical consistent base was obtained by means of the determination and assessment of the physicochemical, mechanical, and thermal properties, as well as the stability, cytotoxicity, and *in vitro* release. Additional studies were carried out to complete this preclinical background.

All the research has been done between the PARAQUASIL Research Group at the Department of Pharmacology, Pharmacy and Pharmaceutical (Faculty of Pharmacy, University of Santiago de Compostela (USC), Santiago de Compostela, Spain), the Clinical Pharmacology Group and the Clinical Neuroscience Group from the Health Research Institute of Santiago de Compostela (IDIS) (University Clinical Hospital of Santiago de Compostela, Santiago de Compostela, Spain). Moreover, molecular imaging (presented in chapters 1, 2 and 3) was performed in close collaboration with the Molecular Imaging Group (UNIME) of the Health Research Institute of Santiago de Compostela (IDIS) (University Clinical Hospital of Santiago de Compostela, Santiago de Compostela, Spain).

This project was included within the area of biomedical research applied to ophthalmology, since a series of knowledge related to the design and development of extended-release pharmaceutical forms could be obtained, with potential practical application. In general, all the conclusions might be susceptible of scientific application once the research was completed, since an important advance would be clinically promoted, by making possible the

USC UNIVERSIDADE DE SANTIAGO

administration of drugs for the treatment of ocular pathologies. Likewise, all the results were susceptible of publication and diffusion through the different media and diffusion specialized in topics related to ocular therapeutics, from Ophthalmology or Hospital Pharmacy to Pharmaceutical Technology or Biopharmacy.

USC
UNIVERSIDADE
DE SANTIAGO
DE COMPOSTELA

Introduction

USC
UNIVERSIDADE
DE SANTIAGO
DE COMPOSTELA

USC
UNIVERSIDADE
DE SANTIAGO
DE COMPOSTELA

INTRODUCTION

DRUG DELIVERY AND RELEASE INTO THE EYE

The human eye is such a complex and isolated sensory organ with a unique structure, physiology, and biochemistry. It is composed of widely varied structures with independent physiological functions, and it is connected to rest of the body by its vascular and nervous networks. The access of exogenous substances to specific ocular tissues is significantly protected by its anatomical and defense mechanisms.

The eye is divided into two different segments, the anterior and the posterior segment, both anatomically divided by the crystalline lens. The anterior segment comprises the front one-third of the eye that includes the cornea, pupil, aqueous humor, iris, lens, and ciliary body. On the other hand, the posterior segment constitutes the back two-third of the eye that includes the sclera posterior to the ciliary body, choroid, retina, vitreous humor, macula, and optic nerve

Ocular drug delivery is one of the most exigent challenges in terms of formulation on delivery systems. The most difficult part in the design and development of ocular drug delivery systems relies on the achievement of therapeutic drug concentrations for adequate time at the target site in order to provide high therapeutic efficacy. The ocular surface is hindered by barriers which protect the eye. Conventional ocular drug delivery systems have shown a poor bioavailability due to these ocular defense mechanisms that hamper to achieve effective drug concentrations in the target tissue. Lacrimation, efficient drainage through the nasolacrimal duct system, the inner and outer blood-retinal barrier, the cornea impermeability, and the absorptive capacity of other non-corneal structures make the eye an immunologically privileged system.

The basic principles of drug delivery are governed by basic thermodynamic functions (1), taking into account several characteristics, such as the diffusion rate, the drug chemical potential, or the drug concentration. The diffusion rate is dependent on drug concentration and time, both variables being related to a mathematical constant, the rate constant, which allows the determination of the diffusion order (2). Generally, the drug diffusion potential from one region to another is directly proportional to its chemical nature, which can usually be

USC UNIVERSIDADE DE SANTIAGO DE COMPOSTELA

approximated by its concentration (1–3). In any case, the achievement of a therapeutic effect is dependent on the drug concentration reached in the biophase, since it must be within the therapeutic range. This concentration is influenced by the sum of the following processes (4): (I) absorption, a process that involves the entry of the drug into the body, (II) distribution, in order to reach the target site, and (III) elimination of the drug. The intensity of these processes is time-dependent and can be estimated, although the existence of interindividual variability phenomena must be considered. This variability mainly depends on pharmacokinetic factors that alter the aforementioned processes. In addition, response variability is dependent on pharmacodynamic factors that alter the body's sensitivity to the drug.

1. Drug delivery to the anterior segment of the eye

Topical ophthalmic delivery is the most chosen route for drug delivery to the anterior segment of the eye due to its several advantages (5), such as: (I) non-invasive pathway, (ii) local effect and dosage reduction, minimizing systemic side effects, (III) no first-pass metabolism, and (IV) improvement of the patient compliance (6). Nevertheless, the application of ophthalmic drugs requires high dose frequency in order to overcome the short half-life and low drug solubility, since the cornea and conjunctival barriers hinder the drug penetration.

Despite the innovations in topical ophthalmic delivery, there remain challenges with regards to drug administration, diffusion, and retention. New strategies would be needed to achieve a long-acting topical ocular drug delivery. Novel anterior eye-targeted drug delivery systems offer many advantages over conventional eye drops and improve patient compliance by increasing drug bioavailability, prolonging drug delivery, and minimizing systemic exposure.

2. Drug delivery to the posterior segment of the eye

Prevalence of posterior segment ocular diseases is increasing every year, being associated with an increase on their severity and difficulty of treatment. Despite numerous efforts, effective intraocular drug delivery remains uncertain and, consequently, it is highly desirable to develop new alternative strategies of diseases affecting the vitreous cavity surroundings.

The standard procedure for the treatment of posterior segment ocular diseases these disorders is usually based on an intravitreal administration, although different approaches have been developed for the treatment of these disorders, including periocular, suprachoroidal, and subretinal administration routes (7).

Direct intravitreal injection has the advantage of being able to achieve immediate therapeutic concentrations in the eye while avoiding systemic exposure. However, drugs are rapidly cleared from the vitreous, usually by a first-order diffusion process, with half-lives of 24 hours or less. If relatively insoluble drug suspensions are injected into the vitreous, their apparent half-life may increase, although the intrinsic half-life of the drug itself does not change. In this case, dissolution of the suspended drug is rate limiting rather than elimination of the drug itself (8). Therefore, repeated injections are required to maintain therapeutic concentrations in the eye, and the associated risks of endophthalmitis, cataract formation, and retinal detachment have reduced the application of this technique to some sight-threatening diseases, such as endophthalmitis and cytomegalovirus retinitis.

Many attempts have been made to achieve sustained intraocular drug levels after intravitreal injection. Novel posterior eye-targeted drug delivery systems are a reasonable strategy intended to circumvent the drawbacks of direct intravitreal injections by offering many advantages in terms of bioavailability, drug delivery, and pharmacokinetics (9).

CORNEA AND ECSTATIC CORNEAL DISORDERS

1. Introduction

The human cornea is a transparent, avascular, richly innervated and resistant-to-deformation connective tissue, located in the most anterior portion of the eyeball, being a part of the anterior external tunic (10). It acts as the primary infectious and structural barrier of the eye.

It is presented as a spherical optical structure and has a dimension of approximately 10.5 mm on its vertical meridian and 11.5 mm on its horizontal meridian, as well as a 0.5 mm thickness at the center, gradually increasing towards the periphery (11–13). Its relative transparency, with a 1.3375 average refractive index, and 7.8 mm anterior radius of central curvature, provides a proper anterior refractive surface for the eye, together with the overlying tear film (10,13,14).

Anterior corneal stromal rigidity seems to be exceptionally significant in maintaining the corneal curvature (10). Organizational differences in the collagen bundles of the anterior stroma may contribute to a tighter cohesive strength in this area and may also explain why the anterior curvature defies alteration to stromal hydration much more than the posterior stroma, which verges to develop folds more easily.

Corneal ectasia is a progressive and degenerative disease, usually with a bilateral and asymmetric pattern, that comprises the corneal protrusion and thinning, as well as an increase

in its curvature (15–17). Corneal ectasia arises when the biomechanical integrity of the cornea is compromised with tissue alteration (beyond a harmless threshold required to preserve its shape and curvature), leading to an irreversible corneal thinning and steepening (16).

This decrease in the corneal thickness is associated with a series of clinical signs, such as (I) progressive astigmatism or myopia after developmental stage, (II) scissors or irregular retinal reflex, (III) decreased visual acuity, (IV) elevated keratometry, and (V) asymmetric corneal topography, among others (18–20). Thus, it can lead to significant ocular morbidity and may require surgical intervention.

Corneal ectasia shows a multifactorial etiology, the main cause being genetics. However, other possible causes of these ecstasies have been found, including recurrent eye rubbing, eye surgery or trauma, hormonal alterations or use of inappropriate contact lenses, among others (21,22). In general, it begins in puberty and progresses until about age 50, although the evolution in imaging technology has enabled a much earlier diagnosis, detecting cases at a much earlier age. Further, the overall prevalence of the ecstatic disorders has increased in the past years, from 50 to almost 300 cases per 100.000 in the general population, with both sexes equally affected (23–25).

There are many criteria for classifying corneal ectasias. They are mainly categorized according to (I) the origin, as natural or post-traumatic, and (II) the shape and location, as axial (localized), generalized or peripheral.

The present section aimed to reach a consensus of ecstatic diseases information focusing, not just the on prevalence and rates of progression, but on the most important scientific and medical information, including etiology, epidemiology, pathogenesis, diagnosis, and therapeutic approaches from documented literature.

2. Signs of corneal disease

2.1. Superficial signs of corneal disease

Clinically, several superficial signs were described as corneal disease's detection and diagnosis signs, including punctate epithelial erosions, subepithelial infiltrates, filaments, and epithelial edema, among others.

Punctate epithelial erosions (PEE) are tiny, faintly visible, and depressed epithelial defects that may be observed as an early sign of epithelial injury and ocular disease, being caused by a

variety of stimuli, where their location can help to discern the disease's etiology (see Table 1). The loss of the epithelial cells is a non-specific and frequently observed response in numerous ocular diseases and may be caused by trauma, exposure, inflammation, or toxic agents (26,27). These lesions are also observed in most ocular inflammatory diseases (e.g., keratoconjunctivitis or vernal keratitis).

Subepithelial infiltrates are observed as tiny foci of inflammatory infiltration below the corneal surface (28) as a consequence of severe or prolonged adenovirus keratoconjunctivitis, herpes zoster keratitis, adult inclusion conjunctivitis, marginal keratitis, acne rosacea and Thygeson's superficial spotted keratitis (29–31).

Table 1. Summary of the different diseases and their relationship with the appearance of punctate epithelial erosions (PEE).

Location	Etiology	Ref.
Superior	Vernal keratoconjunctivitis, Chlamydial conjunctivitis, Upper limbic keratoconjunctivitis, Palpebral laxity syndrome, Mechanical keratoconjunctivitis	(32)
Interpalpebral	Dry eye, Corneal hypesthesia, Ultraviolet keratopathy	(33)
Inferior	Dry eye, Chronic blepharitis, Lagophthalmos, Eyedrops toxicity, Self-inflicted injuries, Entropion.	(33)
Diffuse	Viral and bacterial conjunctivitis, Eyedrops toxicity	(34)
Central	Prolonged use of contact lenses	(35)

Filaments are mucus strands mixed with epithelium that are attached at one end to the corneal surface. Dry eye is by far the most common cause, although it may also be due to upper limbic keratoconjunctivitis, neurotrophic keratopathy, prolonged patch occlusion, and essential blepharospasm (36,37).

Epithelial edema may be caused by endothelial decompensation, leading to a loss of normal corneal brightness, with tiny epithelial vesicles and blisters (in moderate or severe cases) (38–40).

USC DE COMPOSTELA

2.2. Deep-seated signs of corneal disease

In the last decades, several deep-seated signs of corneal diseases have been deeply studied, including infiltrates, ulceration, corneal lysis, vascularization, lipid deposition, Descemet's membrane folding or rupture, and Descemetocele, among others.

Infiltrates are initially yellowish or white-greyish stromal foci opacities of acute inflammation (local or diffuse) composed of inflammatory cells (mainly polymorphonuclear leukocytes (neutrophils), lymphocytes and macrophages, released from the limbal blood vessels), cellular and extracellular debris, and necrosis areas, surrounded by edema (41,42). These signs are usually located in the anterior stroma near to a limbus vascularized region as a response to local tissue damage or associated with chemotactic factors (antigens or environmental toxins), usually associated to limbic or conjunctival hyperemia (43). Thus, it is essential to distinguish between sterile and infectious lesions (see table 2) (41).

Ulceration is a tissue excavation associated with an epithelial defect, usually with infiltration, and underlying inflammation, as well as considerable conjunctival hyperemia, hypopyon (sedimented leukocytes in the anterior chamber), and necrosis (41,44). Corneal neovascularization may also be developed from the limbus Ulceration usually heals with fibrotic tissue, leading to corneal opacification and decreased visual acuity (45).

Table 2. Characteristics of infectious and sterile corneal infiltrates.

Location	Infectious corneal infiltrates	Sterile corneal infiltrates
Size	Bigger	Smaller
Progression	Rapid	Slow
Epithelial failure	Frequent	Infrequent
Pain	Moderate or intense	Mild
Secretion	Purulent	Mucopurulent
Single or multiple	Single	Multiple
Unilateral o bilateral	Unilateral	Bilateral
Anterior chamber reaction	Intense	Mild

USC UNIVERSIDADE DE SANTIAGO DE COMPOSTELA

Location	Central	Periphery
Adjacent corneal reaction	Extensive	Limited

Corneal lysis consists of tissue disintegration by enzymatic activity, often with little or no infiltration, as in peripheral ulcerative keratitis (41). The corneal epithelial and endothelial layers show high superoxide dismutase (SOD) activity but the stroma lacks this enzyme, and thus is virtually unprotected from highly reactive anions biologically generated by numerous mechanisms (46). Consequently, the disruption of the epithelia leads to an increase of the stromal layer vulnerability to oxygen radicals and, thus, incur damage by molecular alteration of the structural components (47).

Descemet's membrane folding, also known as striated keratopathy, appear as a consequence of corneal edema, causing inflammation, trauma and ocular hypotonia (48). Rupture of the Descemet's membrane may also occur due to enlargement (Haab's striae in childhood glaucoma) or corneal deformation, as well as descemetocele (a bubble-shaped herniation of the Descemet's membrane into the cornea), filling an otherwise full-thickness defect (49,50). Vascularization may occur in response to a wide variety of stimuli (51). Venous channels are easily seen, while arterial blood vessels are smaller and require more magnification (52).

Lipid deposition may be a consequence of chronic inflammation with exudation from corneal neovasae (53). Lipids and lipoproteins probably reach the corneal stroma from the limbal vessels. Their distribution within the stroma depends on many different factors (temperature, lipid composition and properties, among others) (54). Lipids and lipoproteins carried to the stroma may be modified upon entrance. Furthermore, blood vessels inflammation or corneal neovascularization may occur, promoting the corneal lipid deposition (55). As a result, a vascular form of lipid deposition, lipid keratopathy, may appear due to an unmodified lipid deposition phenomenon (56).

3. Ecstatic corneal disorders

Corneal ectasias, either natural or secondary to refractive surgery, respond to a set of morphological and structural changes, resulting in the progressive thinning, visual reduction and deterioration of the optical quality (25,57). Ecstatic disorders also have an increasing socioeconomic impact due to the fact that they mainly affect a wide range of age among the general population (58).

The four most common forms are (I) Post-laser-assisted *in situ* keratomileusis corneal ectasia (post-LASIK), (II) Keratotorus or Pellucid marginal degeneration (PMD), (III) Keratoglobus, and (IV) Keratoconus. Table 3 shows the parameters to be determined to carry out a differential diagnosis of different corneal ectasias (59). In any of them, the thinning and protrusion processes make the patient suffer from a whole disease pattern of continuous discomfort and progressive deterioration of the optical quality, coming to not tolerate most of the traditional treatments (glasses or contact lenses) in advanced stages.

Table 3. Key parameters for a differential diagnosis of corneal ectasias.

Parameter	Post-LASIK	PMD	Keratoglobus	Keratoconus
Frequency	Infrequent	Infrequent	Rare	Frequent
Laterality	Bilateral	Bilateral	Bilateral	Bilateral
Onset age	> 6 months after surgery	20-50 years	Birth	Puberty
Thinning	Central or paracentral	Inferior stripe	Bigger on the periphery	Lower paracentral
Protrusion	Generalized	Above the thinning stripe	Generalized	Thinner towards the apex

3.1. Post-laser-assisted *in situ* keratomileusis corneal ectasia (post-LASIK corneal ectasia)

Post-laser-assisted *in situ* keratomileusis (LASIK) corneal ectasia is a corneal disorder firstly described in 1998 (57) and characterized by progressive stromal thinning and central or asymmetric inferior corneal steepening (60), with a 0.01–0.66% estimated incidence (22,61–64). It was suggested that central corneal ectasia is associated with low residual stromal thickness, while inferotemporal ecstatic disorder is a sign of preexisting pellucid marginal degeneration (PMD) or formed fruste keratoconus (FFK) (65). Histologically, several features of post-LASIK corneal ectasia can be similar to other ecstatic disorders, such as stromal bed microstriae and stromal collagen lamellae thinning.

USC UNIVERSIDADE DE SANTIAGO

The exact pathophysiology of post-LASIK corneal ectasia remains unclear, even though corneal biomechanics alterations can lead to thinning and compression of collagen fibrils, resulting in a loss of the global structural integrity (65–69). Low stromal thickness, thin preoperative pachymetry, topographic asymmetry, atypical astigmatic patterns, and high myopia are also observed (58,66,68–70).

Clinical diagnosis of corneal ectasia was made by the assessment of progressive central or inferior corneal steepening based on Scheimpflug tomography, associated with increased and refractive myopia, as well as astigmatism of a 3 or more month period after LASIK surgery, decreased uncorrected distance visual acuity (UDVA), and corrected distance visual acuity (CDVA) (20,71,72). Pachymetry, topography, and slit-lamp biomicroscopy were also applied for confirmation of LASIK flap presence, keratometry, and topography readings (73).

Therapeutic options for post-LASIK treatment traditionally include vision correction (74), rigid gas-permeable contact lenses, and intrastromal corneal ring segments (66). Corneal collagen crosslinking (CXL) (75–80) subsequently emerged as a promising technique to treat post-LASIK ectasia, by combining the use of ultraviolet A irradiation and B2 vitamin (as a photosensitizer) in order to produce reactive oxygen species (ROS), which induce intra- and interfibrillar covalent bonds between stromal collagen fibrils to biomechanically stabilize the cornea (74,81,82).

3.2. Keratotorus or Pellucid Marginal Degeneration (PMD)

Pellucid marginal degeneration is a rare disorder with progressive peripheral corneal thinning that compromises the lower and peripheral area of the cornea (83). It usually appears in adulthood (typically discovered between the second and fifth decades of life) and is shown as a bilateral and asymmetric affectation of the lower portion of the cornea. It adopts a characteristic topographic pattern commonly called "croissant" or "butterfly" shape (84). Unlike other ecstatic corneal disorders, the affected area is located below the ectasia and astigmatism is against the rule, where Fleischer's rings and Vogt's striae do not usually occur (85).

USC UNIVERSIDADE DE SANTIAGO DE COMPOSTELA

PMD usually appears sporadically and may be classified as a hereditary pathology with variable expressiveness, with no family history or associated systemic disease, also influenced by other factors (86). Further, there is presumably no predisposition neither by race nor by gender

(25,83,87,88), although recent studies have revealed a male preponderance in the occurrence of the disease (84,89,90).

Up to the present time, no biostatistical studies have assessed either the incidence or prevalence of PMD. However, PMD is considered a rare illness, less common than other ecstatic diseases (25,83,87).

Classically, slowly progressive visual blurring due to irregular astigmatism is the most common symptom that appears in this ecstatic corneal disorder (41). Nevertheless, several signs have been established as diagnosis parameters of this disease, including: (I) 1-2 mm band of lower corneal thinning in a crescent-shaped pattern in the limbus area, with a slow and bilateral progression, (II) the epithelium is intact, and the cornea above the thinned area shows ectasia and flattening signs, (III) no Fleischer's ring or Vogt's striae, (IV) acute dropsy is rare, and (V) the corneal topography analysis shows a butterfly pattern, associated with significant astigmatism and bending diffuse lower cornea (83,84,87).

The histopathology analysis suggests the likelihood of a variety of keratoconus, as supported by the recently microscopic outcomes (91). However, it was observed an increase in stromal mucopolysaccharides and absence or an irregular Bowman's layer, but the epithelium remained as usual (92,93).

Other disorders reported in patients with PMD include keratoconjunctivitis (94), chronic open-angle glaucoma (95), retinitis pigmentosa (89), retinal lattice degeneration (89), scleroderma (a progressive, eczema (96,97), and hyperthyroidism (98,99). Nevertheless, no pathogenic association with PMD was still confirmed.

The treatment of PMD is very difficult due to abnormal corneal topography. Treatment options are limited by the degree of corneal protrusion. The standard medical treatment is based on glasses and contact lenses correction (41). As for astigmatism increases, glasses correction usually fails in the early stages of PMD (85). However, different contact lenses options remain useful, these being: (I) soft toric hydrophilic contact lenses, which are adequate in early stages (100), (II) hybrid contact lenses, appropriate for patients, but with low oxygen permeability that may result in corneal neovascularization (101), (III) rigid gas-permeable contact lenses, which provide good corneal oxygenation, being often the best in advanced cases (102). Nevertheless, all these contact lens options are symptomatic treatments that can improve the patient's vision and may cause glare and reduced contrast sensitivity. Despite that, there is no evidence that these lenses can prevent disease progression.

USC UNIVERSIDADE DE SANTIAGO

In many cases, medical treatment is not satisfactory, and surgery may be required to restore vision or as an alternative treatment to the patient's intolerance to contact lenses (90,103). Surgical options, none of which are optimal, include eccentric penetrating keratoplasty, thermocautery, crescentic lamellar keratoplasty, wedge resection of the affected tissue, epikeratoplasty or implantation of intrastromal rings, among others (104–109). At this time, the most prevalent treatment may be a peripheral lamellar crescent keratoplasty followed by a central penetrating keratoplasty.

3.3. Keratoglobus

Keratoglobus is an extremely rare bilateral disorder that can be present at birth (when it must be differentiated from congenital glaucoma and megalocornea, and can be associated with other alterations) or acquired, debuting in adulthood (110,111). Topographically, the cornea suffers a globular rather than a conical ectasia, with generalized and extreme thinning, as well as a widespread increase in the corneal curvature. The Bowman's layer is fragmented, and the stroma and Descemet's membrane are thinned (112–114).

Two different forms of keratoglobus were described, these being: (I) a congenital or juvenile form, and (II) an acquired adult form. The congenital form presents a genetic etiology, where at least two different autosomal recessive syndromes (anormal and normal Type VI Ehlers–Danlos syndromes, where lysyl hydroxylase's activity is the key difference) are involved (115). Congenital keratoglobus is also associated with a Bowman's membrane absence, stromal disorganization and Descemet's membrane thickening, whereas acquired keratoglobus pathology is similar to that of keratoconus (116). The acquired form may be presented as an end-stage form of keratoconus. Despite this, no specific histopathological characteristics of keratoglobus that enable to be differentiated from keratoconus were described (116).

The presence of a limbus or tolimbus corneal thinning with globular corneal protrusion is considered the main ocular manifestation of keratoglobus. This corneal thinning is bigger in the corneal periphery or midperiphery. Diffuse corneal thinning with corneal rupture (spontaneously or after minor trauma), perforations, and corneal hydrops may occur, especially in the congenital form of the disease (117).

USC
UNIVERSIDADE
DE SANTIAGO
DE COMPOSTELA

The treatment of keratoglobus is still challenging so far. Conservative therapy is based on the refractive correction for myopia through the use of customized contact lenses (scleral lenses, small and large diameter rigid gas permeable lenses, and reverse-geometry hydrogel lenses)

(118–123). Nevertheless, corneal extreme protrusions and irregularities complicate the lens assembly, requiring a balance between optics and lens stability, where irregular astigmatism and risk of corneal perforation act as limiting factors (124).

Ocular acute hydrops, characterized by the appearance of stromal edema due to the filtration of aqueous humor through a rupture in Descemet's membrane, may appear as a clinical complication, whose treatment can be both conservative and surgical. Conventional treatment is non-specific, being based on the use of scleral contact lenses, patching, topical-ophthalmic hypertonic saline solutions, and cycloplegics eyedrops in order to reduce the edema (114,125). Surgically, there is no known standard procedure for treatment due to the rarity of the disease, so there is a lack of consistent reports of surgical results. Its purpose was restricted to the repair of large and stellate perforations due to the corneal fragility (124,126). Lamellar epikeratoplasty, large penetrating keratoplasty, and corneoscleroplasty were successfully been attempted in order to reinforce thinned corneas (127,128).

3.4. Keratoconus

3.4.1. Epidemiology and pathogenesis

Keratoconus (KC) is a bilateral, degenerative, and progressive disorder with a central or paracentral stromal thinning, apical protrusion, and irregular astigmatism (25,86,129–132). It is the most frequent progressive-character corneal ectasia (prevalence 54.5/100000 and incidence 1/2000), in which the cornea thins and acquires a conical and irregular shape (86,133,134).

The pathogenesis of keratoconus remains unclear. It could be due to a combination of intrinsic factors (that destroy collagen) and other environmental extrinsic, through trauma or rubbing. Despite that, an autosomal dominant transmission pattern with incomplete penetrance has been proposed, affecting all races alike, although there is not much available information that clarify the differences in frequency among them (135).

Recent genetic and epidemiological studies mention an increasing prevalence of the disease in the general population and suggest a strong involvement of genetics in the emergence of the disease. Hence, although a multifactorial origin is not questioned, the genetic component plays a fundamental role (136). Even so, although the identification of genetic mutations remains difficult due to the complex nature of this condition, different familial inheritance mutation

USC UNIVERSIDADE DE SANTIAGO

patterns were found. An autosomal dominant (or partially dominant) inheritance pattern was observed in these cases, leading to the discovery of almost twenty different potential genetic loci (136), of which three might show an independent genetic replication process, these being 14q11, 5q32, and 5q21 (137,138).

Likewise, biochemical studies suggest that corneal stroma loss in patients with keratoconus may be explained by two different mechanisms (which are not mutually exclusive), these being: (I) alteration in the degradation of corneal tissue, by excessive degradation of stromal collagen and other cellular and extracellular components, and (II) alteration in the synthesis of the corneal tissue, either by a decrease in the synthesis of stromal collagen and other components or by an altered synthesis (139,140).

Similarly, the reduction of corneal stiffness and thinning due to the different distribution and reduction of the number of lamellae in the corneal stroma are the main biomechanical factors involved in the development of the keratoconus (141). Oxidative damage is also defined as a co-factor in the progression of the disease (142,143), although the mechanism is still unclear.

Keratoconus usually appears as an isolated ecstatic disorder, unrelated to other diseases. However, a multitude of associations with both systemic diseases (Down's, Ehlers-Danlos and Marfan syndromes, atopic dermatitis, osteogenesis imperfecta, and mitral valve prolapse) (142–150) and ophthalmological pathologies (vernal keratoconjunctivitis, blue sclera, aniridia, lens ectopy, congenital Leber amaurosis, and retinitis pigmentosa) (86,129,136) have been found.

3.4.2. Diagnosis

At present, the diagnosis of keratoconus has been found to affect the upper, nasal, and central corneal areas (151), although new forms of the disease have been recently found (152) thanks to the development of new sophisticated surface observation systems.

Different classifications refer to the evolutionary stage of keratoconus (preclinical, incipient, moderate or severe), such as the Buxton’s classification (four scales based on keratometric readings), the Amsler-Krumeich’s classification (according to disease stages), Ferrara's classification (as a modification of the previous one and the most recently published based on clinical and aberrometric findings) (153,154). Likewise, keratoconus can be classified as mild (< 48 D), moderate (48-54 D) or advanced (> 54 D), according to the axis of maximum corneal power in keratometry. Corneal topography and other novel techniques to represent the corneal

USC UNIVERSIDADE DE SANTIAGO DE COMPOSTELA

contour are also very sensitive in disease detection and monitoring, providing earlier and more accurate information about the corneal distortion.

In order to point out, given the importance of early detection of this type of disease, and thanks to advances in optical diagnosis methods, detection and classification systems based on corneal topographic indexes have also been developed, allowing their severity to be graduated (see Table 4).

Symptoms usually appear in the second decade of life, between the ages of 10 and 30. A slow progression between the ages of 20 and 60 is observed, although detention may be prolonged, depending on the disease's progress and taking into account the interindividual variability (155).

In the early stages, no signs may appear, and keratoconus can be diagnosed by a simple corneal topographical examination. The progression of the disease is manifested by a significant loss of vision that cannot be amended. Photophobia, glare, monocular diplopia, eye irritation, impairment of vision in one eye due to progressive near-sightedness and rapidly advancing myopathic astigmatism, with or without acute dropsy and blurred vision, are also early symptoms (86). Characteristically, astigmatism progresses from a symmetrical bow tie pattern, through an asymmetrical appearance, to a pronounced cone with lower temporal displacement.

Table 4. Index-based system for keratoconus diagnosis.

Index	Description	Ref.
K-value	Central keratometry and the difference in power between the lower and upper cornea	(155)
I-S value	Central keratometry and the difference in power between the lower and upper cornea	(155)
Keratoconus Prediction Index (KPI)	Videokeratography quantitative index	(156)
keratoconus Classification Index (KCI)	Videokeratography quantitative index	(156)
Keratoconus Severity Index (KSI)	Detection and severity with an artificial system	(157)

USC UNIVERSIDADE DE SANTIAGO DE COMPOSTELA

Z3	Height data in Zernique polynomials	(158)
KISA	Surveyor's data analysis indexes (K, I-S, corneal toricity, SRAX)	(159)
Keratoconus Severity Score (KSS)	Biomicroscopy, topography, corneal power and the root mean square value of high-order aberrations of the anterior corneal surface	(153)
Cone Location and Magnitude Index (CLMI)	Presence or not of keratoconic patterns, and determination of cone location and magnitude	(160)

As the disease advances from mild to moderate and advanced stages, external pathognomonic signs may be observed, such as the Munson's sign (deformation of the lower eyelid in a downward glance), the Rizzuti's sign (conical reflex in the nasal limb), the Charleux's oil drop sign, and Vogt's striae (vertical stress lines in the deep stroma) among others (86,161).
The clinical diagnosis of moderate or advanced keratoconus is not difficult due to the classic clinical signs described above. However, the early diagnosis of this disease has become critical in recent years for two main reasons: (I) the need to contraindicate the practice of corneal refractive surgery techniques that can accelerate the evolution of keratoconus, and (II) the possibility of using new therapies that can slow or delay its progression.

3.4.3. Treatment

The treatment of keratoconus depends on the stage of the disease progression. In the initial stages, optical treatment is considered the preferred option, being based on two different methods (24): (I) the use of corrective glasses, and (II) the use of contact lenses (162,163). Glasses do not correct irregular corneal astigmatism, so its isolated use is restricted to the most incipient cases. Once they no longer provide an acceptable visual acuity, the use of contact lenses is necessary. Acute episodes and early stages are also co-treated with hypertonic saline solutions (5%) and protective soft lenses or patches in order to correct the irregular astigmatism (24). If thinning is severe, protective glasses may be worn over the contact lenses. Rigid contact lenses may also improve vision in the early stages by correcting irregular higher degrees of astigmatism, providing a regular refractive surface (163).
Surgery is chosen when contact lenses can no longer be effectively used or when peripheral thinning affects surgery. Corneal transplantation, usually by penetrating keratoplasty (PK), and deep anterior lamellar keratoplasty (DAPK), which avoids the risk of endothelial rejection, may

USC UNIVERSIDADE DE SANTIAGO DE COMPOSTELA

be necessary in patients with advanced progressive disease (especially with significant corneal scarring) in order to regularize the corneal curvature to allow optical correction and visual improvement (86,161).

Penetrating keratoplasty (PK) consists of replacing all the corneal tissue with a healthy cadaver donor cornea (164,165). It is performed in a small number of cases (between 10 and 20%) when there is presence of corneal scarring, excessive corneal thinning, increased corneal astigmatism, intolerance to contact lenses or recurrent keratitis, among others (161,166). Results can be altered by residual astigmatism and anisometropia, requiring correction with contact lenses in order to achieve the optimal visual acuity.

On the other hand, deep anterior lamellar keratoplasty (DAPK) is based on the replacement of damaged tissue, while the healthy one remains intact (167). Certainly, the superficial layers of the cornea are removed, while corneal endothelium remains intact, and it is replaced by donor tissue. This transplantation technique is the one of choice at present (168,169).

These incisional and ablative techniques can be combined with additive procedures based on corneal strengthening (170–172). Implantation of intracorneal rings (ICRs) is a relatively save technique that enables to strengthen the cornea by improving its biomechanics and decreasing the astigmatism's asymmetry and cone's convexity, thus refining visual acuity and facilitating contact lenses tolerance in advanced cases (161,173–175).

On the other hand, crosslinking (CXL) also provides additional corneal strengthening by exposing the eye to ultraviolet A (UVA) light after photosensitization with riboflavin drops (vitamin B2). The degree of collagen fibers crosslinking is increased by intrinsic biomechanical properties, thus stabilizing, reducing or reversing the development and progression of the corneal ectasia (176).

OPTIC NEUROPATHIES: THERAPEUTIC ARSENAL IN LHON

1. Introduction

Optic neuropathies are optic-nerve multicausal diseases, characterized by a visual acuity decrease, dyschromatopsia, variable campimetric, and relative afferent pupillary defects, which may be unilateral or bilateral and asymmetric, where optic-disc ophthalmoscopic appearance is variable (edematous, atrophic or normal) (177).

Optic neuropathies produce diverse clinical profiles, both in appearance (sudden or progressive), topography (unilateral or bilateral), and the magnitude of the visual acuity reduction that they cause. This visual decrease can be isolated or associated with other ophthalmological or extraophthalmological symptoms (177).

Mechanisms responsible for the optic nerve's involvement appear to be vascular, inflammatory, toxic, hereditary, and compressive, although they can also be secondary to intracranial hypertension (178). Optic neuropathies diagnosis is usually carried out by assessing two different circumstances (178), these being: 1) the existence of a visible optic disc anomaly in the fundus (oedema, pallor or malformation) and 2) the existence of a visual acuity decrease (VAD), a dyschromatopsia or a visual field abnormality, associated with a relative afferent pupillary deficit, despite the fact that the fundus may be normal.

In the present section, a general description of the most common optic neuropathies is made, focusing on the Leber's Hereditary Optic Neuropathy (LHON), a primary mitochondrial neurodegenerative disease. The development of the current LHON therapeutic arsenal, as well as the research base and regions of unmet clinical need were also examined.

2. Optic neuropathies

2.1. Optic neuritis

Optic neuritis is defined as the optic nerve inflammatory condition in any of its portions as a consequence of a demyelination process (177,179). It predominantly affects young women and has an incidence of 5 cases per 100,000 inhabitants. Clinically, it is characterized by a series of clinical signs (177,179), these being: (I) decreased visual acuity (usually unilateral) in several degrees (mild to severe), with central scotoma due to macular fibers' involvement, (II) decreased visual field, (III) photomotor-reflex loss, and (IV) papillary atrophy, among others.

Its shows a multifactorial etiology, having studied different causes (179), the most common being: (I) cranial trauma, (II) inflammatory processes secondary to infections, (III) nervous-origin processes (sclerosis or syphilis), (IV) toxic exposure or consumption (alcohol or smoking), and (V) vascular or hereditary processes.

USC UNIVERSIDADE DE SANTIAGO DE COMPOSTELA

2.2. Devic's disease

Devic's disease, also called Neuromyelitis Optica (NMO) (180), is a severe bilateral optic neuropathy derived from an immunological disorder, being based on the involvement of the optic nerve and the spinal cord as a consequence of an autoimmune phenomenon.
The potential symptoms of this disease include (177,180): (I) vision loss or blurred vision, (II) spinal demyelinating lesions that longitudinally affect, at least, three spinal segments, (III) weakness and numbness, and (IV) presence of IgG-NMO antibodies in the blood, among others. Currently, there is no cure for this pathology, although there are palliative treatments that help reduce symptoms (180).

2.3. Neurretinitis

Neuroretinitis is a retinal and optic nerve inflammatory disease, which presents a symptomatic profile based on unilateral vision loss, macular star, and optic nerve oedema, associated with peripapillary retinal exudates, usually in young patients, with no sex preponderance (177,181,182). Its etiology is not completely known and can be triggered as a result of an immune or infectious process (181,183), although most cases still have an idiopathic etiology (181). The severity of the disease may also vary, although clinical progression is similar in all cases. Despite all, it tends to resolve spontaneously (181).

2.4. Ischemic optic neuropathy

Ischemic optic neuropathy (ION) affects the intraocular (90%) and retrobulbar (10%) portions of the optic nerve, giving rise to the sudden loss of central vision, lateral vision or both, as a consequence of a blood flow decrease or an optic nerve interruption (177).
Its etiology is not completely known, although the hypothesis of greater relevance points to the obstruction of the posterior short ciliary arteries that irrigate the optic disc, derived from previous pathological processes, such as thrombosis or hypotension in patients with arteriosclerosis disease (184).

USC

2.5. Traumatic optic neuropathy

Traumatic optic neuropathy is defined as an optic nerve lesion that usually appears after a traumatic episode (185,186) due to a craniofacial trauma, and as a consequence of an upper

orbital contusion. In most cases, damage appears in the intracanalicular segment of the optic nerve (177).

2.6. Compressive optic neuropathy

Compressive optic neuropathy (CON) is mainly characterized by a visual acuity decrease and field constriction as a consequence of a muscle-adipose widening that leads to orbital congestion processes, preventing venous drainage (187). However, its etiology is varied (177,184), from tumors in the visual pathway (gliomas, craniopharyngiomas, ...), to orbital lesions that compress the optic nerve (dysthyroid orbitopathy) or even infiltrative lesions (tuberculosis, sarcoidosis, ...), among others. Thus, a treatment delay or the use of inadequate treatments can lead to a permanent lesion of the visual function (187).

2.7. Toxic optic neuropathy

Toxic optic neuropathy (TON), also known as toxic amblyopia, is defined as optic nerve damage caused by toxin's acute or chronic exposure. It usually presents a multifactorial etiology and is characterized by clinical symptomatology based on papillomacular-bundle damage, with central scotoma and reduced color vision (177,188).

2.8. Nutritional optic neuropathy

Nutritional optical neuropathy is caused by nutritional deficiencies that give rise to an optic nerve atrophy as a result of the toxins production in genetically predisposed patients (189,190), triggering an exacerbated oxidative-stress process. Despite being a pathology with a very low frequency of onset, its diagnosis is often hampered for its unspecific clinical symptomatology, that it is shared with other neuropathies, especially hereditary optic or toxic optic neuropathies (191–194). Clinically, it has been shown that certain nutritional elements (fatty acids, ...) are responsible for the optic nerve's atrophy, based on different biochemical mechanisms (195,196). However, it has been inferred that the interruption of these mechanisms could give rise to a significant ROS minimization, leading to a disease's substantial improvement (195).

USC
UNIVERSIDADE
DE SANTIAGO
DE COMPOSTELA

2.9. Hereditary optic neuropathies

Hereditary optic neuropathies are rare pathologies that are inherited with an autosomal recessive pattern, linked to the X chromosome or with a maternal mitochondrial inheritance (177). They cause subacute or chronic visual loss, painless, with central or cecocentral involvement of the visual field, dyschromatopsia, and optic nerve atrophy. They may also be linked to an extrapyramidal system atrophy, peripheral neuropathies, deposit diseases, and other disorders (177).

3. Impact of genetics on hereditary retinal diseases

In recent years, unprecedented progress has been made in the knowledge of the human genetic material in terms of characteristics and organization. One of the most important advances was the human genome complete sequencing, which allowed knowing the three billion nucleotides that make up the cell's genetic material (184). This achievement has generated a great impact in all scientific areas, but particularly in the ophthalmology field, since it has been possible to identify the genetic cause of a large number of ocular diseases, both of monogenetic origin as of complex and multifactorial etiology. One of the fields with greater benefits has been retinal diseases', since it has been able to identify genetic defects that cause dozens of these diseases in humans (184).

Retina requires the coordinated function of hundreds of genes in order to achieve, not only an adequate embryological formation, but also efficient functionality in postnatal life due to its great structural and functional complexity (177). The knowledge about the molecular pathology of retinal diseases has led to a much better understanding of the disease mechanisms and contributed to a better therapeutic development for many retinal genetic diseases. Molecular analysis is increasingly available in specialized centers and this has a huge impact on retinal diseases diagnosis and genetic counselling (177,179).

4. Leber's Hereditary Optic Neuropathy (LHON)

Leber's Hereditary Optic Neuropathy (LHON) is a hereditary mitochondrial neurodegenerative disease, characterized by a degeneration of retinal ganglion cells (RGCs), a type of axon-myelinated neurons situated in the retinal inner surface and a progressive loss of the optic nerve functionality (197). Despite the fact that the first mention of an LHON patient dates back about 150 years, being diagnosed by von Graefe (198), it was primary explained as a clinical

USC DE SANTIAGO DE COMPOSTELA

pathology in 1871 by Theodor Leber, a German ophthalmologist who described a distinctive pattern of visual loss among members of different families. His observations were subsequently confirmed in pedigrees from different populations (199).

The non-mendelian inheritance pattern and the discovery of the first mitochondrial DNA mutation (nucleotide change at position 11778) associated with it (200) were fully explained by Douglas C. Wallace et al. (1988) (201), becoming the first human disease caused by point mutations within the mitochondrial genome (202).

The disease etiology is not completely known, although all clinically described cases show a maternal hereditary pattern (linked to the X chromosome), being based on the presence of certain mitochondrial DNA point mutations. It produces alterations in the amino acids primary structure of several polypeptides located in the complex I of the mitochondrial transport chain. The most common genetic alterations are: 3460GNA (ND1) (203), 11778GNA (ND4) (201) and 14484TNC (ND6) (204), which represent 95% of all cases, with the 11778GNA mutation as the most prevalent in the world (60-80%) (205). Even so, all currently known mutations are found in Table 5. (32)

Table 5. Summary of the most studied LHON mutations.

Mutation		Subunit	Prevalence (%)	Heredity
Common (> 95%)	G3460A	ND1	13	Maternal
	G11778A	ND4	69	Maternal
	T14484C	ND6	14	Maternal
Rare (< 5%)	G3376A	ND1	Unknown	Maternal
	G11696A	ND4	Unknown	Maternal
	T10663C	ND4L	Unknown	Maternal
	C12848T	ND5	Unknown	Maternal
	G13730A	ND5	Unknown	Maternal
	G14459A	ND6	Unknown	Maternal
	C14482G	ND6	Unknown	Maternal

USC UNIVERSIDADE DE SANTIAGO DE COMPOSTELA

	A14495G	ND6	Unknown	Maternal
	C14498T	ND6	Unknown	Maternal
	C14568T	ND6	Unknown	Maternal
	T14596A	ND6	Unknown	Maternal

All these mutations affect genes that encode complex I mitochondrial subunits and, as a result, a deficient transfer of high energy electrons to complex III is observed, being an essential step in mitochondrial oxidative phosphorylation processes (206). Thus, the complex I dysfunction gives rise to a decrease in the ATP synthesis, high levels of oxidative stress and a glutamate damaged transport, being actions that lead to the RGCs dysfunction and, consequently, to their apoptotic death (207). As a result, neuronal transmission from the retina to the brain is affected, causing neuronal-viability alterations (208).

Physiologically, this pathology manifests itself through several unique clinical features (209–211), including: (I) vascular tortuosity, (II) peripapillary swelling of the retinal nerve fiber layer (RNFL), accompanied by an optic disc pseudo-oedema, (III) circumpapillary telangiectatic microangiopathy during the acute phase, with no leakage in fluorescein angiography, and (IV) temporal optic nerve atrophy or diffuse optic atrophy of the papillomacular bundle's small-caliber fibers in the retina center during the chronic phase.

These clinical changes can be observed even before the patient becomes visually symptomatic. Clinically, an acute and progressive unilateral loss of central vision with ocular involvement is observed in a 2-4 month period, becoming bilateral weeks or months after the onset of ocular deterioration (201,212). Other symptoms reported are usually minor and nonspecific, such as headache, eye discomfort, light flashes, paresthesias, or dizziness (199).

It should also be known that LHON has a 1/30.000 estimated prevalence, predominantly affecting young adults (between 15-30 years) in all ethnic groups, with a male preponderance (80%). Even so, it must be borne in mind that not all people in whom one or several mutations have been identified relative to the LHON will develop visual changes. In addition, the disease's evolution speed and severity are variable and dependent on several factors, with age and sex as the most important ones (211).

Likewise, it should be taken into account that there is a strong bias in terms of patient's sex, linked to the vision loss in LHON carriers, known as incomplete penetration. Causes of this

USC DE SANTIAGO DE COMPOSTELA

incomplete penetration are complex and are influenced, in turn, by several genetic, hormonal and environmental factors (213). Apart from this, it must be mentioned the fact that up to 25% of LHON patients may appear spontaneous visual recovery phenomena, often years after the disease onset (214). Nevertheless, this recovery is invariably incomplete. In addition, the probability of spontaneous visual recovery is higher in patients with the 14484TNC mutation, followed by patients with the 3460GNA mutation and, finally, patients with the 11778GNA mutation (211). Visual perception spontaneous retrieval advocates that vision loss is not a straight outcome of the RGCs degeneration in the initial stages, but may have significance in terms of cellular dysfunction, harming the signals transmission between the retina and the brain (215).

In line with this hypothesis, the RGCs selective loss observed as RNFL thinning only occurs in the disease's late atrophic phase, making visual recovery impossible at this point (216,217). Therefore, the period between cellular dysfunction and cell loss can be considered as an opportunity where vision could be restored by the normalizing mitochondrial function (218). Considering the mitochondrial origin of many ocular diseases, mitochondria as a drug target could be an alternative treatment for optic neuropathies, where symptomatic or untreated options remained as the present ones (215,219).

Nowadays, LHON treatment options remain limited (220). Thus, after having ineffectively resorted to the use of coenzyme Q10 (CoQ10, natural and liposoluble quinone analogue, capable of freely circulating within the mitochondrial inner membrane because of its intrinsic hydrophobic properties) for being the respiratory-chain predominant electron carrier and mediating the electron transport from complexes I and II and other flavoprotein-dehydrogenases to complex III, new drugs have been sought in order to develop an attractive dual strategy so as to improve the electron transfer throughout the respiratory chain, maximizing ATP production, while minimizing ROS levels (220,221). Thus, to reduce the biophysical restriction involved in crossing the blood-brain barrier (BBB) in the case of CoQ10, new generation analogues have been developed, increasing the pharmacophore bioavailability and maximizing its therapeutic potential (212,222,223).

USC
UNIVERSIDADE DE SANTIAGO DE COMPOSTELA

5. Therapeutic arsenal in the LHON treatment

5.1. Classical therapy: physical methods

5.1.1. Hyperbaric oxygen

The first existing record of the hyperbaric oxygen therapy (HBOT) dates from 1870, being used to treat a variety of pathological conditions, expanded during the 1940s for multiple health applications (224). The European Committee for Hyperbaric Medicine (ECHM) defines HBOT as a medical treatment modality based on breathing oxygen (100%) under increased pressure (greater than 1 absolute pressure atmosphere) in a therapeutic hyperbaric pressure chamber (225,226). Oxygen high levels in plasma achieved through HBOT are able to satisfy the oxygen demand in hypoxic areas, independently of hemoglobin and oxyhemoglobin blood levels (224). Clinically, benefits are a consequence of the pressure mechanical effects, as well as of the physiological-and-biochemical effects of the hyperoxia and gas physics (224).

Hyperbaric oxygen therapy for the LHON treatment is based on obtaining higher oxygen levels in the RGCs during the acute phase with the aim of improving mitochondrial biogenesis (227). However, toxic effects linked to oxygen supraphysiological levels are a limiting factor in the disease treatment due to the ROS formation, so the benefit/risk ratio should be assessed for each particular case, where damages could be much more important than benefits (227).

5.1.2. Near-Infrared light therapy (NIR)

Infrared light represents a light broad spectrum with wavelengths ranging from 700 to 1000 nm. At their shorter wavelengths (near infrared interval), fusion occurs with the red spectrum of visible light while, at the longer end (far infrared interval), it is combined with the microwave range (228).

Near-infrared light therapy (NIR), also known as photobiomodulation or low-intensity light therapy, was developed as an alternative therapeutic strategy for the treatment of a series of injuries and diseases, after observation of the beneficial effects on astronauts (229).

USC UNIVERSIDADE DE SANTIAGO DE COMPOSTELA

Its therapeutic use lies in the low-density-wavelengths irradiation. In particular, it has been shown to improve mitochondrial function and cell survival in several wound-healing models, neurodegeneration and retinal toxicity induced by methanol (230). It is believed that NIR

increases ATP synthesis by stimulating the cytochrome C oxidase activity (complex IV), although the mechanisms responsible for its action are currently unknown (230).

Clinically, the NIR application to the anomalous RGCs in LHON patients is done by light emitting diodes (LEDs) or low power lasers as the most accepted therapeutic tools, carrying out their application through the optimal wavelengths use (630-1000 nm) and energy densities (4 J/cm^2) necessary for therapeutic intervention (229,231,232). However, the use of this therapy has not been widely developed at the clinical level, due to the lack of: (I) awareness of the irradiation's penetration impact, (II) a standardization method for the results comparison between different trials, and (III) understanding of the action mechanisms, among others (233).

5.2. Classical therapy: pharmacological methods

5.2.1. Mitochondrial cocktail

In recent years, formulations using vitamin combinations (B2, B3, B19, B12, C, and E) and components with antioxidant activity and mitochondrial bioenergetics (α-lipoic acid, carnitine, creatine, L-arginine or dichloroacetate) (227) have been developed to treat patients with mitochondrial diseases, including LHON patients. However, none of them has shown enough efficacy (234–236).

5.2.2. Pharmacological activators of mitochondrial biogenesis

Mitochondrial biogenesis constitutes a cellular process controlled by transcription factors (coactivators and repressors) (237,238), whose identification and study has been the main goal in the development of alternative treatments (239). The modulation of mitochondrial biogenesis is carried out through the manipulation of molecular processes involving active substances such as AMPK-activated kinase (AMPK), sirtuins, cyclic adenosine monophosphate (cAMP) and cyclic guanosine monophosphate (cGMP), as well as later effectors, including the estrogen-related receptors (ERR) and the peroxisome proliferator activated receptor (PPAR) (239).

Recent studies in animal models have shown that the mitochondrial biogenesis stimulation constitutes an alternative strategy for the treatment of pathologies derived from Oxidative Phosphorylation (OXPHOS) linked mitochondrial alterations (240). Specifically, these studies arose from the hypothesis that an increase in the residual activity of the mitochondrial

USC UNIVERSIDADE DE SANTIAGO DE COMPOSTELA

respiratory chain would lead to an increase in cellular ATP synthesis and, consequently, to a rise in energy production (240).

It has also been observed that an increase in mitochondrial biogenesis has a protective effect in LHON patients (241) as a consequence of an optimal regulation promoted by protein pharmacological activators (242,243), such as the PGC-1α transcriptional activator, a central protein controlled by activated peroxisome proliferator receptors (PPARs) or AMPK activated protein (244). Similarly, one of the pharmacological activators with greater potential is bezafibrate, a fibrate with demonstrated efficacy and safety in pathologies with mitochondrial etiology (245), by promoting a delay in the disease advancement by mitochondrial biogenesis stimulation (246).

5.2.3. Steroids and immunosuppressants

In general, the frequency of steroid use as a LHON alternative treatment has been very low, since its utility is dependent on a previous molecular differential diagnosis to exclude the possibility of the existence of an inflammatory optic neuropathy (234). Corticosteroids, such as prednisone or methylprednisolone, have been the most used steroids in the LHON treatment, although it has been confirmed that they do not prevent a possible affectation of the other eye, besides notifying as doubtful the benefits related to the disease progression (227).

Likewise, it has been shown that pre-treatment with immunosuppressants (e.g., cyclosporin A) exerted an antiapoptotic effect and allowed attenuating ROS harmful consequences by blocking the mitochondrial-transition-pore (MTP) permeability, which indicates a conceivable therapeutic pathway for LHON (247). Specifically, cyclosporin A, a cyclic polypeptide endowed with a powerful immunosuppressive action, is capable of inhibiting the cellular immune response as well as lymphocytes and T-dependent antibodies production-and-release, including proinflammatory cytokines. Thus, cyclosporin A would be a possible line of therapeutic action in the LHON treatment (247).

5.2.4. Brimonidine

USC
DE SANTIAGO
DE COMPOSTELA

Brimonidine belongs to a group of drugs called sympathomimetics, being a highly selective α2 agonist commonly used in the treatment of glaucoma due to its ability to reduce intraocular pressure. High concentrations of α2-receptor in the retina and the optic disk regulate several antiapoptotic factors and block the glutamate excitotoxicity induced by mitochondrial oxidative

stress (248). This antiapoptotic effect could provide a retinal protective effect against oxidative damage (227,249). However, studies in LHON patients with unilateral involvement have demonstrated brimonidine ineffectiveness in the LHON prevention and treatment (250). Even so, since high intraocular pressure may be an aggravating factor for visual loss in LHON patients, brimonidine remains as a drug of choice for patients diagnosed with glaucoma or ocular hypertension (227,250,251).

5.2.5. Ubiquinone analogues

Mitochondrial point mutations observed in LHON patients give rise to a complex I dysfunction, which results in an electron-flow destabilization to complex III, leading to an ATP-synthesis reduction and a ROS increase (252). Consequently, a strategy was designed based on the activation of electron flow from complexes I and II to complex III, through the use of ubiquinone analogues (227,236,250).

Coenzyme Q (CoQ), also known as ubiquinone or ubidecarenone, is a mobile transporter that ensures the efficient electron transfer along the mitochondrial respiratory chain (227), from complexes I and II to complex III (227). The use of coenzyme Q10 (CoQ10) in patients with mitochondrial disorders has been reduced as a consequence of the absence of any scientific evidence (234–236). However, its use was based on potential antioxidant and bioenergetic properties, although it was later found its lipophilic nature as the main difficulty in terms of oral administration, since its passage to the mitochondria was limited (227). Nevertheless, last generation short-chain ubiquinone analogues, such as idebenone or EPI-743, have shown an *in vitro* greater potency compared to CoQ10 (253,254).

Idebenone can cross the blood-brain barrier (BBB) and reach the mitochondria. This drug also has the ability to directly transfer electrons to complex III, allowing the correct ATP synthesis, avoiding lipid peroxidation produced as a consequence of the oxidative damage due to its antioxidant properties (255,256).

The α-tocotrienol quinone or EPI-743 is an experimental drug developed as a specific treatment for mitochondrial diseases. In 2012, Sadun et al. published a study on five LHON patients orally treated with EPI-743 three times a day, observing a pathology slowing-down in 80% of cases, even achieving some visual recovery (227,244,254).

USC UNIVERSIDADE DE SANTIAGO DE COMPOSTELA

5.3. Gene therapy

In recent decades, molecular techniques have experimented an extensive development based on genetic modification, all grouped under the field of gene therapy (257). Gene therapy is defined as the expression of a therapeutic gene introduced into a target cell or tissue in order to repair or block a given function or generate a new one, minimizing the patient's symptomatology (257–259). This type of technique is based on the use of gifted vectors with the ability to transfer therapeutic genes. Currently, there are no optimal application methods, observing the appearance of side effects that, in many cases, are not tolerated by the patient (227,260).

Broadly speaking, gene therapy is classified into two large groups (261), these being: (I) the *in vivo* gene therapy, based on the insertion of genetic material directly into the target cell without performing a previous extraction, and (II) the *ex vivo* gene therapy, based on the extraction of the target cells prior to the inoculation of the genetic material to be reintroduced later once they have been modified.

Gene therapy has proved to be very promising in mitochondrial diseases, particularly in LHON, because RCGs layer accessibility. In addition, the eye is a relatively isolated organ, thus minimizing risks of unwanted transfection to other nearby tissues. On the other hand, cells labelled for gene therapy are not going to undergo cell division, so the oncogenesis risk is potentially reduced (260). However, the heterogeneity and the double mitochondrial layer are the main obstacles when optimizing a therapeutic-genes inoculation method (262–264). In recent years, different strategies have been tested based on the new-genome direct introduction, where problems of mitochondrial efficacy-and-toxicity have been observed (265). The current claim is based on a universal vector synthesis containing all promoters in order to ensure the correct expression of any gene that has been modified (265).

5.4. Advanced therapy: stem cells

The appearance of lesions in ocular tissues or cellular degeneration are typical characteristics of blindness-associated neurodegenerative ocular pathologies. Initially, the treatment methodology was based on the prevention of the initial lesions or, failing that, on the increased cell resistance to lesions (cytoprotection) (266). However, in recent decades and thanks to the development of advanced therapies, stem cell therapy has been introduced as one of the therapeutic alternatives in the LHON treatment. Stem cells are undifferentiated cells capable of

dividing indefinitely, keeping intact the differentiation ability. Generally, they are obtained from embryonic tissues and umbilical cord blood, but also from certain differentiated adult tissues (266), which can be modified through the use of genetic engineering.

Stem cells offer great opportunities to repair the nervous system and the eye (267). However, although this type of therapy is promising, problems such as procurement, transplant methodology, differentiation or immune response reduce its potential application in most cases (266). At the ocular level, stem cell therapy has shown to be useful in the treatment of optic nerve-and-retinal degenerative diseases, although its efficacy and safety is dependent on the type of stem cells used (268,269). Even so, several reports have studied this type of in-depth treatment, with promising results and possible application in LHON patients (270–272).

5.5. Preventive therapy: prevention of germline transmission

The oculo-nervous system can be especially affected by defects in the respiratory chain functions due to its high energy demand (273). Currently, the absence of a LHON cure and the lack of effective treatments aimed at reducing symptoms and slowing the disease progression, giving rise to the study of prevention systems for the transmission of genetic defects (274). Even so, prevention of germline transmission in diseases caused by mtDNA mutations is much more complicated due to the fact that the exclusion mechanism of mutated mitochondria is not fully known (275), being influenced by heteroplasmy and random segregation during oogenesis (276). It also must be added the fact that the detection of the mutations is expression-dependent, since a minimum mtDNA mutation threshold is necessary for the pathology to be expressed (277).

Currently, different methods are available to prevent, in most cases, the transmission of mtDNA mutations responsible for certain pathologies, some of which can be mentioned (274) as: (I) use of oocytes from an unaffected individual, (II) amniocentesis, (III) chorionic villi sampling, (IV) preimplantation genetic diagnosis (PGD), (V) cytoplasmic transfer, (VI) germ vesicles transfer, (VII) pronuclear transfer (PNT), and (VIII) chromosomal spindle transfer (ST). However, all of them require very rigorous safety tests, since none of the techniques is risk-free (227).

USC
UNIVERSIDADE DE SANTIAGO DE COMPOSTELA

REFERENCES

1. Jaffe GJ, Ashton P, Pearson PA. Intraocular Drug Delivery. CRC Press; 2006. 385 p.

2. Subrizi A, del Amo EM, Korzhikov-Vlakh V, Tennikova T, Ruponen M, Urtti A. Design principles of ocular drug delivery systems: importance of drug payload, release rate, and material properties. Drug Discov Today. 2019 Aug 1;24(8):1446–57.

3. Morrison PW, Khutoryanskiy VV. Advances in ophthalmic drug delivery. Ther Deliv. 2014 Dec;5(12):1297–315.

4. Kok-Yong S, Lawrence L. Drug Distribution and Drug Elimination [Internet]. Basic Pharmacokinetic Concepts and Some Clinical Applications. IntechOpen; 2015 [cited 2022 Feb 28]. Available from: https://www.intechopen.com/chapters/48275

5. Kaur IP, Kanwar M. Ocular preparations: the formulation approach. Drug Dev Ind Pharm. 2002 May;28(5):473–93.

6. Cholkar K, Patel SP, Vadlapudi AD, Mitra AK. Novel Strategies for Anterior Segment Ocular Drug Delivery. J Ocul Pharmacol Ther. 2013 Mar;29(2):106–23.

7. Varela-Fernández R, Díaz-Tomé V, Luaces-Rodríguez A, Conde-Penedo A, García-Otero X, Luzardo-Álvarez A, et al. Drug Delivery to the Posterior Segment of the Eye: Biopharmaceutic and Pharmacokinetic Considerations. Pharmaceutics. 2020 Mar 16;12(3).

8. Yasukawa T, Tabata Y, Kimura H, Ogura Y. Recent advances in intraocular drug delivery systems. Recent Pat Drug Deliv Formul. 2011 Jan;5(1):1–10.

9. Gote V, Sikder S, Sicotte J, Pal D. Ocular Drug Delivery: Present Innovations and Future Challenges. J Pharmacol Exp Ther. 2019 Sep 1;370(3):602–24.

10. Adler FH, Hart WM. Adler's physiology of the eye: clinical application. St. Louis: Mosby Year Book; 1992.

11. Wybar K. Wolff's Anatomy of the Eye and Orbit. Br J Ophthalmol. 1977 Apr;61(4):302.

12. Van Buskirk EM. The anatomy of the limbus. Eye Lond Engl. 1989;3 (Pt 2):101–8.

13. Martola EL, Baum JL. Central and peripheral corneal thickness. A clinical study. Arch Ophthalmol Chic Ill 1960. 1968 Jan;79(1):28–30.

USC UNIVERSIDADE DE SANTIAGO DE COMPOSTELA

14. Siu A, Herse P. The effect of age on human corneal thickness. Statistical implications of power analysis. Acta Ophthalmol (Copenh). 1993 Feb;71(1):51–6.

15. Dupps WJ, Wilson SE. Biomechanics and Wound Healing in the Cornea. Exp Eye Res. 2006 Oct;83(4):709–20.

16. Roberts CJ, Dupps WJ. Biomechanics of corneal ectasia and biomechanical treatments. J Cataract Refract Surg. 2014 Jun;40(6):991–8.

17. Salomão MQ, Hofling-Lima AL, Gomes Esporcatte LP, Lopes B, Vinciguerra R, Vinciguerra P, et al. The Role of Corneal Biomechanics for the Evaluation of Ectasia Patients. Int J Environ Res Public Health [Internet]. 2020 Mar [cited 2020 Nov 5];17(6). Available from: https://www.ncbi.nlm.nih.gov/pmc/articles/PMC7143615/

18. Müller LJ, Pels E, Vrensen GF. The specific architecture of the anterior stroma accounts for maintenance of corneal curvature. Br J Ophthalmol. 2001 Apr;85(4):437–43.

19. Dawson DG, Grossniklaus HE, McCarey BE, Edelhauser HF. Biomechanical and wound healing characteristics of corneas after excimer laser keratorefractive surgery: is there a difference between advanced surface ablation and sub-Bowman's keratomileusis? J Refract Surg Thorofare NJ 1995. 2008;24(1):S90-96.

20. Randleman JB, Russell B, Ward MA, Thompson KP, Stulting RD. Risk factors and prognosis for corneal ectasia after LASIK. Ophthalmology. 2003 Feb;110(2):267–75.

21. Piñero DP, Nieto JC, Lopez-Miguel A. Characterization of corneal structure in keratoconus. J Cataract Refract Surg. 2012 Dec;38(12):2167–83.

22. Binder PS. Analysis of ectasia after laser in situ keratomileusis: risk factors. J Cataract Refract Surg. 2007 Sep;33(9):1530–8.

23. Espandar L, Meyer J. Keratoconus: Overview and update on treatment. Middle East Afr J Ophthalmol. 2010 Jan 1;17(1):15.

USC
UNIVERSIDADE DE SANTIAGO DE COMPOSTELA

24. Jhanji V, Sharma N, Vajpayee RB. Management of keratoconus: current scenario. Br J Ophthalmol. 2011 Aug;95(8):1044–50.

25. Krachmer JH, Feder RS, Belin MW. Keratoconus and related noninflammatory corneal thinning disorders. Surv Ophthalmol. 1984 Feb;28(4):293–322.

26. Hirano K, Koide M, Mizoguchi Y, Osakabe Y, Sasaki K-A. Unilateral corneal leukoplakia without limbal involvement. Int Med Case Rep J. 2015 May 18;8:103–6.

27. Weiss JS, Møller HU, Aldave AJ, Seitz B, Bredrup C, Kivelä T, et al. IC3D classification of corneal dystrophies--edition 2. Cornea. 2015 Feb;34(2):117–59.

28. Al-Muammar A. Peripheral sterile corneal infiltrate in two brothers after photorefractive keratectomy. Saudi J Ophthalmol. 2011 Jul;25(3):305–8.

29. Bialasiewicz A. Adenoviral Keratoconjunctivitis. Sultan Qaboos Univ Med J. 2007 Apr;7(1):15–23.

30. Shaikh S, Ta C. Evaluation and Management of Herpes Zoster Ophthalmicus. Am Fam Physician. 2002 Nov 1;66(9):1723.

31. Oxford Handbook of Ophthalmology [Internet]. Oxford Handbook of Ophthalmology. Oxford University Press; [cited 2020 Nov 6]. Available from: https://oxfordmedicine.com/view/10.1093/med/9780198804550.001.0001/med-9780198804550

32. Wilson SE, Mohan RR, Hong JW, Lee JS, Choi R, Mohan RR. The wound healing response after laser in situ keratomileusis and photorefractive keratectomy: elusive control of biological variability and effect on custom laser vision correction. Arch Ophthalmol Chic Ill 1960. 2001 Jun;119(6):889–96.

33. Yanoff M, Sassani JW. 8 - Cornea and Sclera. In: Yanoff M, Sassani JW, editors. Ocular Pathology (Eighth Edition) [Internet]. London: Elsevier; 2020. p. 272-356.

34. Barnes SD, Kumar NM, Pavan-Langston D, Azar DT. 114 - Microbial Conjunctivitis. In: Bennett JE, Dolin R, Blaser MJ, editors. Mandell, Douglas, and Bennett's Principles and Practice of Infectious Diseases (Eighth Edition) [Internet]. Philadelphia: W.B. Saunders; 2015. p. 1392-1401.

USC UNIVERSIDADE DE SANTIAGO DE COMPOSTELA

35. Markoulli M, Papas E, Cole N, Holden B. Corneal erosions in contact lens wear. Contact Lens Anterior Eye J Br Contact Lens Assoc. 2012 Feb;35(1):2–8.

36. Bhattacharya P, Mahadevan R. Case Report: Post-keratoplasty Filamentary Keratitis Managed with Scleral Lens. Optom Vis Sci Off Publ Am Acad Optom. 2018;95(8):682–6.

37. Dawson DG, Randleman JB, Grossniklaus HE, O'Brien TP, Dubovy SR, Schmack I, et al. Corneal ectasia after excimer laser keratorefractive surgery: histopathology, ultrastructure, and pathophysiology. Ophthalmology. 2008 Dec;115(12):2181-2191.e1.

38. Wellish KL, Glasgow BJ, Beltran F, Maloney RK. Corneal ectasia as a complication of repeated keratotomy surgery. J Refract Corneal Surg. 1994 Jun;10(3):360–4.

39. Xie W, Xu Y, Yao Y-F. Case Report: Acute Hydrops with Descemet Membrane Schisis in Corneal Ectasia after Radial Keratotomy. Optom Vis Sci Off Publ Am Acad Optom. 2018;95(1):76–81.

40. Urrego-Díaz JA, Frías-Ordoñez JS, Figueroa-Echandía G, Durán-Silva G. Acute corneal edema without epithelium compromise. A case report and literature review. Rev Fac Med. 2017 Sep;65(3):513–9.

41. Franzo BBFrcseFrco. Kanski. Oftalmología Clínica Y Expertconsult - 8ª Edición: Un enfoque sistemático ... Un enfoque sistemático. Amsterdam; Barcelona, etc.; 2016. 928 p.

42. Alipour F, Khaheshi S, Soleimanzadeh M, Heidarzadeh S, Heydarzadeh S. Contact Lens-related Complications: A Review. J Ophthalmic Vis Res. 2017;12(2):193–204.

43. Szczotka-Flynn L, Lass JH, Sethi A, Debanne S, Benetz BA, Albright M, et al. Risk Factors for Corneal Infiltrative Events during Continuous Wear of Silicone Hydrogel Contact Lenses. Invest Ophthalmol Vis Sci. 2010 Nov;51(11):5421–30.

44. Ladas JG, Mondino BJ. Systemic disorders associated with peripheral corneal ulceration. Curr Opin Ophthalmol. 2000 Dec;11(6):468–71.

USC UNIVERSIDADE DE SANTIAGO DE COMPOSTELA

45. Maung N, Thant CC, Srinivasan M, Upadhyay MP, Priyadarsini B, Mahalakshmi R, et al. Corneal ulceration in South East Asia. II: A strategy for the prevention of fungal keratitis at the village level in Burma. Br J Ophthalmol. 2006 Aug;90(8):968–70.

46. Green K. Free radicals and aging of anterior segment tissues of the eye: a hypothesis. Ophthalmic Res. 1995;27 Suppl 1:143–9.

47. Crouch R, Ling Z, Hayden BJ. Corneal Oxygen Scavenging Systems: Lysis of Corneal Epithelial Cells by Superoxide Anions. In: Simic MG, Taylor KA, Ward JF, von Sonntag C, editors. Oxygen Radicals in Biology and Medicine [Internet]. Boston, MA: Springer US; 1988 [cited 2020 Nov 6]. p. 1043–6. (Basic Life Sciences). Available from: https://doi.org/10.1007/978-1-4684-5568-7_172

48. Turaka K, Rapuano CJ, Eagle RC, Abazari A, Hammersmith KM. Macrostriae and Descemet's membrane folds in the Descemet's stripping endothelial keratoplasty graft. Oman J Ophthalmol. 2011 Jan 5;4(2):90.

49. Narang P, Agarwal A, Kumar DA. Predescemetocele: A distinct clinical entity. Indian J Ophthalmol. 2017 Jan 11;65(11):1224.

50. Sultana N, Chaurasia S, Ramappa M. High-resolution optical coherence tomography in a case of descemetocele managed with amniotic membrane transplantation. Indian J Ophthalmol. 2018 Jan 2;66(2):315.

51. Roshandel D, Eslani M, Baradaran-Rafii A, Cheung AY, Kurji K, Jabbehdari S, et al. Current and Upcoming Therapies for Corneal Neovascularization. Ocul Surf. 2018 Oct;16(4):398–414.

52. Feizi S, Azari AA, Safapour S. Therapeutic approaches for corneal neovascularization. Eye Vis. 2017 Dec;4(1):28.

53. Crispin S. Ocular lipid deposition and hyperlipoproteinaemia. Prog Retin Eye Res. 2002 Mar;21(2):169–224.

USC

54. Chu H-S, Hu F-R, Yang C-M, Yeh P-T, Chen Y-M, Hou Y-C, et al. Subconjunctival injection of bevacizumab in the treatment of corneal neovascularization associated with lipid deposition. Cornea. 2011 Jan;30(1):60–6.

55. Chu HS, Chen TC, Hu FR, Chen WL. Recurrence of corneal neovascularization associated with lipid deposition after subconjunctival injection of bevacizumab. Cornea. 2013 Nov 1;32(11):1446–53.

56. Hall MN, Moshirfar M, Amin-Javaheri A, Ouano DP, Ronquillo Y, Hoopes PC. Lipid Keratopathy: A Review of Pathophysiology, Differential Diagnosis, and Management. Ophthalmol Ther [Internet]. 2020 Oct 15 [cited 2020 Nov 6]; Available from: https://doi.org/10.1007/s40123-020-00309-y

57. Seiler T, Quurke AW. Iatrogenic keratectasia after LASIK in a case of forme fruste keratoconus. J Cataract Refract Surg. 1998 Jul;24(7):1007–9.

58. Randleman JB, Woodward M, Lynn MJ, Stulting RD. Risk assessment for ectasia after corneal refractive surgery. Ophthalmology. 2008 Jan;115(1):37–50.

59. Efron N. Chapter 28 - Endothelial blebs. In: Efron N, editor. Contact Lens Complications (Third Edition) [Internet]. London: W.B. Saunders; 2012 [cited 2020 Nov 6]. p. 278–84. Available from: http://www.sciencedirect.com/science/article/pii/B9780702042690000286

60. Twa MD, Nichols JJ, Joslin CE, Kollbaum PS, Edrington TB, Bullimore MA, et al. Characteristics of corneal ectasia after LASIK for myopia. Cornea. 2004 Jul;23(5):447–57.

61. Meghpara B, Nakamura H, Macsai M, Sugar J, Hidayat A, Yue BYJT, et al. Keratectasia After Laser In Situ Keratomileusis. Arch Ophthalmol. 2008 Dec;126(12):1655–63.

62. Rao SN, Epstein RJ. Early onset ectasia following laser in situ keratomileusus: case report and literature review. J Refract Surg Thorofare NJ 1995. 2002 Apr;18(2):177–84.

63. Lifshitz T, Levy J, Klemperer I, Levinger S. Late bilateral keratectasia after LASIK in a low myopic patient. J Refract Surg Thorofare NJ 1995. 2005 Oct;21(5):494–6.

USC UNIVERSIDAD DE CANTABRIA

64. Spadea L, Cantera E, Cortes M, Conocchia NE, Stewart CW. Corneal ectasia after myopic laser in situ keratomileusis: a long-term study. Clin Ophthalmol Auckl NZ. 2012;6:1801–13.

65. Roberts CJ, Dupps WJ. Biomechanics of corneal ectasia and biomechanical treatments. J Cataract Refract Surg. 2014 Jun;40(6):991–8.

66. Randleman JB. Post-laser in-situ keratomileusis ectasia: current understanding and future directions. Curr Opin Ophthalmol. 2006 Aug;17(4):406–12.

67. Guirao A. Theoretical elastic response of the cornea to refractive surgery: risk factors for keratectasia. J Refract Surg Thorofare NJ 1995. 2005 Apr;21(2):176–85.

68. Klein SR, Epstein RJ, Randleman JB, Stulting RD. Corneal ectasia after laser in situ keratomileusis in patients without apparent preoperative risk factors. Cornea. 2006 May;25(4):388–403.

69. Rabinowitz YS. Ectasia after laser in situ keratomileusis. Curr Opin Ophthalmol. 2006 Oct;17(5):421–6.

70. Tatar MG, Aylin Kantarci F, Yildirim A, Uslu H, Colak HN, Goker H, et al. Risk Factors in Post-LASIK Corneal Ectasia. J Ophthalmol. 2014;2014:204191.

71. Said A, Hamade IH, Tabbara KF. Late onset corneal ectasia after LASIK surgery. Saudi J Ophthalmol. 2011 Jul;25(3):225–30.

72. Wolle MA, Randleman JB, Woodward MA. Complications of Refractive Surgery: Ectasia after Refractive Surgery. Int Ophthalmol Clin. 2016;56(2):129–41.

73. Randleman JB. Ectasia After Corneal Refractive Surgery: Nothing to SMILE About. J Refract Surg. 2016 Jul 13;32(7):434–5.

74. Kymionis GD, Portaliou DM, Diakonis VF, Kounis GA, Panagopoulou SI, Grentzelos MA. Corneal collagen cross-linking with riboflavin and ultraviolet-A irradiation in patients with thin corneas. Am J Ophthalmol. 2012 Jan;153(1):24–8.

75. Greenstein SA, Fry KL, Hersh PS. Corneal topography indices after corneal collagen crosslinking for keratoconus and corneal ectasia: one-year results. J Cataract Refract Surg. 2011 Jul;37(7):1282–90.

76. Hersh PS, Greenstein SA, Fry KL. Corneal collagen crosslinking for keratoconus and corneal ectasia: One-year results. J Cataract Refract Surg. 2011 Jan;37(1):149–60.

77. Richoz O, Mavrakanas N, Pajic B, Hafezi F. Corneal collagen cross-linking for ectasia after LASIK and photorefractive keratectomy: long-term results. Ophthalmology. 2013 Jul;120(7):1354–9.

78. Salgado JP, Khoramnia R, Lohmann CP, Winkler von Mohrenfels C. Corneal collagen crosslinking in post-LASIK keratectasia. Br J Ophthalmol. 2011 Apr;95(4):493–7.

79. Yildirim A, Cakir H, Kara N, Uslu H, Gurler B, Ozgurhan EB, et al. Corneal collagen crosslinking for ectasia after laser in situ keratomileusis: long-term results. J Cataract Refract Surg. 2014 Oct;40(10):1591–6.

80. Viswanathan D, Males J. Prospective longitudinal study of corneal collagen cross-linking in progressive keratoconus. Clin Experiment Ophthalmol. 2013 Aug;41(6):531–6.

81. Gaster RN, Canedo ALC, Rabinowitz YS. Corneal Collagen Cross-Linking for Keratoconus and Post-LASIK Ectasia. Int Ophthalmol Clin. 2013;53(1):79–90.

82. Yam JCS, Cheng ACK. Prognostic factors for visual outcomes after crosslinking for keratoconus and post-LASIK ectasia. Eur J Ophthalmol. 2013 Dec;23(6):799–806.

83. Krachmer JH. Pellucid marginal corneal degeneration. Arch Ophthalmol Chic Ill 1960. 1978 Jul;96(7):1217–21.

84. Sridhar MS, Mahesh S, Bansal AK, Nutheti R, Rao GN. Pellucid marginal corneal degeneration. Ophthalmology. 2004 Jun;111(6):1102–7.

USC UNIVERSIDADE DE SANTIAGO DE COMPOSTELA

85. García-Feijóo J. Manual de oftalmología. Barcelona; 2012. 376 p.

86. Rabinowitz YS. Keratoconus. Surv Ophthalmol. 1998 Feb;42(4):297–319.

87. Robin JB, Schanzlin DJ, Verity SM, Barron BA, Arffa RC, Suarez E, et al. Peripheral corneal disorders. Surv Ophthalmol. 1986 Aug;31(1):1–36.

88. Parker DL, McDonnell PJ, Barraquer J, Green WR. Pellucid marginal corneal degeneration. Cornea. 1986 Jan 1;5(2):115–23.

89. Kompella VB, Aasuri MK, Rao GN. Management of pellucid marginal corneal degeneration with rigid gas permeable contact lenses. CLAO J Off Publ Contact Lens Assoc Ophthalmol Inc. 2002 Jul;28(3):140–5.

90. Tzelikis PF, Cohen EJ, Rapuano CJ, Hammersmith KM, Laibson PR. Management of pellucid marginal corneal degeneration. Cornea. 2005 Jul;24(5):555–60.

91. Sii F, Lee GA, Sanfilippo P, Stephensen DC. Pellucid marginal degeneration and scleroderma. Clin Exp Optom. 2004 May;87(3):180–4.

92. Krachmer JH. Pellucid Marginal Corneal Degeneration. Arch Ophthalmol. 1978 Jul 1;96(7):1217–21.

93. François J, Hanssens M, Stockmans L. [Pellucid marginal degeneration of the cornea]. Ophthalmol J Int Ophtalmol Int J Ophthalmol Z Augenheilkd. 1968;155(5):337–56.

94. Jain V, Nair AG, Jain-Mhatre K, Shome D. Pellucid marginal corneal disease in a case of atopic keratoconjunctivitis. Ocul Immunol Inflamm. 2010 Jun;18(3):187–9.

95. Sahu J, Raizada K. Pellucid Marginal Corneal Degeneration. In: StatPearls [Internet]. Treasure Island (FL): StatPearls Publishing; 2020 [cited 2020 Nov 6]. Available from: http://www.ncbi.nlm.nih.gov/books/NBK562314/

96. Maguire LJ, Klyce SD, McDonald MB, Kaufman HE. Corneal Topography of Pellucid Marginal Degeneration. Ophthalmology. 1987 May 1;94(5):519–24.

97. Guyer DR, Barraquer J, McDonnell PJ, Green WR. Terrien's marginal degeneration: Clinicopathologic case reports. Graefes Arch Clin Exp Ophthalmol. 1987 Feb 1;225(1):19–27.

98. Schlaeppi V. The marginal inferior pelvic cortex dystrophy. Bibl Ophthalmol Suppl Ad Ophthalmol. 1957;12(47):672–7.

99. Liu J, Leach NE, Bergmanson JPG. Reverse-geometry gas-permeable lens design for pellucid marginal degeneration. Eye Contact Lens. 2005 May;31(3):127–9.

100. Gruenauer-Kloevekorn C, Fischer U, Kloevekorn-Norgall K, Duncker GIW. Pellucid marginal corneal degeneration: evaluation of the corneal surface and contact lens fitting. Br J Ophthalmol. 2006 Mar;90(3):318–23.

101. Rathi VM, Dumpati S, Mandathara PS, Taneja MM, Sangwan VS. Scleral contact lenses in the management of pellucid marginal degeneration. Contact Lens Anterior Eye. 2016 Jun 1;39(3):217–20.

102. Dominguez CE, Shah A, Weissman BA. Bitoric gas-permeable contact lens application in pellucid marginal corneal degeneration. Eye Contact Lens. 2005 Sep;31(5):241–3.

103. Rasheed K, Rabinowitz YS. Surgical treatment of advanced pellucid marginal degeneration. Ophthalmology. 2000 Oct;107(10):1836–40.

104. Cheng C-L, Theng JTS, Tan DTH. Compressive C-shaped lamellar keratoplasty: a surgical alternative for the management of severe astigmatism from peripheral corneal degeneration. Ophthalmology. 2005 Mar;112(3):425–30.

105. Cameron JA. Results of lamellar crescentic resection for pellucid marginal corneal degeneration. Am J Ophthalmol. 1992 Mar 15;113(3):296–302.

106. Fronterrè A, Portesani GP. Epikeratoplasty for pellucid marginal corneal degeneration. Cornea. 1991 Sep;10(5):450–3.

107. Kymionis GD, Aslanides IM, Siganos CS, Pallikaris IG. Intacs for early pellucid marginal degeneration. J Cataract Refract Surg. 2004 Jan;30(1):230–3.

108. Mularoni A, Torreggiani A, di Biase A, Laffi GL, Tassinari G. Conservative treatment of early and moderate pellucid marginal degeneration: a new refractive approach with intracorneal rings. Ophthalmology. 2005 Apr;112(4):660–6.

USC UNIVERSIDADE DE SANTIAGO DE COMPOSTELA

109. Akaishi L, Tzelikis PF, Raber IM. Ferrara intracorneal ring implantation and cataract surgery for the correction of pellucid marginal corneal degeneration. J Cataract Refract Surg. 2004 Nov;30(11):2427–30.

110. Wallang BS, Das S. Keratoglobus. Eye. 2013 Sep;27(9):1004–12.

111. Jacobs DS, Green WR, Maumenee AE. Acquired keratoglobus. Am J Ophthalmol. 1974 Mar;77(3):393–9.

112. Jones DH, Kirkness CM. A new surgical technique for keratoglobus-tectonic lamellar keratoplasty followed by secondary penetrating keratoplasty. Cornea. 2001 Nov;20(8):885–7.

113. Biglan AW, Brown SI, Johnson BL. Keratoglobus and blue sclera. Am J Ophthalmol. 1977 Feb;83(2):225–33.

114. Gupta VP, Jain RK, Angra SK. Acute hydrops in keratoglobus with vernal keratoconjunctivitis. Indian J Ophthalmol. 1985 Apr;33(2):121–3.

115. Royce PM, Steinmann B, Vogel A, Steinhorst U, Kohlschuetter A. Brittle cornea syndrome: An heritable connective tissue disorder distinct from Ehlers-Danlos syndrome type VI and fragilitas oculi, with spontaneous perforations of the eye, blue sclerae, red hair, and normal collagen lysyl hydroxylation. Eur J Pediatr. 1990 Apr 1;149(7):465–9.

116. Pouliquen Y, Dhermy P, Espinasse MA, Savoldelli M. [Keratoglobus]. J Fr Ophtalmol. 1985;8(1):43–54.

117. Cameron JA. Corneal abnormalities in Ehlers-Danlos syndrome type VI. Cornea. 1993 Jan;12(1):54–9.

118. Ozkurt Y, Atakan M, Gencaga T, Akkaya S. Contact Lens Visual Rehabilitation in Keratoconus and Corneal Keratoplasty. J Ophthalmol [Internet]. 2012 [cited 2020 Nov 6];2012. Available from: https://www.ncbi.nlm.nih.gov/pmc/articles/PMC3265106/

USC UNIVERSIDADE DE SANTIAGO DE COMPOSTELA

119. O'donnell C, Welham L, Doyle S. Contact lens management of keratectasia after laser in situ keratomileusis for myopia. Eye Contact Lens. 2004 Jul;30(3):144–6.

120. Bromley JG, Randleman JB. Treatment strategies for corneal ectasia. Curr Opin Ophthalmol. 2010 Jul;21(4):255–8.

121. Jacobs DS. Update on scleral lenses. Curr Opin Ophthalmol. 2008 Jul;19(4):298–301.

122. Foss AJ, Trodd TC, Dart JK. Current indications for scleral contact lenses. CLAO J Off Publ Contact Lens Assoc Ophthalmol Inc. 1994 Apr;20(2):115–8.

123. Pullum KW, Buckley RJ. A study of 530 patients referred for rigid gas permeable scleral contact lens assessment. Cornea. 1997 Nov;16(6):612–22.

124. Cameron JA. Keratoglobus. Cornea. 1993 Mar;12(2):124–30.

125. Grewal S, Laibson PR, Cohen EJ, Rapuano CJ. Acute hydrops in the corneal ectasias: associated factors and outcomes. Trans Am Ophthalmol Soc. 1999;97:187–203.

126. Mohamed Hussin H, Biswas S, Majid M, Haynes R, Tole D. A novel technique to treat traumatic corneal perforation in a case of presumed brittle cornea syndrome. Br J Ophthalmol. 2007 Mar;91(3):399.

127. Burk RO, Joussen AM. Corneoscleroplasty with maintenance of the angle in two cases of extensive corneoscleral disease. Eye Lond Engl. 2000 Apr;14 (Pt 2):196–200.

128. Javadi MA, Kanavi MR, Ahmadi M, Yazdani S. Outcomes of epikeratoplasty for advanced keratoglobus. Cornea. 2007 Feb;26(2):154–7.

129. Li X, Yang H, Rabinowitz YS. Longitudinal study of keratoconus progression. Exp Eye Res. 2007 Oct;85(4):502–7.

130. Kennedy RH, Bourne WM, Dyer JA. A 48-year clinical and epidemiologic study of keratoconus. Am J Ophthalmol. 1986 Mar 15;101(3):267–73.

131. Wang Y, Rabinowitz YS, Rotter JI, Yang H. Genetic epidemiological study of keratoconus: evidence for major gene determination. Am J Med Genet. 2000 Aug 28;93(5):403–9.

USC DE SANTIAGO DE COMPOSTELA

132. Zadnik K, Steger-May K, Fink BA, Joslin CE, Nichols JJ, Rosenstiel CE, et al. Between-eye asymmetry in keratoconus. Cornea. 2002 Oct;21(7):671–9.

133. Cristina Kenney M, Brown DJ. The cascade hypothesis of keratoconus. Contact Lens Anterior Eye J Br Contact Lens Assoc. 2003 Sep;26(3):139–46.

134. Wagner H, Barr JT, Zadnik K. Collaborative Longitudinal Evaluation of Keratoconus (CLEK) Study: methods and findings to date. Contact Lens Anterior Eye J Br Contact Lens Assoc. 2007 Sep;30(4):223–32.

135. Pearson AR, Soneji B, Sarvananthan N, Sandford-Smith JH. Does ethnic origin influence the incidence or severity of keratoconus? Eye Lond Engl. 2000 Aug;14 (Pt 4):625–8.

136. Edwards M, McGhee CN, Dean S. The genetics of keratoconus. Clin Experiment Ophthalmol. 2001 Dec;29(6):345–51.

137. Bisceglia L, De Bonis P, Pizzicoli C, Fischetti L, Laborante A, Di Perna M, et al. Linkage analysis in keratoconus: replication of locus 5q21.2 and identification of other suggestive Loci. Invest Ophthalmol Vis Sci. 2009 Mar;50(3):1081–6.

138. Li X, Rabinowitz YS, Tang YG, Picornell Y, Taylor KD, Hu M, et al. Two-stage genome-wide linkage scan in keratoconus sib pair families. Invest Ophthalmol Vis Sci. 2006 Sep;47(9):3791–5.

139. Määttä M, Väisänen T, Väisänen M-R, Pihlajaniemi T, Tervo T. Altered expression of type XIII collagen in keratoconus and scarred human cornea: Increased expression in scarred cornea is associated with myofibroblast transformation. Cornea. 2006 May;25(4):448–53.

140. Määttä M, Heljasvaara R, Sormunen R, Pihlajaniemi T, Autio-Harmainen H, Tervo T. Differential expression of collagen types XVIII/endostatin and XV in normal, keratoconus, and scarred human corneas. Cornea. 2006 Apr;25(3):341–9.

141. Klintworth GK, Damms T. Corneal dystrophies and keratoconus. Curr Opin Ophthalmol. 1995 Aug;6(4):44–56.

USC UNIVERSIDADE DE SANTIAGO DE COMPOSTELA

142. Behndig A, Karlsson K, Johansson BO, Brännström T, Marklund SL. Superoxide dismutase isoenzymes in the normal and diseased human cornea. Invest Ophthalmol Vis Sci. 2001 Sep;42(10):2293–6.

143. Buddi R, Lin B, Atilano SR, Zorapapel NC, Kenney MC, Brown DJ. Evidence of oxidative stress in human corneal diseases. J Histochem Cytochem Off J Histochem Soc. 2002 Mar;50(3):341–51.

144. Lichter H, Loya N, Sagie A, Cohen N, Muzmacher L, Yassur Y, et al. Keratoconus and mitral valve prolapse. Am J Ophthalmol. 2000 May;129(5):667–8.

145. Sharif KW, Casey TA, Coltart J. Prevalence of mitral valve prolapse in keratoconus patients. J R Soc Med. 1992 Aug;85(8):446–8.

146. Street DA, Vinokur ET, Waring GO, Pollak SJ, Clements SD, Perkins JV. Lack of association between keratoconus, mitral valve prolapse, and joint hypermobility. Ophthalmology. 1991 Feb;98(2):170–6.

147. Beckh U, Schönherr U, Naumann GO. [Autosomal dominant keratoconus as the chief ocular symptom in Lobstein osteogenesis imperfecta tarda]. Klin Monatsbl Augenheilkd. 1995 Apr;206(4):268–72.

148. Maumenee IH. The eye in the Marfan syndrome. Trans Am Ophthalmol Soc. 1981;79:684–733.

149. Stoiber J, Muss WH, Ruckhofer J, Thaller-Antlanger H, Alzner E, Grabner G. Recurrent keratoconus in a patient with Leber congenital amaurosis. Cornea. 2000 May;19(3):395–8.

150. Dharmaraj S, Leroy BP, Sohocki MM, Koenekoop RK, Perrault I, Anwar K, et al. The phenotype of Leber congenital amaurosis in patients with AIPL1 mutations. Arch Ophthalmol Chic Ill 1960. 2004 Jul;122(7):1029–37.

151. McMahon TT, Robin JB, Scarpulla KM, Putz JL. The spectrum of topography found in keratoconus. CLAO J Off Publ Contact Lens Assoc Ophthalmol Inc. 1991 Jul;17(3):198–204.

USC UNIVERSIDADE DE SANTIAGO DE COMPOSTELA

152. Abad JC, Rubinfeld RS, Del Valle M, Belin MW, Kurstin JM. Vertical D: a novel topographic pattern in some keratoconus suspects. Ophthalmology. 2007 May;114(5):1020–6.

153. McMahon T, Szczotka-Flynn L, Barr J, Anderson R, Slaughter M, Lass J, et al. A New Method for Grading the Severity of Keratoconus: The Keratoconus Severity Score (KSS). Cornea. 2006;

154. Amsler M. [The “forme fruste” of keratoconus]. Wien Klin Wochenschr. 1961 Dec 8;73:842–3.

155. Rabinowitz YS, McDonnell PJ. Computer-assisted corneal topography in keratoconus. Refract Corneal Surg. 1989 Dec;5(6):400–8.

156. Maeda N, Klyce SD, Smolek MK, Thompson HW. Automated keratoconus screening with corneal topography analysis. Invest Ophthalmol Vis Sci. 1994 May;35(6):2749–57.

157. Maeda N, Klyce SD, Smolek MK. Neural network classification of corneal topography. Preliminary demonstration. Invest Ophthalmol Vis Sci. 1995 Jun;36(7):1327–35.

158. Schwiegerling J, Greivenkamp JE. Keratoconus detection based on videokeratoscopic height data. Optom Vis Sci Off Publ Am Acad Optom. 1996 Dec;73(12):721–8.

159. Rabinowitz YS, Rasheed K. KISA% index: a quantitative videokeratography algorithm embodying minimal topographic criteria for diagnosing keratoconus. J Cataract Refract Surg. 1999 Oct;25(10):1327–35.

160. Mahmoud AM, Roberts CJ, Lembach RG, Twa MD, Herderick EE, McMahon TT, et al. CLMI: the cone location and magnitude index. Cornea. 2008 May;27(4):480–7.

161. Romero-Jiménez M, Santodomingo-Rubido J, Wolffsohn JS. Keratoconus: a review. Contact Lens Anterior Eye J Br Contact Lens Assoc. 2010 Aug;33(4):157–66; quiz 205.

162. Szczotka LB, Barr JT, Zadnik K. A summary of the findings from the Collaborative Longitudinal Evaluation of Keratoconus (CLEK) Study. CLEK Study Group. Optom St Louis Mo. 2001 Sep;72(9):574–84.

USC UNIVERSIDADE

163. Edrington TB, Szczotka LB, Barr JT, Achtenberg JF, Burger DS, Janoff AM, et al. Rigid contact lens fitting relationships in keratoconus. Collaborative Longitudinal Evaluation of Keratoconus (CLEK) Study Group. Optom Vis Sci Off Publ Am Acad Optom. 1999 Oct;76(10):692–9.

164. Colin J, Velou S. Current surgical options for keratoconus. J Cataract Refract Surg. 2003 Feb;29(2):379–86.

165. Gordon MO, Steger-May K, Szczotka-Flynn L, Riley C, Joslin CE, Weissman BA, et al. Baseline factors predictive of incident penetrating keratoplasty in keratoconus. Am J Ophthalmol. 2006 Dec;142(6):923–30.

166. Tuft SJ, Moodaley LC, Gregory WM, Davison CR, Buckley RJ. Prognostic factors for the progression of keratoconus. Ophthalmology. 1994 Mar;101(3):439–47.

167. Jang JH, Chang SD. Tectonic Deep Anterior Lamellar Keratoplasty in Impending Corneal Perforation Using Cryopreserved Cornea. Korean J Ophthalmol KJO. 2011 Apr;25(2):132–5.

168. Watson SL, Ramsay A, Dart JKG, Bunce C, Craig E. Comparison of deep lamellar keratoplasty and penetrating keratoplasty in patients with keratoconus. Ophthalmology. 2004 Sep;111(9):1676–82.

169. Vabres B, Bosnjakowski M, Bekri L, Weber M, Pechereau A. [Deep lamellar keratoplasty versus penetrating keratoplasty for keratoconus]. J Fr Ophtalmol. 2006 Apr;29(4):361–71.

170. Poulsen DM, Kang JJ. Recent advances in the treatment of corneal ectasia with intrastromal corneal ring segments. Curr Opin Ophthalmol. 2015 Jul;26(4):273–7.

171. Garcia-Ferrer FJ, Akpek EK, Amescua G, Farid M, Lin A, Rhee MK, et al. Corneal Ectasia Preferred Practice Pattern®. Ophthalmology. 2019;126(1):P170–215.

172. Imbornoni LM, McGhee CNJ, Belin MW. Evolution of Keratoconus: From Diagnosis to Therapeutics. Klin Monatsbl Augenheilkd. 2018 Jun;235(6):680–8.

USC UNIVERSIDADE DE SANTIAGO DE COMPOSTELA

173. Zare MA, Hashemi H, Salari MR. Intracorneal ring segment implantation for the management of keratoconus: safety and efficacy. J Cataract Refract Surg. 2007 Nov;33(11):1886–91.

174. Shabayek MH, Alió JL. Intrastromal corneal ring segment implantation by femtosecond laser for keratoconus correction. Ophthalmology. 2007 Sep;114(9):1643–52.

175. Sansanayudh W, Bahar I, Kumar NL, Shehadeh-Mashour R, Ritenour R, Singal N, et al. Intrastromal corneal ring segment SK implantation for moderate to severe keratoconus. J Cataract Refract Surg. 2010 Jan;36(1):110–3.

176. Wollensak G, Spoerl E, Seiler T. Riboflavin/ultraviolet-a-induced collagen crosslinking for the treatment of keratoconus. Am J Ophthalmol. 2003 May;135(5):620–7.

177. Rojas Juárez S, Saucedo Castillo A. Oftalmología. Mexico: Editorial El Manual Moderno; 2014.

178. Bidot S, Vignal-Clermont C. Neuropatías ópticas. EMC - Tratado Med. 2013 Mar;17(1):1–6.

179. Busquet L, Gabarel B. Osteopatía y oftalmología. Badalona, Barcelona: Paidotribo; 2008.

180. Rose-John S, Gold R. Devic disease: Translational medicine at work. Neurology. 2014 Apr 15;82(15):1294–5.

181. Valverde-Gubianas M, Ramos-López JF, López-Torres JA, Toribio-García M, Milla-Peñalver C, Gálvez Torres-Puchol J, et al. Neurorretinitis: Casos clínicos. Arch Soc Esp Oftalmol [Internet]. 2009 Aug [cited 2018 Dec 4];84(8). Available from: http://scielo.isciii.es/scielo.php?script=sci_arttext&pid=S0365-66912009000800004&lng=en&nrm=iso&tlng=en

182. Ray S, Gragoudas E. Neuroretinitis. Int Ophthalmol Clin. 2001;41(1):83–102.

183. Suhler EB, Lauer AK, Rosenbaum JT. Prevalence of serologic evidence of cat scratch disease in patients with neuroretinitis. Ophthalmology. 2000 May;107(5):871–6.

USC UNIVERSIDADE DE SANTIAGO DE COMPOSTELA

184. Rojas Juárez S, Saucedo Castillo A. Retina y vitreo [Internet]. 2012 [cited 2018 Nov 16]. Available from: http://site.ebrary.com/lib/interpuertoricosp/Doc?id=10804335

185. Kumaran AM, Sundar G, Chye LT. Traumatic Optic Neuropathy: A Review. Craniomaxillofacial Trauma Reconstr. 2015 Mar;8(1):31–41.

186. Pérez García E, Pola Alvarado L, Juvier Riesgo T, Hernández Martín Y, Hernández Hechevarría O. Neuropatía óptica traumática. Rev Cuba Oftalmol. 2012;25:590–9.

187. Thyparampil P, Yen MT. Compressive Optic Neuropathy in Thyroid Eye Disease: Int Ophthalmol Clin. 2016;56(1):51–67.

188. Sharma R, Sharma P. Toxic optic neuropathy. Indian J Ophthalmol. 2011;59(2):137.

189. Sadun AA. Metabolic optic neuropathies. Semin Ophthalmol. 2002 Jan 1;17(1):29–32.

190. Hsu CT, Miller NR, Wray ML. Optic neuropathy from folic acid deficiency without alcohol abuse. Ophtalmol Int J Ophthalmol Z Augenheilkd. 2002 Feb;216(1):65–7.

191. Miléa D. Nutritional, toxic and drug-induced optic neuropathies. Rev Prat. 2001 Dec 15;51(20):2215–9.

192. Woon C, Tang RA, Pardo G. Nutrition and optic nerve disease. Semin Ophthalmol. 1995 Sep;10(3):195–202.

193. Rizzo JF. Adenosine triphosphate deficiency: a genre of optic neuropathy. Neurology. 1995 Jan;45(1):11–6.

194. López-Hernández N, García-Escrivá A, Pampliega-Pérez A, Alvarez-Saúco M, Martín-Estefanía C, Asensio-Asensio M. Peripheral and optical myeloneuropathy in a folic acid deficient alcoholic patient. Rev Neurol. 2003 Oct 16;37(8):726–9.

195. Orssaud C, Roche O, Dufier JL. Nutritional optic neuropathies. J Neurol Sci. 2007 Nov;262(1–2):158–64.

USC DE SANTIAGO DE COMPOSTELA

196. Gherghel D, Griffiths HR, Hilton EJ, Cunliffe IA, Hosking SL. Systemic reduction in glutathione levels occurs in patients with primary open-angle glaucoma. Invest Ophthalmol Vis Sci. 2005 Mar;46(3):877–83.

197. Klopstock T, Yu-Wai-Man P, Dimitriadis K, Rouleau J, Heck S, Bailie M, et al. A randomized placebo-controlled trial of idebenone in Leber's hereditary optic neuropathy. Brain J Neurol. 2011 Sep;134(Pt 9):2677–86.

198. von Graefe, A. Ein ungewoehnlicher Fall von hereditaerer Amaurose. Arch Ophthalmol. 1858;4:266–8.

199. Newman NJ, Biousse V. Hereditary optic neuropathies. Eye Lond Engl. 2004 Nov;18(11):1144–60.

200. Anderson S. Sequence and organization of the human mitochondrial genome. Nature. 1981;290:451–64.

201. Wallace DC, Singh G, Lott MT, Hodge JA, Schurr TG, Lezza AM, et al. Mitochondrial DNA mutation associated with Leber's hereditary optic neuropathy. Science. 1988 Dec 9;242(4884):1427–30.

202. Yu-Wai-Man P, Griffiths PG, Hudson G, Chinnery PF. Inherited mitochondrial optic neuropathies. J Med Genet. 2009 Mar;46(3):145–58.

203. Huoponen K, Vilkki J, Aula P, Nikoskelainen EK, Savontaus ML. A new mtDNA mutation associated with Leber hereditary optic neuroretinopathy. Am J Hum Genet. 1991 Jun;48(6):1147–53.

204. Zhadanov SI, Atamanov VV, Zhadanov NI, Oleinikov OV, Osipova LP, Schurr TG. A novel mtDNA ND6 gene mutation associated with LHON in a Caucasian family. Biochem Biophys Res Commun. 2005 Jul 15;332(4):1115–21.

205. Guo D-Y, Wang X-W, Hong N, Gu Y-S. A Meta-analysis of the association between different genotypes (G11778A, T14484C and G3460A) of Leber hereditary optic neuropathy and visual prognosis. Int J Ophthalmol. 2016;9(10):1493–8.

USC UNIVERSIDADE DE SANTIAGO DE COMPOSTELA

206. Carelli V, Ross-Cisneros FN, Sadun AA. Mitochondrial dysfunction as a cause of optic neuropathies. Prog Retin Eye Res. 2004 Jan;23(1):53–89.

207. Yu-Wai-Man P, Griffiths PG, Chinnery PF. Mitochondrial optic neuropathies – Disease mechanisms and therapeutic strategies. Prog Retin Eye Res. 2011 Mar;30(2–2):81–114.

208. Rizzo G, Tozer KR, Tonon C, Manners D, Testa C, Malucelli E, et al. Secondary post-geniculate involvement in Leber's hereditary optic neuropathy. PloS One. 2012;7(11):e50230.

209. Yen M-Y, Wang A-G, Wei Y-H. Leber's hereditary optic neuropathy: a multifactorial disease. Prog Retin Eye Res. 2006 Jul;25(4):381–96.

210. Abukhalil F, Lam BL, Guy J. Visual observations of an American patient with Leber hereditary optic neuropathy after purported injections of stem cells in China. Arch Ophthalmol Chic Ill 1960. 2012 Apr;130(4):532–4.

211. Yu-Wai-Man P, Turnbull DM, Chinnery PF. Leber hereditary optic neuropathy. J Med Genet. 2002;39(3):162–9.

212. Klopstock T, Yu-Wai-Man P, Dimitriadis K, Rouleau J, Heck S, Bailie M, et al. A randomized placebo-controlled trial of idebenone in Leber's hereditary optic neuropathy. Brain J Neurol. 2011 Sep;134(Pt 9):2677–86.

213. Schaefer AM, McFarland R, Blakely EL, He L, Whittaker RG, Taylor RW, et al. Prevalence of mitochondrial DNA disease in adults. Ann Neurol. 2008 Jan;63(1):35–9.

214. Fraser JA, Biousse V, Newman NJ. The neuro-ophthalmology of mitochondrial disease. Surv Ophthalmol. 2010 Aug;55(4):299–334.

215. Gueven N. Optic Neurodegeneration: Time to Act. Biol Med. 2014;01(S1).

216. Barboni P, Savini G, Feuer WJ, Budenz DL, Carbonelli M, Chicani F, et al. Retinal nerve fiber layer thickness variability in Leber hereditary optic neuropathy carriers. Eur J Ophthalmol. 2012 Dec;22(6):985–91.

217. Carelli V, La Morgia C, Valentino ML, Barboni P, Ross-Cisneros FN, Sadun AA. Retinal ganglion cell neurodegeneration in mitochondrial inherited disorders. Biochim Biophys Acta. 2009 May;1787(5):518–28.

218. Howell N, Bindoff LA, McCullough DA, Kubacka I, Poulton J, Mackey D, et al. Leber hereditary optic neuropathy: identification of the same mitochondrial ND1 mutation in six pedigrees. Am J Hum Genet. 1991 Nov;49(5):939–50.

219. Gueven N, Nadikudi M, Daniel A, Chhetri J. Targeting mitochondrial function to treat optic neuropathy. Mitochondrion. 2017;36:7–14.

220. Avula S, Parikh S, Demarest S, Kurz J, Gropman A. Treatment of mitochondrial disorders. Curr Treat Options Neurol. 2014 Jun;16(6):292.

221. Jankauskaitė E, Bartnik E, Kodroń A. Investigating Leber's hereditary optic neuropathy: Cell models and future perspectives. Mitochondrion. 2017 Jan;32:19–26.

222. Carelli V, La Morgia C, Valentino ML, Rizzo G, Carbonelli M, De Negri AM, et al. Idebenone treatment in Leber's hereditary optic neuropathy. Brain J Neurol. 2011 Sep;134(Pt 9):e188.

223. Sabet-Peyman EJ, Khaderi KR, Sadun AA. Is Leber hereditary optic neuropathy treatable? Encouraging results with idebenone in both prospective and retrospective trials and an illustrative case. J Neuro-Ophthalmol Off J North Am Neuro-Ophthalmol Soc. 2012 Mar;32(1):54–7.

224. Kumar MA, Radhika B, Gollamudi N, Reddy SP, Yaga US. Hyperbaric Oxygen Therapy—A Novel Treatment Modality in Oral Submucous Fibrosis: A Review. J Clin Diagn Res JCDR. 2015 May;9(5):ZE01–4.

225. Mortensen CR. Hyperbaric oxygen therapy. Curr Anaesth Crit Care. 2008 Oct;19(5–6):333–7.

226. European Committee for Hyperbaric Medicine (ECHM) [Internet]. [cited 2018 Sep 26]. Available from: http://www.echm.org/

USC UNIVERSIDADE DE SANTIAGO DE COMPOSTELA

227. Yu-Wai-Man P, Votruba M, Moore AT, Chinnery PF. Treatment strategies for inherited optic neuropathies: past, present and future. Eye Lond Engl. 2014 May;28(5):521–37.

228. Henderson TA. Multi-watt near-infrared light therapy as a neuroregenerative treatment for traumatic brain injury. Neural Regen Res. 2016 Apr;11(4):563–5.

229. Whelan HT, Smits RL, Buchman EV, Whelan NT, Turner SG, Margolis DA, et al. Effect of NASA light-emitting diode irradiation on wound healing. J Clin Laser Med Surg. 2001 Dec;19(6):305–14.

230. Desmet KD, Paz DA, Corry JJ, Eells JT, Wong-Riley MTT, Henry MM, et al. Clinical and experimental applications of NIR-LED photobiomodulation. Photomed Laser Surg. 2006 Apr;24(2):121–8.

231. Lubart R, Wollman Y, Friedmann H, Rochkind S, Laulicht I. Effects of visible and near-infrared lasers on cell cultures. J Photochem Photobiol B. 1992 Feb 28;12(3):305–10.

232. Beauvoit B, Evans SM, Jenkins TW, Miller EE, Chance B. Correlation between the light scattering and the mitochondrial content of normal tissues and transplantable rodent tumors. Anal Biochem. 1995 Mar 20;226(1):167–74.

233. Fitzgerald M, Hodgetts S, Van Den Heuvel C, Natoli R, Hart NS, Valter K, et al. Red/near-infrared irradiation therapy for treatment of central nervous system injuries and disorders. Rev Neurosci [Internet]. 2013 Jan 1 [cited 2018 Dec 26];24(2). Available from: https://www.degruyter.com/view/j/revneuro.2013.24.issue-2/revneuro-2012-0086/revneuro-2012-0086.xml

234. Newman NJ. Treatment of hereditary optic neuropathies. Nat Rev Neurol. 2012 Oct;8(10):545–56.

235. Pfeffer G, Majamaa K, Turnbull DM, Thorburn D, Chinnery PF. Treatment for mitochondrial disorders. Cochrane Database Syst Rev. 2012 Apr 18;(4):CD004426.

236. Pfeffer G, Horvath R, Klopstock T, Mootha VK, Suomalainen A, Koene S, et al. New treatments for mitochondrial disease-no time to drop our standards. Nat Rev Neurol. 2013 Aug;9(8):474–81.

USC UNIVERSIDADE DE SANTIAGO DE COMPOSTELA

237. Scarpulla RC. Metabolic control of mitochondrial biogenesis through the PGC-1 family regulatory network. Biochim Biophys Acta. 2011 Jul;1813(7):1269–78.

238. Scarpulla RC, Vega RB, Kelly DP. Transcriptional integration of mitochondrial biogenesis. Trends Endocrinol Metab TEM. 2012 Sep;23(9):459–66.

239. Whitaker RM, Corum D, Beeson CC, Schnellmann RG. Mitochondrial Biogenesis as a Pharmacological Target: A New Approach to Acute and Chronic Diseases. Annu Rev Pharmacol Toxicol. 2016;56:229–49.

240. Komen JC, Thorburn DR. Turn up the power - pharmacological activation of mitochondrial biogenesis in mouse models. Br J Pharmacol. 2014 Apr;171(8):1818–36.

241. Giordano C, Iommarini L, Giordano L, Maresca A, Pisano A, Valentino ML, et al. Efficient mitochondrial biogenesis drives incomplete penetrance in Leber's hereditary optic neuropathy. Brain J Neurol. 2014 Feb;137(Pt 2):335–53.

242. Jornayvaz FR, Shulman GI. Regulation of mitochondrial biogenesis. Essays Biochem. 2010;47:69–84.

243. La Morgia C, Carbonelli M, Barboni P, Sadun AA, Carelli V. Medical Management of Hereditary Optic Neuropathies. Front Neurol [Internet]. 2014 Jul 31 [cited 2018 Dec 26];5. Available from: https://www.ncbi.nlm.nih.gov/pmc/articles/PMC4117178/

244. Wenz T, Williams SL, Bacman SR, Moraes CT. Emerging therapeutic approaches to mitochondrial diseases. Dev Disabil Res Rev. 2010;16(2):219–29.

245. Tischner C, Wenz T. Keep the fire burning: Current avenues in the quest of treating mitochondrial disorders. Mitochondrion. 2015 Sep;24:32–49.

246. Wenz T, Diaz F, Spiegelman BM, Moraes CT. Activation of the PPAR/PGC-1alpha pathway prevents a bioenergetic deficit and effectively improves a mitochondrial myopathy phenotype. Cell Metab. 2008 Sep;8(3):249–56.

USC UNIVERSIDADE DE SANTIAGO DE COMPOSTELA

247. Porcelli AM, Angelin A, Ghelli A, Mariani E, Martinuzzi A, Carelli V, et al. Respiratory complex I dysfunction due to mitochondrial DNA mutations shifts the voltage threshold

for opening of the permeability transition pore toward resting levels. J Biol Chem. 2009 Jan 23;284(4):2045–52.

248. Limb GA, Martin KR. Current Prospects in Optic Nerve Protection and Regeneration: Sixth ARVO/Pfizer Ophthalmics Research Institute Conference. Invest Ophthalmol Vis Sci. 2011 Jul 1;52(8):5941–54.

249. Saylor M, McLoon LK, Harrison AR, Lee MS. Experimental and clinical evidence for brimonidine as an optic nerve and retinal neuroprotective agent: an evidence-based review. Arch Ophthalmol Chic Ill 1960. 2009 Apr;127(4):402–6.

250. Newman NJ, Biousse V, David R, Bhatti MT, Hamilton SR, Farris BK, et al. Prophylaxis for second eye involvement in leber hereditary optic neuropathy: an open-labeled, nonrandomized multicenter trial of topical brimonidine purite. Am J Ophthalmol. 2005 Sep;140(3):407–15.

251. Thouin A, Griffiths PG, Hudson G, Chinnery PF, Yu-Wai-Man P. Raised intraocular pressure as a potential risk factor for visual loss in Leber Hereditary Optic Neuropathy. PloS One. 2013;8(5):e63446.

252. Montoya J, López-Pérez MJ, Ruiz-Pesini E. Mitochondrial DNA transcription and diseases: past, present and future. Biochim Biophys Acta. 2006 Oct;1757(9–10):1179–89.

253. Harding AE, Sweeney MG, Miller DH, Mumford CJ, Kellar-Wood H, Menard D, et al. Occurrence of a multiple sclerosis-like illness in women who have a Leber's hereditary optic neuropathy mitochondrial DNA mutation. Brain J Neurol. 1992 Aug;115 (Pt 4):979–89.

254. Sadun AA, Chicani CF, Ross-Cisneros FN, Barboni P, Thoolen M, Shrader WD, et al. Effect of EPI-743 on the clinical course of the mitochondrial disease Leber hereditary optic neuropathy. Arch Neurol. 2012 Mar;69(3):331–8.

USC UNIVERSIDADE DE SANTIAGO DE COMPOSTELA

255. Mordente A, Martorana GE, Minotti G, Giardina B. Antioxidant properties of 2,3-dimethoxy-5-methyl-6-(10-hydroxydecyl)-1,4-benzoquinone (idebenone). Chem Res Toxicol. 1998 Jan;11(1):54–63.

256. Giorgio V, Petronilli V, Ghelli A, Carelli V, Rugolo M, Lenaz G, et al. The effects of idebenone on mitochondrial bioenergetics. Biochim Biophys Acta. 2012 Feb;1817(2):363–9.

257. Camacho ÓFC, Carballo AA, Zenteno JC. Terapia génica para enfermedades hereditarias oftalmológicas: avances y perspectivas. Gac Médica México. 2015;151(4):501–11.

258. Mallela K. Pharmaceutical biotechnology - concepts and applications. Hum Genomics. 2010 Feb 1;4(3):218–9.

259. Kayser O, Kiderlen AF. Nonviral Gene Transfer Systems in Somatic Gene Therapy. In: Pharmaceutical Biotechnology [Internet]. John Wiley & Sons, Ltd; 2005 [cited 2018 Dec 27]. p. 249–63. Available from: https://onlinelibrary.wiley.com/doi/abs/10.1002/3527602410.ch14

260. Martin KRG, Quigley HA. Gene therapy for optic nerve disease. Eye Lond Engl. 2004 Nov;18(11):1049–55.

261. Scheller EL, Krebsbach PH. Gene Therapy. J Dent Res. 2009 Jul;88(7):585–96.

262. DiMauro S, Mancuso M. Mitochondrial diseases: therapeutic approaches. Biosci Rep. 2007 Jun;27(1–3):125–37.

263. Guy J, Qi X, Pallotti F, Schon EA, Manfredi G, Carelli V, et al. Rescue of a mitochondrial deficiency causing Leber Hereditary Optic Neuropathy. Ann Neurol. 2002 Nov;52(5):534–42.

264. Manfredi G, Fu J, Ojaimi J, Sadlock JE, Kwong JQ, Guy J, et al. Rescue of a deficiency in ATP synthesis by transfer of MTATP6, a mitochondrial DNA-encoded gene, to the nucleus. Nat Genet. 2002 Apr;30(4):394–9.

265. Osherovich L. Mitochondrial gene therapy. SciBX Sci-Bus Exch [Internet]. 2012 May 10 [cited 2018 Dec 29];5(19). Available from: https://www.nature.com/scibx/journal/v5/n19/full/scibx.2012.484.html

USC UNIVERSIDADE DE SANTIAGO DE COMPOSTELA

266. Levin LA, Ritch R, Richards JE, Borrás T. Stem cell therapy for ocular disorders. Arch Ophthalmol Chic Ill 1960. 2004 Apr;122(4):621–7.

267. Cao Q, Benton RL, Whittemore SR. Stem cell repair of central nervous system injury. J Neurosci Res. 2002 Jun 1;68(5):501–10.

268. Mead B, Berry M, Logan A, Scott RAH, Leadbeater W, Scheven BA. Stem cell treatment of degenerative eye disease. Stem Cell Res. 2015 May;14(3):243–57.

269. Mead B, Hill LJ, Blanch RJ, Ward K, Logan A, Berry M, et al. Mesenchymal stromal cell-mediated neuroprotection and functional preservation of retinal ganglion cells in a rodent model of glaucoma. Cytotherapy. 2016 Apr;18(4):487–96.

270. Dahlmann-Noor A, Vijay S, Jayaram H, Limb A, Khaw PT. Current approaches and future prospects for stem cell rescue and regeneration of the retina and optic nerve. Can J Ophthalmol J Can Ophtalmol. 2010 Aug;45(4):333–41.

271. Johnson TV, Bull ND, Hunt DP, Marina N, Tomarev SI, Martin KR. Neuroprotective effects of intravitreal mesenchymal stem cell transplantation in experimental glaucoma. Invest Ophthalmol Vis Sci. 2010 Apr;51(4):2051–9.

272. Connick P, Kolappan M, Crawley C, Webber DJ, Patani R, Michell AW, et al. Autologous mesenchymal stem cells for the treatment of secondary progressive multiple sclerosis: an open-label phase 2a proof-of-concept study. Lancet Neurol. 2012 Feb;11(2):150–6.

273. Brown WM, George M, Wilson AC. Rapid evolution of animal mitochondrial DNA. Proc Natl Acad Sci U S A. 1979 Apr;76(4):1967–71.

274. A Turner K. Current Methods for the Prevention of Transmission of Mitochondrial DNA Diseases. J Mol Genet Med [Internet]. 2014 [cited 2018 Dec 18];08(03). Available from: https://www.omicsonline.com/open-access/current-methods-for-the-prevention-of-transmission-of-mitochondrial-dna-diseases-1747-0862.1000127.php?aid=31154

275. Thorburn DR, Dahl HH. Mitochondrial disorders: genetics, counseling, prenatal diagnosis and reproductive options. Am J Med Genet. 2001;106(1):102–14.

USC UNIVERSIDADE DE COMPOSTELA

276. Sato M, Sato K. Maternal inheritance of mitochondrial DNA by diverse mechanisms to eliminate paternal mitochondrial DNA. Biochim Biophys Acta. 2013 Aug;1833(8):1979–84.

277. Carling PJ, Cree LM, Chinnery PF. The implications of mitochondrial DNA copy number regulation during embryogenesis. Mitochondrion. 2011 Sep;11(5):686–92.

USC
UNIVERSIDADE DE SANTIAGO DE COMPOSTELA

Chapter 1.

Design, optimization, and characterization of lactoferrin-loaded chitosan/TPP and chitosan/ sulfobutylether-β-cyclodextrin nanoparticles as a pharmacological alternative for keratoconus treatment

USC
UNIVERSIDADE DE SANTIAGO DE COMPOSTELA

USC
UNIVERSIDADE
DE SANTIAGO
DE COMPOSTELA

Chapter 1

Design, optimization, and characterization of lactoferrin-loaded chitosan and sulfobutylether-β-cyclodextrin/chitosan nanoparticles as a pharmacological alternative for keratoconus treatment

Rubén Varela-Fernández[1,2], Xurxo García-Otero[1,3], Victoria Díaz-Tomé1, Uxía Regueiro[2], Maite López-López[2], Miguel González-Barcia[4], María Isabel Lema[5,*], and Francisco Javier Otero-Espinar[1,6,*].

1. Department of Pharmacology, Pharmacy and Pharmaceutical Technology. University of Santiago de Compostela (USC). Campus vida. Santiago de Compostela. Zip Code: 15782. Spain. francisco.otero@usc.es.
2. Clinical Neurosciences Group. University Clinical Hospital, Health Research Institute of Santiago de Compostela (IDIS). Travesía da Choupana s/n Santiago de Compostela. Zip Code: 15706. Spain. rubenvf1@gmail.com.
3. Molecular Imaging Group. University Clinical Hospital, Health Research Institute of Santiago de Compostela (IDIS). Travesía da Choupana s/n Santiago de Compostela. Zip Code: 15706. Spain. xurxo.garcia.otero@gmail.com
4. Clinical Pharmacology Group. University Clinical Hospital, Health Research Institute of Santiago de Compostela (IDIS). Travesía da Choupana s/n Santiago de Compostela. Zip Code: 15706. Spain. miguel.gonzalez.barcia@sergas.es.
5. Department of Surgery and Medical-Surgical Specialties. Ophthalmology Area. University of Santiago de Compostela (USC).Campus Vida. Santiago de Compostela. Zip Code: 15706. Spain. mariaisabel.lema@usc.es.
6. Paraquasil Group. University Clinical Hospital, Health Research Institute of Santiago de Compostela (IDIS). Travesía da Choupana s/n Santiago de Compostela. Zip Code: 15706. Spain. francisco.otero@usc.es.

ACS Appl Mater Interfaces. 2021 Jan 27;13(3):3559-3575. doi: 10.1021/acsami.0c18926. Epub 2021 Jan 11. PMID: 33428398

INTRODUCTION

Conventional administration routes have been the preferential methods for drug delivery in the treatment of ocular pathologies (1). Nevertheless, micro and nanoparticles developed in the past decades are becoming the most promising ocular drug delivery systems (DDS), showing a great therapeutic potential due to their ability to protect drugs from degradation, enhance ocular penetration, and modulate or control drug pharmacokinetics. As a result, an efficacy improvement, a drug toxicity reduction, and an increase in the residence time in the target tissue were observed (2).

The ability of prolonging the drug release to the target tissue makes these carriers more attractive since they can decrease the frequency of administration, also improving patient compliance to treatment. A more recent strategy based on the incorporation of cyclodextrins (CDs) in nanometric carriers has risen in the past decades. Its aim is focused in the design of versatile DDS that are able to encapsulate drugs with unfavorable physicochemical properties (3).

Keratoconus is a progressive bilateral degenerative corneal ectasia that affects young adults, causing great visual disability, with great impact on life quality and social health, worsening over time (4). The keratoconus prevalence established from 1/2000 in the worldwide population, has evolved to higher rates in several countries with the development of topographic and corneal tomographic techniques that allow an earlier diagnosis (5).

There is no available medical or pharmacological treatment to prevent the development or decrease the progression of this disease. Besides, the optical treatment for visual rehabilitation (glasses or contact lenses) in initial and moderate stages does not stop the ectasia progression, making it necessary to recur to implanting intracorneal ring segments (ICRS) or corneal transplant in advanced stages, with limited visual recovery (6). Currently, the only conservative treatment that has proven effectiveness in slowing or delaying the keratoconus progression was corneal cross linking (CXL). However, CXL is only being performed in progressive stages with visual impairment, and it is not effective in all cases, possibly due to the exclusive use of topographical criteria (7).

Despite the high prevalence of the disease and the visual disability that it causes from an early age, both the etiology and progression determinant factors remain unclear. Besides that, its etiology appears to be multifactorial or represents the final common path of different pathological processes (8).

The cornea is part of the eye surface containing specific and non-specific immune molecules. The tissue degradation in keratoconus involves the expression of inflammatory mediators, such as pro-inflammatory cytokines, cell adhesion molecules, and matrix metalloproteases. Furthermore, a decrease in lactoferrin lacrimal levels in patients with keratoconus was observed (9). These results suggest that immunological processes may be involved in the pathogenesis of the ectasia.

USC UNIVERSIDADE DE SANTIAGO DE COMPOSTELA

Lactoferrin (Lf) is an 80 kDa iron-binding glycoprotein that has shown different biological effects (10). Corneally, Lf was observed to promote *in vivo* and *in vitro* corneal epithelial wound healing (11). This protein modulates the function of humoral and cellular components of the innate and adaptive response, as well as induces extracellular and intracellular signaling pathways involving Toll-Like receptors (TLRs), which regulate the gene expression of cytokines and other inflammatory mediators (12). Recently, our group demonstrated the overexpression of TLR2 and TLR4 receptors in monocytes and neutrophils of keratoconus patients, as well as a decrease in Lf lacrimal levels (13,14).

Two important criteria (corneal contact time and drug penetration) should be taken into account in a topical ophthalmic formulation that improve ocular bioavailability. Novel DDS are required for ocular drug delivery due to the numerous disadvantages of the conventional ocular dosage forms.

Previous studies (15) have confirmed that small proteins (M_W < 66 kDa) showed a slow diffusion rate through the excised corneal tissue (100-fold slower than glucose). Consequently, a low Lf diffusion rate is expected in the experimental conditions due its higher molecular weight. Thus, it is essential to promote a Lf residence time increase on the corneal surface and a penetration improvement into the stroma.

The novelty of this current work relies on challenging both chitosan-based formulations suitability for the improvement of the drug corneal permanence and penetration, as well as assess the ability to sustain and control the drug release. These novel DDS are non-irritant to the eye and produce an enhanced ocular retention time, thus providing greater efficacy and bioavailability. Additional advantages include high biocompatibility, ease of preparation, no need for high restrictions during the preparation procedure, high encapsulation and loading efficiencies, higher physical stability upon storage, and improved drug permeability.

Cyclodextrins can positively influence the protein stability, both thermally (temperature increase, ...) and chemically (inactivation by acids, ...). Furthermore, cyclodextrins can chemically interact with aromatic amino acids and promote the formation of inclusion complexes. Sulfobutylether-β-cyclodextrin (SBE-β-CD), a β-CD derivative, can also stabilize proteins, not only by the formation of inclusion complexes, but also by electrostatic interaction phenomena (16). Moreover, this cyclodextrin can act as a complexing agent in the formation of chitosan nanoparticles by ion gelation technique, being able to act as an alternative substitute

USC UNIVERSIDADE DE SANTIAGO DE COMPOSTELA

to the pentasodium tripolyphosphate (TPP). In addition, it has also been described the role of this cyclodextrin in terms of penetration and adhesion phenomena to corneal and scleral tissue.

Likewise, the main purpose for this site-specific and controlled release strategy is mainly based on the achievement of an improved pharmacokinetic and pharmacodynamic drug profile, as well as a better immunogenicity and system recognition for an enhanced therapeutic efficacy.

The aim of this chapter was based on the design, preparation, and characterization of lactoferrin-loaded CS/TPP and CS/SBE-β-CD nanoparticles as topical ophthalmic drug delivery systems as a pharmacological alternative for keratoconus treatment. A comparison between the traditional CS/TPP nanoparticles and CS/SBE-β-CD nanoparticles in order to carry out the immobilization of high molecular weight proteins intended for topical ophthalmic administration was made. An effort to demonstrate the suitability of both chitosan-based formulations to sustain the lactoferrin release and improve the corneal permeability was also carried out by obtaining a consistent preclinical base, not just through *in vitro* tests, but also with *ex vivo* and *in vivo* assays. Certainly, a novel ocular biopermanence study of polymeric nanoparticles based on a radiolabeling technique with different radiotracers were carried out to assess the bioadhesion of particles intended for ophthalmic topical administration.

MATERIALS

Low molecular weight chitosan (LMWCS; Mw = 150 kDa, 85% deacetylation degree and 85% purity grade) and pentasodium tripolyphosphate (TPP) were purchased from Sigma-Aldrich (St Louis, USA). Glacial acetic acid, sodium hydroxide (NaOH) and hydrochloric acid (HCl) were acquired from Merck (Darmstadt, Germany). Sulfobutylether-β-cyclodextrin (SBE-β-CD; Mw = 2160 Da, substitution degree = 3.00 – 6.50) was provided by Cyclolab Ltd (Budapest, Hungary). Lactoferrin was acquired from Sigma-Aldrich (St Louis, USA). Type II porcine mucin was purchased from Sigma Chemical Co (St Louis, USA). Visking® dialysis tubing cellulose membrane (14,000 g/mole molecular weight cut-off) was purchased from Sigma Aldrich (St. Louis, Missouri, USA). Ultrapure water (Milli-Q®, Millipore Iberica, Madrid, Spain) was used throughout the entire work. All other chemicals and reagents were of the highest purity grade commercially available.

USC UNIVERSIDADE DE SANTIAGO DE COMPOSTELA

EXPERIMENTAL METHODS

1. Screening study: CS/TPP and CS/SBE-β-CD nanoparticles formation

Chitosan-based nanoparticles were prepared by ionotropic gelation. This method is based in the electrostatic interaction of chitosan's positively charged amino groups with negatively charged groups of the TPP (17) or SBE-β-CD (18). Preliminary experiments were carried out before the drug encapsulation process to establish the best ratio between components that enable the nanoparticle's formation.

2. Preparation of blank CS/TPP nanoparticles

A 0.2% (w/v) chitosan solution was prepared by dissolving LMWCS in a 1% (v/v) acetic acid aqueous solution under stirring (500 rpm) for 24 h at room temperature. Dilutions were made in Milli-Q® water to the final desired concentrations. The pH was then adjusted to 5 (pH 5) with a 1M NaOH aqueous solution and stored in refrigeration (4 ± 2°C) until use. A tripolyphosphate (TPP) aqueous solution was prepared by dissolving the salt in Milli-Q® water to a final concentration of 0.2% (w/v) under stirring (500 rpm) for 24 h at room temperature and then stored in refrigeration (4 ± 2°C) until use. All TPP and chitosan solutions were filtered through a 0.22 µm hydrophilic polyvinylidene fluoride (PVDF) membrane (Merck Millipore Durapore™) prior to storage.

CS/TPP nanoparticle's formation occurred by the addition of the TPP solution to the chitosan solution drop-wisely (v = 10 mL/min) at a 5:1 (v/v) CS:TPP ratio under vigorous magnetic stirring (> 750 rpm) at room temperature for 30 min in order to promote nanoparticle's gelation (17). TPP final concentrations in the preparation varied from 0.05% to 0.2% (w/v), while CS final concentrations follow the same pattern, from 0.05% to 0.2% (w/v).

Resulting CS/TPP nanoparticle's suspensions were centrifuged for 1 h at 14000 rpm at 25°C and the obtained sediment was resuspended in double-distilled water, analyzed, and finally lyophilized, using 10% (w/v) trehalose as cryoprotectant. Dried particles were re-dispersed in a specific ocular buffer (pH 7.4) and characterized in terms of size, surface charge and morphology.

USC UNIVERSIDADE DE SANTIAGO DE COMPOSTELA

2.1. Preparation of blank CS/SBE-β-CD nanoparticles

Chitosan and SBE-β-CD solutions were prepared by dissolution in Milli-Q® water. A 0.2% (w/v) chitosan aqueous solution was prepared by dissolving LMWCS in a 1% (v/v) acetic acid aqueous solution under stirring (500 rpm) for 24 h at room temperature, filtered through a 0.22 µm PVDF membrane (Merck Millipore Durapore™) and pH was subsequently adjusted to 5 (pH 5) with a 1M NaOH aqueous solution, and stored in refrigeration (4 ± 2°C) until use. The SBE-β-CD solutions were prepared by jointly dissolving the cyclodextrin in desired concentrations into Milli-Q® water under stirring for 24 h at room temperature.

CS/SBE-β-CD nanoparticle's formation occurred by the addition of the SBE-β-CD solution to the chitosan solution drop-wisely (v = 10 mL/min) at a 5:1 (v/v) CS:SBE-β-CD ratio under vigorous magnetic stirring (> 750 rpm) at room temperature for 30 min, allowing the system's complete stabilization. SBE-β-CD final concentrations in the preparation varied from 0.1% to 0.5% (w/v), while CS final concentrations range from 0.025% to 0.1% (w/v).

Resulting CS/SBE-β-CD nanoparticle's suspensions were centrifuged for 1 h at 14000 rpm and 25°C, and the sediment was then resuspended in double-distilled water, analyzed and subsequently lyophilized, using 10% (w/v) trehalose as cryoprotectant. Dried particles were re-dispersed in a specific ocular buffer (pH 7.4) and characterized in terms of size, surface charge and morphology.

2.2. Preparation of lactoferrin-loaded CS/TPP nanoparticles

Lactoferrin-loaded CS/TPP nanoparticles were prepared by the addition of predetermined amounts of protein (from 0.1 to 1.0 mg/mL) to the TPP aqueous solution under magnetic stirring (> 750 rpm), prior to the nanoparticle's formation by the ionotropic gelation technique, as previously described (see *Preparation of blank CS/TPP nanoparticles*). The lactoferrin was added to the TPP solution due to the protein's isoelectric point (Ip = 7.28), where TPP aqueous solution showed a pH 9, as a way to keep the protein's isoelectric balance during the elaboration process.

USC UNIVERSIDADE DE SANTIAGO DE COMPOSTELA

Resulting lactoferrin-loaded CS/TPP nanoparticle's suspensions were centrifuged for 1 h at 14000 rpm at 25°C and the obtained sediment was resuspended in double-distilled water, analyzed, and lyophilized, using 10% (w/v) trehalose as cryoprotectant. Dried particles were

re-dispersed in a specific ocular buffer (pH 7.4) and characterized in terms of size, surface charge and morphology. The supernatant was recovered for further analysis.

2.3. Preparation of lactoferrin-loaded CS/SBE-β-CD nanoparticles

Predetermined amounts of lactoferrin (from 0.1 to 1 mg/mL) were incubated under magnetic stirring (500 rpm, 1 h) in a SBE-β-CD solution in order to promote the inclusion complex formation. These inclusion-complexed solutions were then used for nanoparticle's formation by the ionotropic gelation technique, as previously described (see *Preparation of blank CS/SBE-β-CD nanoparticles*).

Resulting lactoferrin-loaded CS/SBE-β-CD nanoparticle's suspensions were centrifuged for 1 h at 14000 rpm at 25°C and the obtained sediment was resuspended in double-distilled water, analyzed, and lyophilized, using 10% (w/v) trehalose as cryoprotectant. Dried particles were re-dispersed in a specific ocular buffer (pH 7.4) and characterized in terms of size, surface charge, and morphology. The supernatant was recovered for further analysis.

3. Physicochemical characterization of chitosan-based nanoparticles

3.1. Particle size, size distribution and z potential

The average particle size, polydispersity index (PDI) and ζ potential of the chitosan-based nanoparticles were determined by dynamic light scattering (DLS) with non-invasive back scattering (DLS-NIBS) at 25°C, using a Malvern Zetasizer Nano ZS instrument (ZEN3600, Malvern Instruments Ltd., Malvern, UK). Samples were diluted 1:10 in purified water before measurement in order to reduce the opalescence during size analysis and subsequently placed in disposable polystyrene cuvettes (DTS1070, Malvern Instruments Ltd., Malvern, UK) for the analysis. Each batch was analyzed in triplicate. DLS subsets were defined as presented: (I) 120 seconds temperature stabilization time for each sample, (II) 3 analysis runs for each formulation, and (III) 20 determinations per run for each sample.

USC
UNIVERSIDADE
DE SANTIAGO
DE COMPOSTELA

3.2. Morphological evaluation

The morphological examination of the CS/TPP and CS/SBE-β-CD nanoparticles was performed by scanning electron microscopy (SEM) and transmission electron microscopy (TEM). SEM analyses were carried out by placing the samples on a metal stub double-sided

conductive adhesive tape and iridium sputter-coating the samples prior to observation in an analytical scanning electron microscope (ZEISS EVO LS 15/EDX, ZEISS®) (Jena, Germany), under different magnifications. TEM analyses were performed by staining samples with 2% (w/v) phosphotungstic acid for 10 min, placed on copper grids with Formvar® film and dried overnight for TEM observation by using a JEOL JEM-F200CF-HR microscope (JEOL®) (Peabody, USA). The air-dried samples were imaged using a 200 kV acceleration voltage.

3.3. Production yield (PY) of nanoparticles

The production yield of the resulting nanoparticles was obtained by the application of the centrifugation technique (19), with minor modifications. Briefly, fixed volumes of the nanoparticle's suspensions were centrifuged without glycerol bed (14000 rpm, 1h, 25°C), the supernatants were then discarded, and the sediment was vacuum-dried for 48 h at 50 ± 2°C (until constant weight). The production yield was then estimated by comparing the final weight with the theoretical weight of the nanoparticles, as presented (equation 1):

$$Production\ yield\ (\%) = \frac{Nanoparticles\ weight}{Total\ initial\ solids\ weight} \cdot 100 \qquad Equation\ 1$$

3.4. Encapsulation efficiency (EE) and loading capacity (LC) of nanoparticles

Encapsulation efficiency (EE) and loading capacity (LC) of the nanoparticle preparations were determined after isolation by centrifugation, as previously described. EE denotes the percentage of drug that is entrapped from the total amount of drug initially added to the preparation, while LC refers to the percentage of encapsulated drug into the NPs. The amount of unbound lactoferrin was determined in the supernatant by UV-Vis spectrophotometry (Cary 60 UV-Vis, Agilent Technologies®) (California, USA) at a 280 nm wavelength. The EE (equation 2) and LC (equation 3) of lactoferrin were respectively calculated as presented below:

USC UNIVERSIDADE DE SANTIAGO DE COMPOSTELA

$$EE\ (\%) = \frac{Total\ amount\ of\ drug - Amount\ of\ unbound\ drug}{Total\ amount\ of\ drug} \cdot 100. \qquad Equation\ 2$$

$$LC\ (\%) = \frac{Total\ amount\ of\ drug - Amount\ of\ unbound\ drug}{Nanoparticles\ weight} \cdot 100. \quad Equation\ 3$$

4. Stability studies

The nanoparticle's aggregation or contraction phenomena are expected to be influenced by the drug physicochemical properties. Furthermore, chemical processes, such as oxidation or hydrolysis, may also alter the useful lifespan of chitosan-based nanoparticle suspensions. The stability of chitosan-based nanoparticles should be assessed in terms of structural changes, such as contraction and swelling processes, among others (20).

4.1. Stability to storage

The stability study during storage was designed as per ICH guidelines (21), with minor modifications. Selected nanoparticle's formulations were freshly prepared, isolated by centrifugation and resuspended in a specific ocular buffer (pH 7.4), considering size changes and possible precipitation phenomena. Nanoparticles were incubated at three different temperature conditions: (I) in refrigeration (4 ± 2°C), (II) at room temperature (25 ± 2°C), and (III) oven temperature (37 ± 2°C) for an 8 h (short-time stability) and 3-month (long-term stability) period respectively, under orbital agitation (100 rpm) sheltered from the light. Samples were collected at predetermined time points for both studies. Nanoparticle's size and size distribution were measured by dynamic light scattering (DLS), performing every measurement in triplicate.

4.2. Stability to pH

The pH-dependent nanoparticle's physical stability evaluation was carried out in freshly prepared samples. Once obtained and after a three-times Milli-Q® water washing, suspensions were kept in refrigeration at 4 ± 2°C as stock suspensions. 500 µL of each formulation were taken to test tubes and diluted to a 5 ml volume using Milli-Q® water. pH was then adjusted to predetermined values (2, 4, 6, 7, 8, 10, and 12) by using 0.1M NaOH or 0.1M HCl aqueous solutions, as appropriate. Samples were kept in refrigeration at 4 ± 2°C for 24 h, followed by the particle size, PDI and ζ potential measurements. Each sample was measured in triplicate.

USC UNIVERSIDADE DE SANTIAGO DE COMPOSTELA

4.3. Stability to ionic strength

NPs physical stability assessment in terms of ionic strength was performed in freshly prepared samples. Once obtained and after a three-times Milli-Q® water washing, suspensions were kept in refrigeration at 4 ± 2°C as stock suspensions. 500 µL of each formulation were taken to test tubes and diluted to a 5 ml volume using NaCl aqueous solutions with predetermined molarity values (0.2, 0.4, 0.6, 0.8, 1.2, 1.4, 1.6, and 2M). Samples were kept in refrigeration at 4 ± 2°C for 24 h, followed by the particle size, PDI and ζ potential measurements. Each formulation was tested and measured in triplicate.

5. *In vitro* release study

The dialysis method is one of the most versatile and widespread technique used to assess drug release from nano-sized drug delivery systems. In this method, two different chambers are physically separated by the usage of a dialysis membrane. Several modifications have subsequently been applied in crucial factors as a way to improve the experimental process (22). Furthermore, the ease of the system and sampling procedure make it an appropriate, simple, and uncomplicated technique to evaluate the drug release profile from a wide-ranging variety of nano-sized delivery systems (23).

The release of lactoferrin from CS/TPP and CS/SBE-β-CD nanoparticles was assessed in order to predict the drug diffusion and kinetic behavior from the delivery systems in simulated physiological conditions. The osmolality of formulations was adjusted to better replicate the topical ophthalmic administration. Hence, freshly prepared lactoferrin-loaded CS/TPP and CS/SBE-β-CD nanoparticles were suspended in PBS (pH 7.4 and ionic strength 0.075 M) due to the fact that the buffer osmolality is in the optimal range (from 0.025 to 0.15 M) for a physiological environment proof-of-concept assay and characterization in terms of drug delivery (24).

The lactoferrin release rate from CS/TPP and CS/SBE-β-CD nanoparticles was determined by UV-Visible spectrophotometry (Cary 60 UV-Vis, Agilent Technologies®) (California, USA), using Franz diffusion cells. The receptor chamber was fully filled with 7 mL of phosphate buffer medium (PBS, pH 7.4) containing 0.02% (w/v) sodium azide, while donor chamber was filled 3 mL of a known amount of lactoferrin-loaded nanoparticles. Both chambers were separated by a Visking® dialysis membrane. Sink conditions were established in order to simulate *in vivo* pharmacokinetic behavior.

Franz diffusion cells were subsequently placed in an orbital shaker bath (Unimax 1010/Incubator 1000, Heidolph®) (Schwabach, Germany) which was maintained at 37°C and shaken at 100 rpm. At predetermined time points, 1 mL was taken from the receptor chamber, and refilled with an equivalent volume of fresh PBS solution in order to maintain sink conditions. The study was run for 24 h, and each formulation was tested in triplicate.

Lactoferrin concentrations in the pH 7.4 isotonic PBS solution were measured using UV-Vis spectrophotometry (Cary 60 UV-Vis, Agilent Technologies®) (California, USA) at a 280.0 nm wavelength. Resulting data demonstrated that reference solutions remained stable for at least a week, protected from light exposure and under refrigeration (4 ± 2°C).

6. Cytotoxicity analysis

Success in developing and validating alternative tests to replace the Draize rabbit eye irritation test has remained elusive due to the difficulty of comparing *in vitro* results with historical animal data (more solid and consistent), but some assays showed considerable potential for the evaluation of ocular irritancy. The alternative methods to eye irritation comprise organotypic models such as isolated eyes or components thereof, tissue or cell culture systems, and physicochemical tests (25). The effectiveness of these *in vitro* and *ex vivo* procedures is well established within some national regulatory agencies and within industry for specific and limited purposes.

The Bovine Corneal Opacity and Permeability test (BCOP) is very suitable to select out the moderate, severe, and very severe eye irritants since the depth of injury can be measured in this *ex vivo* tissue model. However, the BCOP resolution for mild to very mild ocular irritancy levels is deficient. Hence, BCOP can be considered as a pre-validation assay, and it is suggested to be used in tandem with other assays measuring different cytotoxicity endpoints, such as the Hen's egg test on the chorioallantoic membrane assay (HETCAM), among others (26). On its behalf, the chorioallantoic membrane (CAM) of the fertilized chicken eggs is also considered a suitable template for modelling the effects of materials on ocular tissues, being able to detect even mild or very mild ocular irritant compounds.

USC UNIVERSIDADE DE SANTIAGO DE COMPOSTELA

6.1. Bovine Corneal Opacity and Permeability test (BCOP)

The Bovine Corneal Opacity and Permeability test (BCOP) is an organotypic assay used to assess the potential ocular irritancy of formulations, avoiding the keeping and killing of laboratory animals (animal replacement compliance).

The use of *in situ* isolated corneas have the advantage that all corneal layers can be screened, i.e., epithelium, Bowman's membrane, stroma, Descemet's membrane, and endothelium. Furthermore, tests on isolated corneas generally involve simple techniques with a number of accurate quantifiable endpoints.

The use of BCOP assay is based on the method developed by Tchao et al. (1988) (27) and adapted by Gautheron et al. (28), with minor modifications. Briefly, freshly excised eyes were collected from a local slaughterhouse and transported in superfusion containers that allow their maintenance for a specified period, enough for the formulation's testing in the laboratory. The eyes were then inspected by macroscopic analysis, and the corneas, free of defects, were dissected and used as the test systems.

Freshly isolated corneas were vertically mounted in Franz diffusion cells, used as holders, with the corneal epithelial surface upwards. The mounted corneas divided the diffusion cell into two different chambers (donor and receptor, respectively). All Franz diffusion cells were incubated in a thermostatic bath with controlled temperature (37 ± 2°C) and under magnetic stirring (100 rpm) during the entire assay.

In the BCOP test, corneal opacity changes were assessed by the onset of two different techniques, these being the luxmetry and the UV-Vis spectrophotometry. Luxmetry is assessed by placing the dissected cornea inside a specially designed luxmeter (Gossen Mavolux 5032C USB) (Nürnberg, Germany). On the other hand, UV-Vis spectrophotometry is determined by transmittance scan (from 200 to 800 nm), positioning the cornea in an specific holder in order to allow the light to pass through, from the source to the receiver of the spectrophotometer (Cary 60 UV-Vis, Agilent Technologies®) (California, USA). Each formulation was evaluated in triplicate.

A procedure for formulation's addition and opacity measurements was established as presented: (I) determination of the initial opacity values for freshly excised corneas by luxmetry and UV-Vis spectrophotometry; a corneal blank was made before luxmetry determination in order to remove basal light, while the cornea itself was used as blank (at a 800 nm wavelength) before spectrophotometry determination, (II) addition of 1 mL PBS into the Franz cell's donor

USC DE COMPOSTELA

compartment and cornea's incubation for 10 minutes, followed by the opacity determination, (III) 1 mL of the formulation was added to the upper compartment (enclosing the corneal epithelial surface) for 10 minutes, followed by its removal and subsequent addition of PBS for 120 minutes; after this time, the opacity determination was repeated.

Likewise, after measuring the opacity, 1 mL of the 0.4% (w/v) fluorescein aqueous solution was added to the corneal epithelial side (i.e., into the upper compartment) in order to determine the corneal permeability by assessment of the optical density (OD) of the medium (PBS) in the lower compartment at a 490 nm wavelength, as a way to assess corneal permeability changes.

The measured numerical values for opacity and permeability can be used to calculate a so-called *in vitro* irritation score (IVIS) (28). Furthermore, classification of test formulations can be done according to the Kay and Calandra score (28). The mathematical equation used for the IVIS determination is presented as:

$$IVIS = mean\ opacity\ value + (15 \times mean\ permeability\ OD_{490}\ value) \quad Equation\ 4$$

6.2. Hen's egg test on the chorioallantoic membrane (HET-CAM)

The universal test for the irritant and corrosive potential assessment of substances is based on a rabbit eye test, developed by Draize et al. (1944) (29) and has become the international standard assay for acute eye irritation and corrosion (OECD TG 405, 2002; EC B.5). However, different validated alternative tests (animal replacement principle) showed considerable promise for ocular irritancy evaluation. The HET-CAM test is one of the new organotypic models that allows the identification of irritative reactions, similarly to those which occur in the eye using the standard Draize rabbit eye test (30).

In the HET-CAM test, three reactions are measured, these being: (I) hemorrhage, (II) lysis, and (III) coagulation of the chorioallantoic membrane at the ninth day of embryonation, when nerve tissue and pain perception have not been developed yet. These reactions can be quantified through an irritation score (IS) and subsequently classified as follows: (I) 0-0.9 as no irritation, (II) 1-4.9 as slight irritation, (III) 5-8.9 as moderate irritation, and (IV) 9-21 as severe irritation, following the Kalweit et al. criteria (31). All procedures with eggs were followed by the regulations and procedures for handling of animal materials.

USC
UNIVERSIDADE DE SANTIAGO DE COMPOSTELA

The protocol used was adapted from the procedure previously described by Spielmann and Liebsch (32). Briefly, fertilized Broiler eggs (50 – 60 g weight) were obtained from the regional

hatchery technology center and incubated for nine days in specific conditions (37 ± 0.5°C and 65% ± 5% RH). The trays containing eggs were automatically rotated in every 2 h until eighth day, where rotation was stopped, and the eggs were kept in the axial position for the proper placement of the chorioallantoic membrane (CAM).

At ninth day of incubation, viable embryos were used by creating a window on the head of the eggs through which formulations (300 µL) were instilled. After directly placing the formulation onto the CAM, an evaluation of the aforementioned parameters over a 5 min observation period was performed by using an Olympus SZ61TR Stereomicroscope and an Olympus CellSens Entry software. Images were taken at the beginning (before formulation's administration) and at the end (after the trial period) of the assay and each replicate was recorded during the entire process in order to carefully assess the presence or absence of toxic effects (if required). These measurements were considered individually and then combined to derive a score, which was used to classify the irritancy level of each formulation. A 0.9% (w/v) NaCl aqueous solution was used as negative control, while a 1M NaOH aqueous solution was employed as positive control. Each formulation was evaluated in triplicate.

7. Mucoadhesion study

The interaction between chitosan and mucin determines the behavior of chitosan-based nanosystems. Interactions between chitosan and mucin depend on both intrinsic factors (directly associated with the polymer nature) and external factors (environment where the interaction occurs). It must be taken into account that some external factors have a direct impact on different intrinsic factors, modulating the interaction. Thus, four different outcomes could be observed as a result of the interaction between chitosan-based nanoparticles and the ocular mucin layer (see Figure S-1, Supporting Information): (I) adsorption of the nanoparticles to the mucus layer, (II) nanoparticle's removal with the mucus layer renewal, (III) loss of functionality of the nanoparticles when covered by mucin or (IV) passage through the mucin layer and reach the cornea.

Thus, it is of great importance to study the mucoadhesive properties of chitosan and chitosan-based nanomaterials. Two different approaches were used to assess the ocular retention time of the formulations after topical ophthalmic administration into the eye, as presented: (I) *in vitro* ocular retention study by biophysical techniques (ζ potential measurements), (II) *ex vivo* ocular

USC UNIVERSIDADE DE SANTIAGO

retention study by using excised bovine eyes, and (III) *in vivo* ocular retention study by using male Sprague-Dawley rats as an animal model.

7.1. *In vitro* ocular mucoadhesion study

The *in vitro* ocular surface retention study was based on a mucoadhesion assay procedure, considering the electrostatic interaction between the chitosan's positively charged amino groups and the negatively charged groups of the mucin (33).

Experimentally, mucoadhesion study was performed following the procedure described by Mazzarino et al. (34), with minor modifications. Equal volumes of 0.04% (w/v) mucin solution and CS/TPP or CS/SBE-β-CD nanoparticles were vortexed for 1 min and furtherly kept in an orbital incubator (37 ± 2°C, 100 rpm) for 2 h. Mucin activity was then stopped by maintaining the nanoparticle's suspensions on an ice bath for 45 min and the ζ potential of the resulting mixtures was subsequently measured. It must be taken into account that nanoparticle's ζ potential was measured before and after the incubation process with the mucin solution, and the mucoadhesion ability was measured as the difference between both values.

7.2. *Ex vivo* ocular mucoadhesion study

The *ex vivo* corneal surface retention study was adapted from the original procedure described by Belgamwar et al, (2009) (35), with minor modifications. For this purpose, freshly excised eyes were collected from a local abattoir and transported in superfusion containers that allow their maintenance for a specified period, enough for the formulation's testing in the laboratory. The eyes were then inspected by macroscopic analysis and viable ones were selected for further analysis.

Viable excised eyes were washed with PBS (pH 7.4) in order to remove possible impurities, and then placed on manually developed specific holders, positioning the corneal epithelial surface upwards. 500 µL of the 0.4% (w/v) fluorescein-stained chitosan-based nanoparticles were added drop wisely, and excess was collected and reapplied, repeating this procedure 10 times. The final residual solution was measured for fluorescence intensity by UV-Vis spectrophotometry (Cary 60 UV-Vis, Agilent Technologies®) (California, USA) at a 490.0 nm wavelength, comparing it to the initial intensity values, obtained by measuring the suspension prior to the instillation.

The *ex vivo* corneal mucoadhesion of the CS/TPP and CS/SBE-β-CD nanoparticles was subsequently quantified through the following mathematical equation (equation 5):

$$Mucoadhesion\ (\%) = (Ab_{S0} - V_0) - \frac{(Ab_{SF} - V_F)}{(Ab_{S0} - V_0)} \cdot 100 \quad Equation\ 5$$

Where Abs_0 and Abs_F represent the absorbance value for the initial and final fluorescein-stained chitosan-based suspensions, V_0 refers to the volume applied to the viable excised eyes, and V_F indicates the final volume of the suspension not adsorbed to the mucosa. Each formulation was tested in triplicate.

7.3. *In vivo* mucoadhesion study

7.3.1. Evaluation of the radiolabeling stability and efficiency of chitosan-based nanoparticles

Radioactive fluoride (^{18}F) is one of the most commonly used positron emitter due to its optimal positron characteristics ($t_{1/2}$ = 109.7 min, $E_{\beta+,max}$ = 635 keV, and β^+ intensity = 97%), making it almost ideal for Positron Emission Tomography (PET) imaging. In spite of all these benefits, ^{18}F is mostly clinically used in two different forms, these being 2-(^{18}F)fluoro-2-deoxy-D-glucose (^{18}F-FDG) and ^{18}F-Choline.

Recently, different approaches were studied to track different types of colloidal systems using ^{18}F-FDG or ^{18}F-Choline labeling (36,37). Based on this literature review, the assessment of the radiolabeling stability and efficiency of ^{18}F-FDG or ^{18}F-Choline chitosan-based nanoparticles was carried out by incubation with a known amount of the radiotracer for a 45 min period at room temperature (25 ± 2ºC) and 200 rpm in an orbital shaker (ThermoCell® Mixing Block, Tamar Laboratory Supplies Ltd., Israel). Samples were then centrifuged at predetermined times (0.5, 1.5 and 3.0 h) (14000 rpm and 4ºC) (Eppendorf® 5427R, Eppendorf Iberica, Spain), supernatant and remnant were separated into two different centrifuge tubes, and radiotracer activity was finally measured by using an activimeter (Capintec® CRC 15R Dose Calibrator, New Jersey, USA). In order to point out, both types of the ^{18}F-based aqueous solution (^{18}F-FDG and ^{18}F-Choline) were provided by the PET Radiopharmaceutical Unit (Cyclotron) of the University Hospital Complex of Santiago de Compostela (CHUS).

The radiolabeling efficiency of chitosan-based nanoparticles was assessed by measuring the ^{18}F-FDG or ^{18}F-Choline activity respectively, both in the supernatant and the remnant vials,

taking into account the incubation time and the radiotracer decay. Mathematical analysis was then applied to the resulting data in order to obtain the radiolabeling efficiency and to assess the labeling stability over time.

7.3.2. Experimental *in vivo* evaluation of the ocular biopermanence

The *in vivo* assessment of the ocular surface retention time of the formulations was carried out by Positron Emission Tomography (PET) and Computed Tomography (CT) combined technique. Both methodologies for conducting the radiolabeling and the subsequent quantitative ocular permanence evaluation of topical ophthalmic formulations were described in previous works (38).

In vivo studies were carried out on male Sprague-Dawley rats (250 ± 35 g), supplied by the animal facility at the University of Santiago Compostela (Spain). The animals were kept in individual cages under controlled temperature (22 ± 1ºC) and relative humidity (60 ± 5%), with day-night cycles regulated by artificial light (12/12 hours) and fed ad libitum. Animals were acclimatized for a week prior to the beginning of the experiments. All animals were treated according to the ARVO Statement for the Use of Animals in Ophthalmic and Vision Research, as well as the approved guidelines for laboratory animals (39). Each formulation was tested in quadruplicate (four eyes, two animals) in order to accomplish the 3Rs regulatory frameworks (40).

The microPET and CT acquisition was performed by using the Albira PET/CT Preclinical Imaging System (Bruker Biospin, Woodbridge, Connecticut, United States). Anesthetized animals were positioned into the imaging bed with a face mask (2.5% (v/v) isoflurane/oxygen), monitoring the respiration frequency during the acquisition period. Then, 7.5 µL of ^{18}F-FDG radiolabeled chitosan-based nanoparticles were instilled into the conjunctival sac eye. After the instillation, static PET frames at predetermined times (0, 30, 75, 120, 240 and 300 minutes) were acquired in order to estimate the pharmacokinetic behavior. An Elizabethan collar was placed in each animal between PET studies to prevent the rat from scratching their eyes and removing the previously instilled formulation.

USC
UNIVERSIDADE DE SANTIAGO DE COMPOSTELA

Imaging reconstruction (0.5 x 0.5 x 0.5 mm^3 pixel size) was carried out by using the maximum likelihood expectation maximization algorithm (MLEM) (6 iterations). Image analysis was performed using the Amide's Medical Image Data Analysis Tool (41). Regions of Interest (ROIs) were manually acquired and processed after imaging reconstruction for the different

frames over time by delimiting the total radiotracer's uptake of each eye (15 x 15 x 15 mm, 1767.10 mm^3), and the resulting data were adjusted by the radiotracer's radioactive decay (half-life time: 109.7 min). Results were replicated on the different temporal image frames. The mean radiotracer uptake obtained from the first frame just after topical ophthalmic instillation of the formulations was considered as the reference value. The subsequent measurements from the successive frames were reported as percentage of the reference value. The average amount from both eyes of the same animal was used for the pharmacokinetic analysis. Graphical representations of formulation's radioactivity versus time were subsequently obtained, comparing the results against a control solution (^{18}F-FDG buffered solution).

The fitting of the remaining formulation versus time to a mono-exponential decay equation using a single compartmental model was performed by non-lineal regression using the GraphPad Prism® software (42). Non-compartmental analysis was also carried out by estimating the mean residence time (MRT) and the total area under the curve (AUC) of the remaining percentage of formulations versus time.

8. Data analysis

Pairs of groups were compared by carrying out one-tailed Student's t-test and multiple group comparison was conducted by one-way or two-way analysis of variance (one-way or two-way ANOVA), or by non-parametric Kruskal Wallis test with a 95% significance level ($p < 0.05$) throughout these studies, using the GraphPad Prism v.8.00 software (GraphPad Software, Inc. CA, USA). All data are presented as a mean value with its standard deviation indicated (mean ± SD). Tukey's, Bonferroni's or Dunnet's tests were subsequently applied for post-hoc contrast.

RESULTS AND DISCUSSION

1. Screening study: CS/TPP and CS/SBE-β-CD nanoparticles formation

1.1. Preparation of CS/TPP nanoparticles

CS/TPP NPs were prepared via the ionotropic gelation technique, based on the ionic interaction between positively charged amino groups of CS and the negatively charged ions of TPP, leading to the formation of inter- and intramolecular linkages (17). The ion gelation method was mild, and a few minutes were taken to create the final nanoparticles.

CS/TPP NPs preparation was carried out in acidic conditions due to the fact that the pH of the medium influenced the protonation of the CS amino groups (pH interval = 5 - 6). Preliminary experiments were addressed to the selection of the optimal ratio for the CS/TPP nanoparticle's formation. The presence of opalescence in the resulting solutions was used as an indicator of nanoparticle's formation, subsequently confirmed by DLS.

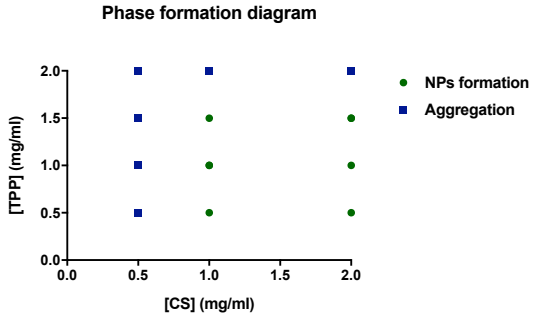


Figure 1. Phase diagram formation of CS/TPP NPs.

The increase in the turbidity of the suspensions (CS/TPP NPs formation) was directly proportional to the amount of TPP used, but particle aggregation rapidly and drastically occurred (see Figure 1). Higher available amount of TPP led to the formation of larger nanoparticles and flocculating aggregates as a consequence of dominantly inter- and intramolecular cross-links. All the suspensions prepared in the selected interval of TPP and CS concentrations were deeply analyzed in terms of particle size, size distribution and surface charge (see Figure S-2, Supporting Information).

The preliminary results of these preparations indicate that a 1:1 (w/w) CS/TPP ratio and a 5:1 (v/v) phase ratio turned out to be the best proportion for CS/TPP nanoparticle's formation.

1.2. Preparation of CS/SBE-β-CD nanoparticles

The ratio between CS and SBE-β-CD is a critical parameter in the nanoparticle's formation and restricts the resulting particle size. Hence, it was necessary to establish the best CS/SBE-β-CD ratio to promote the best conditions for the formation of the nanosystems before the drug encapsulation. Different concentrations of CS and SBE-β-CD were used to establish the optimum preparation conditions for nanoparticle's formation. The CS/SBE-β-CD NPs

preparation was carried out in acidic conditions since the pH of the medium influenced the protonation of the CS amino groups (pH 5).

In the present study, SBE-β-CD was incorporated into final formulations to improve drug stability, water solubility, encapsulation efficiency, and release profile into the nanocarriers. Carried-out studies have shown that all NPs were in the nano-sized range and exhibited a positive ζ potential. Likewise, the phase diagram of nanoparticle formation (see Figure 2) revealed the existence of an interval with different specific ratios of SBE-β-CD and CS in order to make nanoparticle's formation possible. Two different systems were identified in the phase diagram, including (I) opalescent dispersion, and (II) aggregates (see Figure 2) for the tested concentration interval.

The increase in the turbidity of the suspensions (CS/SBE-β-CD NPs formation) was directly proportional to the amount of SBE-β-CD used, but particle aggregation promptly and significantly occurred (see Figure 2). Higher available amount of SBE-β-CD led to the formation of larger nanoparticles or flocculating aggregates as a consequence of dominantly inter- and intramolecular interactions between both components. All the suspensions were deeply analyzed in terms of particle size, size distribution and surface charge (see Figure S-3, Supporting Information).

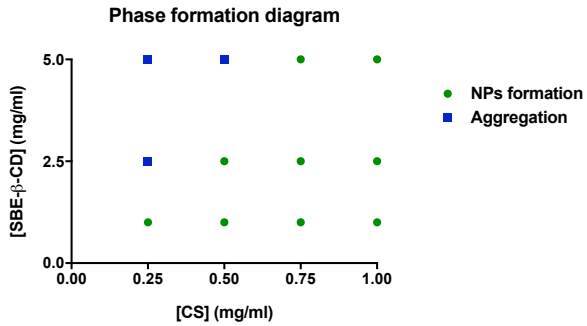


Figure 2. Phase diagram formation of CS/SBE-β-CD NPs.

Based on the resulting data, an optimum CS/SBE-β-CD ratio was selected for the preparation of drug-loaded nanoparticles, these being composed of 0.05% (w/v) chitosan and 0.25% (w/v) SBE-β-CD solutions in a 5:1 (v/v) phase ratio.

USC UNIVERSIDADE DE SANTIAGO DE COMPOSTELA

2. Physicochemical characterization of nanoparticles

2.1. Particle size, size distribution and ζ potential

Particle size and size distribution of novel nanoparticulate systems are important factors in view of their potential application for topical ophthalmic administration. Indeed, it is well known that particles in the nanometric range influence biological parameters, such as the *in vivo* distribution through biological barriers, drug delivery to the target tissue, drug content, stability, or toxicity, among others (43).

Preliminary results of CS/TPP nanoparticles indicate that a 5:1 (v/v) CS/TPP ratio turned out to be the best proportion for nanoparticle's formation. The average size was 160.56 ± 20.65 nm. The polydispersity index (PDI) was lower than 0.3 for the chosen CS/TPP ratio (about 0.170 ± 0.067), indicating that a homogeneous dispersion was obtained. The distribution curve suggested the presence of two different particle size populations: a small fraction of 1000 nm (< 2%) (nanoparticle aggregates) and a major population of around 150 nm (> 98%) (nanoparticles). Nevertheless, during the elaboration procedure, nanoparticle's suspensions were filtered through a 0.45 μm PVDF membrane filter in order to remove the larger aggregates. Regarding the surface charge, compact complexes were spontaneously formed as a consequence of the interaction between CS and TPP; hence, final formulations were measured by DLS, obtaining high positively ζ potential values (16.13 ± 1.67 mV) (see Table 1) due to the CS presence in the surface (44). This positively charged is desirable to prevent particle aggregation and promote electrostatic interaction with the overall cell membranes (negatively charged) (45).

On its behalf, CS/SBE-β-CD nanoparticles were developed under the assumption that these systems could be prepared in the absence of TPP, by only mixing CS with different amounts of SBE-β-CD, a negatively charged CD derivative, which could be more effectively incorporated into nanoparticles as a consequence of strong ionic interactions with the positively charged amino groups of the CS. The average size was 227.3 ± 20.52 nm. The polydispersity index (PDI) was found to be smaller than 0.3 (0.182 ± 0.07), indicating a relative homogeneity in the resulting formulation. The ζ potential studies of the nanoparticles showed high positive values (about 17.2 ± 1.25 mV), revealing that the NPs surface was mostly composed of CS (see Table 1).

USC DE COMPOSTELA

Table 1. Physicochemical characterization for blank and lactoferrin-loaded chitosan-based nanoparticles

Formulation	(LF) (mg/mL)	Size (nm)	PDI	ζ Potential (mV)
Blank CS/TPP NPs	-	160.56 ± 20.56	0.170 ± 0.067	16.13 ± 1.67
Blank CS/SBE-β-CD NPs	-	227.3 ± 20.52	0.182 ± 0.070	17.2 ± 1.25
Lactoferrin-loaded CS/TPP NPs	0.1	125.59 ± 10.01	0.244 ± 0.050	9.42 ± 0.76
	0.5	166.46 ± 42.27	0.287 ± 0.040	9.41 ± 1.90
	1.0	150.48 ± 13.44	0.294 ± 0.150	8.69 ± 1.36
Lactoferrin-loaded CS/SBE-β-CD NPs	0.1	221.83 ± 9.48	0.220 ± 0.038	15.53 ± 1.55
	0.5	242.01 ± 20.26	0.266 ± 0.040	16.62 ± 3.10
	1.0	196.07 ± 3.02	0.213 ± 0.014	14.54 ± 2.49

2.2. Morphological evaluation

SEM images were examined to demonstrate that the nanoparticle's size was maintained after the dehydration process. SEM analysis after the freeze-drying process confirmed the presence of monodisperse population of spherical-in-shape and irregular surface particles with size below 300 nm, although some aggregation phenomena due to the drying process was observed (see Figure S-4, Supporting Information). Thus, the freeze-dried formulations guaranteed the nanoscale size, where the microstructural analysis confirmed the morphology and size of the nanoparticles. These results were aligned with TEM morphological evaluation for both types of nanoparticles.

The TEM images provided information about the particle size and morphology of nanoparticles, as well as confirmed previous DLS measurements. The microstructural analysis confirmed that both types of nanoparticles were presented as a predominantly monodisperse population of isolated and spherical particles with well-defined, solid, and consistent structure (see Figure 3).

USC UNIVERSIDADE DE SANTIAGO DE COMPOSTELA

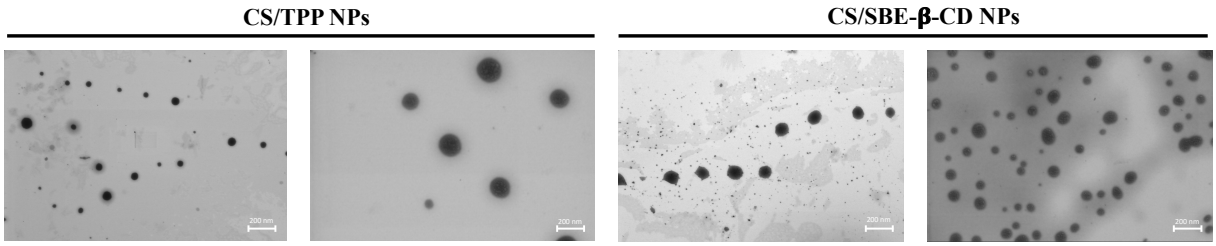


Figure 3. TEM images of chitosan-based nanoparticles.

A diameter interval of 103.7 ± 13.2 nm (CS/TPP NPs) and 185.0 ± 12.1 nm (CS/SBE-β-CD NPs) was obtained for the resulting nanoparticulate systems based on the TEM micrographs, smaller than the diameter determined by DLS. This could have been expected since the nanoparticles were dispersed in an aqueous phase for DLS analysis (CS swelling in water), while the TEM trials were performed in dry samples (46).

2.3. Production yield, encapsulation efficiency, and loading capacity of nanoparticles

Two different chitosan-based nanosystems were developed for protein encapsulation. It is known that chitosan in acidic media (pH 5) can interact with the negatively charged TPP or SBE-β-CD, forming inter- and intra-molecular cross-linkages, yielding ionically crosslinked chitosan-based nanoparticles (47).

Table 2 shows the production yield (PY), encapsulation efficiency (EE), and loading capacity (LC) values of the resulting lactoferrin-loaded CS/TPP and CS/SBE-β-CD nanoparticles. The encapsulation efficiency determination demonstrated that the elaboration process of lactoferrin-loaded CS/TPP and CS/SBE-β-CD nanoparticles was reproducible and efficient with production yield values above 31.53 ± 3.94% and 24.00 ± 2.69%, respectively (see Table 2). It must be considered that the drug:polymer ratio in this study ranged from 1:1 to 1:1.4. A directly proportional increase in the EE and LC values was observed with the increase in the amount of drug added into the formulation (e.g., 5:1 or 10:1 ratios). A two-way ANOVA analysis was applied to the resulting data in order to determine the existence of differences between CS/TPP and CS/SBE-β-CD nanoparticles. The results indicated that there were no significant differences in terms of PY, and between formulations with the same Lf concentration in terms of EE and LC, but significant differences ($p < 0.05$) were observed between increasing Lf-concentration formulations in terms of EE and LC.

Table 2. Production yield (PY), Encapsulation Efficiency (EE), and Loading Capacity (LC) values for chitosan-based nanoparticles.

Formulation	(Lf) (mg/mL)	Size (nm)	PY (%)	EE (%)	LC (%)
Blank CS/TPP NPs	-	130 ± 20.65	84.39 ± 2.65	-	-
Blank CS/SBE-β-CD NPs	-	227.28 ± 20.52	85.80 ± 3.42	-	-
Lactoferrin-loaded CS/TPP NPs	0.1	135.59 ± 10.01	85.89 ± 4.96	24.78 ± 3.60	12.39 ± 1.80
	0.5	146.46 ± 22.27	84.13 ± 2.96	34.85 ± 2.24	26.14 ± 1.68
	1.0	150.48 ± 13.44	84.19 ± 2.67	47.19 ± 2.97	43.47 ± 5.04
Lactoferrin-loaded CS/SBE-β-CD NPs	0.1	221.83 ± 19.48	83.86 ± 2.02	20.49 ± 6.00	11.18 ± 3.27
	0.5	242.01 ± 20.26	85.37 ± 3.51	38.67 ± 1.01	30.26 ± 0.79
	1.0	215.51 ± 18.77	84.91 ± 2.95	52.84 ± 1.05	43.44 ± 3.69

2.4. Effect of protein loading on size, surface charge, EE (%) and LC (%)

Lactoferrin, which shows an isoelectric point (Ip) around 7.28 (48), was directly added to the anionic solution (pH 9, where the protein would be positively charged) and then TPP or SBE-β-CD aqueous solutions were added drop wisely. As shown in Table 2, the presence of the model protein has a small influence on particle size. In order to point out, ζ potential values of both lactoferrin-loaded CS/TPP and CS/SBE-β-CD NPs were lower than blank formulations (see Table 2), suggesting that the protein could not be just encapsulated inside the nanosystems, but also attached to the nanoparticle's external shell, partly masking the CS's inherent positive charges. This finding is supported by the study carried out by Tantra el al. (49), where it is suggested that NPs external charges are influenced by the molecular organization of all the compounds at the NPs shell and the net constituted by the chemical positions.

Likewise, visual analysis of the resulting data (see Figure 4) seems to indicate that an upsurge in the EE and LC values is observed by increasing the amount of lactoferrin added to the formulation, but without significant modifications in size. A two-way ANOVA analysis confirmed this hypothesis, where statistically significant differences ($p < 0.05$) were observed

USC UNIVERSIDADE DE SANTIAGO DE COMPOSTELA

for both types of nanoparticles in terms of EE (%) and LC (%), but not in terms of size ($p > 0.05$). Thus, an increase in the initial amount of lactoferrin could improve EE and LC values in this kind of chitosan-based nanosystems.

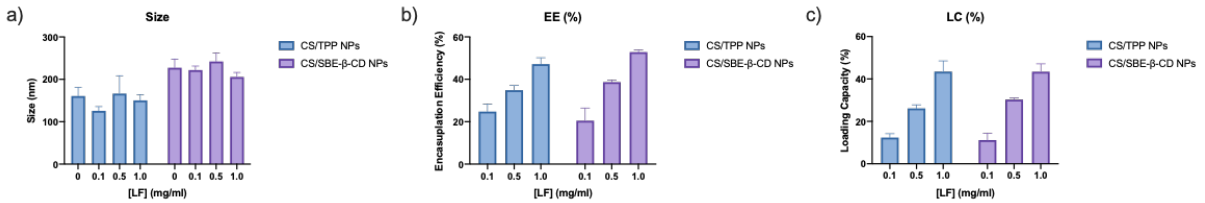


Figure 4. (a) Evolution of size (nm) over increased lactoferrin concentration for CS/TPP and CS/SBE-β-CD nanoparticles. PDI values were under 0.3 (from 0.194 to 0.244 for CS/TPP NPs, and from 0.213 to 0.287 for CS/SBE-β-CD NPs), associated with a uniform and monodisperse population. (b) EE (%) values over increased lactoferrin concentration for CS/TPP and CS/SBE-β-CD nanoparticles. (c) LC (%) values over increased lactoferrin concentration for CS/TPP and CS/SBE-β-CD nanoparticles.

A Dunnet's multiple comparisons test was also applied to assess the existence or absence of statistically significant differences in terms of size. No differences were observed for both types of formulations ($p > 0.05$). Similarly, a Tukey's multiple comparisons test was applied to evaluate the existence or absence of statistically significant differences in terms of EE (%) and LC (%), where statistically noteworthy variances were detected for both chitosan-based nanosystems ($p < 0.0001$) over the increased amount of incorporated lactoferrin.

3. Stability studies

3.1. Stability to storage

The short-term stability determination of CS/TPP and CS/SBE-β-CD nanoparticles was performed by determining the size, size distribution, and surface charge by keeping samples at three different temperature sets (4 ± 2°C, 25 ± 2°C/60 ± 5% RH and 37 ± 2°C/60 ± 5% RH) for 8 h, while the long-term stability study was carried out under the same conditions but for a 3-month period.

Previous studies have also shown the CDs role in the nanoparticle's stabilization. Certainly, β-CD derivatives have been widely used to improve the aqueous solubility and the chemical stability of different active substances, by forming host−guest complexes. This complexation

process usually leads to a modulation of the drug physicochemical properties of the guest molecule (i.e., solubility, ocular penetration, or stability) (50).

The results for the short-term stability study showed that both formulations (CS/TPP and CS/SBE-β-CD nanoparticles) did not suffer a significant change in their size following incubation for 8 h (data not shown, included into the long-term stability study; see Figure S-5, Supporting Information). Same results were observed for long-term stability over a 3-month period (see Figure 5).

Resulting data were analyzed and no changes in size were observed during the studied period, where size varied within an interval of less than 10% of the initial average size. A two-way ANOVA analysis was also applied, and no statistically significant differences ($p < 0.05$) were observed for the studied period. Thus, it can be concluded that both types of nanoparticles are stable over time.

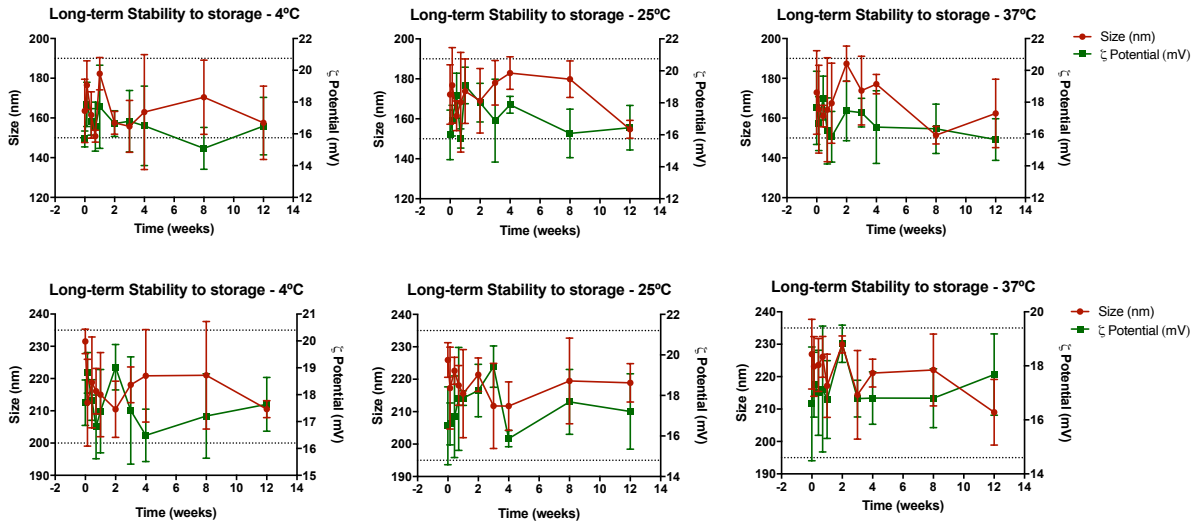


Figure 5. Long-term stability-to-storage study for CS/TPP and CS/SBE-β-CD NPs (up and down, respectively) over a 3-month period. Stripped lines show the 10% variation size interval from the initial mean size values, which comprises the nanoparticle stability range.

3.2. Stability to pH

Changes in the pH conditions of the media may be generally associated with nanoparticle's collapse, breakage, or coalescence phenomena. Figure 6 shows particle size and ζ potential changes of CS/TPP and CS/ SBE-β-CD nanoparticles for the tested pH interval.

A transition from positive to negative ζ potential values was gradually observed with increasing pH values. Nevertheless, no particle size changes were observed from pH 2 to 7, while aggregation phenomenon appears in basic pH range (up to pH 8). In order to point out, although topical ophthalmic formulations should have a pH value similar to the tear film (pH 7), the presence of salts, proteins, and others ocular substances, provides the ocular surface a buffering ability, increasing the pH interval that can be tolerated by the eye without causing ocular surface damages or tearing (pH interval: from 4 to 8) (51); hence, these formulations could be safely applied into the eye by topical ophthalmic administration.

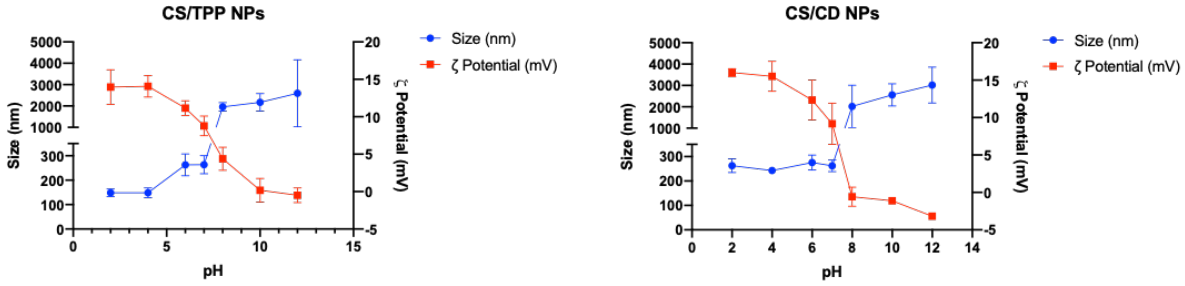


Figure 6. Changes in size and ζ potential values of CS/TPP and CS/SBE-β-CD NPs over the studied pH interval.

3.3. Stability to ionic strength

Changes in the ionic strength conditions of the media may be generally associated with nanoparticle's collapse, breakage, or coalescence phenomena. This statement is supported by the electrical double-layer theory, which explains a reduction in the thickness of the diffuse double layer with increasing ionic strength values (52). Thus, an increase in the particle-particle interaction leads to a rise in the nanoparticle's aggregation phenomenon.

The physical stability to ionic strength depends on possible time-dependent aggregation, flocculation, or sedimentation phenomena of the nanoparticles (53). Changes in the particle compactness over time may also influence either of these processes. Figure 7 shows the resulting data for the stability-to-ionic-strength study of CS/TPP and CS/SBE-β-CD NPs for the ionic strength tested interval.

Both CS/TPP and CS/SBE-β-CD NPs were in the nanometric size range for normal values of ionic strength in an ocular medium (from 0.075 to 0.15M). The colloidal stability of CS/TPP

nanoparticles was kept constant regardless of the increased ionic strength conditions of the media, although a ζ potential lowering was observed with the increasing salt concentration of the media. Indeed, as observed in Figure 7, CS/TPP formulations stored in the presence of NaCl were mostly stable with respect to changes in size, turbidity, and particle compactness over the studied period.

Nevertheless, a coalescence process was observed in the CS/SBE-β-CD NPs with increasing amounts of NaCl in the media. This phenomenon suggests that electrostatic repulsion is the predominant stabilization mechanism for this type of formulation. Aggregation process may be associated with the high concentration of monovalent ions (mainly Na^+) of the cyclodextrin formulation (~ 135 mOsm/kg, see SBE-β-CD technical sheet specifications), which in turn contributes to an increase in the final nanoparticle formulation osmolality. Even so, the CS/SBE-β-CD NPs remained stable over the normal ionic strength interval (0.075M to 0.15M), making them appropriate DDS for topical ophthalmic administration.

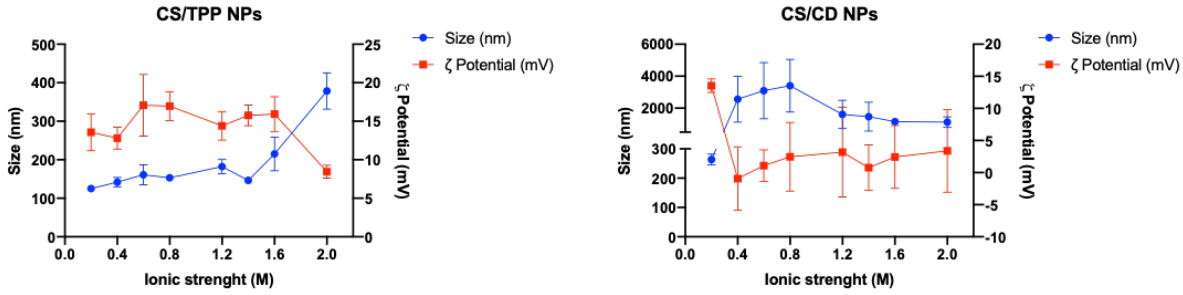


Figure 7. Changes in size and ζ potential values of CS/TPP and CS/SBE-β-CD NPs over the ionic strength studied interval.

4. *In vitro* release study

The preliminary *in vitro* release study from lactoferrin-loaded CS/TPP and CS/SBE-β-CD nanoparticles proves that both formulations present a sustained release pattern, compared to the control solution (Lf buffer solution) as shown in Figure 8. The *in vitro* protein release profiles obtained for each formulation showed two different release phases, as follows: (I) a first initial burst release due to the drug desorbed from the particles surface, and (II) a plateau release phase, resulting from the protein diffusion from the polymer matrix as a consequence of bioerosion processes.

USC UNIVERSIDADE DE SANTIAGO DE COMPOSTELA

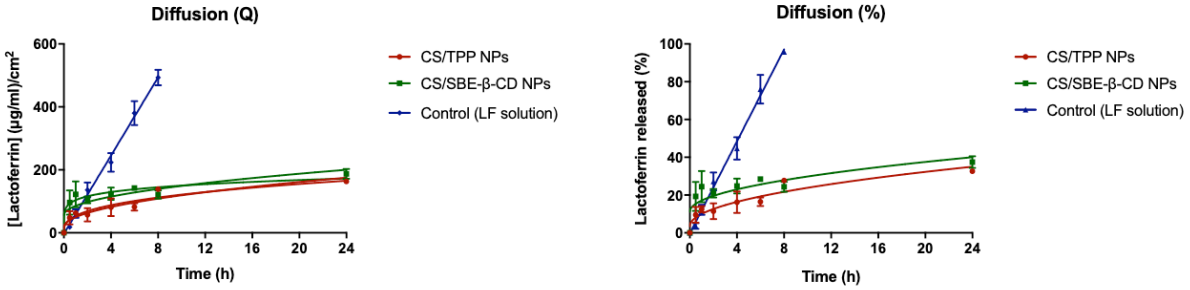


Figure 8. *In vitro* release study of CS/TPP and CS/SBE-β-CD NPs. The first graph shows the raw cumulative amount of lactoferrin released over time (h), while the second graph presents the cumulative percentage of lactoferrin released over time (h).

The resulting data from lactoferrin cumulative release from CS/TPP and CS/SBE-β-CD NPs were fitted to two different kinetic models (Higuchi and Peppas and Korsmeyer) in order to identify the release mechanism. The best correlation data was obtained with the Higuchi kinetic model, suggesting that diffusion was the main release mechanism (see details in Table 3).

Table 3. Release data of chitosan-based nanoparticles to the Higuchi diffusion kinetics and Peppas and Korsmeyer equation.

Formulation	Higuchi		Pepas and Korsmeyer		
	k ($mg \cdot cm^{-2} \cdot min^{-0.5}$)	R^2	k ($mg \cdot cm^{-2} \cdot min^{-n}$)	n	R^2
CS/TPP NPs	32.13	0.8663	52.50	0.3585	0.8451
CS/SBE-β-CD NPs	29.42	0.8245	102.7	0.1614	0.8211

5. Cytotoxicity analysis

5.1. Bovine Corneal Opacity and Permeability test (BCOP)

Endpoints measured during the BCOP test for both types of formulations were assessed in terms of opacity (determined by the amount of light transmission through the cornea by luxmetry and UV-Vis spectrophotometry) and permeability (determined by the amount of fluorescein that passes through the entire corneal tissue).

USC UNIVERSIDADE DE SANTIAGO

Firstly, opacity and permeability values were independently studied to evaluate whether formulations induce corrosivity or severe irritation (see Figure S-6, Supporting Information). Resulting data indicate that no significant structural changes were observed in terms of corneal opacity and fluorescein permeability, comparing them with the negative control solution (PBS and ethanol as negative and positive control solutions, respectively) (see Figure 9).

Likewise, opacity and permeability data were corrected for background or control values prior to further statistical determinations were calculated. The IVIS score was then calculated by combination of both types of empirically derived values for each formulation. Both formulations (CS/TPP and CS/SBE-β-CD NPs) resulted in an *in vitro* Irritation Score of 0 (IVIS = 0), showing no cytotoxicity effects compared to control formulations (see Figure 9).

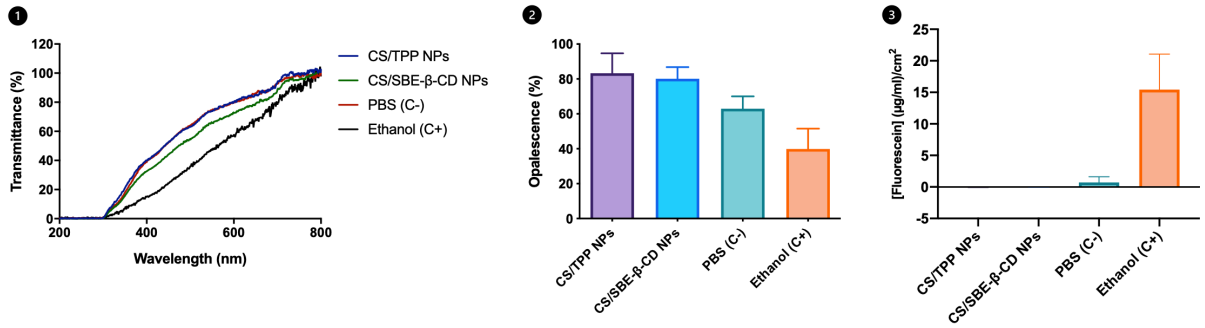


Figure 9. BCOP results for chitosan-based nanoparticles. (1) Resulting data of corneal transparency for both chitosan-based nanoparticles, compared to the results of the control solutions. (2) Opalescence data of corneal tissue after the administration of chitosan-based formulations, compared to control values. (3) Fluorescein corneal permeability for CS/TPP and CS/SBE-β-CD nanoparticles compared to the control solution results.

5.2. Hen's egg test on the chorioallantoic membrane (HET-CAM)

The CAM is a no innervated tissue and constitutes a well-developed vascularization model and an easy-to-study alternative strategy for ocular irritation assessment due to the complete inflammatory process response, similar to that induced in the Draize test, as it can be performed with greater efficiency and faster measurements than other *in vivo* tests (54). Thus, the HET-CAM assay was used to assess the cytotoxicity and biocompatibility of prepared nanoparticles. CS/TPP and CS/SBE-β-CD nanoparticles were evaluated, and the resulting data were compared with those obtained for the BSS and NaOH solutions, used as negative and positive control

USC UNIVERSIDADE DE SANTIAGO

formulations, respectively. All formulations show no cytotoxicity effects (Irritation Score = 0), comparing them with both control formulations (see Figure S-7, Supporting Information). This is in good agreement with previously published works (55), as well as in accordance with the results of the BCOP test, confirming that the materials used and the developed nanosystems are non-toxic and biocompatible.

6. Ocular surface mucoadhesion study

6.1. *In vitro* mucoadhesion study

Ocular mucus layer is a heterogeneous three-dimensional network composed of a mucin fiber's network where nanoparticles may diffuse through and be retained (56,57). Hence, the mucus layer can affect the stability of CS/TPP and CS/SBE-β-CD nanoparticles (58). Chitosan is a mucoadhesive polymer that may increase the residence time of the formulation, consequently improving the drug bioavailability (59). In this study, the interaction between mucin and CS/TPP and CS/SBE-β-CD nanoparticles was determined by DLS (60), evaluating the size and ζ potential changes before and after the nanoparticle/mucin interaction (61).

Figure 10 shows the size and ζ potential values for CS/TPP and CS/SBE-β-CD nanoparticles, before and after the incubation in the mucin suspensions. The increased size after the incubation procedure suggests that the interaction between mucin and CS/TPP or CS/SBE-β-CD nanoparticles led to the formation of nanoaggregates and a decrease in ζ potential values, probably due to the electrostatic interaction between positively charged amino groups of chitosan and the negatively charged groups of mucin (61). Furthermore, a strong ability of CS/TPP and CS/SBE-β-CD nanoparticles to interact with mucin through electrostatic forces was observed, highlighting their potential as mucoadhesive drug delivery systems (34).

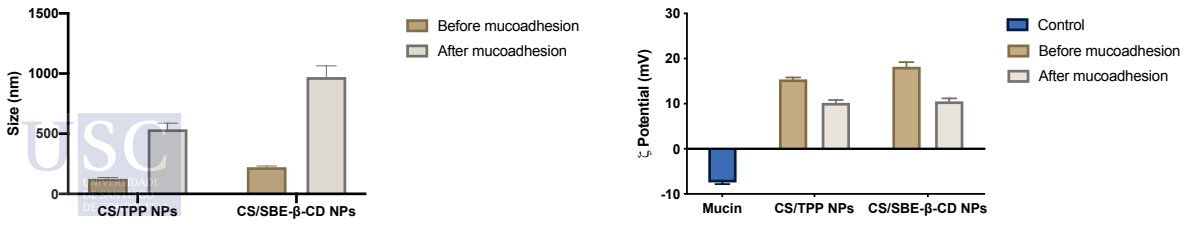


Figure 10. Changes in size and ζ potential values for chitosan-based nanoparticles during the *in vitro* ocular surface retention study.

6.2. *Ex vivo* corneal mucoadhesion study

Mucin layer in the corneal surface is a key factor that must be considered in the design and development of pharmaceutical forms intended for the topical ophthalmic administration. Figure 11 shows the mucoadhesion variation for both types of chitosan-based nanoparticles in terms of the difference in the fluorescein concentration before and after the *ex vivo* ocular surface retention study.

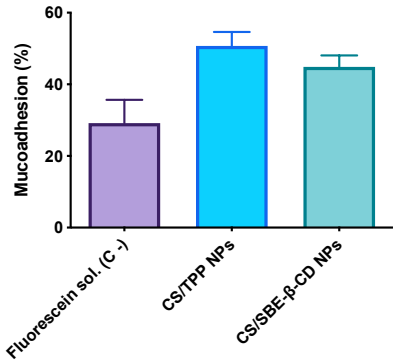


Figure 11. Mucoadhesion values (%) for chitosan-based nanoparticles during the *ex vivo* ocular surface retention study.

It was found that mucoadhesive properties of chitosan-based formulations were greater in the *in vitro* studies than *ex vivo* studies. This may be since formulations were instilled in a single administration during the *ex vivo* study, reducing the contact time between the formulation and the mucin layer, compared to the *in vitro* ocular surface retention study, where formulations were kept in contact with the mucin solution for a predetermined time. Thus, a reduction in the mucoadhesive strength of nanoparticles was observed.

In addition, a one-way ANOVA analysis was applied, and statistically significant differences ($p < 0.05$) were observed by comparing the resulting data obtained for both formulations with the control fluorescein solution.

6.3. *In vivo* ocular surface permanence study

USC UNIVERSIDADE DE SANTIAGO

6.3.1. Evaluation of the radiolabeling stability and efficiency of chitosan-based nanoparticles

Figure S-8 (Supporting Information) shows the ^{18}F-FDG or ^{18}F-Choline radiolabeling stability and efficiency for chitosan-based nanoparticles, respectively. As presented, ^{18}F-FDG chitosan-

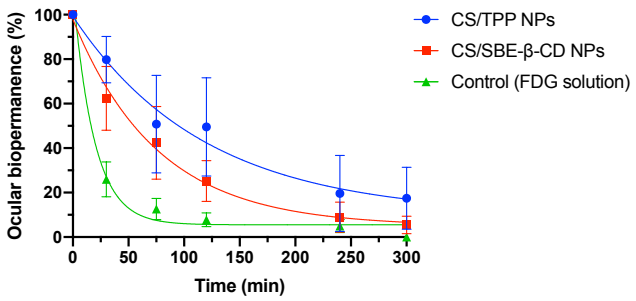
based nanoparticles showed a high radiolabeling efficiency (up to 70%) and great stability along the studied period (up to 3h), while ^{18}F-Choline radiolabeling efficiency was lower (around 20%) but maintaining stability over time.

It must be taken into account that ^{18}F-Choline radiolabeling efficiency increased over time (from 10 to 25%), possibly due to the fact that more incubation time is needed for the radiolabeling process to take place. Based on these results, ^{18}F-FDG was selected as the radiotracer for further *in vivo* radiolabeling assays.

6.3.2. Experimental in vivo evaluation of the residence time on the ocular surface

Figure 12 shows the ^{18}F-FDG-radiolabeled chitosan-based ocular biopermanence along the studied interval, compared to a control solution (^{18}F-FDG aqueous buffered solution, pH 7.4). The ocular permanence of both chitosan-based nanoparticles was characterized on male rats by ^{18}F-FDG radiolabeling, followed by the radioactivity assessment in a microPET system over a 5 h (300 min) period. It is a useful and non-invasive technique employed in the determination of the pharmacokinetic profiles of topical ophthalmic DDS (38,62,63).

In the present study, a higher residence time was observed for both types of nanoparticles, compared to the control solution, despite the fact that all formulations showed a composition close to the tears. The resulting data was properly fitted to a monoexponential decay profile using a single compartmental model ($R^2 = 0.9813$ for CS/TPP NPs, $R^2 = 0.9935$ for CS/SBE-β-CD NPs, and $R^2 = 0.9930$ for ^{18}F-FDG control solution) (see Figure 12). These results support the idea that both formulations exhibit good mucoadhesive, headline penetration and, presumably, direct cell uptake properties, being in good agreement with the PET data described in previous studies (39-41).



USC UNIVERSIDADE DE SANTIAGO DE COMPOSTELA

Figure 12. ^{18}F-FDG radiolabeled chitosan-based NPs clearance ratio (%) from the ocular surface determined by PET, compared to a control solution (^{18}F-FDG buffered aqueous solution). Ocular biopermanence (%) remaining on the ocular surface over time was calculated assuming initial biopermanence value (%) recorded in the ROI.

Table 4 shows the pharmacokinetics parameters ($t_{1/2}$, MRT, and k) of the ^{18}F-FDG radiolabeled chitosan-based nanoparticles and ^{18}F-FDG control formulations. Statistically significant differences ($p < 0.05$) were observed between both types of formulation compared to the control solution in terms of diffusion coefficient (k, min^{-1}) and half-life time ($t_{1/2}$, min), but no differences between both chitosan-based nanoparticle formulations. Similar behavior was also observed for MRT, AUC, and % dose 30 min parameters.

Table 4. Release data of chitosan-based nanoparticles into the diffusion

Formulation	K (min^{-1})		$t_{1/2}$ (min)		MRT (min)		AUC		% dose 30 min	
	Mean	SD	Mean	SD	Mean	SD	Mean	SD	Mean	SD
CS/TPP NPs	0.008	0.005	114.4	72.0	127.3	47.1	17114	9874.0	79.8	10.5
CS/SBE-β-CD NPs	0.013	0.005	60.5	20.1	89.9	13.7	9316	2553.7	62.4	14.3
^{18}F-FDG Control solution	0.041	0.012	17.7	4.5	59.1	17.6	4131	919.9	26.0	7.8

Both types of nanoparticles show greater biopermanence than the control formulation. However, the apparent lower ocular permanence of the CS/SBE-β-CD NPs observed in the monoexponential decay curve shown in Figure 12 may be associated with their more sensitivity to the presence of salts in the tear film that produces a decrease of the NP surface charge with a possible increase in the aggregation phenomena, causing a slight decrease in the adherence to the corneal mucous layer.

USC UNIVERSIDADE DE SANTIAGO DE COMPOSTELA

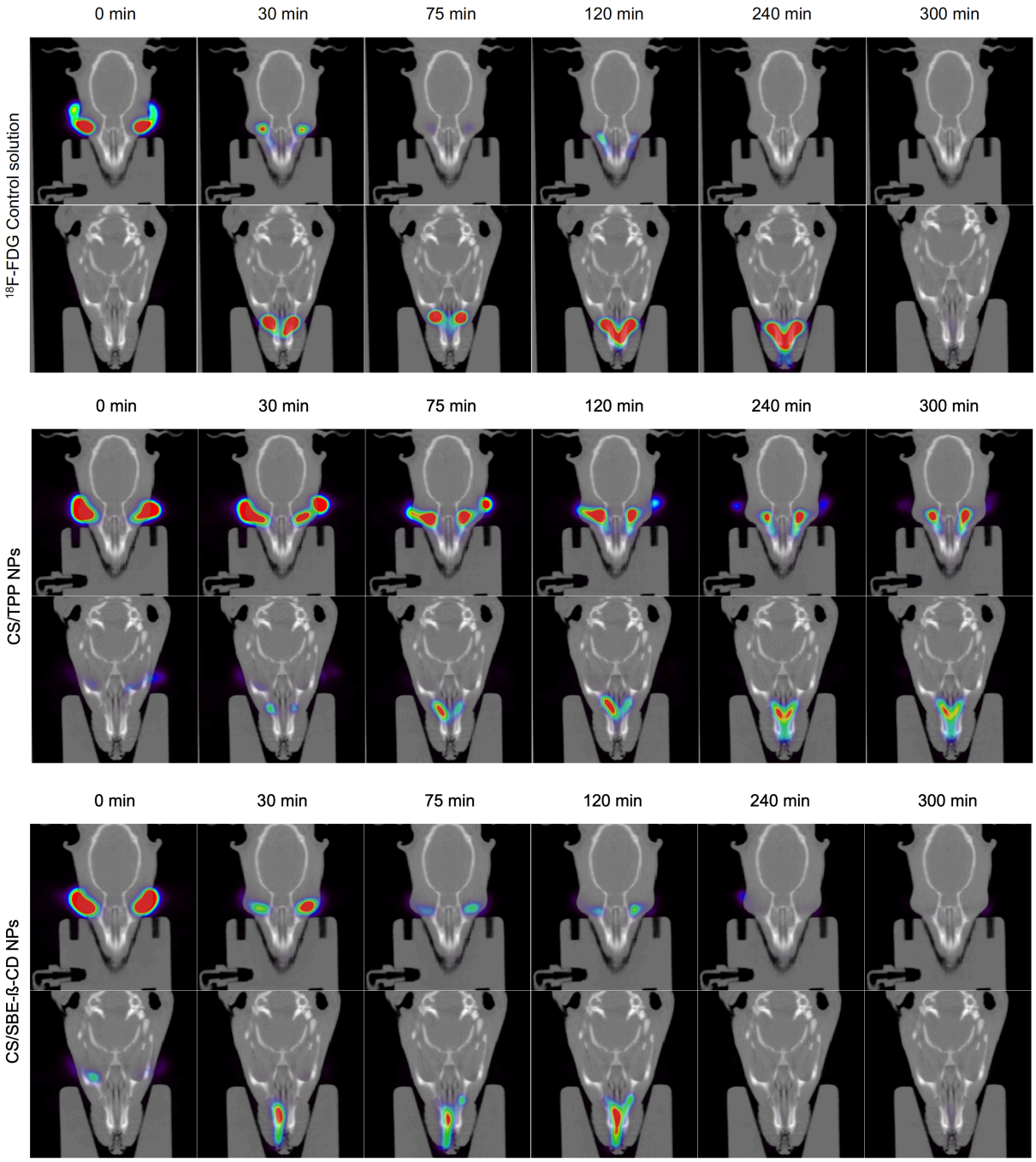


Figure 13. Fused PET/CT images displayed in coronal plane representing rat's eye and nasolacrimal duct at different time points (0, 30, 75, 120, 240 and 300 min) post-administration.

CONCLUSION

The preparation of CS/TPP and CS/SBE-β-CD nanoparticles by ionotropic gelation is highly sensitive to numerous environmental variables, as well as component and process conditions. The elaboration process of both types of nanoparticles involves several critical parameters,

including the optimization of chitosan's, TPP's or SBE-β-CD's concentration, pH, and ionic strength of the media or CS/TPP or CS/SBE-β-CD ratio, among others, in order to obtain stable nanoparticles of tunable size and charge (64,65).

In the present work, low molecular weight chitosan with highest degree of deacetylation was selected and novel ionic crosslinked nanoparticles composed of CS/TPP and CS/SBE-β-CD loaded with lactoferrin were successfully prepared. An average particle size of 160.56 ± 20.65 nm and 227.3 ± 20.52 nm, as well as a surface potential of 16.13 ± 1.67 mV and 17.2 ± 1.25 mV were obtained for CS/TPP and CS/SBE-β-CD nanoparticles, respectively. Both formulations were spherical in shape and irregular surface with size below 300 nm.

Similarly, both formulations show good stability to storage for, at least, three months, as well as no particle size changes were observed from pH 2 to 7 interval and were in the nanometric size range for normal values of ionic strength in an ocular medium (from 0.075 to 0.15M). A controlled release of lactoferrin was also achieved from both types of nanoparticles, confirming their use as potential drug delivery systems for protein drugs.

Results also demonstrated mucoadhesive nanoparticles without relevant cytotoxicity. A strong ability of CS/TPP and CS/SBE-β-CD nanoparticles to interact with mucin through electrostatic forces was observed, showing a higher ocular retention profile for, at least, 240 min.

In conclusion, it is proposed, for the first time, two different chitosan-based formulations as biodegradable mucoadhesive nanocarriers for delivery of lactoferrin. This is supported by extensive *in vitro* and *in vivo* characterization studies. A preclinical consistent basis was achieved for the first pharmacological treatment for keratoconus as an alternative to the current invasive clinical methods, since there are no therapeutic alternatives, only existing non-pharmacological (use of contact lenses or glasses) or surgical procedures as palliative or supportive treatments.

Analogously, both types of nanoparticles show appropriate physicochemical properties suitable for topical ophthalmic administration, supporting the idea that they are retained in the corneal layer, prolonging the drug release time from the tissue itself, something that may guarantee the patient's adherence to the treatment, since a lower dosage frequency would be required. Furthermore, the versatility of these systems would allow including them in different pharmaceutical forms for ophthalmic administration based on the requirements and characteristics of the patient, as a new way to partially personalize and individualize the therapeutic strategy. Nevertheless, a better correlation with *in vivo* data should be profoundly

USC DE SANTIAGO DE COMPOSTELA

explored in order to deeply understand the real potential of these nanocarriers as a topical ophthalmic alternative strategy for the prevention and treatment of keratoconus.

REFERENCES

1. Patel A, Cholkar K, Agrahari V, Mitra AK. Ocular drug de-livery systems: An overview. World J Pharmacol. 2013;2(2):47–64.

2. Kammona O, Kiparissides C. Recent advances in nanocarrier-based mucosal delivery of biomolecules. J Control Release Off J Control Release Soc. 2012 Aug 10;161(3):781–94.

3. Trapani A, Garcia-Fuentes M, Alonso MJ. Novel drug nanocarriers combining hydrophilic cyclodextrins and chitosan. Nanotechnology. 2008 May 7;19(18):1851-01.

4. Kymes SM, Walline JJ, Zadnik K, Sterling J, Gordon MO, Collaborative Longitudinal Evaluation of Keratoconus Study Group. Changes in the quality-of-life of people with kerato-conus. Am J Ophthalmol. 2008 Apr;145(4):611–7.

5. Godefrooij DA, de Wit GA, Uiterwaal CS, Imhof SM, Wisse RPL. Age-specific Incidence and Prevalence of Keratoconus: A Nationwide Registration Study. Am J Ophthalmol. 2017 Mar;175:169–72.

6. Romero-Jiménez M, Santodomingo-Rubido J, Wolffsohn JS. Keratoconus: a review. Contact Lens Anterior Eye J Br Con-tact Lens Assoc. 2010 Aug;33(4):157–66.

7. Meiri Z, Keren S, Rosenblatt A, Sarig T, Shenhav L, Varssano D. Efficacy of Corneal Collagen Cross-Linking for the Treatment of Keratoconus: A Systematic Review and Meta-Analysis. Cornea. 2016 Mar;35(3):417–28.

8. Sharif R, Bak-Nielsen S, Hjortdal J, Karamichos D. Pathogenesis of Keratoconus: The intriguing therapeutic potential of Prolactin-inducible protein. Prog Retin Eye Res. 2018 Nov;67:150–67.

9. Lema I, Brea D, Rodríguez-González R, Díez-Feijoo E, Sobrino T. Proteomic analysis of the tear film in patients with keratoconus. Mol Vis. 2010 Oct 13;16:2055–61.

10. Hayashida K, Kaneko T, Takeuchi T, Shimizu H, Ando K, Harada E. Oral administration of lactoferrin inhibits inflammation and nociception in rat adjuvant-induced arthritis. J Vet Med Sci. 2004 Feb;66(2):149–54.

11. Pattamatta U, Willcox M, Stapleton F, Cole N, Garrett Q. Bovine lactoferrin stimulates human corneal epithelial alkali wound healing in vitro. Invest Ophthalmol Vis Sci. 2009 Apr;50(4):1636–43.

USC DE SANTIAGO DE COMPOSTELA

12. Flanagan JL, Willcox MDP. Role of lactoferrin in the tear film. Biochimie. 2009 Jan;91(1):35–43.
13. Sobrino T, Regueiro U, Malfeito M, Vieites-Prado A, Pérez-Mato M, Campos F, Lema I. Higher Expression of Toll-Like Receptors 2 and 4 in Blood Cells of Keratoconus Patiens. Sci Rep. 2017 Oct 11;7(1):1–7.
14. Gesto MIL, Sánchez JAC, Moreiras TS, Perez FC. Biomarkers for diagnosis and prognosis of corneal ectatic disorders.
15. Charalel RA, Engberg K, Noolandi J, Cochran JR, Frank C, Ta CN. Diffusion of protein through the human cornea. Ophthalmic Res. 2012;48(1):50-55.
16. Serno T, Geidobler R, Winter G. Protein stabilization by cyclodextrins in the liquid and dried state. Adv Drug Deliv Rev. 2011 Oct 1;63(13):1086–106.
17. Kawashima Y, Tetsuro H, Akihiro K, Hideo T, Shan Yang L. The effect of thickness and hardness of the coating film on the drug release of theophylline granules. Chem. Pharm Bull. 1985; 33:2469–2474.
18. Zhang P, Liu X, Hu W, Bai Y, Zhang L. Preparation and evaluation of naringenin-loaded sulfobutylether-β-cyclodextrin/chitosan nanoparticles for ocular drug delivery. Carbohydr Polym. 2016 20;149:224–30.
19. Jithan A, Madhavi K, Madhavi M, Prabhakar K. Preparation and characterization of albumin nanoparticles encapsulating curcumin intended for the treatment of breast cancer. Int J Pharm Invetig. 2011;1(2):119–25.
20. Morris G, Castile J, Smith A, Adams G, Harding SE. The effect of prolonged storage at different temperatures on the particle size distribution of tripolyphosphate (TPP)-chitosan nanoparticles. Carbohydr Polym. 2011 Apr;84(4):1430–4.
21. Q 1 A (R2) Stability Testing of new Drug Substances and Products. 2006;20.
22. Chidambaram N, Burgess DJ. A novel in vitro release method for submicron-sized dispersed systems. AAPS PharmSci. 1999 Aug 31;1(3):32–40.
23. Muthu MS, Singh S. Poly (D, L-lactide) nanosuspensions of risperidone for parenteral delivery: formulation and in-vitro evaluation. Curr Drug Deliv. 2009 Jan;6(1):62–8.
24. Orthner MP, Lin G, Avula M, Buetefisch S, Magda J, Rieth LW, Solzbacher F. Hydrogel based sensor arrays (2 × 2) with perforated piezoresistive diaphragms for metabolic monitoring (in vitro). Sens Actuators B Chem. 2010 Mar 19;145(2):807–16.

USC UNIVERSIDADE DE SANTIAGO

25. Chamberlain M, Gad SC, Gautheron P, Prinsen MK. IRAG working group 1. Organotypic models for the assessment/prediction of ocular irritation. Interagency Regulatory Alternatives Group. Food Chem Toxicol Int J Publ Br Ind Biol Res Assoc. 1997 Jan;35(1):23–37.
26. Loprieno N. Alternative Methodologies for the Safety Evaluation of Chemicals in the Cosmetic Industry. CRC Press; 2019. 233 p.
27. Salem H, Katz SA. Alternative Toxicological Methods. CRC Press; 2003. 618 p.
28. Eskes C, Bessou S, Bruner L, Curren R, Harbell J, Jones P, Kreiling R, Liebsch M, McNamee P, Pape W, Prinsen MK, Seidle T, Vanparys P, Worth A, Zuang V. 3.3. Eye Irritation. Alternatives to Laboratory Animals. 2005; 33, 47–81.
29. Wallig MA, Haschek WM, Rousseaux CG, Bolon B, edi-tors. Chapter 22 - Special Senses. In: Fundamentals of Toxicologic Pathology (Third Edition) (Internet). Academic Press; 2018 (cited 2020 Mar 21). p. 673–747.
30. Luepke NP. Hen's egg chorioallantoic membrane test for irritation potential. Food Chem Toxicol Int J Publ Br Ind Biol Res Assoc. 1985 Feb;23(2):287–91.
31. Kalweit S, Besoke R, Gerner I, Spielmann H. A national vali-dation project of alternative methods to the Draize rabbit eye test. Toxicol Vitro Int J Publ Assoc BIBRA. 1990;4(4–5):702–6.
32. Spielmann H, Kalweit S, Liebsch M, Wirnsberger T, Gerner I, Bertram-Neis E, Krauser K, Kreiling R, Miltenburger HG, Pape W, Steiling W. Validation study of alternatives to the Draize eye irritation test in Germany: Cytotoxicity testing and HET-CAM test with 136 industrial chemicals. Toxicol Vitro Int J Publ Assoc BIBRA. 1993 Jul;7(4):505–10.
33. Collado-González M, González Espinosa Y, Goycoolea FM. Interaction Between Chitosan and Mucin: Fundamentals and Applications. Biomimetics (Internet). 2019 Apr 25.
34. Mazzarino L, Travelet C, Ortega-Murillo S, Otsuka I, Pig-not-Paintrand I, Lemos-Senna E, Borsali R. Elaboration of chitosan-coated nanoparticles loaded with curcumin for mu-coadhesive applications. J Colloid Interface Sci. 2012 Mar 15;370(1):58–66.
35. Belgamwar V, Shah V, Surana SJ. Formulation and evaluation of oral mucoadhesive multiparticulate system containing metoprolol tartarate: an in vitro-ex vivo characterization. Curr Drug Deliv. 2009 Jan;6(1):113–21.
36. Rojas S, Gispert JD, Abad S, Buaki-Sogo M, Victor VM, Garcia H, Herance JR. In vivo biodistribution of amino-functionalized ceria nanoparticles in rats using positron emission tomography. Mol Pharm. 2012 Dec 3;9(12):3543–50.

USC UNIVERSIDADE DE SANTIAGO DE COMPOSTELA

37. Pérez-Campaña C, Gómez-Vallejo V, Martin A, Sebastián ES, Moya SE, Reese T, Ziolo R, Llop J. Tracing nanoparticles in vivo: a new general synthesis of positron emitting metal oxide nanoparticles by proton beam activation. Analyst. 2012 Oct 1;137(21):4902–6.
38. Fernández-Ferreiro A, Silva-Rodríguez J, Otero-Espinar FJ, González-Barcia M, Lamas MJ, Ruibal A, Luaces-Rodriguez A, Vieites-Prado A, Sobrino T, Herranz, M., García-Varela L, Blanco-Mendez J, Gil-Martínez M, Pardo M, Moscoso A, Medín-Aguerre S, Pardo-Montero J, Aguiar P. Positron Emission Tomography for the Development and Characterization of Corneal Permanence of Ophthalmic Pharmaceutical Formulations. Invest Ophthalmol Vis Sci. 2017 01;58(2):772–80.
39. The Association for Research in Vision and Ophthalmology Statement for the Use of Animals in Ophthalmic and Vision Research (Internet).
40. Burden N, Aschberger K, Chaudhry Q, Clift MJD, Doak SH, Fowler P, Johnston H, Landsiedel R, Rowland J, Sotne V. The 3Rs as a framework to support a 21st century approach for nanosafety assessment. Nano Today. 2017 Feb 1;12:10–3.
41. Loening AM, Gambhir SS. AMIDE: a free software tool for multimodality medical image analysis. Mol Imaging. 2003 Jul;2(3):131–7.
42. Zhang Y, Huo M, Zhou J, Xie S. PKSolver: An add-in pro-gram for pharmacokinetic and pharmacodynamic data analysis in Microsoft Excel. Comput Methods Programs Biomed. 2010 Sep;99(3):306–14.
43. Csaba N, Garcia-Fuentes M, Alonso MJ. The performance of nanocarriers for transmucosal drug delivery. Expert Opin Drug Deliv. 2006 Jul;3(4):463–78.
44. Oyarzun-Ampuero FA, Brea J, Loza MI, Torres D, Alonso MJ. Chitosan-hyaluronic acid nanoparticles loaded with heparin for the treatment of asthma. Int J Pharm. 2009 Nov 3;381(2):122–9.
45. Schiffelers RM, Woodle MC, Scaria P. Pharmaceutical prospects for RNA interference. Pharm Res. 2004 Jan;21(1):1–7.
46. Aktaş Y, Andrieux K, Alonso MJ, Calvo P, Gürsoy RN, Couvreur P, Capan Y. Preparation and in vitro evaluation of chitosan nanoparticles containing a caspase inhibitor. Int J Pharm. 2005 Jul 25;298(2):378–83.
47. Mahmoud AA, El-Feky GS, Kamel R, Awad GEA. Chitosan/sulfobutylether-β-cyclodextrin nanoparticles as a potential approach for ocular drug delivery. Int J Pharm. 2011 Jul 15;413(1–2):229–36.

USC UNIVERSIDADE DE SANTIAGO

48. Sohrabi SM, Niazi A, Chahardoli M, Hortamani A, Se-toodeh P. In silico investigation of lactoferrin protein characterizations for the prediction of anti-microbial properties. Mol Biol Res Commun. 2014 Jun;3(2):85–100.
49. Tantra R, Tompkins J, Quincey P. Characterisation of the de-agglomeration effects of bovine serum albumin on nanoparticles in aqueous suspension. Colloids Surf B Biointerfaces. 2010 Jan 1;75(1):275–81.
50. Krauland AH, Alonso MJ. Chitosan/cyclodextrin nanoparticles as macromolecular drug delivery system. Int J Pharm. 2007 Aug 1;340(1–2):134–42.
51. Abdelkader H, Fathalla Z, Moharram H, Ali TFS, Pierscion-ek B. Cyclodextrin Enhances Corneal Tolerability and Reduc-es Ocular Toxicity Caused by Diclofenac. Oxid Med Cell Longev. 2018;2018:52609-76.
52. Partheniades E. Chapter 3 - Forces between Clay Particles and the Process of Flocculation. In: Partheniades E, editor. Cohesive Sediments in Open Channels (Internet). Boston: Butter-worth-Heinemann; 2009 (cited 2020 Jun 24). p. 47–88.
53. Sreekumar S, Goycoolea FM, Moerschbacher BM, Rivera-Rodriguez GR. Parameters influencing the size of chitosan-TPP nano- and microparticles. Sci Rep. 2018 Dec;8(1):46-95.
54. Saw CLL, Heng PWS, Liew CV. Chick Chorioallantoic Membrane as an In Situ Biological Membrane for Pharmaceutical Formulation Development: A Review. Drug Dev Ind Pharm. 2008 Jan 1;34(11):1168–77.
55. Kean T, Thanou M. Biodegradation, biodistribution and toxicity of chitosan. Adv Drug Deliv Rev. 2010 Jan 31;62(1):3–11.
56. Olmsted SS, Padgett JL, Yudin AI, Whaley KJ, Moench TR, Cone RA. Diffusion of macromolecules and virus-like particles in human cervical mucus. Biophys J. 2001 Oct;81(4):1930–7.
57. das Neves J, Bahia MF, Amiji MM, Sarmento B. Mucoadhesive nanomedicines: characterization and modulation of mucoadhesion at the nanoscale. Expert Opin Drug Deliv. 2011 Aug;8(8):1085–104.
58. de Campos AM, Diebold Y, Carvalho ELS, Sánchez A, Alonso MJ. Chitosan nanoparticles as new ocular drug delivery systems: in vitro stability, in vivo fate, and cellular toxicity. Pharm Res. 2004 May;21(5):803–10.
59. Sarmento B, das Neves J. Chitosan-Based Systems for Biopharmaceuticals: Delivery, Targeting and Polymer Therapeutics (Internet). (cited 2020 Mar 24).

USC UNIVERSIDADE DE SANTIAGO

60. Takeuchi H, Thongborisute J, Matsui Y, Sugihara H, Yamamoto H, Kawashima Y. Novel mucoadhesion tests for polymers and polymer-coated particles to design optimal mucoadhesive drug delivery systems. Adv Drug Deliv Rev. 2005 Nov 3;57(11):1583–94.
61. Jintapattanakit A, Junyaprasert VB, Kissel T. The role of mucoadhesion of trimethyl chitosan and PEGylated trimethyl chitosan nanocomplexes in insulin uptake. J Pharm Sci. 2009 Dec 1;98(12):4818–30.
62. Allmeroth M, Moderegger D, Gündel D, Buchholz H-G, Mohr N, Koynov K, Rösch F, Thews O, Zentel R. PEGylation of HPMA-based block copolymers enhances tumor accumulation in vivo: A quantitative study using radiolabeling and positron emission tomography. J Controlled Release. 2013 Nov;172(1):77–85.
63. Varela-Fernández R, Díaz-Tomé V, Luaces-Rodríguez A, Con-de-Penedo A, García-Otero X, Luzardo-Álvarez A, Fernández-Ferreiro A, Otero-Espinar FJ. Drug Delivery to the Posterior Segment of the Eye: Biopharmaceutic and Pharmaco-kinetic Considerations. Pharmaceutics. 2020 Mar 16;12(3): 269.
64. Fàbregas A, Miñarro M, García-Montoya E, Pérez-Lozano P, Carrillo C, Sarrate R, Sánchez N, Ticó JR, Suñé-Negre JM. Impact of physical parameters on particle size and reaction yield when using the ionic gelation method to obtain cationic polymeric chitosan-tripolyphosphate nanoparticles. Int J Pharm. 2013 Mar 25;446(1–2):199–204.
65. Morris GA, Castile J, Smith A, Adams GG, Harding SE. The effect of prolonged storage at different temperatures on the particle size distribution of tripolyphosphate (TPP) – chitosan nanoparticles. Carbohydr Polym. 2011 Apr 2;84(4):1430–4.

USC
UNIVERSIDADE DE SANTIAGO DE COMPOSTELA

SUPPLEMENTARY INFORMATION

1. Experimental methods

1.1. Mucoadhesion study

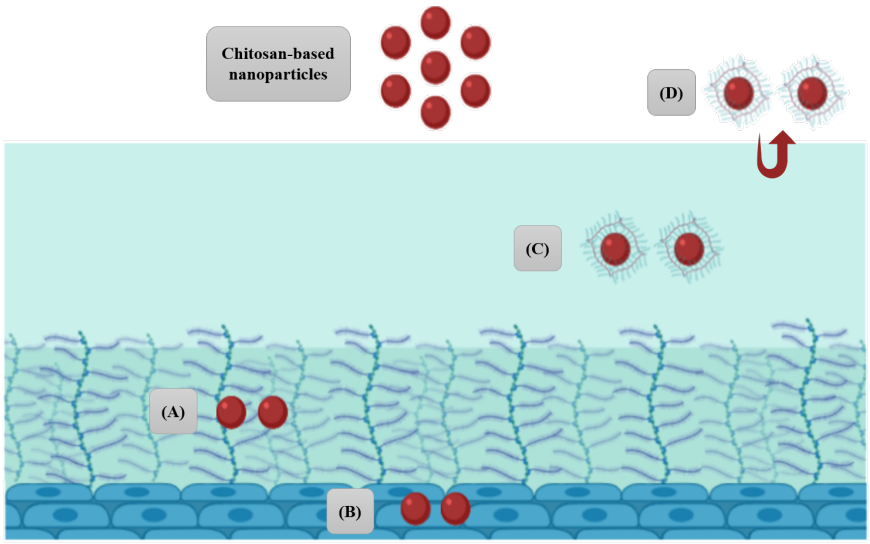


Figure S-1. Different approaches of the interaction between chitosan-based nanoparticles and the ocular mucin layer. (A) adsorption of the nanoparticles to the mucus layer, (B) passage through the mucin layer and reach the cornea, (C) loss of functionality of the nanoparticles when covered by mucin, or (D) nanoparticle's removal with the mucus layer renewal.

2. Results and discussion

2.1. Screening study: CS/TPP and CS/SBE-β-CD nano-particles formation.

2.1.1. Preparation of CS/TPP nanoparticles

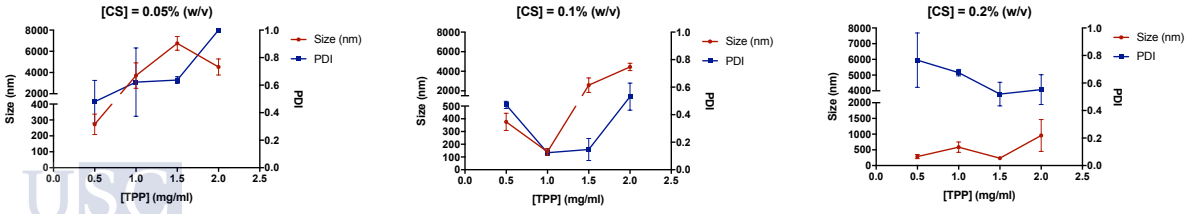


Figure S-2. Changes in size and PDI values during the optimization procedure of CS/TPP nanoparticles.

2.1.2. Preparation of CS/SBE-β-CS nanoparticles

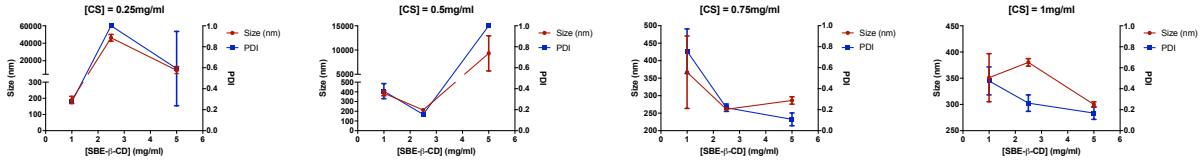


Figure S3. Changes in size and PDI values during the optimization procedure of CS/SBE-β-CD nanoparticles.

2.2. Morphological evaluation

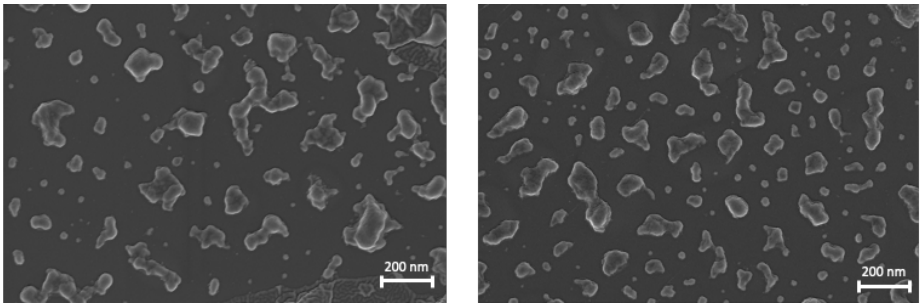


Figure S-4. SEM images of chitosan-based nanoparticles (CS/TPP NPs and CS/SBE-β-CD NPs, respectively).

2.3. Stability studies

2.3.1. Stability to storage

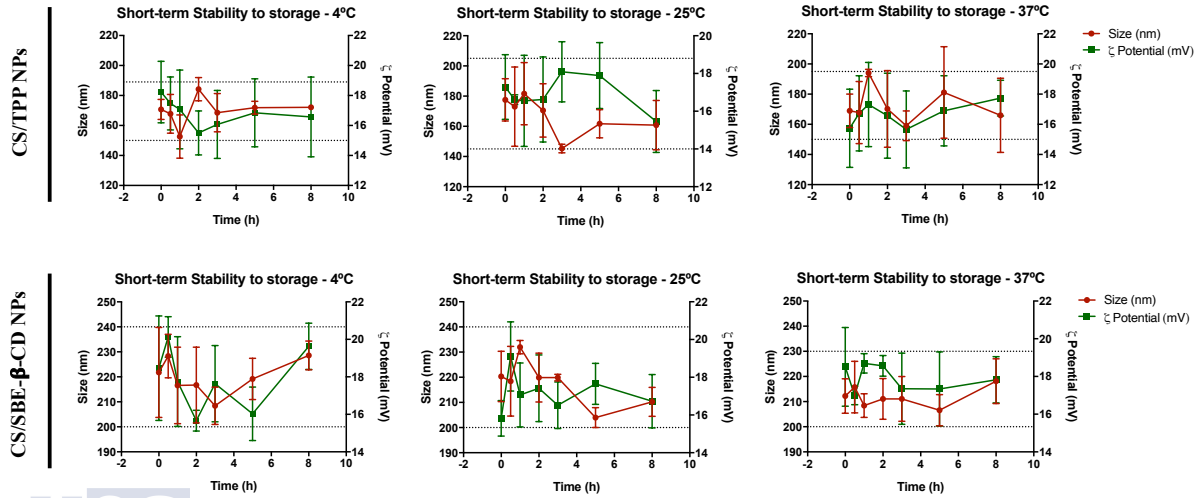


Figure S-5. Long-term stability-to-storage study for CS/TPP and CS/SBE-β-CD NPs (up and down, respectively) over a 3-month period. Stripped lines show the 10% variation size interval from the initial size values, which comprises the nanoparticle stability range.

USC UNIVERSIDADE DE SANTIAGO

2.4. Cytotoxicity analysis

2.4.1. Bovine Corneal Opacity and Permeability test (BCOP)

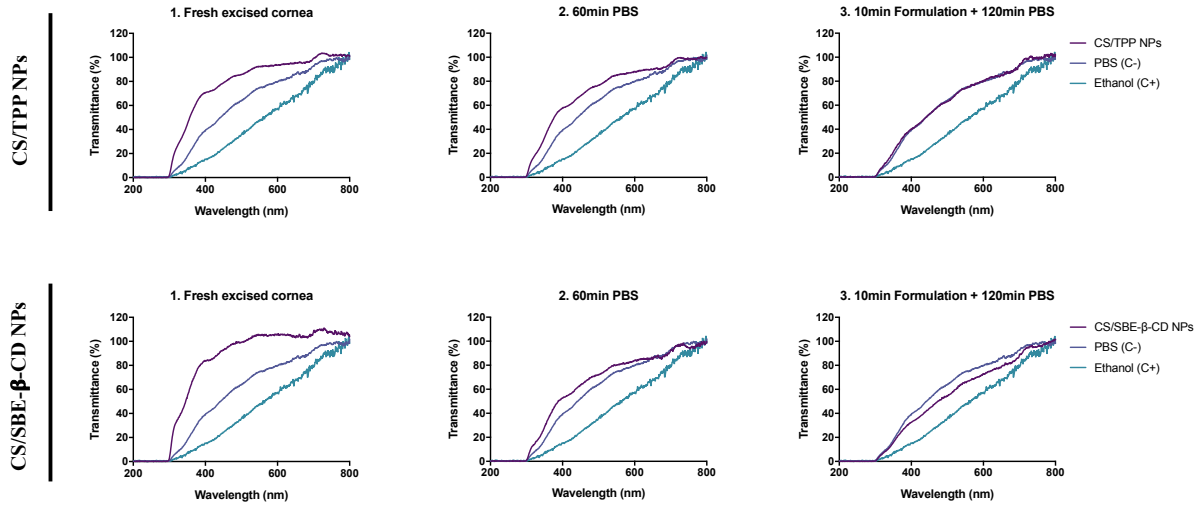


Figure S-6. BCOP results for chitosan-based nanoparticles. (I) Evolution of corneal transparency for CS/TPP nanoparticles over time during BCOP assay, (II) Evolution of corneal transparency for CS/SBE-β-CD nanoparticles over time during BCOP assay, and (III) Resulting data of corneal transparency, opalescence and fluorescein permeability for CS/TPP and CS/SBE-β-CD nanoparticles.

2.4.2. Hen's egg test on the chorioallantoic membrane (HET-CAM) (page 13)

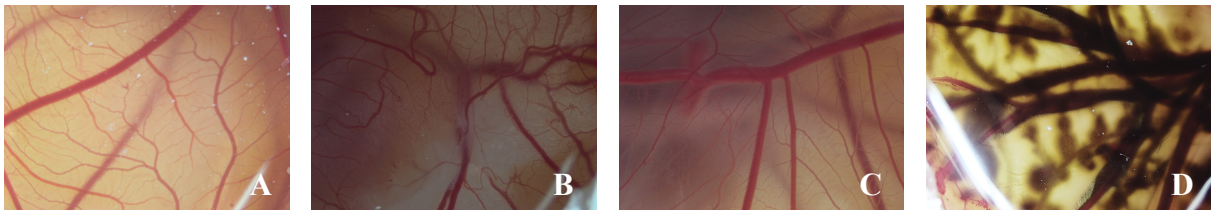


Figure S-7. Images of CAM membranes after the chitosan-based nanoparticles administration during the HET-CAM test, compared to the control solutions. (A) CS/TPP nanoparticles, (B) CS/SBE-β-CD nanoparticles, (C) BSS (negative control), and (D) NaOH (positive control).

USC
UNIVERSIDADE DE SANTIAGO DE COMPOSTELA

2.5. In vivo ocular surface permanence study

2.5.1. Evaluation of the radiolabeling stability and efficiency of chitosan-based nanoparticles

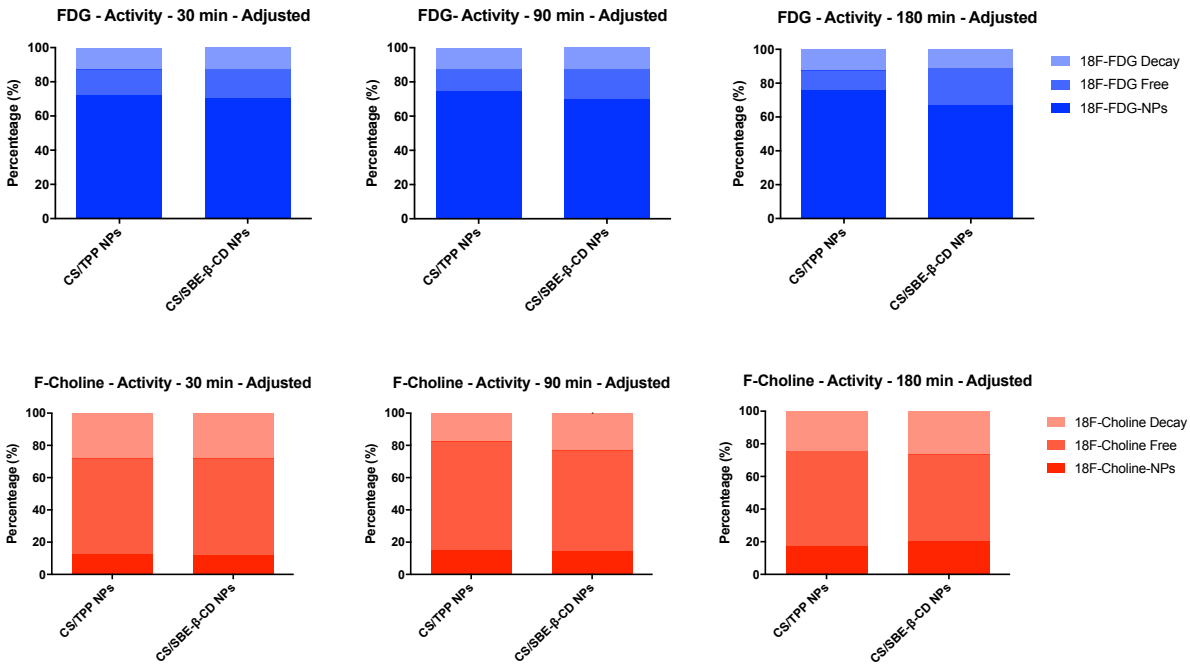


Figure S-8. Radiotracer labeling stability and efficiency for chitosan-based nanoparticles over time. (I) 18F-FDG (above), and (II) 18F-Choline (below).

USC UNIVERSIDADE DE SANTIAGO DE COMPOSTELA

Chapter 2.

Lactoferrin-loaded nanostructured lipid carriers (NLCs) as a new formulation for optimized ocular drug delivery

USC
UNIVERSIDADE DE SANTIAGO DE COMPOSTELA

USC
UNIVERSIDADE
DE SANTIAGO
DE COMPOSTELA

Chapter 2

Lactoferrin-loaded nanostructured lipid carriers (NLCs) as a new formulation for optimized ocular drug delivery

Rubén Varela-Fernández[1,2], Xurxo García-Otero[1,3], Victoria Díaz-Tomé[1], Uxía Regueiro[2], Maite López-López[2], Miguel González-Barcia[4], María Isabel Lema[5,*] and Francisco Javier Otero-Espinar[1,6,*].

1. Department of Pharmacology, Pharmacy and Pharmaceutical Technology. University of Santiago de Compostela (USC). Campus vida. Santiago de Compostela. Zip Code: 15782. Spain. francisco.otero@usc.es.
2. Clinical Neurosciences Group. University Clinical Hospital, Health Research Institute of Santiago de Compostela (IDIS). Travesía da Choupana s/n Santiago de Compostela. Zip Code: 15706. Spain. mariaisabel.lema@usc.es.
3. Molecular Imaging Group. University Clinical Hospital, Health Research Institute of Santiago de Compostela (IDIS). Travesía da Choupana s/n Santiago de Compostela. Zip Code: 15706. Spain. xurxo.garcia.otero@gmail.com
4. Clinical Pharmacology Group. University Clinical Hospital, Health Research Institute of Santiago de Compostela (IDIS). Travesía da Choupana s/n Santiago de Compostela. Zip Code: 15706. Spain. miguel.gonzalez.barcia@sergas.es.
5. Department of Surgery and Medical-Surgical Specialties. Ophthalmology Area. University of Santiago de Compostela (USC).Campus Vida. Santiago de Compostela. Zip Code: 15706. Spain. mariaisabel.lema@usc.es.
6. Paraquasil Group. University Clinical Hospital, Health Research Institute of Santiago de Compostela (IDIS). Travesía da Choupana s/n Santiago de Compostela. Zip Code: 15706. Spain. francisco.otero@usc.es.

Eur J Pharm Biopharm. 2022 Mar;172:144-156. doi: 10.1016/j.ejpb.2022.02.010. Epub 2022 Feb 17. PMID: 35183717.

INTRODUCTION

The eye is one of the daintiest, highly protected, and complex organs, with distinctive structure, composition, and biochemistry. In contrast to the conventional systemic drug delivery pathways, topical ophthalmic administration is a non-invasive and the most favored pathway for drug delivery, particularly to the anterior segment of the eye. Nevertheless, the ocular bioavailability of the active substances may be very low due to the different barriers that may hinder the drug transport and its subsequent low residence time at the target site. Hence, an idyllic drug delivery system (DDS) that effectively ranges the target site without disturbing the ocular structural barriers is needed (1–4).

Nanostructured lipid carriers (NLC) have shown great promise properties (e.g., drug protection, enhanced bioavailability, dose reduction, or prolonged circulation time, among others) as controlled DDS in recent years (5,6). Nanoparticulate lipidic DDS have reached enough interest in the recent years, predominantly due to their biocompatibility with the ocular surface, as well as to their lipophilicity and capability of permeating physiological barriers. Other properties, such as simplicity in the elaboration method, cost-effectiveness ratio, and the practicability of large-scale manufacture, turn them into attractive and marketable drug delivery alternatives to the anterior segment of the eye (7,8).

NLC are a novel generation of lipid nano-sized systems which were designed to surpass the drawbacks of previously developed lipidic colloidal systems (liposomes, solid lipid nanoparticles, …). NLC exist as a solid lipid matrix at body and room temperature, where a percentage is changed for a mixture of liquid lipids, resulting in a less ordered lipid matrix. NLC formulations were deeply studied due to their potential as ocular DDS to enhance corneal permeation and increase the drug bioavailability, as well as safety, non-invasive, and improved patient's compliance (1,9). Moreover, the mucoadhesive nature of NLC improves their contact with the eye surface, leading to a sustained residence time, greater bioavailability, and reduced side effects (10). NLC have also shown high drug encapsulation and loading efficiencies for both lipophilic and hydrophilic drugs (11,12), long shelf-life, and large scale production (13–16).

Keratoconus (KC) is a degenerative ecstatic corneal disorder with a progressive bilateral pattern that mainly appears in young adults, leading to pronounced visual disability, deteriorating over time (17). Currently, there is no available treatment related to the prevention of the development or progression delay of this disease. Moreover, the palliative care does not curb the progression of the ecstatic disorder; invasive surgical procedures are used as the ultimate alternative, preferably intracorneal ring segments (ICRS) implantation, corneal transplant, or corneal cross linking (CXL), with incomplete visual upturn (18,19). The etiology and its progression determinants are still unclear despite its high prevalence, although a multi-factorial pattern is dilucidated as the last common trail of several pathological processes (20).

Keratoconus progression is related to a gradual increase of inflammatory intermediaries, comprising cytokines and cell adhesion glycoproteins. Certainly, different studies have proven the correlation between the overexpression of type-α Tumor Necrosis Factor (TNF-α), Interleukin-6 (IL-6), and Matrix-9-Metalloprotease (MMP-9), described as a key factor in the

USC UNIVERSIDADE DE SANTIAGO

KC progression (21,22). Additionally, a noteworthy diminution in lactoferrin lacrimal levels, as well as other glycoproteins, was also noticed in the KC pathogenesis (23,24). These findings may indicate that immunological courses may be related to the appearance and development of this corneal ectasia.

Lactoferrin (Lf) is a globular protein (two homologous globular N- and C- lobes) with iron-binding capacity (25,26), as well as different biological effects, including anti-inflammatory (27,28), antibacterial (29–31), antiviral (32–34), and antitumoral (35,36), among others. This protein has also proven to modulate the humoral and cellular response involving Toll-Like receptors (TLRs) and to stimulate the corneal wound healing (37–39). A TLR 2-4 receptors overexpression, an increase in pro-inflammatory cytokines, and a Lf lacrimal levels decrease in granulocytes of keratoconus patients were previously demonstrated by our group (40–42).

The aim of the present chapter was grounded on the design, development, and characterization of Lf-loaded NLCs as nanosized systems intended for the topical ophthalmic treatment of KC. Similarly, the central commitment of this site-specific and controlled-delivery approach is predominantly centered on the understanding of enhanced pharmacokinetics and pharmacodynamics drug properties, together with better immunogenicity to improve the therapeutic effect. An effort to prove the appropriateness of NLC to control the Lf release and improve its corneal permeability was also studied by acquiring a strong preclinical foundation. Indeed, a new ocular biopermanence assay based on a radiolabeling method was performed to evaluate the NLC bioadhesion proposed for topical instillation.

MATERIALS

Glycerol monostearate 40-55 was purchased from Roig Farma S.A. (Barcelona, Spain). Soy lecithin was acquired from Acofarma® (Barcelona, Spain). Cholesterol from lanolin was provided by Sigma Aldrich Chemie GmbH (St Louis, USA). Compritol 888 ATO (a mixture of mono-, di- and triglycerides of behenic acid (C22)) and Capryol® 90 (propylene glycol monocaprylate) were generously presented by Gattefosse (Paris, France). Miglyol® 812 N (medium-chain triglycerides) was kindly donated by IOI Oleochemical GmbH (Witten, Germany). Poloxamer 407 (Kolliphor® P 407), Poloxamer 188 (Kolliphor® P 188) and D-α-Tocopherol Polyethylene Glycol 1000 Succinate were supplied by Sigma Aldrich Chemie GmbH (St Louis, USA). Lactoferrin was acquired from Sigma-Aldrich (St Louis, USA). All supplementary elements and reagents were of the uppermost available pureness score.

USC
UNIVERSIDADE DE COMPOSTELA

EXPERIMENTAL METHODS

1. Preparation of lactoferrin-loaded NLC

Lf-loaded NLC were obtained by a customized double emulsion/solvent evaporation technique (DE/SE) (see details of the NLC composition in Table 1). Briefly, the mixture of solid and liquid lipids was dissolved in 5 mL dichloromethane (organic phase). Inner aqueous phase (W1) was prepared by dissolving predetermined amounts of Lf in PBS, containing a 30% (w/v) Kolliphor® P407. The first emulsion was obtained by emulsification of the aqueous phase with the organic phase in a 1:5 (v/v) ratio by sonication (Bandelin Sonoplus® HD3200, Germany) at 15% sonication amplitude for 2 minutes (pulse: 30 s – 5 s). The second emulsion (W2) was obtained by adding the first emulsion to an α-Tocopherol PEG aqueous solution in a 1:10 (v/v) ratio by sonication at 20% sonication amplitude for 5 min (pulse: 30 s – 5 s). The organic solvent in the double emulsion was evaporated during the sonication process. Double emulsion was then included into a maturation medium, composed of a 0.5% (w/v) Kolliphor® P188 aqueous solution (included into an ice-bath) for 3 h under magnetic stirring (100 rpm). Resulting NLC were then filtered through a 0.8 mm cellulose acetate filter and subsequently ultracentrifugated at 50000 rpm and 25°C for 1 h (TL-100 Ultracentrifuge, Beckman Coulter). The final NLC concentrate was resuspended in Milli-Q® water, examined and subsequently lyophilized. The supernatant was retrieved for additional studies.

Table 1. Composition of the previously optimized Lf-loaded NLC formulation.

Solid lipid		**Liquid lipid**		**Surfactant**	
Name	*Ratio (w/v)*	*Name*	*Ratio (w/v)*	*Name*	*Ratio (w/v)*
Glycerol monostearate	12%	Capryol® 90	15%	Kolliphor® P 407	30%
Compritol® 888 ATO	12%	Miglyol® 812 N	45%	Kolliphor® P 188	0.5%
Soy lecithin	12-30%			a-Tocopherol-PEG	0.5%
Cholesterol	5-7.5%				

USC DE SANTIAGO DE COMPOSTELA

2. Physicochemical characterization of lactoferrin-loaded NLC

2.1. Particle size, size distribution and ζ potential

Particle size and size distribution are crucial characteristics due to their influence on the final formulation properties (stability, solubility, release rate or biological behavior, among others). The average size, PDI, and surface charge of the NLCs were determined by dynamic light scattering with non-invasive back scattering (DLS-NIBS) at 25°C (ZEN3600, Malvern Instruments Ltd., UK). Sample preparation was described in previous works (43). Each batch was tested in triplicate.

2.2. Morphology evaluation

Morphology denotes the outer features of nanoparticles. NLC are presumably anisometric particles (high surface area), where oil droplets are included between the solid platelets and the surfactant layer (44). In addition, particle morphology significantly influences a lot of physicochemical characteristics, such as the encapsulation efficiency, loading capacity, drug release, pharmacokinetics, biodistribution or cellular uptake, among others (45,46).

The NLC morphological examination was carried out by Scanning Electron Microscopy (SEM) and Transmission Electron Microscopy (TEM), as previously described (43). Briefly, SEM analysis were carried out by positioning the freeze-dried NLCs on a metal specific holder and iridium coating was further applied preceding the microscopical analysis under different magnifications. An appropriate preparation procedure was also performed over the samples prior to TEM analysis (JEM-F200CF-HR microscope) by dyeing formulations with a 2% (w/v) phosphotungstic acid aqueous solution and ulterior all-night drying.

2.3. Determination of production yield, encapsulation efficiency, and loading capacity

The production yield (PY) of the resulting NLC was obtained by the centrifugation procedure (47), with negligeable changes. Briefly, fixed NLCs volumes were ultracentrifuged at 50000 rpm and 25°C for an 1 h. Ultracentrifugation led the NLC concentration in the surface of the suspension. Aqueous residue was then discarded, and the concentrated NLC were finally freeze-dried. The PY was then estimated as presented (equation 1):

$$Production\ yield\ (\%) = \frac{Nanoparticles\ weight}{Total\ initial\ solids\ weight} \cdot 100 \quad Equation\ 1$$

Encapsulation efficiency (EE) and loading capacity (LC) of NLCs were obtained after separation by centrifugation, as previously described (see methods section 1). The amount of boundless Lf was measured in the resulting aqueous residue by UV-Vis spectrophotometry (λ = 280.0 nm). EE (equation 2) and LC (equation 3) were finally estimated as presented below:

$$EE\ (\%) = \frac{Total\ amount\ of\ drug - Amount\ of\ unbound\ drug}{Total\ amount\ of\ drug} \cdot 100 \quad Equation\ 2$$

$$LC\ (\%) = \frac{Total\ amount\ of\ drug - Amount\ of\ unbound\ drug}{Nanoparticles\ weight} \cdot 100 \quad Equation\ 3$$

3. Stability studies

Several colloidal structures (micelles, liposomes or nanoemulsions) included into the NLC formulations may have an important impact on the NLC stability. Aggregation or coagulation phenomena may arise because of collisions among particles, leading to caking or flocculation throughout long-term stability (48).

3.1. Stability to storage

The stability-to-storage assay was planned according to the ICH guidelines (49), with negligeable adjustments. Resulting NLC formulations were freshly prepared, contemplating size changes and probable aggregation phenomena. Three different temperature subsets were established for the NLC incubation (4°C, 25°C, and 37°C for an 8 h and 3-month period for short and long-term stability respectively, under magnetic stirring, protected from light. Samples were taken at predefined intervals for particle size and distribution determination, carrying out every measurement in triplicate.

USC
UNIVERSIDADE DE SANTIAGO DE COMPOSTELA

3.2. Stability to pH

The NLC stability assessment to pH changes was performed in newly prepared formulations. NLC were preserved at 4 ± 2°C as standard formulations. A prefixed volume of each NLC suspension (500 µL) was included and diluted to a final volume using double-distilled water (5 mL). pH was subsequently changed to prearranged values (from 2 to 12). Resulting formulations were preserved in cooling temperature for 1 day, prior to the measurement by DLS analysis. Each sample was triplicate measured.

3.3. Stability to ionic strength

Newly prepared NLC formulations were subjected to ionic strength changes to complete the assessment of their physical stability. NLC were preserved at 4 ± 2°C as standard formulations. A prefixed volume of each NLC suspension (500 µL) was included into a final volume using double-distilled water (5 mL). The ionic concentration was subsequently changed to prearranged values (from 0.2 to 2.0M). Resulting formulations were preserved in cooling temperature for a day, prior to the measurement by DLS analysis. Each sample was measured thrice.

4. *In vitro* release study

The dialysis method is commonly used to quantify the drug release from nanosized systems. In the present system, two compartments are divided by a dialysis membrane, as previously described (43), building an appropriate system to evaluate the drug release behavior from different types of DDS (50–52).

The Lf release from NLC was evaluated to forecast the drug diffusion and kinetic profile from the delivery systems. The Lf release rate from NLC was measured by UV-Vis spectrophotometry, using Franz diffusion cells. The assembly, filling, and conditioning processes were explained in detail in previous works (43). The assay was performed for a 1-day period, and NLCs were tested in triplicate. The diffused protein was finally measured by UV-Vis spectrophotometry at a 280.0 nm wavelength. Analytic validation was previously obtained by our group and showed linearity (R = 0.999) over a concentration interval of 0.4882 – 500 µg/mL and LOD and LOQ values of 0.9765 µg/mL and 1.9531 µg/mL, respectively (data

not published). Results proved that NLCs remained stable for at least 7 days, sheltered from light and under cooling.

5. Ophthalmic toxicity analysis

The achievement in planning and creating alternative experiments to swap the Draize test has persisted slippery because of the complications of matching the *in vitro* outcomes and animal information. The alternative approaches encompass organotypic models, whose effectiveness was well proven for specific and limited purposes (53–55).

The Bovine Corneal Opacity and Permeability test (BCOP) is an appropriate assay for the evaluation of mild, moderate, and severe ocular irritants. Nonetheless, the BCOP steadfastness is limited for mild irritancy levels. Henceforth, BCOP may be contemplated as a pre-validation test, whose results can be used in combination with alternative irritancy tests, such as the Hen's Egg Test on the Chorioallantoic Membrane assay (HET-CAM) assay (56–59). In turn, the HET-CAM test is also contemplated a suitable template for modelling the consequences of materials on ocular tissues (55).

5.1. Bovine Corneal Opacity and Permeability test (BCOP)

The BCOP is an organ-like trial that permits the appraisal of the hypothetical ocular irritancy of formulations, safeguarding the animal replacement compliance. A complete scan of all corneal layers can be performed by using *in situ* isolated corneas, enabling the assessment of accurate quantifiable endpoints.

The BCOP basis were previously described by Tchao et al. (1988) (60) and improved by Gautheron et al. (61), with negligeable variations. The assembly, conditioning, application procedure of the formulations, and opacity measurements were explained in detail in previous works (43). Briefly, the initial corneal opacity was firstly determined by luxmetry and UV-Vis spectrophotometry, taking into account the corneal blank values prior to measurement determination to remove background light exposure. Second, 1 mL PBS was added into the Franz cell's donor chamber, followed by cornea's incubation for 60 min and subsequently opacity determination. Third, 1 mL formulation was incorporated into the upper compartment for 10 min, trailed by its removal and posterior PBS addition for 2 h; the opacity establishment was then made again. Finally, the permeability assessment was furtherly quantified by adding a prefixed volume of a 0.4% (w/v) fluorescein solution (1 mL) to the donor chamber for 90 min

USC UNIVERSIDADE DE SANTIAGO DE COMPOSTELA

and subsequently assessing the PBS optical density (OD) in the receptor compartment at 490.0 nm to estimate the potential corneal permeability variations. The resulting data were finally used to estimate the so-called *in vitro* irritation score (IVIS) (61,62), by applying the following mathematical equation (equation 4):

$$IVIS = mean\ opacity\ value + (15 \times mean\ permeability\ OD_{490}\ value) \quad Equation\ 4$$

5.2. Hen's egg test on the chorioallantoic membrane (HET-CAM)

The HET-CAM test is one of the most common organotypic models used for the identification of irritative compounds as an alternative to the standard Draize test (63). In this test, three potential consequences were determined (hemorrhage, lysis, and coagulation) and subsequently quantified by means of an irritation score (IS), considering the Kalweit et al. criteria (64). All practices with eggs were trailed by the appropriate principles and techniques for management of animal supplies.

The procedure was adjusted from the guidelines formerly developed by Spielmann and Liebsch (65), with minor modifications. The assembly, conditioning, application procedure of the formulations, and irritancy measurements were explained in detail in previous works (43). Each NLC suspension was evaluated in triplicate.

6. Ocular surface retention study

6.1. *Ex vivo* ocular surface retention study

The protocol previously developed by Belgamwar et al, (2009) and Gradauer et al, (2012) was taken as a reference to perform the *ex vivo* corneal surface retention study (66,67), with negligible changes. Thereby, newly removed eyes were obtained from a home-grown abattoir and macroscopically inspected, where feasible ones were chosen for additional exploration. Excised eyes were placed on individual containers, with the corneal surface up. Then, a prefixed volume of a 0.4% (w/v) fluorescein stained NLC suspension (500 µL) were instilled, repeating this process ten times. The residual NLC suspension was measured at a 490.0 nm wavelength by UV-Vis spectrophotometry in order to determine the fluorescence intensity. Each

USC UNIVERSIDADE DE SANTIAGO DE COMPOSTELA

formulation was tested in triplicate. The NLC mucoadhesion data was finally quantified as presented (equation 5):

$$Mucoadhesion\ (\%) = (Ab_{S0} - V_0) - \frac{(Ab_{SF} - V_F)}{(Ab_{S0} - V_0)} \cdot 100 \quad Equation\ 5$$

Where Abs_0 and Abs_F represent the absorbance value for the initial and final fluorescein-stained chitosan-based suspensions, V_0 refers to the volume applied to the viable excised eyes, and V_F indicates the final volume of the suspension not adsorbed to the mucosa. Each formulation was tested in triplicate.

6.2. *In vivo* ocular surface retention study

6.2.1. Radiolabeling stability and efficiency of NLC

Radioactive fluoride (^{18}F) is one of the most employed positron emitter because of its ideal positron properties ($t_{1/2}$ = 109.7 min, $E_{\beta+,max}$ = 635 keV, and β^+ intensity = 97%). In recent years, a series of approaches were studied to trace nanosized systems using the 2-(^{18}F)-fluoro-2-deoxy-D-glucose (^{18}F-FDG) labeling technique (68–71). The experimental procedure for the labeling of NLCs and the subsequent assessment of the labeling efficiency was already detailed in previous works (43).

The NLC radiolabeling efficiency was evaluated by the ^{18}F-FDG activity measurement, together in the supernatant (containing the NLC) and the aqueous residue, in view of the maturation period, as well as the radiotracer disintegration. Finally, a mathematical treatment was applied to the subsequent results to calculate the radiolabeling efficiency and to evaluate the labeling stability over time.

6.2.2. *In vivo* evaluation of the ocular biopermanence

The NLC's biopermanence was executed by Positron Emission Tomography (PET) and Computed Tomography (CT) combined procedure. Both approaches were described in previous works in order to guide the radiolabeling and the successive quantitative biopermanence assessment of new DDS intended for topical ophthalmic administration (43,72).

The *in vivo* studies were performed on male rats, provided by the university's animal-housing unit. The animals were firstly acclimatized and maintained in separate containers under precise

USC UNIVERSIDADE DE SANTIAGO

environmental and feeding conditions. All animals were manipulated taking into account the ARVO frameworks, together with the standard guidelines for laboratory animals (73). NLC were analyzed in quadruplicate to undertake the 3Rs governing outlines (74). The assembly, conditioning, application procedure of the formulations, and the measurements of the *in vivo* ocular biopermanence were explained in detail in previous works (43). The GraphPad Prism® and pKSolver® software were used to establish the appropriate correlation fitting between the remaining formulation activity and time into a single exponential decay equation by means of a single compartment prototype (75). Non-compartmental approach was additionally performed by approximating the mean residence time (MRT) and the total area under the curve (AUC) of the NLC remaining percentage versus time.

7. Data analysis

Pairs of groups were compared by carrying out one-tailed Student's t-test and multiple group comparison was conducted by one-way or two-way analysis of variance (one-way or two-way ANOVA), or by non-parametric Kruskal Wallis test with a 95% significance level ($p < 0.05$) throughout these studies, using the GraphPad Prism v.8.00 software (GraphPad Software, Inc. CA, USA). All data are presented as a mean value with its standard deviation indicated (mean ± SD). Tukey's, Bonferroni's or Dunnet's tests were subsequently applied for post-hoc contrast.

RESULTS AND DISCUSSION

1. Preparation of lactoferrin-loaded NLC

The choice of an adequate technique for the NLC elaboration is highly dependent on the drug physicochemical characteristics. A great variety of methods were successfully developed for the incorporation of hydrophobic compounds into the NLC, but there are hardly any described methods for the encapsulation of hydrophilic drugs (e.g., proteins) into NLC, due to the difficulties involved (drugs with high hydrophilicity are significantly ejected from the hydrophobic matrix into the dispersing aqueous phase) (76–79). Nevertheless, the modified DE/SE preparation method, where the first emulsion acts as a reservoir, is typically employed to encapsulate hydrophilic drugs, whereas the second emulsion serves as a diffusion barrier, preventing drug leakage from internal to external aqueous phase.

Initial screening studies were carried out to assess the formulation and processing parameters of the NLC preparation procedure. Drug:lipid ratio, oil:aqueous phase ratio, surfactant

concentration, volume of the maturation medium, and sonication time were identified as critical factors in producing stable formulations. The results from the initial screening trials (data not shown) suggested that specific values of these parameters are required in the obtention of NLC. Likewise, colloidal systems involve small particle size and narrow size distribution for high stability and low ocular toxicity (13). Optimized NLC formulations were in the nanometric range, as a unimodal population with a relatively narrow size distribution, and negatively charged surface. These are several of the most important prerequisites for ocular application of nanoparticulate systems (80).

2. Physicochemical characterization of NLC

2.1. Particle size, size distribution, and surface charge

The NLC traditional diameter varies from 10 to 1000 nm, although a 50–300 nm size interval is especially desired for site-specific drug release (13). A higher barrier permeability, improved uptake, rapid action, and controlled release are one of the most important advantages of these lipid nanocarriers.

The average size of both blank and lactoferrin-loaded NLC was below 150 nm (see Table 2). The PDI was found to be lower than 0.3, denoting a relative uniformity in the final NLC suspension. The NLC surface charge revealed high negative values (-18.25 ± 2.20 and -17.98 ± 2.54 for blank and lactoferrin-loaded NLC, respectively), being attributed to the chemical nature of the lipid matrix and the surfactants included into the maturation medium (Kolliphor® P188).

Table 2. Particle size, polydispersity index, and surface charge of blank and Lf-loaded NLC formulations. Results are represented as the mean ± S.D. (n = 3).

Formulation	[Lf] (mg/mL)	Size (nm)	PDI	ζ Potential (mV)
Blank NLC	-	115.97 ± 15.58	0.152 ± 0.037	-18.25 ± 2.20
Lactoferrin-loaded NLC	0.1	117.91 ± 12.90	0.146 ± 0.042	-18.57 ± 2.47
	0.5	123.09 ± 8.29	0.165 ± 0.040	-17.86 ± 1.51
	1.0	119.45 ± 11.44	0.151 ± 0.045	-17.50 ± 2.53

USC UNIVERSIDADE DE SANTIAGO DE COMPOSTELA

Moreover, at lower amounts of lipids, the ability of surfactant to stabilize particles could be enhanced (81). Surfactant amount also had a significant effect on PDI that could feasibly be associated with the lower predisposition to form aggregates (82,83). Even though, surfactants proportion in the optimized NLC formulations may stabilize the system without causing an increase in the PDI values.

2.2. Morphological evaluation

The TEM analysis offered evidence about the NLC's particle size and morphology and confirmed previous DLS data, where a size below 200 nm was found for the final NLC. Further, the microstructural analysis confirmed that NLC were mostly composed of a uniform population of isometric, spherical-in-shape, and well-defined size particles (see Figure 1).

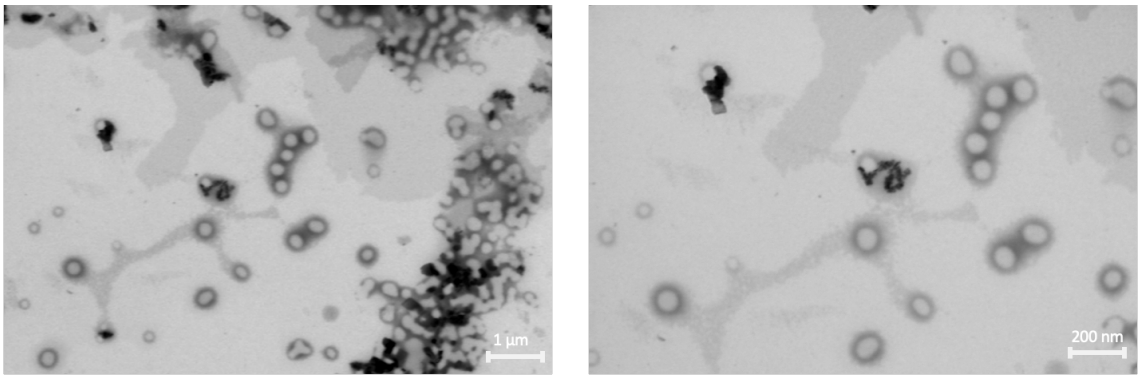


Figure 1. TEM micrographs of Lf-loaded NLC.

SEM analysis demonstrated that the NLC external characteristics were maintained after the elaboration process. SEM analysis also proved the presence of a population of isometric particles. Accordingly, the lyophilized NLC suspensions guaranteed the nanoscale size, being these results aligned with the TEM morphological evaluation. To point out, it must be considered that the NLC's irregular shape observed in SEM images could be caused by the water extraction from the NLC core as consequence of the lyophilization process (see Figure 2).

USC
UNIVERSIDADE DE SANTIAGO DE COMPOSTELA

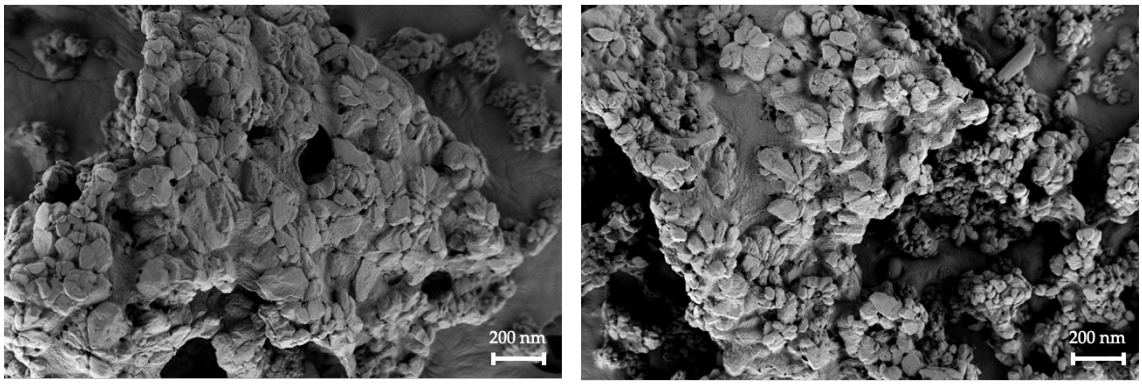


Figure 2. SEM images of lactoferrin-loaded NLC formulations.

2.3. Production yield, encapsulation efficiency, and loading capacity of NLC

Figure 3 shows the PY, EE, and LC data of the final Lf-loaded NLC. The EE assessment confirmed that the preparation process of the Lf-loaded NLC was reproducible and efficient with PY values above 78.92 ± 9.12% for the optimized lactoferrin-loaded NLC (C_{Lf} = 1 mg/mL) (see Table 2). A correlation in the EE and LC data was perceived with the proportional Lf increase into the NLC suspension (see section 2.4). It must be considered that the drug:lipid ratio varied from 1:7.5 to 1:45, reaching high values of EE and LC (up to 75%) for a 1 mg/mL lactoferrin concentration, as presented in Figure 3.

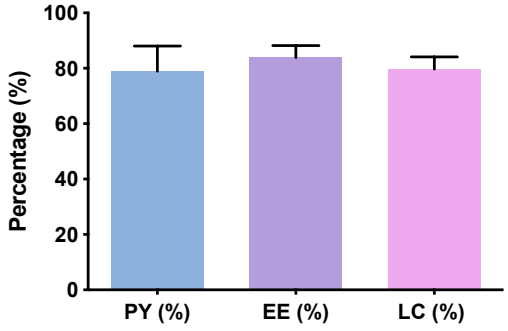


Figure 3. Production yield (PY), encapsulation efficiency (EE), and loading capacity (LC) values for 1 mg/ml lactoferrin-loaded NLC.

USC
UNIVERSIDADE DE SANTIAGO DE COMPOSTELA

2.4. Effect of protein loading on size, EE, and LC

Figure 4 displays the Lf loading effect on size, EE, and LC for Lf-loaded NLC over the increased amount of Lf (from 0.1 to 1.0 mg/mL). Resulting data suggest that Lf amount has a negligeable effect on particle size, although it must be considered that the drug:lipid ratio ranged from 1:7.5 to 1:45, so that the influence may be masked by the large amount of lipidic components. Nevertheless, a correlation in the EE and LC data was found over the increased Lf amount (from 0.1 to 1 mg/mL), although no difference was found in terms of size increase.

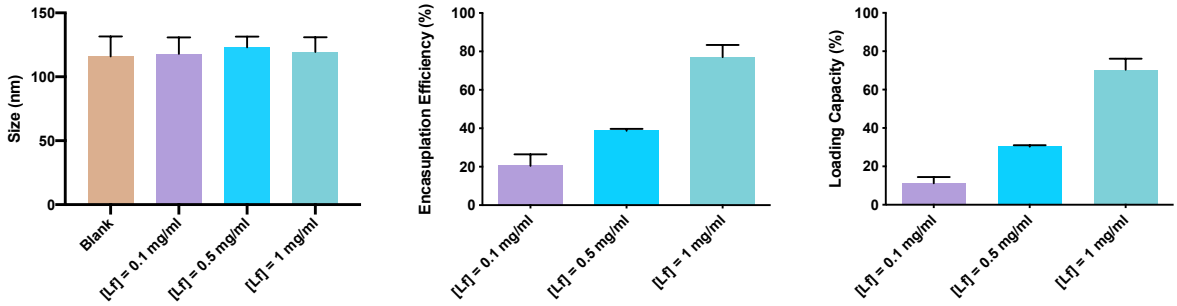


Figure 4. Evolution of size (nm) and ζ potential (mV), as well as EE (%) and LC (%) values, over increased lactoferrin concentration for NLC formulations.

Resulting data was subsequently evaluated by a one-way ANOVA analysis, where differences among the Lf-loaded NLC might be observed. EE (%) and LC (%) data were found to be significantly different between NLC formulations ($F = 124.7$, $P < 0.0001$ for EE and $F = 175.4$, $P < 0.0001$ for LC) (see Figure 4). These results suggest that NLCs might further encapsulate the drug into their matrix, leading to high drug uptake.

These results showed that NLCs have a greater ability to immobilize Lf than previously developed chitosan-based nanoparticles (43). In this previous study, a consistent preclinical base was obtained by our group based on the design, development, and characterization of chitosan-based NPs to immobilize and promote a controlled release of Lf. Certainly, the ability of chitosan/tripolyphosphate nanoparticles (CS/TPP NPs) and chitosan/sulfobutylether-β-cyclodextrin nanoparticles (CS/SBE-β-CD NPs) to immobilize and release Lf was studied. In this previous research, EE values of 47.19 ± 2.97% and 52.84 ± 1.05% and LC values of 43.47 ± 5.04% and 43.44 ± 3.69% for CS/TPP and CS/SBE-β-CD NPs were obtained for a 1 mg/mL

USC UNIVERSIDADE DE SANTIAGO DE COMPOSTELA

(43). Nevertheless, these results were lower than those obtained for the present NLC formulations, which showed values greater than 75% for the same Lf concentration.

3. Stability studies

The physical stability of NLC dispersions is one of the key product characteristics to be assessed. NLC formulations are usually heterogeneous and thermodynamically unstable systems. Hence, a noteworthy predisposition to lose physical stability during storage is presumably observed in this type of formulations (84), although the use of an optimized stabilizer composition may maintain the physical stability for several years (85).

3.1. Stability to storage

The NLC's stability study was carried out by measuring the size, PDI, and ζ potential at three different temperature sets (see methods section 3.1.) for two different periods (8 h and 3 months, for short and long-term stability study, respectively). Resulting data for both stability studies proved that NLCs were stable in terms of size and size distribution along the studied periods (see Figures 5 and 6). A one-way ANOVA analysis was finally employed, and no differences ($p > 0.05$) were spotted along the predefined interval, agreeing with the experimental results.

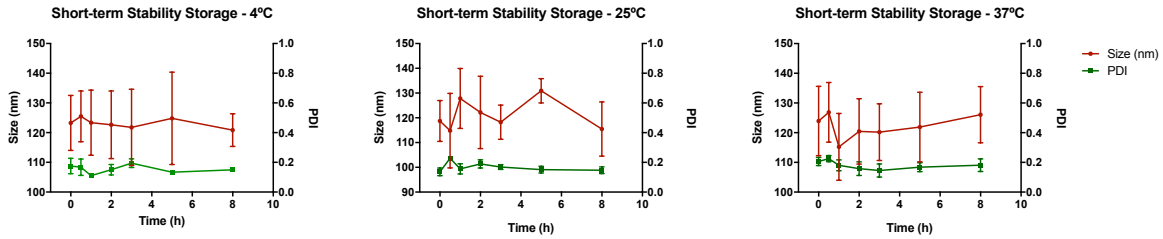


Figure 5. Short-term stability-to-storage study for lactoferrin-loaded NLC over an 8-hour period.

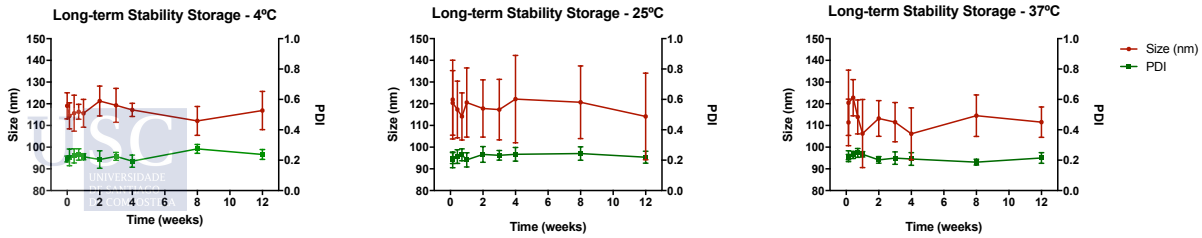


Figure 6. Long-term stability-to-storage study for lactoferrin-loaded NLC over a 3-month period.

3.2. Stability to pH

Figure 7 shows particle size and surface charge variations of NLC formulations for the tested pH interval. Changes along the studied pH interval are presumably associated with the composition of the resulting formulation, where both solid and liquid lipids determine the nanocarrier's surface charge. Hence, aggregation phenomena were detected in the lower acidic pH interval (from pH 2 to 4), because of the interaction between the acidic media (high proton concentration) and the negatively charged groups of the lipid nanocarriers, annulling the nanoparticle's surface charge (ζ potential ≈ 0). Nevertheless, from a pH 6 value, NLC remained stable in size, where high negatively ζ potential values were also observed, supporting these results. Thus, NLC would be suitable for topical ophthalmic administration without producing corneal injuries or lacrimation (pH interval: from 4 to 8) (86).

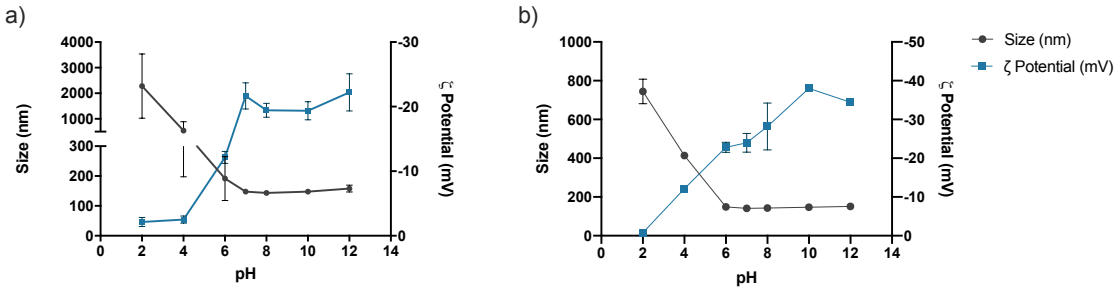


Figure 7. Fluctuations in size and surface charge values of NLC along the studied pH interval. Graph a) represents the changes for NLC formulations in PBS, while Graph b) shows the changes for NLC formulations in Milli-Q® water.

3.3. Stability to ionic strength

The collapse, rupture, or coalescence of the NLC may be associated with modifications in the ionic concentration of the media. This report is reinforced by the electrical double-layer theory, where increased ionic strength values are associated with a decrease in the double layer thickness (87). Therefore, an upsurge in the contact between particles may produce an intensification in the NLC's aggregation.

The time-dependent caking, flocculation or deposition phenomena may occur on NLC suspensions due to changes on ionic strength of the media (88). Figure 8 shows the changes in size and surface charge of NLC formulations along the ionic strength range.

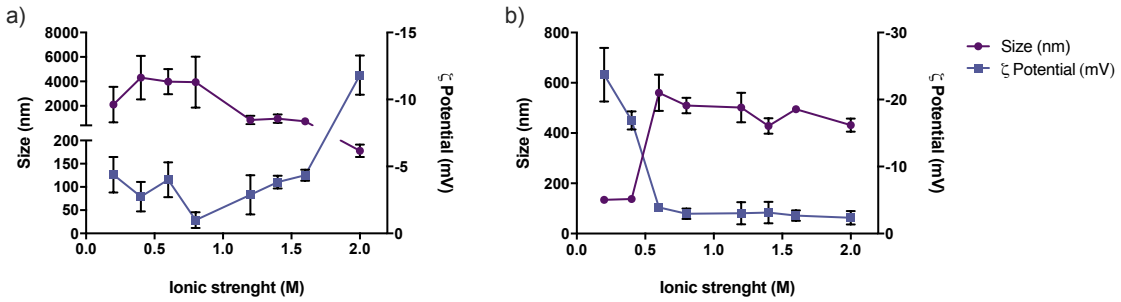


Figure 8. Changes in size and surface charge values of NLC over the ionic strength predefined range. Graph a) represents the changes for NLC formulations in PBS, while Graph b) shows the changes for NLC formulations in Milli-Q® water.

In the absence of additional NaCl salt and at a pH 7.4 value, lactoferrin-loaded NLC aqueous dispersions are stable systems, exhibiting no signal of caking or aggregation for, at least, 3 months (see section 3.1.). NLC stability is determined by electrostatic repulsive forces from the negative surface charge, being supported by previous studies (89,90). Nevertheless, aggregation phenomena occurred in almost the entire studied ionic strength interval, possibly since NLC were just dispersed in PBS (pH 7.4 and 0.15 M ionic strength). A shift from a steady to an unsteady NLC formulation occurs for additional ionic strength values higher than 0.2 M and lower than 1.6 M, as presented in the Figure 8a). A similar pattern was observed for the NLC formulations using Milli-Q® water instead of PBS for high ionic strength values (see figure 8b)), while for the 0.2 to 0.5 M range, the NLC size has remained unchanged, supporting the idea that PBS conditions such stability. Hence, an upsurge in the sodium ions concentration to the NLC colloidal suspension presumably weakened or nullified the magnitude of electrostatic repulsive influence, producing a noteworthy decrease of the ζ potential. Consequently, a minimum increase in the ionic strength led to the coalescence of the NLC. In any case, the NLC suspension in the final formulation (PBS pH 7.4) presented suitable values of ionic strength and osmolarity for topical ophthalmic administration, without the need to add additional salts to the medium.

USC UNIVERSIDADE DE SANTIAGO

4. *In vitro* release study

Compared to the Lf buffered solution, the pilot *in vitro* release study from Lf-loaded NLC proved a controlled and maintained delivery behavior, as presented in Figure 9. The *in vitro* Lf delivery profiles acquired for the NLC replicates exhibited two dissimilar release stages, as presented: (I) a burst release due to the Lf desorption from the NLC surface, and (II) a sustained release because of Lf diffusion from the NLC matrix due to the lipidic bioerosion progression.

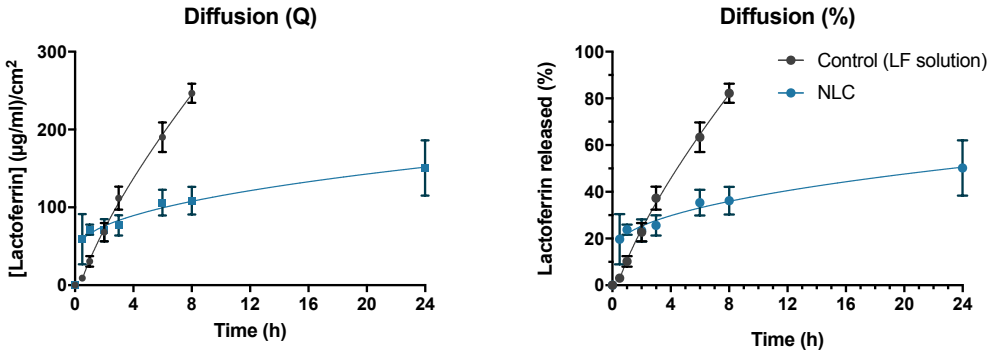


Figure 9. *In vitro* release study of NLC, compared to a control solution. The first diagram illustrates the raw cumulative amount of Lf. The second diagram shows the cumulative percentage of Lf.

Results from Lf cumulative release from NLC were adjusted to several kinetic models to find the pharmacokinetics and release behavior, where Higuchi and the Peppas and Korsmeyer kinetic models showed the best correlation data. In the latter model, a *n* value of 0.45 was obtained, advocating diffusion as the leading delivery mechanism (see details in Table 3). In absence of *in vivo* proteins with catalytic behavior (e.g., lipase, colipase), the main Lf delivery mechanism from the lipid NPs and NLC is assumed to be based on drug diffusion and lipid matrix erosion processes, but once the systems penetrate tissues, the *in vivo* lipid degradation by enzymes could be taken by increasing the intracellular release of the cargo. On the other hand, Robciuc et al. (91) have previously described the presence of sphingolipid-specific enzymes and acid-and-neutral sphingomyelinases, as well as ceramidases in tears of healthy patients, forming part of the homeostatic system of the ocular surface. This enzymatic composition can be modified by the presence of bacterial lipases or extracellular stress. Thus, lipids and lipidic nanosystems can be altered on the ocular surface by the presence of enzymes,

USC UNIVERSIDADE DE SANTIAGO

both in tear fluid or within the corneal epithelial cells and, therefore, the *in vivo* release could be faster.

Table 3. Release data of NLC into the Higuchi and Peppas and Korsmeyer diffusion kinetics equation.

	Higuchi		Peppas and Korsmeyer		
Formulation	k ($mg \cdot cm^{-2} \cdot min^{-0.5}$)	R	k ($mg \cdot cm^{-2} \cdot min^{-n}$)	n	R
NLC	22.08	0.9754	26.67	0.45	0.9761

5. Ophthalmic toxicity analysis

5.1. Bovine Corneal Opacity and Permeability test (BCOP)

Corneal changes due to NLC administration were expressed as opacity and permeability values. Firstly, results were individually analyzed to assess whether NLC produce corneal irritation. No noteworthy variations were detected for NLC formulations, compared to the control solutions results (see Figure 10). The IVIS score was finally obtained, where NLC showed a IVIS = 0, suggesting no corneal toxicity consequences compared to control formulations (see Figure 11).

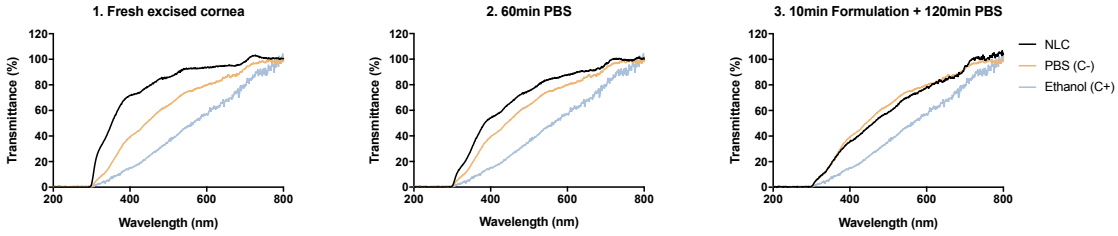


Figure 10. Evolution of corneal transparency for NLC formulations over time during BCOP assay.

USC UNIVERSIDADE DE SANTIAGO DE COMPOSTELA

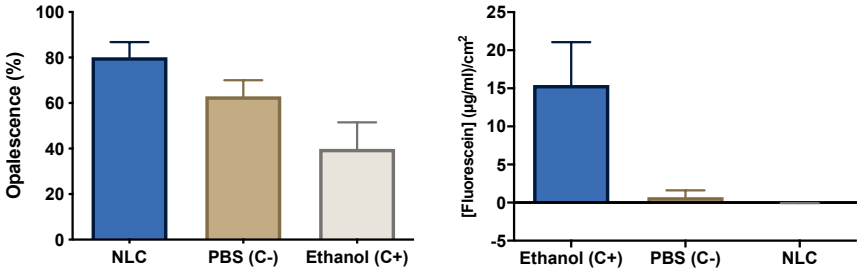


Figure 11. Resulting data of opalescence and fluorescein permeability for NLC formulations, compared to control solutions, respectively.

5.2. Hen's egg test on the chorioallantoic membrane (HET-CAM)

NLC formulations were assessed, comparing results with those acquired for the negative and positive control solutions (NaCl and NaOH aqueous solutions, respectively). NLC showed no cytotoxicity effects (IS = 0), being in accordance with the BCOP test results (see methods section 5.1.). Thus, resulting data confirmed that the constituents and the final lipidic formulations are non-toxic and biocompatible.

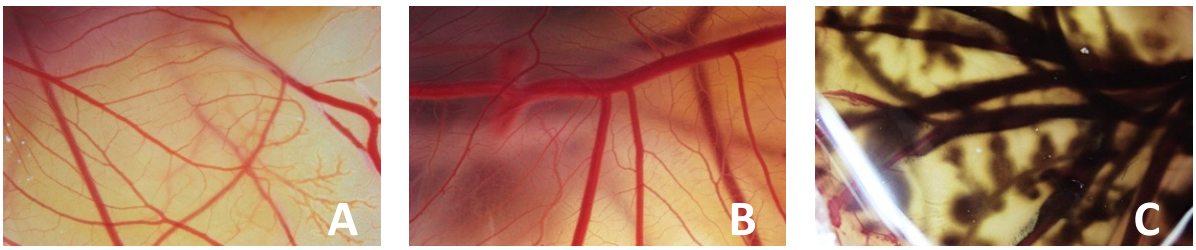


Figure 11. Images of CAM membranes after the administration of NLC during the HET-CAM test, compared to the control solutions. (A) lactoferrin-loaded NLC, (B) NaCl aqueous solution (negative control), and (C) NaOH aqueous solution (positive control).

6. Ocular surface retention study

6.1. *Ex vivo* ocular surface retention study

USC UNIVERSIDADE DE SANTIAGO DE COMPOSTELA

Corneal mucin layer is a critical parameter that should be considered in the NLC design and development for ophthalmic delivery. The mucoadhesion variation for NLC formulations was expressed as the difference in the fluorescein concentration before and after the study.

Thus, a mucoadhesion percentage of 29.16 ± 6.54% and 47.23 ± 4.41% was obtained for the control solution and the NLC formulation, respectively. Furthermore, a one-way ANOVA analysis was then performed, and statistically noteworthy differences ($p < 0.05$) were spotted by comparison of the results for NLCs with the standard data. This is in good agreement with previously published works (92,93), where NLC have proven a prolonged corneal MRT and a significant uptake along the corneal epithelium, conditioned by the small particle size and homogeneous particle size distribution.

6.2. *In vivo* ocular surface retention study

6.2.1. Radiolabeling efficiency and stability of NLC

Figure 12 displays the ^{18}F-FDG radiolabeling efficiency and stability for NLC formulations, respectively. As observed, ^{18}F-FDG NLC formulations presented an appropriate radiolabeling efficiency (higher than 75%) and stability for, at least, 3 hours. ^{18}F-FDG was confirmed as a suitable radiotracer for NLC, and it was used in further *in vivo* radiolabeling assays.

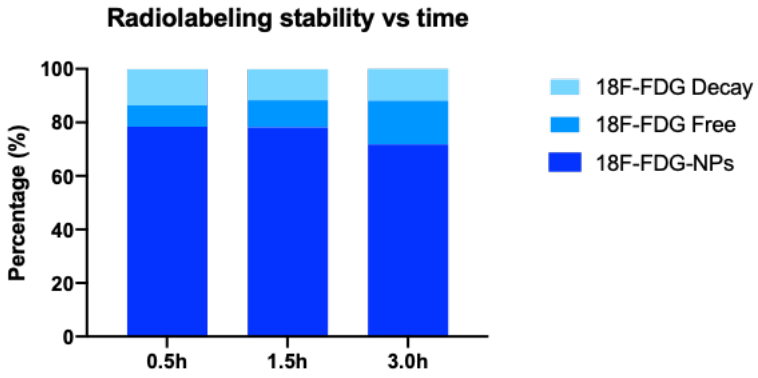


Figure 13. ^{18}F-FDG radiolabeling efficiency and stability for NLCs over time.

6.2.2. Experimental *in vivo* evaluation of ocular biopermanence

Figure 14 displays the ^{18}F-FDG-radiolabeled NLC ocular biopermanence for a 300-min period, compared to the standard solution. The corneal surface retention study of the NLC formulations was evaluated by the ^{18}F-FDG radioactivity assessment in a PET system.

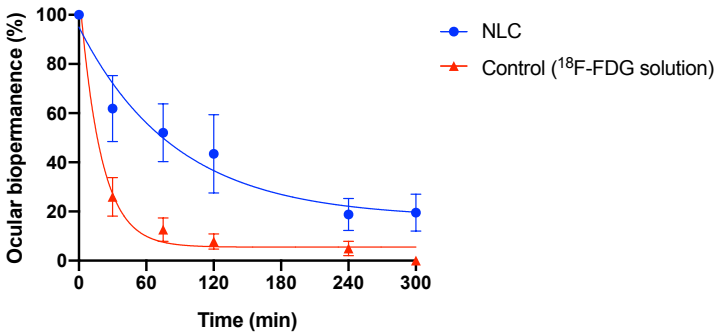
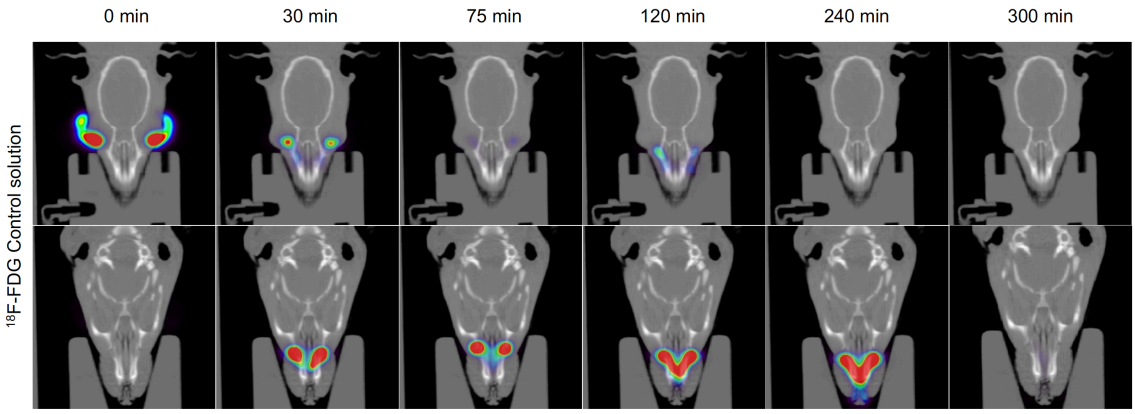


Figure 14. Ocular biopermanence of a ^{18}F-FDG radiolabeled NLC and a ^{18}F-FDG aqueous solution (control), estimated considering the primary biopermanence data (%) in the ROI.

The NLC ocular biopermanence was carried out on rats using ^{18}F-FDG as a radiotracer, trailed by the radioactivity evaluation in a PET equipment over the studied time (see details in Figure 15). In this study, a higher MRT was detected for the NLCs, compared to the standard solution, even though both formulations consist of an ocular buffered solution (PBS, pH 7.4), whose composition is close to tears. Results were accurately adjusted to a monoexponential decline outline by a single compartmental model (R = 0.9578 for NLC and R = 0.9930 for the standard solution) (see Figure 14). The resulting data are in good agreement with the idea that NLCs exhibit appropriate mucoadhesive, direct cell uptake, and corneal penetration, being in accordance to the PET data of previous studies (94–96).



USC
UNIVERSIDADE DE SANTIAGO DE COMPOSTELA

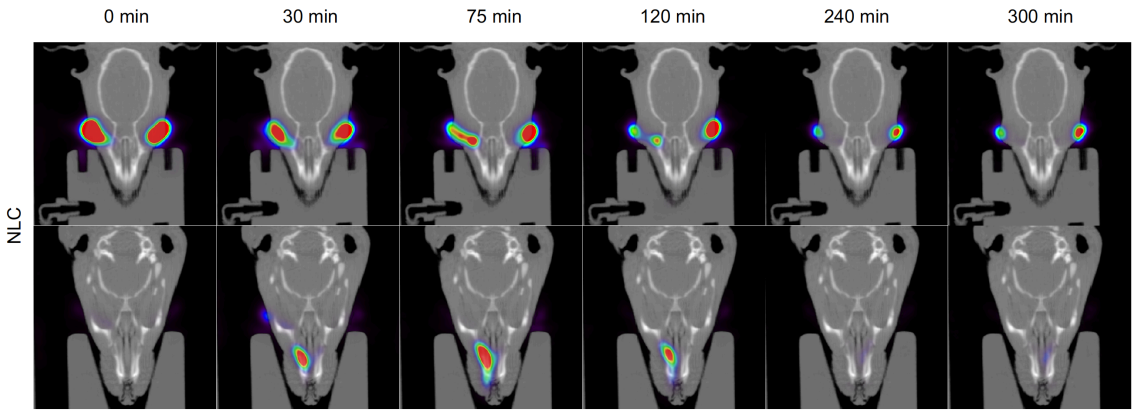


Figure 15. Fused PET/CT images during the 5 h-studied interval. (I) ^{18}F-FDG buffered aqueous solution, (II) ^{18}F-FDG radiolabeled NLC.

Table 4 displays the pharmacokinetics factors (k, $t_{1/2}$, MRT, AUC and R) of the ^{18}F-FDG radiolabeled NLC and ^{18}F-FDG standard solution. Statistically significant differences ($p < 0.05$) were spotted concerning NLC and control solution for the studied interval, where NLC showed a higher ocular retention profile.

Table 4. Ocular biopermanence parameters for ^{18}F-FDG radiolabeled NLC and ^{18}F-FDG control (named as "control" in the table) formulations.

Formulation	K (min^{-1})		$t_{1/2}$ (min)		MRT (min)		R^2	
	Mean	SD	Mean	SD	Mean	SD	Mean	SD
NLC	0.0071	0.0027	107.82	38.10	141.33	26.21	81.1	9.5
Control	0.041	0.012	17.7	4.5	59.1	17.6	26.0	7.8

The NLC ocular permanence obtained by PET was similar to that previously observed for the mucoadhesive Lf-loaded CS/TPP and CS/SBE-β-CD NPs (43). Corneally, chitosan-based NPs showed a $t_{1/2}$ and MRT of 114 ± 72 h and 127 ± 47 h for CS/TPP NPs, and 60 ± 20 h and 90 ±

14 h for CS/SBE-β-CD NPs, respectively. Thus, results confirmed the great bioadhesive ability of the NLC in the ocular mucosa.

CONCLUSION

In the biomedical field, nanoparticulate DDS have been extensively studied in the latest decades. Certainly, NLC have risen as a promising alternative to the conventional pharmaceutical forms in terms of the efficient delivery of therapeutics by different administration routes, including the topical ophthalmic pathway. Likewise, additional physicochemical properties of their excipients (such as high biocompatibility, biodegradability, and non-toxicity) support the use of NLC as new suitable DDS. The ease of scale, the controlled release profile, high stability and improved also reinforce the use of these novel nanosystems.

The elaboration of stable and tunable-size Lf-loaded NLC by double emulsion/solvent evaporation method is highly complex and is determined by different key process conditions, including the optimization of lipids concentration (both solid and liquid lipids), sonication, and thermal shock conditions, among others.

In the present work, lactoferrin-loaded NLC showed an average particle size of 119.45 ± 11.44 nm, a 0.151 ± 0.045 nm PDI and a 17.50 ± 2.53 mV ζ potential, as well as spherical and uniform shape. Similarly, these lipid nanosystems show good stability to storage (up to 3 months), to a 6-12 pH interval and to a 0.075-0.6 M ionic strength range in appropriate media. A controlled release of Lf was also proven, corroborating their use as possible DDS for hydrophilic drugs. Resulting data also confirmed their mucoadhesive properties through electrostatic forces for, at least, 240 min, with no evidence of tissue cytotoxicity.

To sum up, a NLC system was proposed, for the first time, for the topical ophthalmic delivery of lactoferrin, as an alternative to the present aggressive clinical approaches. Its design and development were reinforced by a consistent *in vitro* and *in vivo* characterization preclinical basis. Similarly, NLC showed suitable physicochemical characteristics for ocular administration, delaying the drug release, and assuring the patient's adherence-to-treatment. Additionally, these lipid nanosystems versatility would permit their use in a huge variety of pharmaceutical forms for topical ophthalmic delivery, as a new method of personalized pharmacological therapy.

USC DE COMPOSTELA

REFERENCES

1. Gaudana, R.; Ananthula, H.K.; Parenky, A.; Mitra, A.K. Ocular Drug Delivery. AAPS J. 2010, 12, 348–360, doi:10.1208/s12248-010-9183-3.
2. Varela-Fernández, R.; Díaz-Tomé, V.; Luaces-Rodríguez, A.; Conde-Penedo, A.; García-Otero, X.; Luzardo-Álvarez, A.; Fernández-Ferreiro, A.; Otero-Espinar, F.J. Drug Delivery to the Posterior Segment of the Eye: Biopharmaceutic and Pharmacokinetic Considerations. Pharmaceutics 2020, 12, doi:10.3390/pharmaceutics12030269.
3. Bourlais, C.L.; Acar, L.; Zia, H.; Sado, P.A.; Needham, T.; Leverge, R. Ophthalmic Drug Delivery Systems--Recent Advances. Prog. Retin. Eye Res. 1998, 17, 33–58, doi:10.1016/s1350-9462(97)00002-5.
4. Seyfoddin, A.; Shaw, J.; Al-Kassas, R. Solid Lipid Nanoparticles for Ocular Drug Delivery. Drug Deliv. 2010, 17, 467–489, doi:10.3109/10717544.2010.483257.
5. Saha, R.N.; Vasanthakumar, S.; Bende, G.; Snehalatha, M. Nanoparticulate Drug Delivery Systems for Cancer Chemotherapy. Mol. Membr. Biol. 2010, 27, 215–231, doi:10.3109/09687688.2010.510804.
6. T, T.; T, O. Recent Trends in Clinical Trials Related to Carrier-Based Drugs. J. Pharm. Sci. 2017, 106, 2219–2226, doi:10.1016/j.xphs.2017.02.026.
7. Tapeinos, C.; Battaglini, M.; Ciofani, G. Advances in the Design of Solid Lipid Nanoparticles and Nanostructured Lipid Carriers for Targeting Brain Diseases. J. Control. Release Off. J. Control. Release Soc. 2017, 264, 306–332, doi:10.1016/j.jconrel.2017.08.033.
8. Naseri, N.; Valizadeh, H.; Zakeri-Milani, P. Solid Lipid Nanoparticles and Nanostructured Lipid Carriers: Structure, Preparation and Application. Adv. Pharm. Bull. 2015, 5, 305–313, doi:10.15171/apb.2015.043.
9. Patel, A.; Cholkar, K.; Agrahari, V.; Mitra, A.K. Ocular Drug Delivery Systems: An Overview. World J. Pharmacol. 2013, 2, 47–64, doi:10.5497/wjp.v2.i2.47.
10. Sánchez-López, E.; Espina, M.; Doktorovova, S.; Souto, E.B.; García, M.L. Lipid Nanoparticles (SLN, NLC): Overcoming the Anatomical and Physiological Barriers of the Eye - Part II - Ocular Drug-Loaded Lipid Nanoparticles. Eur. J. Pharm. Biopharm. Off. J. Arbeitsgemeinschaft Pharm. Verfahrenstechnik EV 2017, 110, 58–69, doi:10.1016/j.ejpb.2016.10.013.

USC UNIVERSIDADE DE SANTIAGO DE COMPOSTELA

11. Chen, D.B.; Yang, T.Z.; Lu, W.L.; Zhang, Q. In vitro and in vivo Study of Two Types of Long-Circulating Solid Lipid Nanoparticles Containing Paclitaxel. Chem. Pharm. Bull. (Tokyo) 2001, 49, 1444–1447, doi:10.1248/cpb.49.1444.

12. Fundarò, A.; Cavalli, R.; Bargoni, A.; Vighetto, D.; Zara, G.P.; Gasco, M.R. Non-Stealth and Stealth Solid Lipid Nanoparticles (SLN) Carrying Doxorubicin: Pharmacokinetics and Tissue Distribution after IV Administration to Rats. Pharmacol. Res. 2000, 42, 337–343, doi:10.1006/phrs.2000.0695.

13. Müller, R.H.; Mäder, K.; Gohla, S. Solid Lipid Nanoparticles (SLN) for Controlled Drug Delivery - a Review of the State of the Art. Eur. J. Pharm. Biopharm. Off. J. Arbeitsgemeinschaft Pharm. Verfahrenstechnik EV 2000, 50, 161–177, doi:10.1016/s0939-6411(00)00087-4.

14. Dingler, A.; Gohla, S. Production of Solid Lipid Nanoparticles (SLN): Scaling up Feasibilities. J. Microencapsul. 2002, 19, 11–16, doi:10.1080/02652040010018056.

15. Freitas, C.; Müller, R.H. Correlation between Long-Term Stability of Solid Lipid Nanoparticles (SLN) and Crystallinity of the Lipid Phase. Eur. J. Pharm. Biopharm. Off. J. Arbeitsgemeinschaft Pharm. Verfahrenstechnik EV 1999, 47, 125–132, doi:10.1016/s0939-6411(98)00074-5.

16. Mehnert, W.; Mäder, K. Solid Lipid Nanoparticles: Production, Characterization and Applications. Adv. Drug Deliv. Rev. 2001, 47, 165–196, doi:10.1016/s0169-409x(01)00105-3.

17. Kymes, S.M.; Walline, J.J.; Zadnik, K.; Sterling, J.; Gordon, M.O.; Collaborative Longitudinal Evaluation of Keratoconus Study Group Changes in the Quality-of-Life of People with Keratoconus. Am. J. Ophthalmol. 2008, 145, 611–617, doi:10.1016/j.ajo.2007.11.017.

18. Romero-Jiménez, M.; Santodomingo-Rubido, J.; Wolffsohn, J.S. Keratoconus: A Review. Contact Lens Anterior Eye J. Br. Contact Lens Assoc. 2010, 33, 157–166; quiz 205, doi:10.1016/j.clae.2010.04.006.

19. Meiri, Z.; Keren, S.; Rosenblatt, A.; Sarig, T.; Shenhav, L.; Varssano, D. Efficacy of Corneal Collagen Cross-Linking for the Treatment of Keratoconus: A Systematic Review and Meta-Analysis. Cornea 2016, 35, 417–428, doi:10.1097/ICO.0000000000000723.

USC UNIVERSIDADE DE SANTIAGO

20. Sharif, R.; Bak-Nielsen, S.; Hjortdal, J.; Karamichos, D. Pathogenesis of Keratoconus: The Intriguing Therapeutic Potential of Prolactin-Inducible Protein. Prog. Retin. Eye Res. 2018, 67, 150–167, doi:10.1016/j.preteyeres.2018.05.002.

21. Lema, I.; Durán, J.A. Inflammatory Molecules in the Tears of Patients with Keratoconus. Ophthalmology 2005, 112, 654–659, doi:10.1016/j.ophtha.2004.11.050.

22. Balasubramanian, S.A.; Mohan, S.; Pye, D.C.; Willcox, M.D.P. Proteases, Proteolysis and Inflammatory Molecules in the Tears of People with Keratoconus. Acta Ophthalmol. (Copenh.) 2012, 90, e303-309, doi:10.1111/j.1755-3768.2011.02369.x.

23. Lema, I.; Brea, D.; Rodríguez-González, R.; Díez-Feijoo, E.; Sobrino, T. Proteomic Analysis of the Tear Film in Patients with Keratoconus. Mol. Vis. 2010, 16, 2055–2061.

24. Balasubramanian, S.A.; Pye, D.C.; Willcox, M.D.P. Levels of Lactoferrin, Secretory IgA and Serum Albumin in the Tear Film of People with Keratoconus. Exp. Eye Res. 2012, 96, 132–137, doi:10.1016/j.exer.2011.12.010.

25. González-Chávez, S.A.; Arévalo-Gallegos, S.; Rascón-Cruz, Q. Lactoferrin: Structure, Function and Applications. Int. J. Antimicrob. Agents 2009, 33, 301.e1-301.e8, doi:10.1016/j.ijantimicag.2008.07.020.

26. Legrand, D.; Pierce, A.; Elass, E.; Carpentier, M.; Mariller, C.; Mazurier, J. Lactoferrin Structure and Functions. Adv. Exp. Med. Biol. 2008, 606, 163–194, doi:10.1007/978-0-387-74087-4_6.

27. Appelmelk, B.J.; An, Y.Q.; Geerts, M.; Thijs, B.G.; de Boer, H.A.; MacLaren, D.M.; de Graaff, J.; Nuijens, J.H. Lactoferrin Is a Lipid A-Binding Protein. Infect. Immun. 1994, 62, 2628–2632.

28. Hayashida, K.; Kaneko, T.; Takeuchi, T.; Shimizu, H.; Ando, K.; Harada, E. Oral Administration of Lactoferrin Inhibits Inflammation and Nociception in Rat Adjuvant-Induced Arthritis. J. Vet. Med. Sci. 2004, 66, 149–154, doi:10.1292/jvms.66.149.

29. Schryvers, A.B.; Morris, L.J. Identification and Characterization of the Human Lactoferrin-Binding Protein from Neisseria Meningitidis. Infect. Immun. 1988, 56, 1144–1149.

30. Ellison, R.T.; Giehl, T.J. Killing of Gram-Negative Bacteria by Lactoferrin and Lysozyme. J. Clin. Invest. 1991, 88, 1080–1091.

31. Takakura, N.; Wakabayashi, H.; Ishibashi, H.; Teraguchi, S.; Tamura, Y.; Yamaguchi, H.; Abe, S. Oral Lactoferrin Treatment of Experimental Oral Candidiasis in Mice. Antimicrob. Agents Chemother. 2003, 47, 2619–2623, doi:10.1128/AAC.47.8.2619-2623.2003.

32. Marchetti, M.; Superti, F.; Ammendolia, M.G.; Rossi, P.; Valenti, P.; Seganti, L. Inhibition of Poliovirus Type 1 Infection by Iron-, Manganese- and Zinc-Saturated Lactoferrin. Med. Microbiol. Immunol. (Berl.) 1999, 187, 199–204, doi:10.1007/s004300050093.

USC UNIVERSIDADE DE SANTIAGO

33. Murphy, M.E.; Kariwa, H.; Mizutani, T.; Tanabe, H.; Yoshimatsu, K.; Arikawa, J.; Takashima, I. Characterization of in vitro and in vivo Antiviral Activity of Lactoferrin and Ribavirin upon Hantavirus. J. Vet. Med. Sci. 2001, 63, 637–645, doi:10.1292/jvms.63.637.

34. Berkhout, B.; Floris, R.; Recio, I.; Visser, S. The Antiviral Activity of the Milk Protein Lactoferrin against the Human Immunodeficiency Virus Type 1. Biometals 2004, 17, 291–294, doi:10.1023/B:BIOM.0000027707.82911.be.

35. Eliassen, L.T.; Berge, G.; Sveinbjørnsson, B.; Svendsen, J.S.; Vorland, L.H.; Rekdal, Ø. Evidence for a Direct Antitumor Mechanism of Action of Bovine Lactoferricin. Anticancer Res. 2002, 22, 2703–2710.

36. Tsuda, H.; Sekine, K.; Fujita, K.; Ligo, M. Cancer Prevention by Bovine Lactoferrin and Underlying Mechanisms--a Review of Experimental and Clinical Studies. Biochem. Cell Biol. Biochim. Biol. Cell. 2002, 80, 131–136, doi:10.1139/o01-239.

37. Pattamatta, U.; Willcox, M.; Stapleton, F.; Cole, N.; Garrett, Q. Bovine Lactoferrin Stimulates Human Corneal Epithelial Alkali Wound Healing in vitro. Invest. Ophthalmol. Vis. Sci. 2009, 50, 1636–1643, doi:10.1167/iovs.08-1882.

38. Flanagan, J.L.; Willcox, M.D.P. Role of Lactoferrin in the Tear Film. Biochimie 2009, 91, 35–43, doi:10.1016/j.biochi.2008.07.007.

39. Akira, S.; Takeda, K. Toll-like Receptor Signalling. Nat. Rev. Immunol. 2004, 4, 499–511, doi:10.1038/nri1391.

40. Sobrino, T.; Regueiro, U.; Malfeito, M.; Vieites-Prado, A.; Pérez-Mato, M.; Campos, F.; Lema, I. Higher Expression of Toll-Like Receptors 2 and 4 in Blood Cells of Keratoconus Patiens. Sci. Rep. 2017, 7, 1–7, doi:10.1038/s41598-017-13525-7.

41. Ueta, M.; Kinoshita, S. Ocular Surface Inflammation Is Regulated by Innate Immunity. Prog. Retin. Eye Res. 2012, 31, 551–575, doi:10.1016/j.preteyeres.2012.05.003.

42. Gesto, M.I.L.; Sánchez, J.A.C.; Moreiras, T.S.; Perez, F.C. Biomarkers for Diagnosis and Prognosis of Corneal Ectatic Disorders 2016.

43. Varela-Fernández, R.; García-Otero, X.; Díaz-Tomé, V.; Regueiro, U.; López-López, M.; González-Barcia, M.; Lema, M.I.; Otero-Espinar, F.J. Design, Optimization, and Characterization of Lactoferrin-Loaded Chitosan/TPP and Chitosan/Sulfobutylether-β-Cyclodextrin Nanoparticles as a Pharmacological Alternative for Keratoconus Treatment. ACS Appl. Mater. Interfaces 2021, 13, 3559–3575, doi:10.1021/acsami.0c18926.

USC UNIVERSIDADE DE SANTIAGO

44. Jores, K.; Haberland, A.; Wartewig, S.; Mäder, K.; Mehnert, W. Solid Lipid Nanoparticles (SLN) and Oil-Loaded SLN Studied by Spectrofluorometry and Raman Spectroscopy. Pharm. Res. 2005, 22, 1887–1897, doi:10.1007/s11095-005-7148-5.

45. Moghimi, S.M.; Hunter, A.C.; Andresen, T.L. Factors Controlling Nanoparticle Pharmacokinetics: An Integrated Analysis and Perspective. Annu. Rev. Pharmacol. Toxicol. 2012, 52, 481–503, doi:10.1146/annurev-pharmtox-010611-134623.

46. Truong, N.P.; Whittaker, M.R.; Mak, C.W.; Davis, T.P. The Importance of Nanoparticle Shape in Cancer Drug Delivery. Expert Opin. Drug Deliv. 2015, 12, 129–142, doi:10.1517/17425247.2014.950564.

47. Jithan, A.; Madhavi, K.; Madhavi, M.; Prabhakar, K. Preparation and Characterization of Albumin Nanoparticles Encapsulating Curcumin Intended for the Treatment of Breast Cancer. Int. J. Pharm. Investig. 2011, 1, 119–125, doi:10.4103/2230-973X.82432.

48. Selvamuthukumar, S.; Velmurugan, R. Nanostructured Lipid Carriers: A Potential Drug Carrier for Cancer Chemotherapy. Lipids Health Dis. 2012, 11, 159, doi:10.1186/1476-511X-11-159.

49. Q 1 A (R2) Stability Testing of New Drug Substances and Products. 2006, 20.

50. Muthu, M.S.; Singh, S. Poly (D, L-Lactide) Nanosuspensions of Risperidone for Parenteral Delivery: Formulation and in-Vitro Evaluation. Curr. Drug Deliv. 2009, 6, 62–68, doi:10.2174/156720109787048302.

51. Calvo, P.; Vila-Jato, J.L.; Alonso, M.J. Comparative in vitro Evaluation of Several Colloidal Systems, Nanoparticles, Nanocapsules, and Nanoemulsions, as Ocular Drug Carriers. J. Pharm. Sci. 1996, 85, 530–536, doi:10.1021/js950474+.

52. Yan, G.-P.; Zong, R.-F.; Li, L.; Fu, T.; Liu, F.; Yu, X.-H. Anticancer Drug-Loaded Nanospheres Based on Biodegradable Amphiphilic ε-Caprolactone and Carbonate Copolymers. Pharm. Res. 2010, 27, 2743–2752, doi:10.1007/s11095-010-0275-7.

53. Chamberlain, M.; Gad, S.C.; Gautheron, P.; Prinsen, M.K. IRAG Working Group 1. Organotypic Models for the Assessment/Prediction of Ocular Irritation. Interagency Regulatory Alternatives Group. Food Chem. Toxicol. Int. J. Publ. Br. Ind. Biol. Res. Assoc. 1997, 35, 23–37, doi:10.1016/s0278-6915(96)00100-7.

54. Balls, M.; Botham, P.A.; Bruner, L.H.; Spielmann, H. The EC/HO International Validation Study on Alternatives to the Draize Eye Irritation Test. Toxicol. Vitro Int. J. Publ. Assoc. BIBRA 1995, 9, 871–929, doi:10.1016/0887-2333(95)00092-5.

USC UNIVERSIDADE DE SANTIAGO DE COMPOSTELA

55. Christian, M.S.; Diener, R.M. Soaps and Detergents: Alternatives to Animal Eye Irritation Tests. J. Am. Coll. Toxicol. 1996, 15, 1–44, doi:10.3109/10915819609008705.
56. Loprieno, N. Alternative Methodologies for the Safety Evaluation of Chemicals in the Cosmetic Industry; CRC Press, 2019; ISBN 978-1-00-069678-3.
57. Sina, J.F.; Gautheron, P.D. A Multitest Approach to Evaluating Ocular Irritation in vitro. Toxicol. Methods 1994, 4, 41–49, doi:10.3109/15376519409049111.
58. Barile, F.A. Validating and Troubleshooting Ocular In vitro Toxicology Tests. J. Pharmacol. Toxicol. Methods 2010, 61, 136–145, doi:10.1016/j.vascn.2010.01.001.
59. Wagner, B.M. Book Review: Handbook of Toxicology, 2nd Edition, Edited by Derelanko MJ and Hollinger MA, CRC Press, 1,414 Pages, Numerous Tables and Figures, 2001, Price $149.95. Toxicol. Pathol. 2002, 30, 534–534, doi:10.1080/01926230290105730.
60. Salem, H.; Katz, S.A. Alternative Toxicological Methods; CRC Press, 2003; ISBN 978-0-203-00879-9.
61. Eskes, C.; Bessou, S.; Bruner, L.; Curren, R.; Jones, P.; Kreiling, R.; Liebsch, M.; McNamee, P.; Pape, W.; Prinsen, M.K.; et al. Subgroup 3. Eye Irritation. 76.
62. Sina, J.F.; Galer, D.M.; Sussman, R.G.; Gautheron, P.D.; Sargent, E.V.; Leong, B.; Shah, P.V.; Curren, R.D.; Miller, K. A Collaborative Evaluation of Seven Alternatives to the Draize Eye Irritation Test Using Pharmaceutical Intermediates. Fundam. Appl. Toxicol. 1995, 26, 20–31, doi:10.1006/faat.1995.1071.
63. Luepke, N.P. Hen's Egg Chorioallantoic Membrane Test for Irritation Potential. Food Chem. Toxicol. Int. J. Publ. Br. Ind. Biol. Res. Assoc. 1985, 23, 287–291, doi:10.1016/0278-6915(85)90030-4.
64. Kalweit, S.; Besoke, R.; Gerner, I.; Spielmann, H. A National Validation Project of Alternative Methods to the Draize Rabbit Eye Test. Toxicol. Vitro Int. J. Publ. Assoc. BIBRA 1990, 4, 702–706, doi:10.1016/0887-2333(90)90147-l.
65. Spielmann, H.; Kalweit, S.; Liebsch, M.; Wirnsberger, T.; Gerner, I.; Bertram-Neis, E.; Krauser, K.; Kreiling, R.; Miltenburger, H.G.; Pape, W.; et al. Validation Study of Alternatives to the Draize Eye Irritation Test in Germany: Cytotoxicity Testing and HET-CAM Test with 136 Industrial Chemicals. Toxicol. Vitro Int. J. Publ. Assoc. BIBRA 1993, 7, 505–510, doi:10.1016/0887-2333(93)90055-a.

USC UNIVERSIDADE DE SANTIAGO

66. Belgamwar, V.; Shah, V.; Surana, S.J. Formulation and Evaluation of Oral Mucoadhesive Multiparticulate System Containing Metoprolol Tartarate: An in vitro-Ex vivo Characterization. Curr. Drug Deliv. 2009, 6, 113–121, doi:10.2174/156720109787048285.

67. Gradauer, K.; Vonach, C.; Leitinger, G.; Kolb, D.; Fröhlich, E.; Roblegg, E.; Bernkop-Schnürch, A.; Prassl, R. Chemical Coupling of Thiolated Chitosan to Preformed Liposomes Improves Mucoadhesive Properties. Int. J. Nanomedicine 2012, 7, 2523–2534, doi:10.2147/IJN.S29980.

68. Rojas, S.; Gispert, J.D.; Abad, S.; Buaki-Sogo, M.; Victor, V.M.; Garcia, H.; Herance, J.R. In vivo Biodistribution of Amino-Functionalized Ceria Nanoparticles in Rats Using Positron Emission Tomography. Mol. Pharm. 2012, 9, 3543–3550, doi:10.1021/mp300382n.

69. Pérez-Campaña, C.; Gómez-Vallejo, V.; Martin, A.; Sebastián, E.S.; Moya, S.E.; Reese, T.; Ziolo, R.F.; Llop, J. Tracing Nanoparticles in vivo: A New General Synthesis of Positron Emitting Metal Oxide Nanoparticles by Proton Beam Activation. Analyst 2012, 137, 4902–4906, doi:10.1039/C2AN35863H.

70. M, A.; D, M.; B, B.; K, K.; F, R.; O, T.; R, Z. Modifying the Body Distribution of HPMA-Based Copolymers by Molecular Weight and Aggregate Formation. Biomacromolecules 2011, 12, 2841–2849, doi:10.1021/bm2005774.

71. Allmeroth, M.; Moderegger, D.; Gündel, D.; Buchholz, H.-G.; Mohr, N.; Koynov, K.; Rösch, F.; Thews, O.; Zentel, R. PEGylation of HPMA-Based Block Copolymers Enhances Tumor Accumulation in vivo: A Quantitative Study Using Radiolabeling and Positron Emission Tomography. J. Controlled Release 2013, 172, 77–85, doi:10.1016/j.jconrel.2013.07.027.

72. Fernández-Ferreiro, A.; Silva-Rodríguez, J.; Otero-Espinar, F.J.; González-Barcia, M.; Lamas, M.J.; Ruibal, A.; Luaces-Rodriguez, A.; Vieites-Prado, A.; Sobrino, T.; Herranz, M.; et al. Positron Emission Tomography for the Development and Characterization of Corneal Permanence of Ophthalmic Pharmaceutical Formulations. Invest. Ophthalmol. Vis. Sci. 2017, 58, 772–780, doi:10.1167/iovs.16-20766.

73. The Association for Research in Vision and Ophthalmology- Statement for the Use of Animals in Ophthalmic and Vision Research Available online: https://www.arvo.org/About/policies/statement-for-the-use-of-animals-in-ophthalmic-and-vision-research/ (accessed on 22 July 2020).

74. Burden, N.; Aschberger, K.; Chaudhry, Q.; Clift, M.J.D.; Doak, S.H.; Fowler, P.; Johnston, H.; Landsiedel, R.; Rowland, J.; Stone, V. The 3Rs as a Framework to Support a 21st

USC UNIVERSIDADE DE SANTIAGO

Century Approach for Nanosafety Assessment. Nano Today 2017, 12, 10–13, doi:10.1016/j.nantod.2016.06.007.

75. Zhang, Y.; Huo, M.; Zhou, J.; Xie, S. PKSolver: An Add-in Program for Pharmacokinetic and Pharmacodynamic Data Analysis in Microsoft Excel. Comput. Methods Programs Biomed. 2010, 99, 306–314, doi:10.1016/j.cmpb.2010.01.007.

76. García-Fuentes, M.; Torres, D.; Alonso, M.J. Design of Lipid Nanoparticles for the Oral Delivery of Hydrophilic Macromolecules. Colloids Surf. B Biointerfaces 2003, 27, 159–168, doi:10.1016/S0927-7765(02)00053-X.

77. Almeida, A.J.; Runge, S.; Müller, R.H. Peptide-Loaded Solid Lipid Nanoparticles (SLN): Influence of Production Parameters. Int. J. Pharm. 1997, 149, 255–265, doi:10.1016/S0378-5173(97)04885-0.

78. Cerreto, F.; Scalzo, M.; Cesa, S.; Paolicelli, P.; Casadei, M.A. Solid Lipid Nanosuspensions Based on Low Melting Lipids as Protective System of Retinyl Palmitate. J. Drug Deliv. Sci. Technol. 2011, 21, 479–483, doi:10.1016/S1773-2247(11)50077-2.

79. Jensen, L.B.; Magnussson, E.; Gunnarsson, L.; Vermehren, C.; Nielsen, H.M.; Petersson, K. Corticosteroid Solubility and Lipid Polarity Control Release from Solid Lipid Nanoparticles. Int. J. Pharm. 2010, 390, 53–60, doi:10.1016/j.ijpharm.2009.10.022.

80. Doktorovová, S.; Araújo, J.; Garcia, M.L.; Rakovský, E.; Souto, E.B. Formulating Fluticasone Propionate in Novel PEG-Containing Nanostructured Lipid Carriers (PEG-NLC). Colloids Surf. B Biointerfaces 2010, 75, 538–542, doi:10.1016/j.colsurfb.2009.09.033.

81. Liu, J.; Qiu, Z.; Wang, S.; Zhou, L.; Zhang, S. A Modified Double-Emulsion Method for the Preparation of Daunorubicin-Loaded Polymeric Nanoparticle with Enhanced in vitro Anti-Tumor Activity. Biomed. Mater. Bristol Engl. 2010, 5, 065002, doi:10.1088/1748-6041/5/6/065002.

82. Singh, S.; Dobhal, A.K.; Jain, A.; Pandit, J.K.; Chakraborty, S. Formulation and Evaluation of Solid Lipid Nanoparticles of a Water Soluble Drug: Zidovudine. Chem. Pharm. Bull. (Tokyo) 2010, 58, 650–655, doi:10.1248/cpb.58.650.

83. Hu, L.; Tang, X.; Cui, F. Solid Lipid Nanoparticles (SLNs) to Improve Oral Bioavailability of Poorly Soluble Drugs. J. Pharm. Pharmacol. 2004, 56, 1527–1535, doi:10.1211/0022357044959.

USC UNIVERSIDADE DE SANTIAGO

84. Huang, Z.; Hua, S.; Yang, Y.; Fang, J. Development and Evaluation of Lipid Nanoparticles for Camptothecin Delivery: A Comparison of Solid Lipid Nanoparticles, Nanostructured Lipid Carriers, and Lipid Emulsion. Acta Pharmacol. Sin. 2008, 29, 1094–1102, doi:10.1111/j.1745-7254.2008.00829.x.

85. Bunjes, H.; Koch, M.H.J.; Westesen, K. Influence of Emulsifiers on the Crystallization of Solid Lipid Nanoparticles. J. Pharm. Sci. 2003, 92, 1509–1520, doi:10.1002/jps.10413.

86. Abdelkader, H.; Fathalla, Z.; Moharram, H.; Ali, T.F.S.; Pierscionek, B. Cyclodextrin Enhances Corneal Tolerability and Reduces Ocular Toxicity Caused by Diclofenac. Oxid. Med. Cell. Longev. 2018, 2018, 5260976, doi:10.1155/2018/5260976.

87. Partheniades, E. Chapter 3 - Forces between Clay Particles and the Process of Flocculation. In Cohesive Sediments in Open Channels; Partheniades, E., Ed.; Butterworth-Heinemann: Boston, 2009; pp. 47–88 ISBN 978-1-85617-556-2.

88. Sreekumar, S.; Goycoolea, F.M.; Moerschbacher, B.M.; Rivera-Rodriguez, G.R. Parameters Influencing the Size of Chitosan-TPP Nano- and Microparticles. Sci. Rep. 2018, 8, 4695, doi:10.1038/s41598-018-23064-4.

89. Jin, H.; Zhou, W.; Cao, J.; Stoyanov, S.D.; Blijdenstein, T.B.J.; Groot, P.W.N. de; Arnaudov, L.N.; Pelan, E.G. Super Stable Foams Stabilized by Colloidal Ethyl Cellulose Particles. Soft Matter 2012, 8, 2194–2205, doi:10.1039/C1SM06518A.

90. Bizmark, N.; Ioannidis, M.A.; Henneke, D.E. Irreversible Adsorption-Driven Assembly of Nanoparticles at Fluid Interfaces Revealed by a Dynamic Surface Tension Probe. Langmuir ACS J. Surf. Colloids 2014, 30, 710–717, doi:10.1021/la404357j.

91. Robciuc, A.; Rantamäki, A.H.; Jauhiainen, M.; Holopainen, J.M. Lipid-Modifying Enzymes in Human Tear Fluid and Corneal Epithelial Stress Response. Invest. Ophthalmol. Vis. Sci. 2014, 55, 16–24, doi:10.1167/iovs.13-12577.

92. Liu, R.; Liu, Z.; Zhang, C.; Zhang, B. Nanostructured Lipid Carriers as Novel Ophthalmic Delivery System for Mangiferin: Improving in vivo Ocular Bioavailability. J. Pharm. Sci. 2012, 101, 3833–3844, doi:10.1002/jps.23251.

93. Luo, Q.; Zhao, J.; Zhang, X.; Pan, W. Nanostructured Lipid Carrier (NLC) Coated with Chitosan Oligosaccharides and Its Potential Use in Ocular Drug Delivery System. Int. J. Pharm. 2011, 403, 185–191, doi:10.1016/j.ijpharm.2010.10.013.

USC UNIVERSIDADE DE SANTIAGO

94. A, L.-R.; R, T.-P.; I, A.-R.; X, G.-O.; M, G.-B.; Mt, R.-A.; L, M.-P.; P, A.; N, G.-L.; J, S.-R.; et al. Preclinical Characterization and Clinical Evaluation of Tacrolimus Eye Drops. Eur. J. Pharm. Sci. Off. J. Eur. Fed. Pharm. Sci. 2018, 120, doi:10.1016/j.ejps.2018.04.038.

95. Mazet, R.; García-Otero, X.; Choisnard, L.; Wouessidjewe, D.; Verdoot, V.; Bossard, F.; Díaz-Tomé, V.; Blanc-Marquis, V.; Otero-Espinar, F.-J.; Fernandez-Ferreiro, A.; et al. Biopharmaceutical Assessment of Dexamethasone Acetate-Based Hydrogels Combining Hydroxypropyl Cyclodextrins and Polysaccharides for Ocular Delivery. Pharmaceutics 2020, 12, 717, doi:10.3390/pharmaceutics12080717.

96. Zaki, I.; Fitzgerald, P.; Hardy, J.G.; Wilson, C.G. A Comparison of the Effect of Viscosity on the Precorneal Residence of Solutions in Rabbit and Man. J. Pharm. Pharmacol. 1986, 38, 463–466, doi:10.1111/j.2042-7158.1986.tb04611.x.

USC
UNIVERSIDADE DE SANTIAGO DE COMPOSTELA

Chapter 3.

Design, optimization, and characterization of lactoferrin-loaded PLGA nanoparticles for keratoconus treatment

USC
UNIVERSIDADE DE SANTIAGO DE COMPOSTELA

USC
UNIVERSIDADE
DE SANTIAGO
DE COMPOSTELA

Chapter 3

Mucoadhesive PLGA Nanospheres and Nanocapsules for Lactoferrin Controlled Ocular Delivery

Rubén Varela-Fernández[1,2], Xurxo García-Otero[1,3], Victoria Díaz-Tomé[1], Uxía Regueiro[2], Maite López-López[2], Miguel González-Barcia[4], María Isabel Lema[5,*] and Francisco Javier Otero-Espinar[1,6,*].

1. Department of Pharmacology, Pharmacy and Pharmaceutical Technology. University of Santiago de Compostela (USC). Campus vida. Santiago de Compostela. Zip Code: 15782. Spain. francisco.otero@usc.es.
2. Clinical Neurosciences Group. University Clinical Hospital, Health Research Institute of Santiago de Compostela (IDIS). Travesía da Choupana s/n Santiago de Compostela. Zip Code: 15706. Spain. mariaisabel.lema@usc.es.
3. Molecular Imaging Group. University Clinical Hospital, Health Research Institute of Santiago de Compostela (IDIS). Travesía da Choupana s/n Santiago de Compostela. Zip Code: 15706. Spain. xurxo.garcia.otero@gmail.com
4. Clinical Pharmacology Group. University Clinical Hospital, Health Research Institute of Santiago de Compostela (IDIS). Travesía da Choupana s/n Santiago de Compostela. Zip Code: 15706. Spain. miguel.gonzalez.barcia@sergas.es.
5. Department of Surgery and Medical-Surgical Specialties. Ophthalmology Area. University of Santiago de Compostela (USC).Campus Vida. Santiago de Compostela. Zip Code: 15706. Spain. mariaisabel.lema@usc.es.
6. Paraquasil Group. University Clinical Hospital, Health Research Institute of Santiago de Compostela (IDIS). Travesía da Choupana s/n Santiago de Compostela. Zip Code: 15706. Spain. francisco.otero@usc.es.

Pharmaceutics. 2022 Apr 6;14(4):799. doi: 10.3390/pharmaceutics14040799. PMID: 35456633. PMCID: PMC9029159

INTRODUCTION

The eye is an airtight organ and presents a high resistance to all external xenobiotics (1,2). In the past decades, different strategies were deeply studied to improve the ocular drug retention, ameliorating the topical ophthalmic therapeutic effects, and minimizing the limitations of conventional drug delivery systems (DDS). At present, several drug-loaded colloidal systems, intended for ophthalmic applications, are reported to provide controlled drug release and better retention in the ocular surface as opposed to the well-known of typical eye drops (3).

Biodegradable polymers, such as poly(lactic-co-glycolic) acid (PLGA), are widely used as novel DDS due to their compliance with the desirable requirements intended for topical

ophthalmic administration (safety, biodegradability, biocompatibility, non-toxicity, sustained drug release, and drug site-specific targeting) (4). PLGA chemical structure is composed of different ratios of lactic acid and glycolic acid, providing a large range of physicochemical properties depending on the lactic/glycolic acid ratio.

PLGA nanocarriers may be generally prepared by using different techniques, where nanoprecipitation method is one of the most used ones. Nanoprecipitation involves the addition of a water-miscible organic solution, containing a hydrophobic polymer, into an aqueous solution, prompting a diffusion process that leads to the polymer precipitation (5). Monomodal and uniform particle size distribution of nanoparticles is obtained with this technique, leading to an enhanced colloidal stability (6–8), reduced production times and expenditures (9,10), and high production yields (11). Depending on the preparation process, the nanoparticle structure may differ. The drug may be either entrapped into the matrix or adsorbed on the surface (12,13). The resultant nanoparticles provide a controlled drug release depending on the degradation rate of the polymer (14). During the design and development procedure, the selection of the most appropriate type of PLGA is the main key factor in order to obtain an effective drug delivery (15). Although PLGA nanoparticles achieved good results as DDS, the lack of mucoadhesiveness hinders its use in topical ophthalmic administration (16).

Lactoferrin (Lf) is an iron-binding single-chain glycoprotein composed of two lobes to which Fe^{3+} ions may strongly bind. Lf is acknowledged as a first-line defense protein with a pleotropic functional pattern in humans, including anti-inflammatory (17,18), anti-bacterial (19–21), antiviral (22–24), and antitumoral (25,26) actions, among others. Unlike other iron-binding proteins, Lf was observed to promote iron retention in inflamed tissue, as well as stimulate corneal epithelial wound healing (27–29), thereby restricting free radical production and avoiding oxidative damage and inflammation. As consequence of the functions of this glycoprotein, Lf has been proposed for the treatment of different surface ocular pathologies such as (I) dry eye, including Sjögren syndrome and idiopathic dry eye, (II) keratoconjunctivitis, (III) giant papillary conjunctivitis, (IV) irritative and vernal conjunctivitis, or (V) viral and bacterial ocular infections, among others.

USC UNIVERSIDADE DE SANTIAGO

Additionally, Lf have been identified as a candidate to inhibit hypoxia-inducible factors (HIFs), whose main objective is based on the expression regulation of various gene, including VEGF and, consequently, they are considered as a target for treatment of neovascular ocular diseases

such as age-related macular degeneration (AMD), diabetic retinopathy, and diabetic macular edema (30).

Likewise, Lf has also been recognized as a key molecule in the pathogenesis of Keratoconus (KC). KC is a progressive and bilateral degenerative ecstatic disorder, characterized by disorder distinguished by stromal thinning, corneal steepening, and irregular astigmatism, which lead to great visual acuity and impaired social health and life quality that affects young adults causing, worsening over time (31). KC affects all ethnicities and both genders in the same way, whose initial prevalence (1/2000) has significantly increased in the last few years due to new diagnosis techniques (32). The etiology of KC remains unclear, where environmental, genetic, and behavioral factors act as the main pathophysiological contributors (33,34), not existing approved treatment to prevent or decrease its progression (35), only aimed to slow down its progress (36).

Furthermore, numerous research have recognized the role of oxidative stress and lipid peroxidation pathways in the KC pathogenesis (37–39). Under physiological conditions, the generation of reactive oxygen species (ROS) during metabolism is counter-acted by the action of antioxidant enzymes, particularly catalase, superoxide dismutase and glutathione peroxidase, among others. Thus, any alteration in this balance would promote the generation of an oxidative stress phenomenon (40). Likewise, increased oxidative stress is also associated with several types of non-apoptotic cell death, one of them being ferroptosis. Ferroptosis is an iron-dependent cell death process, inducted by the malfunction of the glutathione-dependent antioxidant shield, resulting in the ac-cumulation of lipid peroxidation products (41). Nevertheless, lipophilic antioxidants s (e.g., α-tocopherol, butylated hydroxytoluene or β-carotene) and iron chelators have proven efficacy as strong suppressors in the ferroptosis cell death prevention (42,43).

In recent years, different works were published aiming at an improve on the Lf ocular bioavailability due to its great potential in the treatment of several ophthalmic diseases (44). This improvement may be achieved by increasing the permanence of Lf on the ocular surface or improving Lf corneal permeation. In the present work, Lf-loaded PLGA nanoparticles were prepared by two different modified nanoprecipitation techniques, using a three-component mixture of drug/polymer/surfactant (Lf/PLGA/Poloxamer), as a way to overcome conventional PLGA NPs inherent limitations. These modified polymeric nanocarriers, intended for topical

USC UNIVERSIDADE DE SANTIAGO

ophthalmic administration, were subjected to in vitro characterization, surface-modification, and in vitro and *in vivo* assessments.

MATERIALS

Resomer® RG 502 (Mw: 10000 Da; lactide:glycolide = 50:50), Resomer® RG 502H (Mw: 17000 Da; lactide:glycolide = 50:50), Resomer® RG 503 (Mw: 24000 Da; lactide:glycolide = 50:50) and Resomer® RG 503 H (Mw: 38000 Da; lactide:glycolide = 50:50) were purchased from Evonik (Essen, Germany). Sodium hydroxide (NaOH) and hydrochloric acid (HCl) were acquired from Merck (Darmstadt, Germany). Lactoferrin, Polyvinyl Alcohol (PVA) and Pluronic® F68 were acquired from Sigma-Aldrich (St Louis, USA). All other chemicals and reagents were of the highest purity grade commercially available.

EXPERIMENTAL METHODS

1. Preparation of PLGA nanoparticles

1.1. One-step nanoprecipitation method: nanospheres

The preparation of PLGA nanospheres (NSs) was performed by a modified one-step nanoprecipitation method, based on the elaboration procedure previously developed by Bilati et al. (45), with minor modifications. The polymer was firstly dissolved in DMSO, at different drug:polymer ratios. This phase was added by means of a syringe/needle system by inserting the needle directly into the dispersing phase, an 0.5% (w/v) Pluronic® F68 aqueous solution, under magnetic stirring (up to 750 rpm) at room temperature for 30 minutes. A 1:10 organic:aqueous phase ratio was established for the nanoparticles preparation. Nanoprecipitation immediately occurred when the organic solution was in contact with the aqueous phase. Resulting suspensions were centrifuged three times at 4°C and 50000 rpm for 1-h cycles and washed with double-distilled water in order to remove the residual DMSO, gradually replacing it with water for subsequent freeze-drying using trehalose as cryoprotectant (0.5% w/v). Lactoferrin-loaded PLGA NSs were prepared following the same procedure used for blank nanoparticles, although adding the protein to the aqueous phase before the addition of the organic phase and the subsequently nanoparticle's formation.

USC UNIVERSIDADE DE SANTIAGO DE COMPOSTELA

1.2. Two-step nanoprecipitation method: nanocapsules

The preparation of PLGA nanocapsules (NCs) was performed by a modified two-step nanoprecipitation method, using a method as developed by Weber et al. (46) and subsequently described by Morales-Cruz et al. (47), with negligible changes. Briefly, Lf (0.01% w/v) was dissolved in an aqueous solution and then solvent-precipitated by adding acetonitrile (a water-miscible solvent) at a 1:4 (v/v) ratio. The resulting protein suspension was stirred for 5 minutes under magnetic stirring and at room temperature.

Furthermore, PLGA (0.05% w/v) was also dissolved in acetonitrile under magnetic stirring (500 rpm) at room temperature, and subsequently added to the Lf suspension drop wisely. The resulting mixture was finally added into a maturation medium in a 1:10 (v/v) ratio, composed of a 1% (w/v) PVA aqueous solution, under vigorous stirring (> 750 rpm) and room temperature to promote the nanoparticle formation.

Polymer nanoprecipitation immediately occurred upon infusion of the protein suspension. The resulting lactoferrin-loaded PLGA NCs were the centrifuged for 1 h at 14000 rpm, the supernatant discarded, and the sediment re-suspended in double distilled water. This washing step was thrice repeated, and the samples subsequently freeze-dried using trehalose as cryoprotectant (0.5% w/v).

2. Physicochemical characterization of nanoparticles

2.1. Particle size, size distribution, and z potential

The average particle size, polydispersity index (PDI), and ζ potential of the nanoparticles were determined by Dynamic Light Scattering with non-invasive back scattering (DLS-NIBS) at 25°C, using a Malvern Zetasizer Nano ZS instrument (ZEN3600, Malvern Instruments Ltd., Malvern) (Worcestershire, UK). PLGA NPs were 1:10 diluted prior to the analysis. Each batch was analyzed in triplicate. DLS subsets were defined as previously described (44,48).

2.2. Morphological evaluation

USC UNIVERSIDADE DE SANTIAGO DE COMPOSTELA

The morphological examination of the PLGA NSs and NCs was performed by Scanning Electron Microscopy (SEM) and Transmission Electron Microscopy (TEM). An appropriate sample preparation was made prior to the SEM and TEM analysis, as previously described (44,48). Different batches were used for both types of analysis.

2.3. Production yield (PY) of nanoparticles

The production yield (PY) of the resulting PLGA NPs was obtained by a centrifugation procedure (49), with slight changes. Briefly, fixed volumes of the PLGA NSs or NCs were centrifuged (14000 rpm, 1 h, 25°C), the supernatants were discarded, and the sediment was vacuum-dried until constant weight. The PY values were finally estimated as follows (equation 1):

$$Production\ yield\ (\%) = \frac{Nanoparticles\ weight}{Total\ initial\ solids\ weight} \cdot 100 \quad Equation\ 1$$

2.4. Encapsulation efficiency (EE) and loading capacity (LC) of nanoparticles

Encapsulation efficiency (EE) and loading capacity (LC) of the PLGA NPs were determined after isolation by centrifugation as previously described (44). The amount of unbound Lf was determined by UV-Vis spectrophotometry (Cary 60 UV-Vis, Agilent Technologies®) (California, USA) at a 280.0 nm wavelength, using a method previously validated by our group. The EE (equation 2) and LC (equation 3) of Lf were respectively calculated as follows:

$$EE = \frac{Total\ amount\ of\ drug - Amount\ of\ unbound\ drug}{Total\ amount\ of\ drug} \cdot 100 \quad Equation\ 2$$

$$LC = \frac{Total\ amount\ of\ drug - Amount\ of\ unbound\ drug}{Nanoparticles\ weight} \cdot 100 \quad Equation\ 3$$

3. Stability studies

3.1. Stability to storage

ICH guidelines were followed to design the procedure for determining storage stability (46), with negligeable adjustments. PLGA NSs and NCs were freshly prepared, isolated by centrifugation, and resuspended in PBS (pH 7.4). Samples were incubated at three different temperature conditions: (a) 4 ± 2°C, (b) 25 ± 2°C, and (c) 37 ± 2°C for two different periods: 8 hours (short-time stability) and 3 months (long-term stability), at 100 rpm and protected from

USC UNIVERSIDADE DE SANTIAGO

light. Size and size distribution were measured by DLS, performing every measurement in triplicate.

3.2. Stability to pH

A complete pH interval (2, 4, 6, 7, 8, 10, and 12) was pre-established for the stability study of PLGA NSs and NCs, as previously described (44,48). Samples (500 µL) were 1:10 diluted in double-distilled water and subsequently refrigerated at 4 ± 2°C for 24 h. Particle size, size distribution, and surface charge measurements were finally analyzed by means of a DLS system (Zetasizer Nano, Malvern Instruments Ltd, Worcestershire, UK).

3.3. Stability to ionic strength

A complete ionic strength interval (0.2, 0.4, 0.6, 0.8, 1.2, 1.4, 1.6, and 2 M) was pre-established for the stability study of PLGA NSs and NCs, as previously described (44,48). Samples (500 µL) were 1:10 diluted in double-distilled water and subsequently refrigerated at 4 ± 2°C for 24 h. Particle size, size distribution, and surface charge measurements were finally analyzed by means of a DLS system (Zetasizer Nano, Malvern Instruments Ltd, Worcestershire, UK).

4. *In vitro* release study

The Lf delivery from PLGA NSs and NCs was determined following the dialysis fundamentals previously described as a way to establish the drug diffusion and kinetic behavior from these colloidal systems in a simulated physiological environment. Henceforward, freshly prepared lactoferrin-loaded PLGA NSs and NCs were suspended in PBS (pH 7.4 and ionic strength 0.075 M) for a physiological background proof-of-concept test (51). The experimental procedure was extensively described in previous works (44,48). The protein release rate from PLGA NSs and NCs was determined at predetermined times by UV-Vis spectrophotometry at a 280.0 nm wavelength (Cary 60 UV-Vis, Agilent Technologies®) (California, USA). Analytic validation was previously acquired by our group and demonstrated linearity (R = 0.999) over a 0.4882 – 500 µg/mL concentration interval and LOD and LOQ values of 0.9765 µg/mL and 1.9531 µg/mL, respectively. Results proved that reference solutions remained stable for at least a week, safeguarded from light exposure and under cooling (4 ± 2°C).

USC
DE SANTIAGO
DE COMPOSTELA

5. Cytotoxicity analysis

5.1. Bovine Corneal Opacity and Permeability test (BCOP)

The Bovine Corneal Opacity and Permeability test (BCOP) is an organotypic model commonly employed in the assessment of a great variety of formulations with potential ocular irritancy in order to accomplish the animal replacement frameworks.

The BCOP test fundamentals were based on the methodology earlier established by Tchao et al. (52) and improved by Gautheron et al. (53), with minimal adjustments. A standardized procedure for PLGA NPs addition, as well as the opacity and permeability measurements were established and considerably described in previous works (44,48). In this test, corneal opacity changes were estimated by two different experimental techniques (luxmetry and the spectrophotometry), while permeability data was exclusively obtained by UV-Vis spectrophotometry (490.0 nm wavelength). Each formulation was evaluated in triplicate. The resulting opacity and permeability values were used to calculate an *in vitro* score value (if necessary, see equation 4) (53,54). Furthermore, the classification of PLGA NPs may be performed according to the Kay and Calandra score (53).

$$IVIS = mean\ opacity\ value + (15 \times mean\ permeability\ OD_{490}\ value) \quad Equation\ 4$$

5.2. Hen's egg test on the chorioallantoic membrane (HET-CAM)

The HET-CAM test has turn into an international standard assay for acute eye irritation and corrosion (55,56), where three potential consequences (hemorrhage, lysis, and coagulation) of the CAM may be observed and subsequently measured by an Irritation Score (IS), following the Kalweit et al. criteria (57). The experimental procedure was extensively described in previous works (44,48). Briefly, viable eggs were employed after nine days on incubation at specific environmental conditions (37 ± 0.5°C and 65% ± 5% relative humidity), using the CAM as the target tissue. Once the formulation was placed onto the CAM, a 5 min inspection period was carried out, where images were taken at the beginning and at the end of the assay. Results were both individually and combined analyzed. Each formulation was evaluated in triplicate.

USC
DE SANTIAGO
DE COMPOSTELA

6. Ocular surface retention study

6.1. *Ex vivo* corneal surface retention study

The *ex vivo* corneal surface retention study was based on the procedure firstly defined by Belgamwar et al. and Gradauer et al. (58,59), with minimal adjustments. The experimental procedure was extensively described in previous works (44,48). Briefly, freshly excised eyes were placed upwards on specifically designed holders. Fluorescein-stained PLGA NSs and NCs were then added, where the formulation's excess was collected and reapplied. The residual formulation volume was finally measured for fluorescence intensity by UV-Vis spectrophotometry (Cary 60 UV-Vis, Agilent Technologies®) (California, USA) at a 490.0 nm wavelength. Each formulation was tested in triplicate. Resulting data was compared with the initial intensity values, and the *ex vivo* corneal mucoadhesion of the PLGA-based NPs was subsequently quantified as follows (equation 5):

$$Mucoadhesion\ (\%) = \frac{(Abs_0 - V_0) - (Abs_F - V_F)}{(Abs_0 - V_0)} \cdot 100 \quad Equation\ 5$$

Where Abs_0 and Abs_F indicate the absorbance value for the initial and final fluorescein-stained chitosan-based suspensions, V_0 denotes the volume applied to the viable excised eyes, and V_F designates the final volume of the suspension not adsorbed to the mucosa.

6.2. *In vivo* corneal surface retention study

6.2.1. Evaluation of the radiolabeling stability and efficiency of PLGA-based nanoparticles

Radioactive fluoride (^{18}F) and gallium (^{68}Ga) are two of the most commonly used positron emitters due to their optimal positron features (see details in Table 1), making them suitable for the Positron Emission Tomography (PET) imaging technique. In any case, ^{18}F is mostly clinically used in two different forms, these being 2-(^{18}F)-fluoro-2-deoxy-D-glucose (^{18}F-FDG) and ^{18}F-Choline, while ^{68}Ga is mainly used in binary or ternary complexes, such as the ^{68}Ga-DOTA (1,4,7,10-tetraazacyclododecane-tetraacetic acid).

Table 1. Physicochemical characteristics of different radiotracers (^{18}F and ^{68}Ga).

Radiotracer	$t_{1/2}$ (min)	$E_{\beta+,max}$ (KeV)	b^+ Intensity (%)
^{18}F	109.7	635	97
^{68}Ga	67.71	1899	89

Lately, several methodologies were studied to track different types of nanosized systems using ^{18}F-FDG, ^{18}F-Choline, and ^{68}Ga-DOTA labeling (56–59). The evaluation of the radiolabeling stability and efficiency of PLGA-based NPs was performed by an incubation procedure, as previously described (44,48). It must be considered that ^{18}F-FDG and ^{18}F-Choline were provided by the PET Radiopharmaceutical Unit (Cyclotron) of the University Hospital Complex of Santiago de Compostela (CHUS), while and ^{68}Ga-DOTA was provided by the Galician Radiopharmacy Unit. The radiolabeling efficiency of PLGA-based nanoparticles was assessed by quantifying the radiotracer activity, both in the supernatant and the remnant vials, considering the incubation interval and the radiotracer decay. Mathematical analysis was later employed to acquire the radiolabeling efficiency and labeling stability data over time.

6.2.2. Experimental *in vivo* evaluation of the ocular biopermanence of PLGA-based nanoparticles

The Positron Emission Tomography (PET) and Computed Tomography (CT) combined technique was used for the *in vivo* assessment of the ocular surface retention time of the PLGA NPs, as previously described (64). The *in vivo* experimental procedure was performed in male Sprague-Dawley rats, whose environmental and feeding conditions were controlled throughout the procedure, according to the ARVO approved guidelines for laboratory animals (65). The PET/CT acquisition and data processing were extensively described in previous works (44,48). Each formulation was tested in quadruplicate (four eyes, two animals) in order to accomplish the 3Rs regulatory outlines (66).

The formulation's radioactivity versus time diagrams were finally acquired, comparing the resulting data against a control solution (^{18}F-Choline buffered solution). A monoexponential decay equation based on a single compartmental model was applied for the remaining formulation versus time fitting by means of the GraphPad Prism® and pKSolver® software (67). Non-compartmental analysis was also performed by assessing the mean residence time (MRT)

USC UNIVERSIDADE DE SANTIAGO DE COMPOSTELA

and the total area under the curve (AUC) of the labelled PLGA NPs remaining percentage versus time.

7. Data analysis

Pairs of groups were compared by carrying out one-tailed Student's t-test and multiple group comparison was conducted by one-way or two-way analysis of variance (one-way or two-way ANOVA), with a 95% significance level ($p < 0.05$) throughout these studies, using the GraphPad Prism® v.8.41 software (GraphPad Software, Inc. CA, USA). All data are presented as a mean value with its standard deviation indicated (mean ± SD). Tukey's or Bonferroni's tests were subsequently applied for post-hoc contrast.

RESULTS AND DISCUSSION

1. Preparation of lactoferrin-loaded PLGA nanoparticles

1.1. One-step nanoprecipitation method: lactoferrin-loaded PLGA nanospheres

Conventional nanoprecipitation technique is usually based on a solvent displacement phenomenon, where a suitable solvent condition shifted into an inappropriate solvent condition (68). Nevertheless, the modified one-step nanoprecipitation methodology applied in the present work made possible to successfully entrapped Lf into PLGA nanospheres. Certainly, both protein and polymer were individually dissolved into two different proper solvents, which were then converted into one unsuitable solvent in a one-step mixing process. The formation of lactoferrin-loaded PLGA NSs was based on the interfacial deposition of polymer and drug by an interfacial solvent displacement phenomenon between two different unstable liquid solvents (69).

1.2. Two-step nanoprecipitation method: lactoferrin-loaded PLGA nanocapsules

The modified two-step nanoprecipitation method designed for the obtention of lactoferrin-loaded PLGA NCs was successfully applied. This method was based on the assumptions previously described by Giteau et al. (70), who precipitated proteins to ensure their stability upon subsequent encapsulation into PLGA microspheres.

The modified two-step nanoprecipitation method previously described (see methods section 1.2.) was based on a double solvent displacement process, by using a desolvating agent (acetonitrile) to precipitate the protein and to promote the polymer dissolution. The original methodology was also slightly changed to assure the obtention of nanosized PLGA nanocarriers with high Lf content, avoiding enzyme inactivation or aggregation phenomena.

2. Physicochemical characterization of nanoparticles

2.1. Particle size, size distribution, and ζ potential

Particle size and size distribution of novel nanoparticulate systems are important factors in view of their potential application for topical ophthalmic administration. Indeed, it is well known that particles in the nanometric range influence biological parameters, such as the *in vivo* distribution through biological barriers, drug delivery to the target tissue, drug content, stability or toxicity, among others (71–74).

Tables 2 and 3 show the average size for PLGA NSs and NCs, respectively. The polydispersity index (PDI) was lower than 0.3 for all formulations, suggesting that a homogeneous population of nanoparticles was obtained. Regarding the surface charge, final formulations were measured by DLS, obtaining high negatively ζ potential values due to the PLGA presence in the surface (75). This negatively charged net indicates that the colloidal system is stable over time, desirable to prevent particle aggregation or coalescence (76).

Table 2. Physicochemical characterization for blank and lactoferrin-loaded PLGA NSs.

Formulation	[Lf] (mg/mL)	Size (nm)	PDI	ζ Potential (mV)
Blank 502 NSs	-	103.6 ± 4.9	0.068 ± 0.04	-28.3 ± 3.4
Blank 502H NSs	-	113.7 ± 8.3	0.111 ± 0.04	-31.6 ± 8.9
Blank 503 NSs	-	109.3 ± 6.7	0.113 ± 0.05	-28.3 ± 3.6
Blank 503H NSs	-	110.6 ± 9.6	0.136 ± 0.03	-30.3 ± 2.8
Lf-loaded 502 NSs	0.1	134.0 ± 3.9	0.078 ± 0.02	-26.4 ± 7.2
Lf-loaded 502H NSs	0.1	116.3 ± 5.5	0.164 ± 0.05	-18.5 ± 5.4

USC UNIVERSIDADE DE SANTIAGO DE COMPOSTELA

Lf-loaded 503 NSs	0.1	133.4 ± 4.4	0.108 ± 0.03	-17.9 ± 1.9
Lf-loaded 503H NSs	0.1	127.7 ± 7.4	0.131 ± 0.05	-22.3 ± 3.9

Table 3. Physicochemical characterization for blank and lactoferrin-loaded PLGA NCs.

Formulation	[Lf] (mg/mL)	Size (nm)	PDI	ζ Potential (mV)
Blank 502 NCs	-	271.6 ± 13.7	0.158 ± 0.04	-15.2 ± 0.9
Blank 502H NCs	-	166.0 ± 8.3	0.148 ± 0.04	-15.5 ± 1.7
Blank 503 NCs	-	235.2 ± 10.8	0.157 ± 0.03	-16.5 ± 1.0
Blank 503H NCs	-	156.4 ± 4.6	0.156 ± 0.04	-19.4 ± 3.2
Lf-loaded 502 NCs	0.1	270.1 ± 22.9	0.152 ± 0.04	-14.9 ± 0.9
Lf-loaded 502H NCs	0.1	170.7 ± 6.6	0.162 ± 0.03	-16.9 ± 1.3
Lf-loaded 503 NCs	0.1	258.4 ± 14.6	0.147 ± 0.03	-17.7 ± 1.8
Lf-loaded 503H NCs	0.1	157.7 ± 5.3	0.154 ± 0.04	-15.7 ± 2.8

2.2. Effect of protein loading on size and surface charge

Figure 1 shows the average size for blank and lactoferrin-loaded PLGA-based nanoparticles. Resulting data suggest that the presence of the protein has a small influence on particle size, although it must be taken into account that the drug:polymer ratio was 1:40, so that the influence may be masked by the large amount of polymer (see Tables 2 and 3, methods section 2.1.). A one-way ANOVA statistical analysis was applied, and no statistically significant differences were found among the formulations ($F = 2.753$ and $P = 0.0550$ for PLGA NSs, and $F = 3.715$ and $P = 0.0558$ for PLGA NCs), regardless of the polymer used.

USC UNIVERSIDADE DE SANTIAGO DE COMPOSTELA

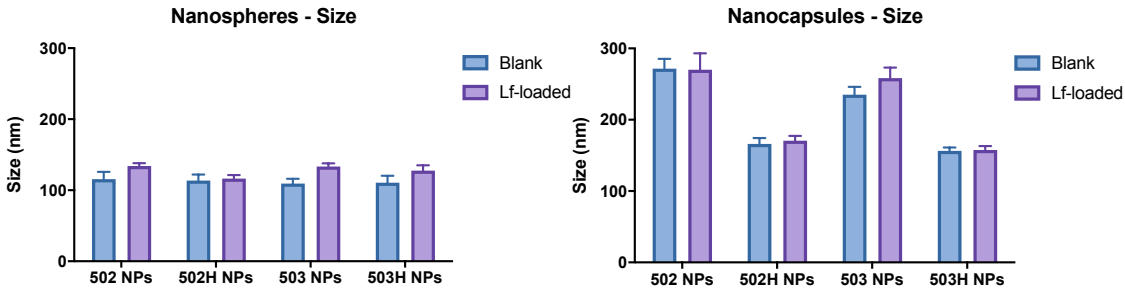


Figure 1. Comparison of size differences for blank and lactoferrin-loaded PLGA-based nanoparticles.

In order to point out, ζ potential values of lactoferrin-loaded PLGA NSs were lower than blank formulations (see Figure 2), suggesting that the protein could not be just encapsulated inside the nanocarriers, but also attached to the polymeric external shell. A one-way ANOVA statistical analysis was applied, and no statistically significant differences were found among the formulations ($F = 50.90$ and $P < 0.001$), regardless of the polymer used. These results are supported by previous studies (77), where it is suggested that the external charges of the nanoparticles are affected by the molecular organization of all the compounds and the net formed by the chemical positions. Nevertheless, these ζ potential differences are not significantly observed in the lactoferrin-loaded PLGA NCs ($F = 0.05051$ and $P = 0.8231$) (see Figure 2), supporting the idea that Lf is encapsulated and protected by a polymeric shell, typical of a reservoir colloidal system, without being massively adhered to the polymeric surface.

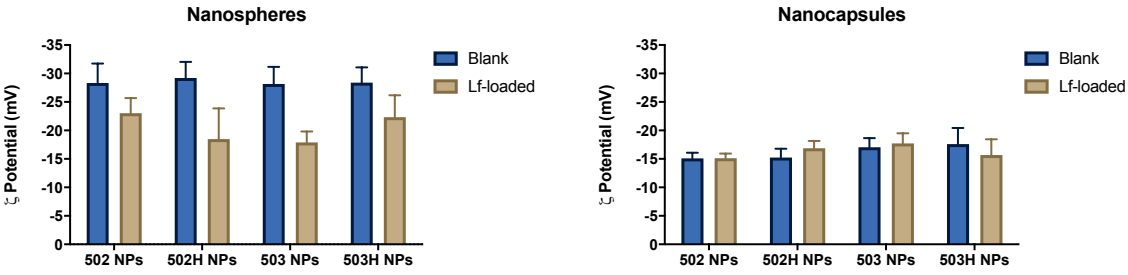


Figure 2. Comparison of ζ potential differences for blank and lactoferrin-loaded PLGA-based nanoparticles.

USC
UNIVERSIDADE DE SANTIAGO DE COMPOSTELA

2.3. Morphological evaluation

SEM images were examined in order to demonstrate that the nanoparticle's size was maintained after the dehydration process. SEM analysis after the vacuum-drying process confirmed the presence of monodisperse populations of spherical in shape and irregular surface particles with size below 300 nm, although some aggregation phenomena due to the drying process was observed (see Figure 3). Thus, the vacuum-dried formulations guarantee the nanoscale size, where the microstructural analysis confirmed the morphology and size of the nanoparticles. The size and morphology results were aligned with the TEM morphological evaluation for both types of nanoparticles.

The TEM images provide information about the particle size and morphology of nanoparticles, as well as confirm previous DLS measurements. The microstructural analysis confirmed that PLGA-based nanoparticles were presented as individual spherical entities, with a homogeneous distribution (monodisperse population), spherical in shape and irregular surface particles with well-defined sizes (see Figure 3). These results agree well with previous studies (80–82), clearly differentiating the NSs from the NCs structure.

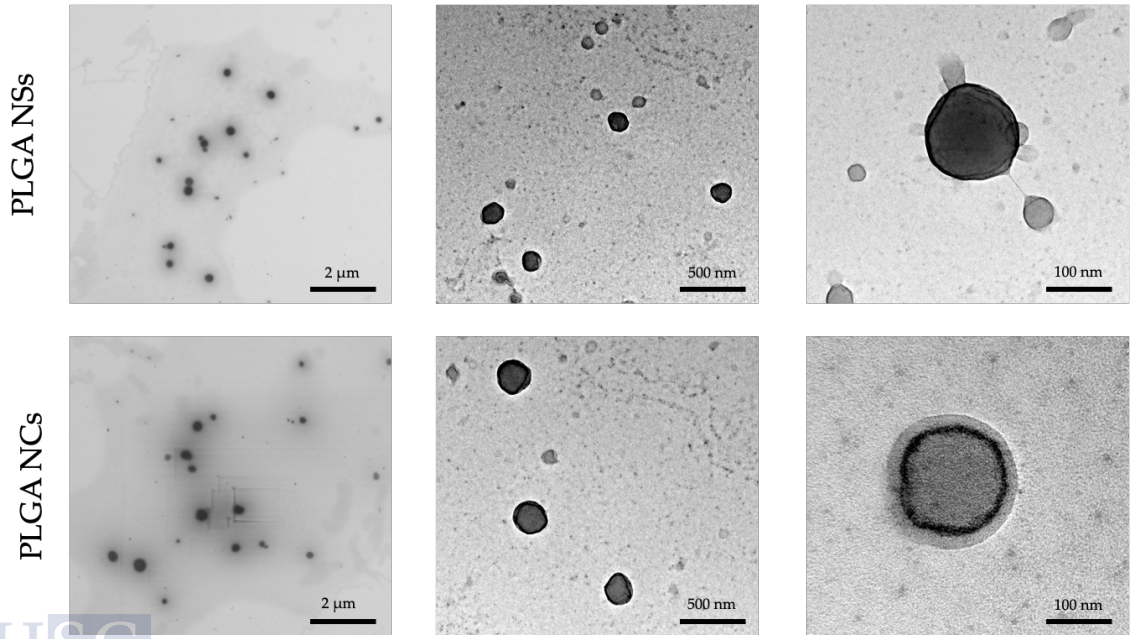


Figure 3. TEM images of lactoferrin-loaded PLGA NSs and lactoferrin-loaded PLGA NCs.

USC UNIVERSIDADE DE SANTIAGO DE COMPOSTELA

2.4. Production yield (PY), encapsulation efficiency (EE), and loading capacity (LC) of nanoparticles

Two different types of PLGA-based NPs were developed for Lf encapsulation. Figure 4 shows the PY, EE, and LC of resulting lactoferrin-loaded PLGA-based nanoparticles. The encapsulation efficiency determination demonstrated that the elaboration process of these nanosystems was reproducible and efficient, with the PY values (above 80%). A one-way ANOVA analysis was applied to the resulting data in order to determine the existence of differences among the prepared formulations. The results indicate that there were no statistically significant differences in terms of PY and EE. Nevertheless, considerable differences were observed for LC values, where NCs-based formulations permitted the obtention of high Lf-embedded content into the polymer matrix, compared to the NSs-based formulations, which barely showed any loading capacity (less than 10%). These data are consistent with the nanoparticle preparation method, where NCs show a large amount of drug inside the polymer matrix while, in the NSs, the drug is mostly adhered to the polymeric matrix surface, presumably by electrostatic bonds.

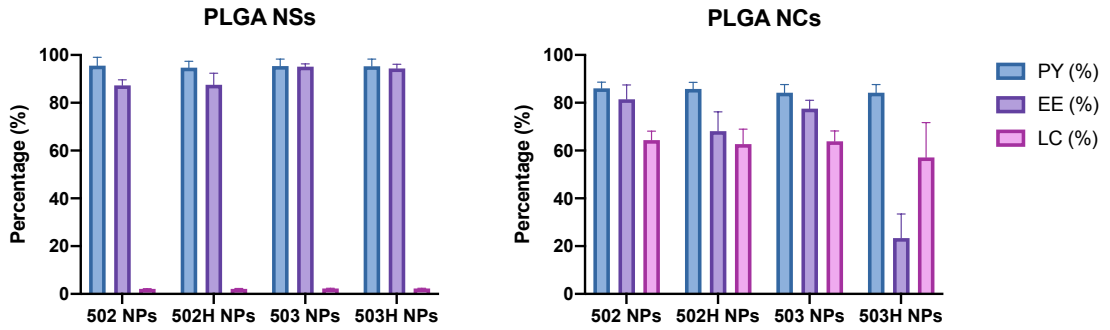


Figure 4. PY, EE and LC values for PLGA-based nanoparticles.

3. Stability studies

3.1. Stability study during storage

The long-term stability determination of PLGA NSs and NCs was performed by determining the size, size distribution, and surface charge by keeping samples at three different temperature sets (4 ± 2°C, 25 ± 2°C/60 ± 5% RH and 37 ± 2°C/60 ± 5% RH) for a 3-month period.

The results for the long-term stability study showed that both formulations did not suffer a significant change in their size following incubation over a 3-month period (see Figures 5 and 6) for two different temperature sets (4 ± 2°C and 25 ± 2°C/60 ± 5% RH). Nevertheless, aggregation phenomena were observed in the third temperature set (37 ± 2°C/60 ± 5% RH) as of the second month. This process may be associated with the glass transition temperature of the PLGA, which varies from 40 to 60°C (near the studied temperature), leading to an increase in the brittle characteristics of the polymer in physiological-like conditions (81).

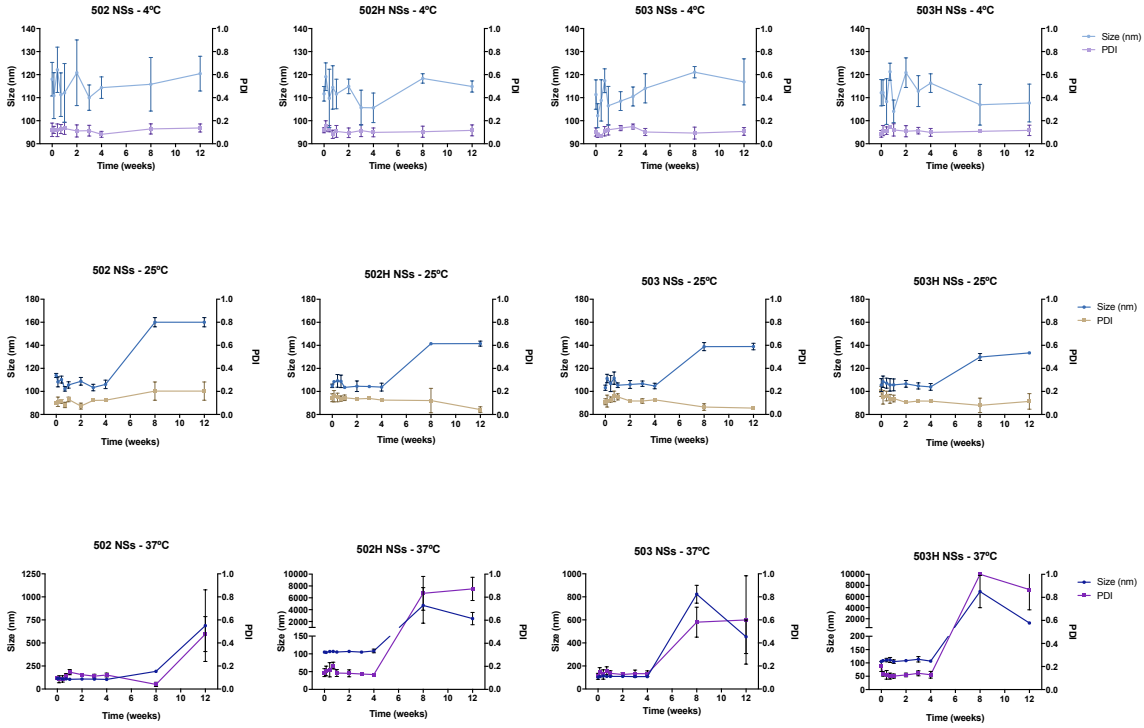


Figure 5. Stability-to-storage study for PLGA-based NSs at three different temperature conditions: (I) 4 ± 2°C, (II) 25 ± 2°C, and (III) 37 ± 2°C, respectively.

USC
UNIVERSIDADE DE SANTIAGO DE COMPOSTELA

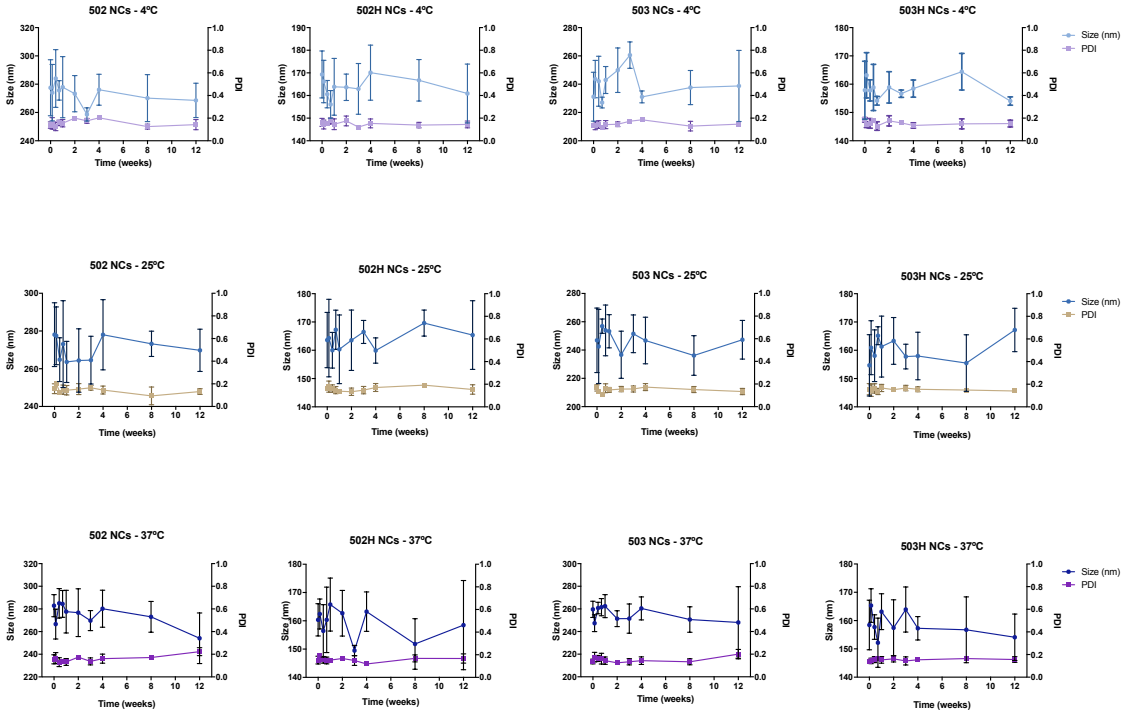


Figure 6. Stability-to-storage study for PLGA-based NCs at three different temperature conditions: (I) 4 ± 2°C, (II) 25 ± 2°C, and (III) 37 ± 2°C, respectively.

3.2. Stability to pH

Changes in the pH conditions of the media may be generally associated with nanoparticle's collapse, breakage, or coalescence phenomena. Figures 7 and 8 show the particle size and ζ potential changes for both PLGA-based nanoparticles along the tested pH interval.

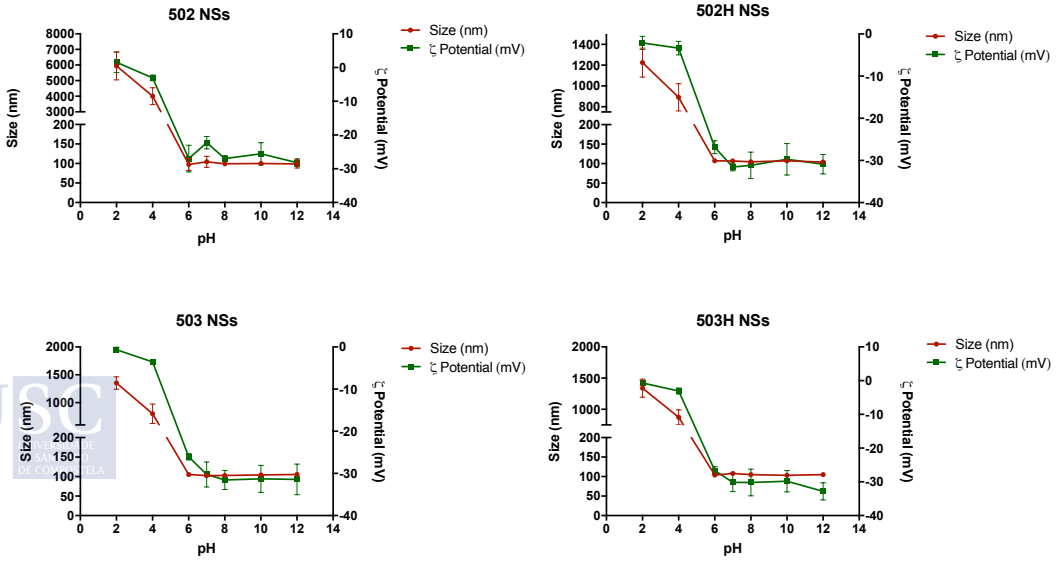


Figure 7. Changes in size and ζ potential values of lactoferrin-loaded PLGA NSs over the studied pH interval.

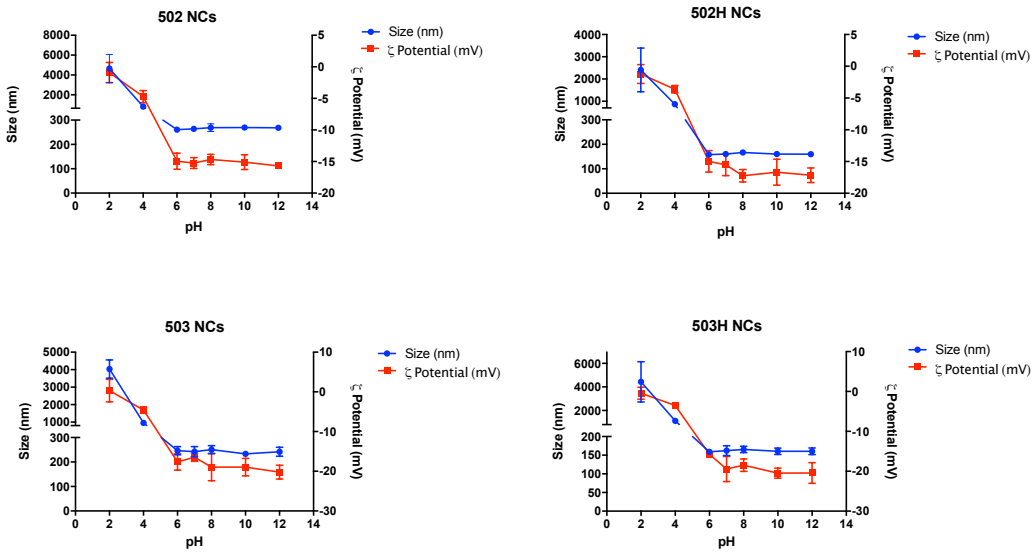


Figure 8. Changes in size and ζ potential values of lactoferrin-loaded PLGA NCs along the studied pH interval.

The same pattern was observed along the pH interval in terms of size and ζ potential values for both types of PLGA nanoparticles. These changes are presumably associated with the polymeric nature of the resulting formulations, where PLGA determines the nanoparticle's surface charge. Hence, aggregation phenomena were observed in the lower acidic pH range (from pH 2 to 4), because of the interaction between the acidic media (high proton concentration) and the negatively charged groups of the polymeric nanocarriers, nullifying the nanoparticle's surface charge (ζ potential ≈ 0). Nevertheless, from a pH 6 value, PLGA-based nanoparticles remained stable in size, where high negatively ζ potential values were also observed, supporting these results. Thus, PLGA-based colloidal systems would be suitable for topical ophthalmic administration without causing ocular surface damages or tearing (pH interval: from 4 to 8) (82).

3.3. Stability study to ionic strength

Changes in the ionic strength conditions of the media may be generally associated with nanoparticle's collapse, breakage, or coalescence phenomena. Figures 9 and 10 show the resulting data for the stability study to ionic strength of lactoferrin-loaded PLGA NSs and NCs for the ionic strength tested interval, respectively.

USC
DE SANTIAGO
DE COMPOSTELA

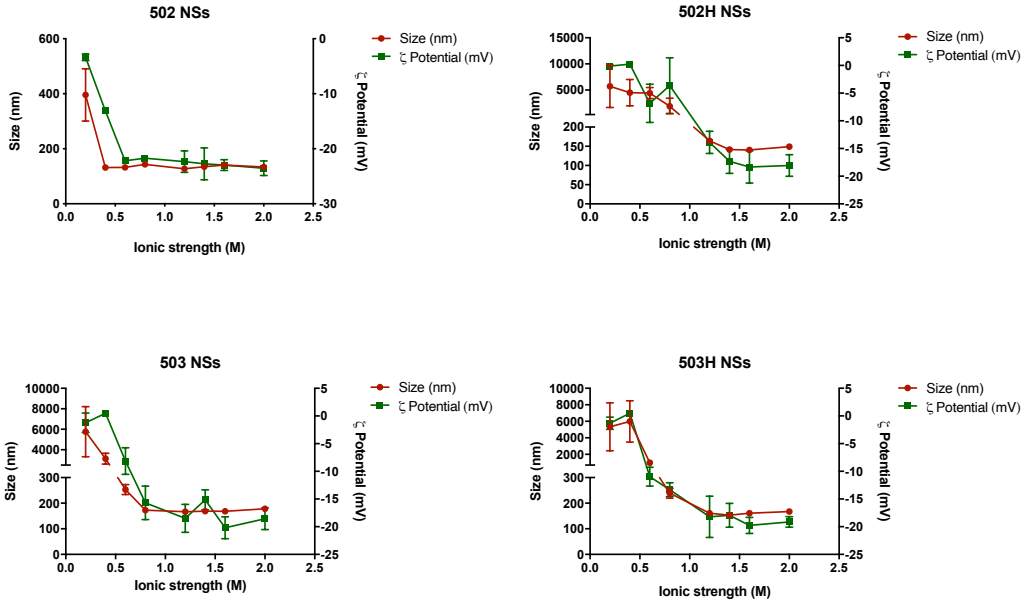


Figure 9. Changes in size and ζ potential values of lactoferrin-loaded PLGA nanospheres over the studied ionic strength interval.

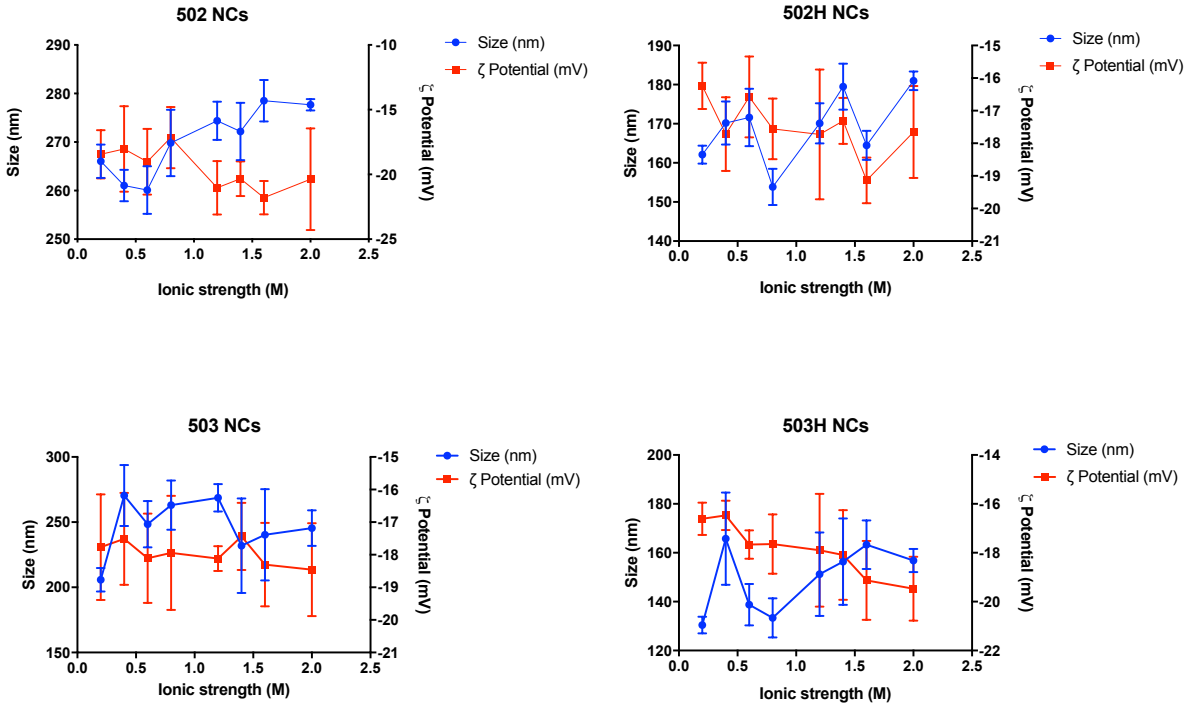


Figure 10. Changes in size and ζ potential values of lactoferrin-loaded PLGA NCs over the studied ionic strength interval.

USC UNIVERSIDADE DE SANTIAGO DE COMPOSTELA

The colloidal stability of both types of nanoparticles were kept constant regardless of the increased ionic strength conditions of the media, where a ζ potential rise was observed with the increasing salt concentration of the media.

The physical stability to ionic strength depends on possible time-dependent aggregation, flocculation or sedimentation phenomena of the nanoparticles (83). Changes in the particle compactness over time may also influence either of these processes. Nevertheless, all formulations stored in the presence of NaCl aqueous solution were mostly stable with respect to changes in size, turbidity, and particle compactness over the studied period.

4. *In vitro* release study

The two main release mechanisms associated with drug loaded PLGA nanosystems are diffusion and bioerosion/degradation. The release rate is initially controlled by the diffusion mechanism while the bioerosion/degradation processes modulate the final stage of the release period. Previous studies have also proven the influence of drug release mechanisms and many other factors (porosity, water content, polymer-drug and drug-drug interactions, among others) in drug diffusion and degradation kinetics from PLGA-based DDS (84).

The preliminary *in vitro* release study from lactoferrin-loaded PLGA nanoparticles proves that both formulations present a sustained release form, compared to a control solution, as shown in Figures 11 and 12. The *in vitro* protein release profiles obtained for each formulation showed two different release phases, as follows: (I) a first initial burst release due to the drug desorbed from the particles surface, and (II) a plateau release phase, resulting from the protein diffusion from the polymer matrix as a consequence of the polymer bioerosion processes. It must be considered that the polymer's autocatalytic degradation is based on the excision of ester bonds, resulting in a decrease in the molecular weight, being faster in the matrix center and becoming more pronounced in larger systems (84).

USC
UNIVERSIDADE DE SANTIAGO DE COMPOSTELA

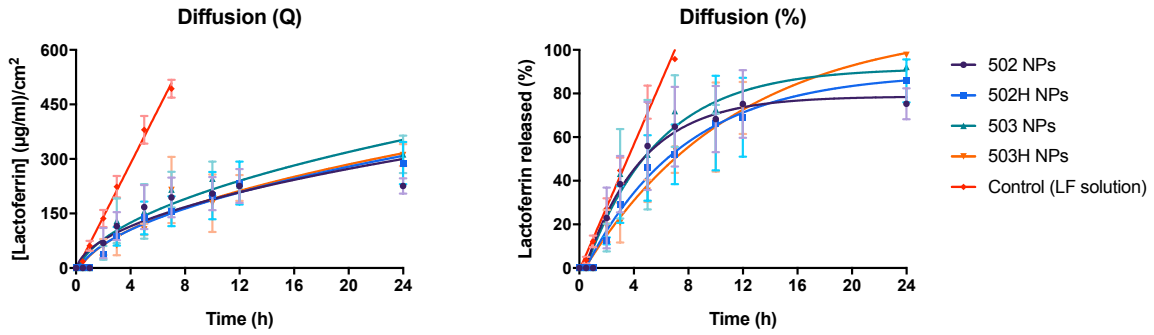


Figure 11. *In vitro* release study of Lf from PLGA NSs. The first graph embodies the raw amount of Lf corrected by the available surface released from the PLGA NSs over the 24 h-period. The second graph represents the percentage of Lf released from the PLGA NSs along the 24 h-period.

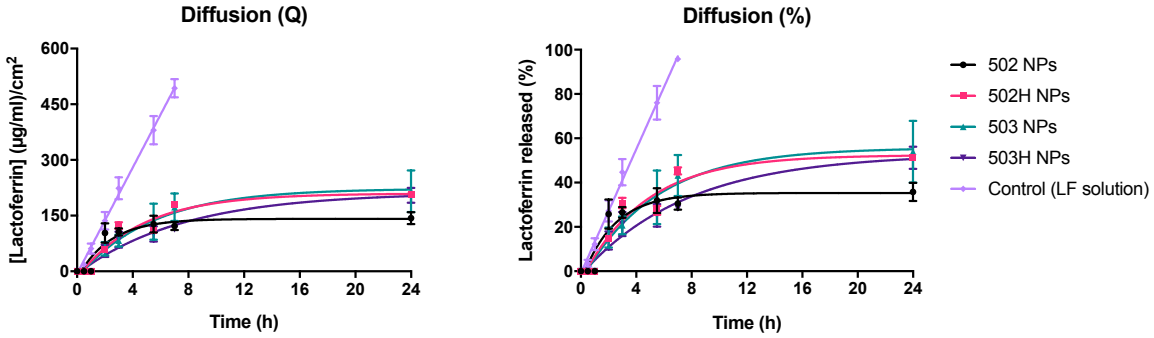


Figure 12. *In vitro* release study of Lf from PLGA NCs. The first graph embodies the raw amount of Lf corrected by the available surface released from the PLGA NCs over the 24 h-period. The second graph represents the percentage of Lf released from the PLGA NCs along the 24 h-period.

On the other hand, a lower molecular weight leads to a less hydrophobic and higher water absorption capability, increasing their hydrolysis and bioerosion rate. Thus, the release of Lf was expected to be faster in the nanoparticles made with Resomer® RG 502 and Resomer® RG 502H, compared to those made with Resomer® RG 503 and Resomer® RG 503H. Nevertheless, no statistically significant differences were observed among all the formulations.

In addition, the release rate can be also affected by interactions between the drug and the polymer. These interactions and their impact on the subsequent release profiles have been deeply examined in previous studies (85–87). However, no statistically significant differences were noticed among all the formulations despite differences in the hydrophobicity of the polymers, possibly due to the similarity on the lactic and glycolic acids' content.

Table 4. Release data of Lf-loaded PLGA NSs and NCs into the Hopfenberg ($M_t/M_\infty=1-[kt]^n$), Higuchi ($M_t/M_\infty = k\sqrt{t}$), Peppas and Korsmeyer ($M_t/M_\infty = kt^n$) diffusion kinetics models.

	Hopfenberg			Higuchi			Peppas and Korsmeyer		
Formulation	k	n	R	**k ($mg \cdot cm^{-2} \cdot min^{-n}$)**	**n**	**R**	**K (min^{-1})**	**Tau**	**R**
502 NSs	0.0377	3	0.9418	34.81	0.2868	0.8415	0.2378	4.205	0.8704
502H NSs	0.0302	3	0.9679	27.16	0.1517	0.5799	0.1378	7.259	0.8977
503 NSs	0.0394	3	0.9340	24.66	0.3866	0.8864	0.1868	5.353	0.8700
503H NSs	0.0293	3	0.9789	27.61	0.4138	0.9123	0.0902	11.08	0.9370
502 NCs	0.0215	3	0.7839	25.41	0.1077	0.9176	0.4312	2.319	0.8606
502H NCs	0.0243	3	0.8798	21.07	0.2950	0.8943	0.2177	4.593	0.9246
503 NCs	0.0237	3	0.9639	18.92	0.3489	0.8316	0.1879	5.321	0.8877
503H NCs	0.0170	3	0.8914	13.09	0.4195	0.9435	0.1305	7.665	0.9388

In the present study, the resulting *in vitro* release profiles were adjusted to different kinetic models. The best correlation was obtained with the Hopfenberg and Peppas-and-Korsmeyer kinetic models (with n values in the range of 0.57 – 0.93), indicating that diffusion was the main release mechanism (see details in Table 4). These results are supported by data showed in previous scientific articles (88–92).

5. Cytotoxicity analysis

5.1. Bovine Corneal Opacity and Permeability test (BCOP)

The BCOP test is an appropriate *ex vivo* tissue model to select out the moderate, severe, and very severe ocular irritant substances since the depth of injury can be measured with this approach. Figures 13a) and 14a) show the transparency variations measured by UV-Vis spectrophotometry for the lactoferrin-loaded PLGA NSs and NCs, respectively. Figures 13b) and 14b) show the transparency variations measured by luxmetry for the lactoferrin-loaded PLGA NSs and NCs, respectively.

USC DE SANTIAGO DE COMPOSTELA

All PLGA-based formulations resulted in an *in vitro* Irritation Score (IS) of 0 (IS = 0), showing no cytotoxicity effects in terms of transparency modification, compared to control formulations. These results are also supported by the fluorescein permeability data (see Figures 13c) and 14c)), where no fluorescein passage was observed through the corneas after the administration of the formulations.

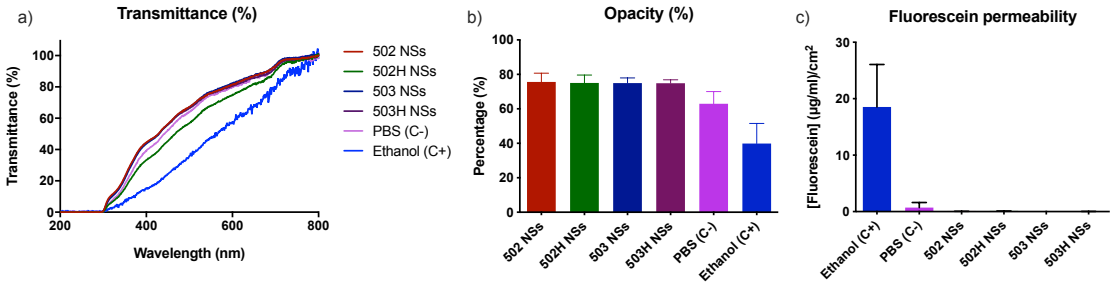


Figure 13. Resulting data of the BCOP test for PLGA-based NSs. (I) final corneal transparency values measured by UV-Vis spectrophotometry, (II) final corneal transparency values measured by luxmetry, and (III) fluorescein permeability measured by UV-Vis spectrophotometry.

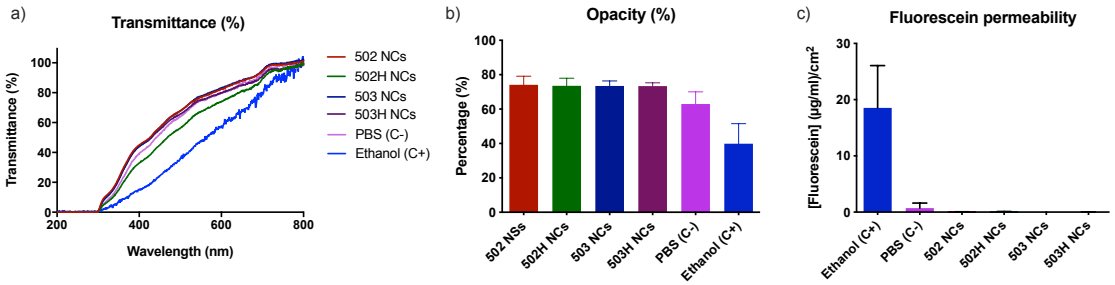


Figure 14. Resulting data of the BCOP test for PLGA-based NCs. (I) final corneal transparency values measured by UV-Vis spectrophotometry, (II) final corneal transparency values measured by luxmetry, and (III) fluorescein permeability measured by UV-Vis spectrophotometry.

5.2. Hen's egg test on the chorioallantoic membrane (HET-CAM)

The CAM is a no innervated tissue and constitutes a well-developed vascularization model and an easy-to-study alternative strategy for ocular irritation assessment due to the complete inflammatory process response, similar to that induced in the Draize test, as it can be performed with greater efficiency and faster measurements than other *in vivo* tests (87–89). Thus, the HET-

CAM assay was used to assess the cytotoxicity and biocompatibility of the prepared nanoparticles.

PLGA-based nanoparticles were evaluated, and the resulting data were compared with those obtained for the 0.9% (w/v) NaCl and 1.8% (w/v) NaOH aqueous solutions, used as negative and positive control formulations, respectively. All formulations show no cytotoxicity effects (Irritation Score = 0), comparing them with control formulations (see Figure 15). This is in good agreement with previously published works (90), as well as in accordance with the results of the BCOP test (see methods section 5.1.) confirming that the materials used and the developed nanosystems are non-toxic and biocompatible.

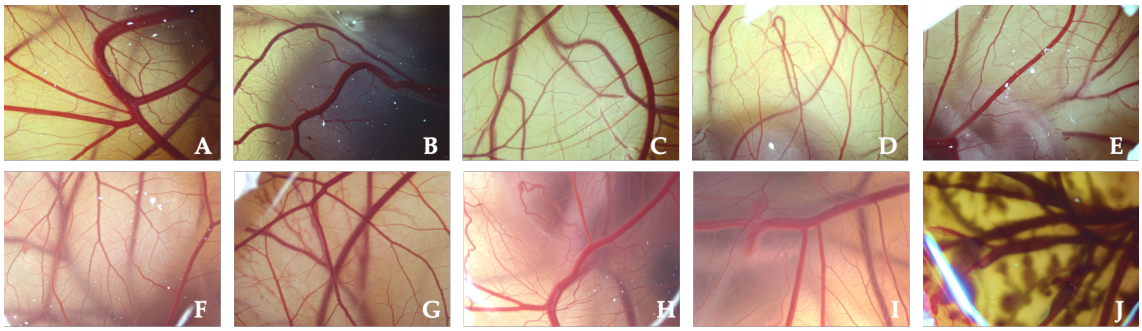


Figure 15. Resulting images of CAM membranes after the PLGA-based nanoparticles administration during the HET-CAM test, compared to the control solutions. (A) 502 PLGA NSs, (B) 502H PLGA NSs, (C) 503 PLGA NSs, (D) 503H PLGA NSs, (E) 502 PLGA NCs, (F) 502H PLGA NCs, (G) 503 PLGA NCs, (H) 503H PLGA NCs, (I) NaCl aqueous solution, and (J) NaOH aqueous solution.

6. Ocular surface retention study

6.1. *Ex vivo* corneal surface model

The *ex vivo* corneal surface retention study was adapted from the original procedure described by Belgamwar et al. (2009) and Gradauer et al. (2012) (58,59), with minor modifications. Figure 16 shows the mucoadhesion percentage for both types of PLGA-based nanoparticles. The resulting data reinforce the possibility of using PLGA-based nanoparticles as an alternative technological strategy for the topical ophthalmic administration of Lf.

USC
UNIVERSIDADE DE SANTIAGO DE COMPOSTELA

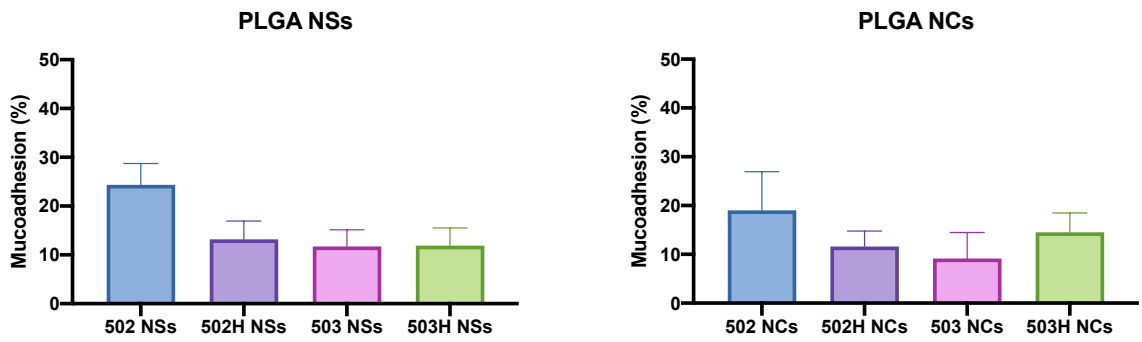


Figure 16. Mucoadhesion data for PLGA-based nanoparticles.

A one-way ANOVA analysis was applied for the PLGA NSs, showing no differences among the formulations, except for the 502 PLGA NSs, which showed a higher muco-adhesion than the rest, being statistically significant. Nevertheless, the same one-way ANOVA analysis was applied for the PLGA NCs, and no significant differences were observed between the prepared formulations, even for the 502 PLGA NCs compared to the others.

The PLGA NSs and NCs ex vivo mucoadhesion values are lower than observed in our group for previous studies made with chitosan and sulfobutylether-β-cyclodextrin/chitosan nanoparticles (44) and nanostructured lipid carriers (48), so it seems that PLGA based nanoparticles have less mucoadhesiveness. This is presumably associated with the surface charge of the nanoparticles, where chitosan-based NPs showed a positive surface charge, which allowed electrostatic interactions with the sialic acid groups of mucin, whereas PLGA nanoparticles showed a negative surface charge, so that their main mechanism of ocular adhesion may be associated with ease of permeation through the corneal layers. Likewise, it must be considered that the *ex vivo* conditions directly correlate with *in vivo* conditions, where different factors are involved and influence the pharmaceutical form administration, such as tearing and blinking, among others (see details in methods section 7.2.).

6.2. *In vivo* corneal biopermanence study

6.2.1. Evaluation of the radiolabeling stability and efficiency of PLGA-based nanoparticles

USC UNIVERSIDADE DE SANTIAGO DE COMPOSTELA

Figure 17 shows the ^{18}F-FDG, ^{18}F-Choline and ^{68}Ga-DOTA radiolabeling stability and efficiency for PLGA-based nanoparticles, respectively. As presented, ^{18}F-FDG and ^{68}Ga-DOTA led to low radiolabeling efficiency (under 50%), although a radiolabeling stability was

observed along the studied interval time, while ^{18}F-Choline displayed a great radiolabeling efficiency (over 80%) and stability over the studied period (up to 3 h) along the studied period, assuring suitable properties for PLGA NPs radiolabeling study. Based on these results, ^{18}F-Choline was selected as the radiotracer for further *in vivo* radiolabeling assays.

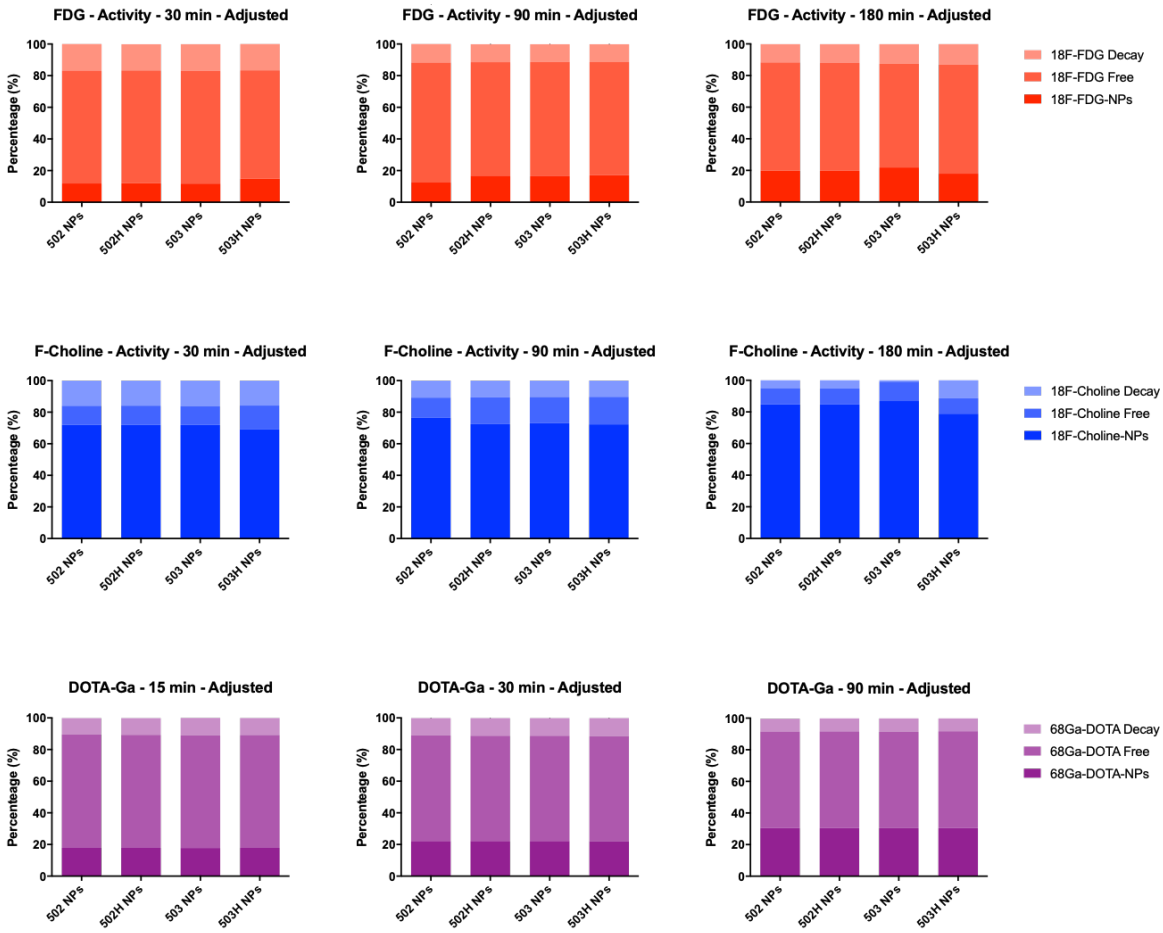


Figure 17. ^{18}F-Choline, ^{18}F-FDG, and ^{68}Ga-DOTA radiolabeling stability and efficiency for PLGA-based nanoparticles over time.

6.2.2. Experimental *in vivo* evaluation of ocular biopermanence

Figure 18 shows the ocular biopermanence of the ^{18}F-Choline-radiolabeled PLGA-based nanoparticles for a 300-min period, compared to the ^{18}F-FDG solution, used as control. A ^{18}F-FDG solution was used as a standard due to the fact that the ^{18}F-Choline is positively charged in its free form, so that it would ionically interact with the negative charge of the sialic acid groups of the mucin layer, resulting in erroneous biodistribution values. On the contrary, ^{18}F-

FDG, presenting a free negative charge, would not bind to the mucin layer, perfectly simulating the administration of a control substance. For the sake of clarification, an analysis of the ^{18}F-Choline-labeled PLGA nanoparticles was carried out to see if this radiotracer modified the size and surface charge, and the results showed that there was no change in either parameter (unpublished data), ensuring that the labeling procedure is suitable for this type of delivery system. The corneal surface retention study of the PLGA-based formulations was measured by the ^{18}F-Choline radioactivity assessment in a PET system.

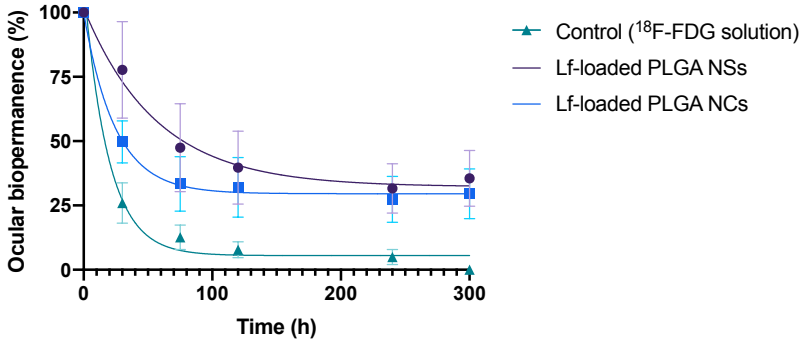


Figure 18. Ocular biopermanence of a ^{18}F-Choline radiolabeled PLGA-based nanoparticles and a ^{18}F-FDG aqueous solution (control), assessed pondering the primary biopermanence data (%) in the ROI.

The ocular biopermanence of the PLGA-based nanoparticles was carried out on rats using ^{18}F-Choline as a radiotracer, trailed by the radioactivity evaluation in a PET equipment over the studied time (see details in Figure 19). In this study, a higher MRT was detected for both Lf-loaded PLGA NSs and NCs, compared to the ^{18}F-FDG solution, even though both formulations consist of an ocular buffered solution (PBS, pH 7.4), whose composition is close to tears. Results were accurately adjusted to a monoexponential decline outline by a single compartmental model (R = 0.9875 for Lf-loaded PLGA NSs, R = 0.9977 for Lf-loaded PLGA NCs, and R = 0.9930 for the ^{18}F-FDG solution) (see Figure 19). The resulting data are in good agreement with the idea that PLGA-based nanoparticles exhibit appropriate mucoadhesive, direct cell uptake, and corneal penetration, being supported the PET data of previous studies (55).

USC UNIVERSIDADE DE SANTIAGO DE COMPOSTELA

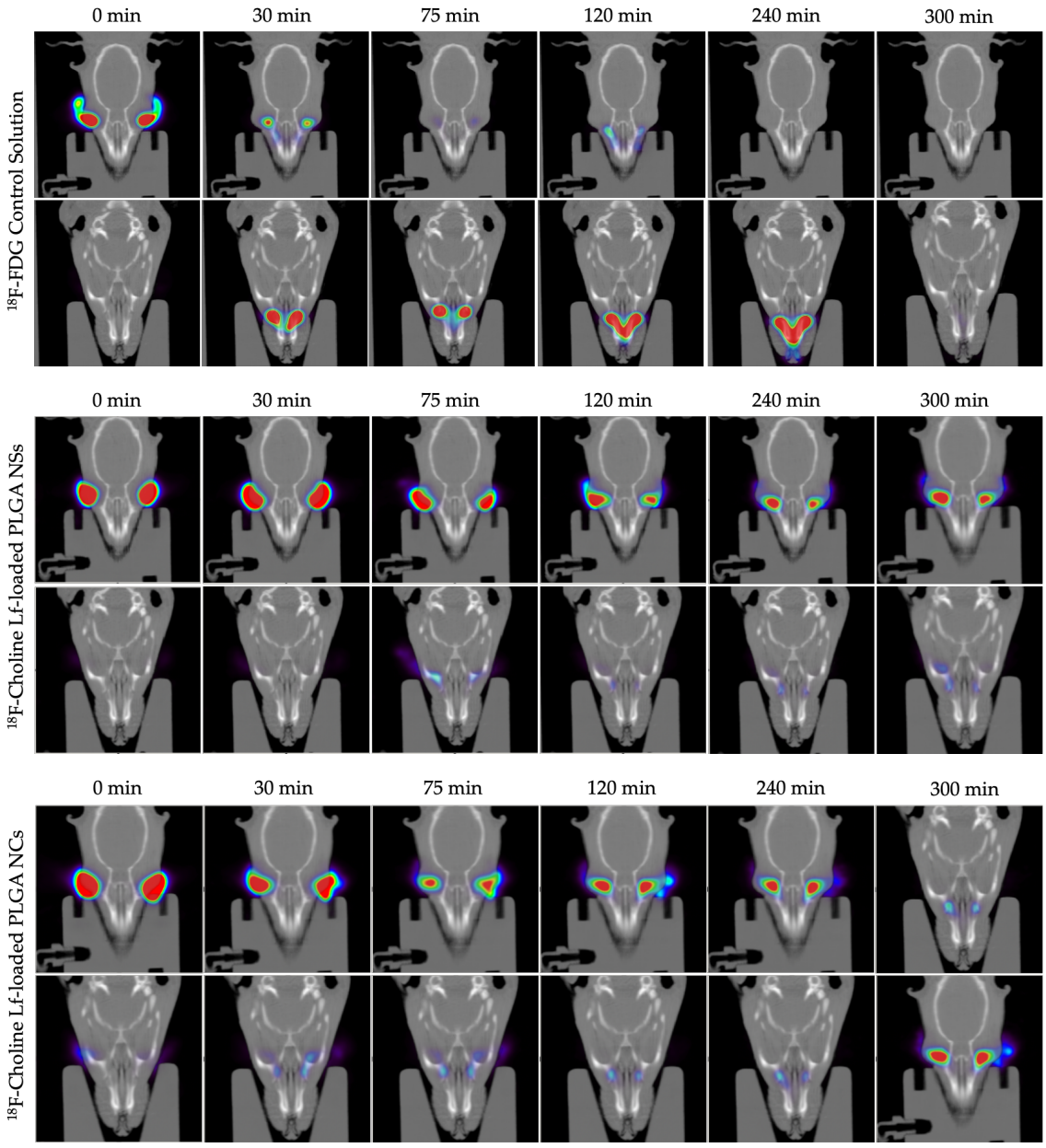


Figure 19. Fused PET/CT images during the 5 h-studied interval. (I) ^{18}F-FDG buffered aqueous solution, (II) ^{18}F-Choline radiolabeled PLGA NSs, and (III) ^{18}F-Choline radiolabeled PLGA NCs.

Table 5 shows the pharmacokinetics factors (k, $t_{1/2}$, MRT, AUC and % dose 30 min) of the ^{18}F-Choline radiolabeled PLGA-based nanoparticles and ^{18}F-FDG standard solution. Statistically significant differences ($p < 0.05$) were spotted concerning PLGA-based formulations and control solution for the studied interval, where Lf-loaded polymeric nanoparticles showed a higher ocular retention profile.

Table 5. Ocular biopermanence parameters for ^{18}F-Choline radiolabeled PLGA-based nanoparticles and ^{18}F-FDG control (named as "control" in the table) formulations.

Formulation	K (min^{-1})		$t_{1/2}$ (min)		% dose 30 min	
	Mean	SD	Mean	SD	Mean	SD
PLGA NSs	0.008	0.0092	93.31	37.71	77.73	18.78
PLGA NCs	0.014	0.0107	51.32	17.45	49.72	8.19
^{18}F-FDG Control	0.044	0.012	16.27	3.81	23.31	5.89
^{18}F-Choline Control	0.013	0.012	53.19	11.28	42.90	5.33

The ocular permanence of the PLGA-based nanoparticles obtained by the PET technique followed the same pattern that the mucoadhesive Lf-loaded CS/TPP and CS/SBE-β-CD NPs, as well as the Lf-loaded NLC (44). Corneally, chitosan-based NPs displayed a $t_{1/2}$ of 114 ± 72 h for CS/TPP NPs, and 60 ± 20 h for CS/SBE-β-CD NPs, respectively, while Lf-loaded NLC showed a t*1/2* of 107.82 ± 38.10 h. Thus, results confirmed the great bioadhesive capability of the PLGA-based formulations in the ocular mucosa.

CONCLUSION

In the biomedical field, polymeric nanoparticles have been extensively studied in the latest decades. Certainly, PLGA-based formulations have risen as a promising alternative to the conventional pharmaceutical forms in terms of the efficient delivery of therapeutics by different administration routes, including the topical ophthalmic pathway. Likewise, additional physicochemical properties of their excipients, such as high biocompatibility, biodegradability, and non-toxicity, support the use of PLGA-based nanoparticles as new promising DDS. The ease of scale, the controlled release profile, high stability, and improved physicochemical properties also reinforce the use of these novel nanosystems.

The obtention of stable and tunable-size Lf-loaded PLGA-based nanoparticles by modified nanoprecipitation methods is highly complex and it is determined by different key process conditions. In the present work, Lf-loaded PLGA-based nanoparticles showed appropriate average particle size, size distribution and ζ potential, as well as spherical and uniform shape. Similarly, these polymeric nanosystems show good stability to storage (up to 3 months), to a 6-

USC UNIVERSIDADE DE SANTIAGO DE COMPOSTELA

12 pH interval, and to a 0.5-2.0 M ionic strength range in appropriate media. A controlled release of Lf was also proven, corroborating their use as possible DDS for hydrophilic drugs. Resulting data also confirmed their mucoadhesive properties through electrostatic forces for, at least, 300 min, with no evidence of tissue cytotoxicity.

To sum up, different PLGA-based formulations were proposed as biodegradable nanocarriers for the delivery of lactoferrin, supported by extensive preclinical studies in order to achieve a consistent base as the first pharmacological treatment for keratoconus as an alternative to current invasive clinical methods. Nevertheless, a better correlation with *in vivo* data should be profoundly explored to deeply understand the real potential of these nanocarriers as a topical ophthalmic alternative strategy for the prevention and treatment of keratoconus.

REFERENCES

1. Bucolo, C.; Drago, F.; Salomone, S. Ocular Drug Delivery: A Clue from Nanotechnology. Front. Pharmacol. 2012, 3, 188, doi:10.3389/fphar.2012.00188.
2. Sahoo, S.K.; Dilnawaz, F.; Krishnakumar, S. Nanotechnology in Ocular Drug Delivery. Drug Discov. Today 2008, 13, 144–151, doi:10.1016/j.drudis.2007.10.021.
3. Rc, N.; S, K.; Pn, S.; P, M.; Jk, P. Polymeric Nanoparticulate System: A Potential Approach for Ocular Drug Delivery. J. Con-trol. Release Off. J. Control. Release Soc. 2009, 136, 2–13, doi:10.1016/j.jconrel.2008.12.018.
4. Danhier, F.; Ansorena, E.; Silva, J.M.; Coco, R.; Le Breton, A.; Préat, V. PLGA-Based Nanoparticles: An Overview of Biomed-ical Applications. J. Control. Release Off. J. Control. Release Soc. 2012, 161, 505–522, doi:10.1016/j.jconrel.2012.01.043.
5. Fessi, H.; Puisieux, F.; Devissaguet, J.Ph.; Ammoury, N.; Benita, S. Nanocapsule Formation by Interfacial Polymer Deposition Following Solvent Displacement. Int. J. Pharm. 1989, 55, R1–R4, doi:10.1016/0378-5173(89)90281-0.
6. Lepeltier, E.; Bourgaux, C.; Couvreur, P. Nanoprecipitation and the “Ouzo Effect”: Application to Drug Delivery Devices. Adv. Drug Deliv. Rev. 2014, 71, 86–97, doi:10.1016/j.addr.2013.12.009.
7. Beck-Broichsitter, M.; Nicolas, J.; Couvreur, P. Solvent Selection Causes Remarkable Shifts of the “Ouzo Region” for Poly(Lactide-Co-Glycolide) Nanoparticles Prepared by Nanoprecipitation. Nanoscale 2015, 7, 9215–9221, doi:10.1039/C5NR01695A.

USC DE SANTIAGO DE COMPOSTELA

8. Vitale, S.A.; Katz, J.L. Liquid Droplet Dispersions Formed by Homogeneous Liquid−Liquid Nucleation: “The Ouzo Effect.” Langmuir 2003, 19, 4105–4110, doi:10.1021/la026842o.

9. Aubry, J.; Ganachaud, F.; Cohen Addad, J.-P.; Cabane, B. Nanoprecipitation of Polymethylmethacrylate by Solvent Shifting: 1. Boundaries. Langmuir ACS J. Surf. Colloids 2009, 25, 1970–1979, doi:10.1021/la803000e.

10. Legrand, P.; Lesieur, S.; Bochot, A.; Gref, R.; Raatjes, W.; Barratt, G.; Vauthier, C. Influence of Polymer Behaviour in Organic Solution on the Production of Polylactide Nanoparticles by Nanoprecipitation. Int. J. Pharm. 2007, 344, 33–43, doi:10.1016/j.ijpharm.2007.05.054.

11. Yang, Z.; Foster, D.; Dhinojwala, A. Continuous Production of Polymer Nanoparticles Using a Membrane-Based Flow Cell. J. Colloid Interface Sci. 2017, 501, 150–155, doi:10.1016/j.jcis.2017.04.044.

12. Hans, M.L.; Lowman, A.M. Biodegradable Nanoparticles for Drug Delivery and Targeting. Curr. Opin. Solid State Mater. Sci. 2002, 9.

13. Soppimath, K.S.; Aminabhavi, T.M.; Kulkarni, A.R.; Rudzinski, W.E. Biodegradable Polymeric Nanoparticles as Drug De-livery Devices. J. Control. Release Off. J. Control. Release Soc. 2001, 70, 1–20, doi:10.1016/s0168-3659(00)00339-4.

14. Corrigan, O.I.; Li, X. Quantifying Drug Release from PLGA Nanoparticulates. Eur. J. Pharm. Sci. Off. J. Eur. Fed. Pharm. Sci. 2009, 37, 477–485, doi:10.1016/j.ejps.2009.04.004.

15. Mu, L.; Feng, S.S. A Novel Controlled Release Formulation for the Anticancer Drug Paclitaxel (Taxol): PLGA Nanoparticles Containing Vitamin E TPGS. J. Control. Release Off. J. Control. Release Soc. 2003, 86, 33–48, doi:10.1016/s0168-3659(02)00320-6.

16. Lemoine, D.; Préat, V. Polymeric Nanoparticles as Delivery System for Influenza Virus Glycoproteins. J. Control. Release Off. J. Control. Release Soc. 1998, 54, 15–27, doi:10.1016/s0168-3659(97)00241-1.

17. Appelmelk, B.J.; An, Y.Q.; Geerts, M.; Thijs, B.G.; de Boer, H.A.; MacLaren, D.M.; de Graaff, J.; Nuijens, J.H. Lactoferrin Is a Lipid A-Binding Protein. Infect. Immun. 1994, 62, 2628–2632.

18. Hayashida, K.; Kaneko, T.; Takeuchi, T.; Shimizu, H.; Ando, K.; Harada, E. Oral Administration of Lactoferrin Inhibits Inflammation and Nociception in Rat Adjuvant-Induced Arthritis. J. Vet. Med. Sci. 2004, 66, 149–154, doi:10.1292/jvms.66.149.

USC UNIVERSIDADE DE SANTIAGO

19. Schryvers, A.B.; Morris, L.J. Identification and Characterization of the Human Lactoferrin-Binding Protein from Neisseria Meningitidis. Infect. Immun. 1988, 56, 1144–1149.
20. Ellison, R.T.; Giehl, T.J. Killing of Gram-Negative Bacteria by Lactoferrin and Lysozyme. J. Clin. Invest. 1991, 88, 1080–1091.
21. Takakura, N.; Wakabayashi, H.; Ishibashi, H.; Teraguchi, S.; Tamura, Y.; Yamaguchi, H.; Abe, S. Oral Lactoferrin Treatment of Experimental Oral Candidiasis in Mice. Antimicrob. Agents Chemother. 2003, 47, 2619–2623, doi:10.1128/AAC.47.8.2619-2623.2003.
22. Marchetti, M.; Superti, F.; Ammendolia, M.G.; Rossi, P.; Valenti, P.; Seganti, L. Inhibition of Poliovirus Type 1 Infection by Iron-, Manganese- and Zinc-Saturated Lactoferrin. Med. Microbiol. Immunol. (Berl.) 1999, 187, 199–204, doi:10.1007/s004300050093.
23. Murphy, M.E.; Kariwa, H.; Mizutani, T.; Tanabe, H.; Yoshimatsu, K.; Arikawa, J.; Takashima, I. Characterization of in vitro and in vivo Antiviral Activity of Lactoferrin and Ribavirin upon Hantavirus. J. Vet. Med. Sci. 2001, 63, 637–645, doi:10.1292/jvms.63.637.
24. Berkhout, B.; Floris, R.; Recio, I.; Visser, S. The Antiviral Activity of the Milk Protein Lactoferrin against the Human Immunodeficiency Virus Type 1. Biometals 2004, 17, 291–294, doi:10.1023/B:BIOM.0000027707.82911.be.
25. Eliassen, L.T.; Berge, G.; Sveinbjørnsson, B.; Svendsen, J.S.; Vorland, L.H.; Rekdal, Ø. Evidence for a Direct Antitumor Mechanism of Action of Bovine Lactoferricin. Anticancer Res. 2002, 22, 2703–2710.
26. Tsuda, H.; Sekine, K.; Fujita, K.; Ligo, M. Cancer Prevention by Bovine Lactoferrin and Underlying Mechanisms--a Review of Experimental and Clinical Studies. Biochem. Cell Biol. Biochim. Biol. Cell. 2002, 80, 131–136, doi:10.1139/o01-239.
27. Pattamatta, U.; Willcox, M.; Stapleton, F.; Cole, N.; Garrett, Q. Bovine Lactoferrin Stimulates Human Corneal Epithelial Alkali Wound Healing in vitro. Invest. Ophthalmol. Vis. Sci. 2009, 50, 1636–1643, doi:10.1167/iovs.08-1882.
28. Flanagan, J.L.; Willcox, M.D.P. Role of Lactoferrin in the Tear Film. Biochimie 2009, 91, 35–43, doi:10.1016/j.biochi.2008.07.007.
29. Akira, S.; Takeda, K. Toll-like Receptor Signalling. Nat. Rev. Immunol. 2004, 4, 499–511, doi:10.1038/nri1391.
30. Ibuki, M.; Shoda, C.; Miwa, Y.; Ishida, A.; Tsubota, K.; Kurihara, T. Lactoferrin Has a Therapeutic Effect via HIF Inhibition in a Murine Model of Choroidal Neovascularization. Front. Pharmacol. 2020, 11.

USC UNIVERSIDADE DE SANTIAGO DE COMPOSTELA

31. Kymes, S.M.; Walline, J.J.; Zadnik, K.; Sterling, J.; Gordon, M.O.; Collaborative Longitudinal Evaluation of Keratoconus Study Group Changes in the Quality-of-Life of People with Keratoconus. Am. J. Ophthalmol. 2008, 145, 611–617, doi:10.1016/j.ajo.2007.11.017.
32. Godefrooij, D.A.; de Wit, G.A.; Uiterwaal, C.S.; Imhof, S.M.; Wisse, R.P.L. Age-Specific Incidence and Prevalence of Kerato-conus: A Nationwide Registration Study. Am. J. Ophthalmol. 2017, 175, 169–172, doi:10.1016/j.ajo.2016.12.015.
33. Sharif, R.; Bak-Nielsen, S.; Hjortdal, J.; Karamichos, D. Pathogenesis of Keratoconus: The Intriguing Therapeutic Potential of Prolactin-Inducible Protein. Prog. Retin. Eye Res. 2018, 67, 150–167, doi:10.1016/j.preteyeres.2018.05.002.
34. Mas Tur, V.; MacGregor, C.; Jayaswal, R.; O'Brart, D.; Maycock, N. A Review of Keratoconus: Diagnosis, Pathophysiology, and Genetics. Surv. Ophthalmol. 2017, 62, 770–783, doi:10.1016/j.survophthal.2017.06.009.
35. Romero-Jiménez, M.; Santodomingo-Rubido, J.; Wolffsohn, J.S. Keratoconus: A Review. Contact Lens Anterior Eye J. Br. Contact Lens Assoc. 2010, 33, 157–166; quiz 205, doi:10.1016/j.clae.2010.04.006.
36. Meiri, Z.; Keren, S.; Rosenblatt, A.; Sarig, T.; Shenhav, L.; Varssano, D. Efficacy of Corneal Collagen Cross-Linking for the Treatment of Keratoconus: A Systematic Review and Meta-Analysis. Cornea 2016, 35, 417–428, doi:10.1097/ICO.0000000000000723.

37. Buddi, R.; Lin, B.; Atilano, S.R.; Zorapapel, N.C.; Kenney, M.C.; Brown, D.J. Evidence of Oxidative Stress in Human Corneal Diseases. J. Histochem. Cytochem. Off. J. Histochem. Soc. 2002, 50, 341–351, doi:10.1177/002215540205000306.
38. Gondhowiardjo, T.D.; van Haeringen, N.J.; Völker-Dieben, H.J.; Beekhuis, H.W.; Kok, J.H.; van Rij, G.; Pels, L.; Kijlstra, A. Analysis of Corneal Aldehyde Dehydrogenase Patterns in Pathologic Corneas. Cornea 1993, 12, 146–154, doi:10.1097/00003226-199303000-00010.
39. Atilano, S.R.; Coskun, P.; Chwa, M.; Jordan, N.; Reddy, V.; Le, K.; Wallace, D.C.; Kenney, M.C. Accumulation of Mitochondrial DNA Damage in Keratoconus Corneas. Invest. Ophthalmol. Vis. Sci. 2005, 46, 1256–1263, doi:10.1167/iovs.04-1395.
40. Lubrano, V.; Balzan, S. Enzymatic Antioxidant System in Vascular Inflammation and Coronary Artery Disease. World J. Exp. Med. 2015, 5, 218–224, doi:10.5493/wjem.v5.i4.218.

USC UNIVERSIDADE DE SANTIAGO

41. Cao, J.Y.; Dixon, S.J. Mechanisms of Ferroptosis. Cell. Mol. Life Sci. CMLS 2016, 73, 2195–2209, doi:10.1007/s00018-016-2194-1.

42. Zilka, O.; Shah, R.; Li, B.; Friedmann Angeli, J.P.; Griesser, M.; Conrad, M.; Pratt, D.A. On the Mechanism of Cytoprotection by Ferrostatin-1 and Liproxstatin-1 and the Role of Lipid Peroxidation in Ferroptotic Cell Death. ACS Cent. Sci. 2017, 3, 232–243, doi:10.1021/acscentsci.7b00028.

43. Dixon, S.J.; Lemberg, K.M.; Lamprecht, M.R.; Skouta, R.; Zaitsev, E.M.; Gleason, C.E.; Patel, D.N.; Bauer, A.J.; Cantley, A.M.; Yang, W.S.; et al. Ferroptosis: An Iron-Dependent Form of Nonapoptotic Cell Death. Cell 2012, 149, 1060–1072, doi:10.1016/j.cell.2012.03.042.

44. Varela-Fernández, R.; García-Otero, X.; Díaz-Tomé, V.; Regueiro, U.; López-López, M.; González-Barcia, M.; Lema, M.I.; Otero-Espinar, F.J. Design, Optimization, and Characterization of Lactoferrin-Loaded Chitosan/TPP and Chitosan/Sulfobutylether-β-Cyclodextrin Nanoparticles as a Pharmacological Alternative for Keratoconus Treatment. ACS Appl. Mater. Interfaces 2021, 13, 3559–3575, doi:10.1021/acsami.0c18926.

45. Bilati, U.; Allémann, E.; Doelker, E. Nanoprecipitation versus Emulsion-Based Techniques for the Encapsulation of Proteins into Biodegradable Nanoparticles and Process-Related Stability Issues. AAPS PharmSciTech 2005, 6, E594-604, doi:10.1208/pt060474.

46. Weber, C.; Coester, C.; Kreuter, J.; Langer, K. Desolvation Process and Surface Characterisation of Protein Nanoparticles. Int. J. Pharm. 2000, 194, 91–102, doi:10.1016/s0378-5173(99)00370-1.

47. Morales-Cruz, M.; Flores-Fernández, G.M.; Morales-Cruz, M.; Orellano, E.A.; Rodriguez-Martinez, J.A.; Ruiz, M.; Griebe-now, K. Two-Step Nanoprecipitation for the Production of Protein-Loaded PLGA Nanospheres. Results Pharma Sci. 2012, 2, 79–85, doi:10.1016/j.rinphs.2012.11.001.

48. Varela-Fernández, R.; García-Otero, X.; Díaz-Tomé, V.; Regueiro, U.; López-López, M.; González-Barcia, M.; Lema, M.I.; Otero-Espinar, F.J. Lactoferrin-loaded nanostructured lipid carriers (NLCs) as a new formulation for optimized ocular drug delivery. Eu. J. Pharm. Biopharm. 2022, S0939-6411(22)00031-5, doi.org/10.1016/j.ejpb.2022.02.010.

49. Jithan, A.; Madhavi, K.; Madhavi, M.; Prabhakar, K. Preparation and Characterization of Albumin Nanoparticles Encapsulating Curcumin Intended for the Treatment of Breast Cancer. Int. J. Pharm. Investig. 2011, 1, 119–125, doi:10.4103/2230-973X.82432.

USC UNIVERSIDADE DE SANTIAGO

50. Q 1 A (R2) Stability Testing of New Drug Substances and Products. 2006, 20.

51. Orthner, M.P.; Lin, G.; Avula, M.; Buetefisch, S.; Magda, J.; Rieth, L.W.; Solzbacher, F. Hydrogel Based Sensor Arrays (2 × 2) with Perforated Piezoresistive Diaphragms for Metabolic Monitoring (in vitro). Sens. Actuators B Chem. 2010, 145, 807–816.

52. Salem, H.; Katz, S.A. Alternative Toxicological Methods; CRC Press, 2003; ISBN 978-0-203-00879-9.

53. Eskes, C.; Bessou, S.; Bruner, L.; Curren, R.; Jones, P.; Kreiling, R.; Liebsch, M.; McNamee, P.; Pape, W.; Prinsen, M.K.; et al. Subgroup 3. Eye Irritation. 76.

54. Sina, J.F.; Galer, D.M.; Sussman, R.G.; Gautheron, P.D.; Sargent, E.V.; Leong, B.; Shah, P.V.; Curren, R.D.; Miller, K. A Collaborative Evaluation of Seven Alternatives to the Draize Eye Irritation Test Using Pharmaceutical Intermediates. Fundam. Appl. Toxicol. 1995, 26, 20–31, doi:10.1006/faat.1995.1071.

55. Chapter 22 - Special Senses. In Fundamentals of Toxicologic Pathology (Third Edition); Wallig, M.A., Haschek, W.M., Rousseaux, C.G., Bolon, B., Eds.; Academic Press, 2018; pp. 673–747 ISBN 978-0-12-809841-7.

56. Luepke, N.P. Hen's Egg Chorioallantoic Membrane Test for Irritation Potential. Food Chem. Toxicol. Int. J. Publ. Br. Ind. Biol. Res. Assoc. 1985, 23, 287–291, doi:10.1016/0278-6915(85)90030-4.

57. Kalweit, S.; Besoke, R.; Gerner, I.; Spielmann, H. A National Validation Project of Alternative Methods to the Draize Rabbit Eye Test. Toxicol. Vitro Int. J. Publ. Assoc. BIBRA 1990, 4, 702–706, doi:10.1016/0887-2333(90)90147-l.

58. Belgamwar, V.; Shah, V.; Surana, S.J. Formulation and Evaluation of Oral Mucoadhesive Multiparticulate System Containing Metoprolol Tartarate: An in vitro-Ex vivo Characterization. Curr. Drug Deliv. 2009, 6, 113–121, doi:10.2174/156720109787048285.

59. Gradauer, K.; Vonach, C.; Leitinger, G.; Kolb, D.; Fröhlich, E.; Roblegg, E.; Bernkop-Schnürch, A.; Prassl, R. Chemical Cou-pling of Thiolated Chitosan to Preformed Liposomes Improves Mucoadhesive Properties. Int. J. Nanomedicine 2012, 7, 2523–2534, doi:10.2147/IJN.S29980.

60. Rojas, S.; Gispert, J.D.; Abad, S.; Buaki-Sogo, M.; Victor, V.M.; Garcia, H.; Herance, J.R. In vivo Biodistribution of Ami-no-Functionalized Ceria Nanoparticles in Rats Using Positron Emission Tomography. Mol. Pharm. 2012, 9, 3543–3550, doi:10.1021/mp300382n.

USC UNIVERSIDADE DE SANTIAGO DE COMPOSTELA

61. Pérez-Campaña, C.; Gómez-Vallejo, V.; Martin, A.; Sebastián, E.S.; Moya, S.E.; Reese, T.; Ziolo, R.F.; Llop, J. Tracing Nanoparticles in vivo: A New General Synthesis of Positron Emitting Metal Oxide Nanoparticles by Proton Beam Activation. Analyst 2012, 137, 4902–4906, doi:10.1039/C2AN35863H.

62. M, A.; D, M.; B, B.; K, K.; F, R.; O, T.; R, Z. Modifying the Body Distribution of HPMA-Based Copolymers by Molecular Weight and Aggregate Formation. Biomacromolecules 2011, 12, 2841–2849, doi:10.1021/bm2005774.

63. Allmeroth, M.; Moderegger, D.; Gündel, D.; Buchholz, H.-G.; Mohr, N.; Koynov, K.; Rösch, F.; Thews, O.; Zentel, R. PEGylation of HPMA-Based Block Copolymers Enhances Tumor Accumulation in vivo : A Quantitative Study Using Radiolabeling and Positron Emission Tomography. J. Controlled Release 2013, 172, 77–85, doi:10.1016/j.jconrel.2013.07.027.

64. Fernández-Ferreiro, A.; Silva-Rodríguez, J.; Otero-Espinar, F.J.; González-Barcia, M.; Lamas, M.J.; Ruibal, A.; Luaces-Rodriguez, A.; Vieites-Prado, A.; Sobrino, T.; Herranz, M.; et al. Positron Emission Tomography for the Development and Characterization of Corneal Permanence of Ophthalmic Pharmaceutical Formulations. Invest. Ophthalmol. Vis. Sci. 2017, 58, 772–780, doi:10.1167/iovs.16-20766.

65. The Association for Research in Vision and Ophthalmology- Statement for the Use of Animals in Ophthalmic and Vision Research Available online: https://www.arvo.org/About/policies/statement-for-the-use-of-animals-in-ophthalmic-and-vision-research/ (accessed on 22 July 2020).

66. Burden, N.; Aschberger, K.; Chaudhry, Q.; Clift, M.J.D.; Doak, S.H.; Fowler, P.; Johnston, H.; Landsiedel, R.; Rowland, J.; Stone, V. The 3Rs as a Framework to Support a 21st Century Approach for Nanosafety Assessment. Nano Today 2017, 12, 10–13, doi:10.1016/j.nantod.2016.06.007.

67. Zhang, Y.; Huo, M.; Zhou, J.; Xie, S. PKSolver: An Add-in Program for Pharmacokinetic and Pharmacodynamic Data Analysis in Microsoft Excel. Comput. Methods Programs Biomed. 2010, 99, 306–314, doi:10.1016/j.cmpb.2010.01.007.

68. Capretto, L.; Cheng, W.; Carugo, D.; Katsamenis, O.L.; Hill, M.; Zhang, X. Mechanism of Co-Nanoprecipitation of Organic Actives and Block Copolymers in a Microfluidic Environment. Nanotechnology 2012, 23, 375602, doi:10.1088/0957-4484/23/37/375602.

USC UNIVERSIDADE DE SANTIAGO

69. Othman, R.; Vladisavljević, G.T.; Shahmohamadi, H.; Nagy, Z.K.; Holdich, R.G. Formation of Size-Tuneable Biodegradable Polymeric Nanoparticles by Solvent Displacement Method Using Micro-Engineered Membranes Fabricated by Laser Drilling and Electroforming. Chem. Eng. J. 2016, 304, 703–713, doi:10.1016/j.cej.2016.07.010.

70. Giteau, A.; Venier-Julienne, M.-C.; Marchal, S.; Courthaudon, J.-L.; Sergent, M.; Montero-Menei, C.; Verdier, J.-M.; Benoit, J.-P. Reversible Protein Precipitation to Ensure Stability during Encapsulation within PLGA Microspheres. Eur. J. Pharm. Biopharm. Off. J. Arbeitsgemeinschaft Pharm. Verfahrenstechnik EV 2008, 70, 127–136, doi:10.1016/j.ejpb.2008.03.006.

71. Csaba, N.; Garcia-Fuentes, M.; Alonso, M.J. The Performance of Nanocarriers for Transmucosal Drug Delivery. Expert Opin. Drug Deliv. 2006, 3, 463–478, doi:10.1517/17425247.3.4.463.

72. Varela-Fernández, R.; Díaz-Tomé, V.; Luaces-Rodríguez, A.; Conde-Penedo, A.; García-Otero, X.; Luzardo-Álvarez, A.; Fernández-Ferreiro, A.; Otero-Espinar, F.J. Drug Delivery to the Posterior Segment of the Eye: Biopharmaceutic and Pharmacokinetic Considerations. Pharmaceutics 2020, 12, doi:10.3390/pharmaceutics12030269.

73. Kumari, A.; Yadav, S.K.; Pakade, Y.B.; Singh, B.; Yadav, S.C. Development of Biodegradable Nanoparticles for Delivery of Quercetin. Colloids Surf. B Biointerfaces 2010, 80, 184–192, doi:10.1016/j.colsurfb.2010.06.002.

74. Mohanraj, V.J.; Chen, Y. Nanoparticles - A Review. Trop. J. Pharm. Res. 2006, 5, 561–573, doi:10.4314/tjpr.v5i1.14634.

75. Oyarzun-Ampuero, F.A.; Brea, J.; Loza, M.I.; Torres, D.; Alonso, M.J. Chitosan-Hyaluronic Acid Nanoparticles Loaded with Heparin for the Treatment of Asthma. Int. J. Pharm. 2009, 381, 122–129, doi:10.1016/j.ijpharm.2009.04.009.

76. Schiffelers, R.M.; Woodle, M.C.; Scaria, P. Pharmaceutical Prospects for RNA Interference. Pharm. Res. 2004, 21, 1–7, doi:10.1023/b:pham.0000012145.49054.6c.

77. Tantra, R.; Tompkins, J.; Quincey, P. Characterisation of the De-Agglomeration Effects of Bovine Serum Albumin on Nano-particles in Aqueous Suspension. Colloids Surf. B Biointerfaces 2010, 75, 275–281, doi:10.1016/j.colsurfb.2009.08.049.

78. Parveen, S.; Sahoo, S.K. Long Circulating Chitosan/PEG Blended PLGA Nanoparticle for Tumor Drug Delivery. Eur. J. Pharmacol. 2011, 670, 372–383, doi:10.1016/j.ejphar.2011.09.023.

USC UNIVERSIDADE DE SANTIAGO

79. Zahr, A.S.; Davis, C.A.; Pishko, M.V. Macrophage Uptake of Core-Shell Nanoparticles Surface Modified with Poly(Ethylene Glycol). Langmuir ACS J. Surf. Colloids 2006, 22, 8178–8185, doi:10.1021/la060951b.

80. Prego, C.; Torres, D.; Fernandez-Megia, E.; Novoa-Carballal, R.; Quiñoá, E.; Alonso, M.J. Chitosan-PEG Nanocapsules as New Carriers for Oral Peptide Delivery. Effect of Chitosan Pegylation Degree. J. Control. Release Off. J. Control. Release Soc. 2006, 111, 299–308, doi:10.1016/j.jconrel.2005.12.015.

81. Park, P.I.P.; Jonnalagadda, S. Predictors of Glass Transition in the Biodegradable Poly-Lactide and Poly-Lactide-Co-Glycolide Polymers. J. Appl. Polym. Sci. 2006, 100, 1983–1987, doi:https://doi.org/10.1002/app.22135.

82. Abdelkader, H.; Fathalla, Z.; Moharram, H.; Ali, T.F.S.; Pierscionek, B. Cyclodextrin Enhances Corneal Tolerability and Reduces Ocular Toxicity Caused by Diclofenac. Oxid. Med. Cell. Longev. 2018, 2018, 5260976, doi:10.1155/2018/5260976.

83. Sreekumar, S.; Goycoolea, F.M.; Moerschbacher, B.M.; Rivera-Rodriguez, G.R. Parameters Influencing the Size of Chi-tosan-TPP Nano- and Microparticles. Sci. Rep. 2018, 8, 4695, doi:10.1038/s41598-018-23064-4.

84. Fredenberg, S.; Wahlgren, M.; Reslow, M.; Axelsson, A. The Mechanisms of Drug Release in Poly(Lactic-Co-Glycolic Acid-Based Drug Delivery Systems--a Review. Int. J. Pharm. 2011, 415, 34–52, doi:10.1016/j.ijpharm.2011.05.049.

85. A, B.; Sj, S.; Ki, W. Controlling the in vitro Release Profiles for a System of Haloperidol-Loaded PLGA Nanoparticles. Int. J. Pharm. 2007, 346, 151–159, doi:10.1016/j.ijpharm.2007.06.011.

86. Gasper, M.M.; Blanco, D.; Cruz, M.E.; Alonso, M.J. Formulation of L-Asparaginase-Loaded Poly(Lactide-Co-Glycolide) Nanoparticles: Influence of Polymer Properties on Enzyme Loading, Activity and in vitro Release. J. Control. Release Off. J. Control. Release Soc. 1998, 52, 53–62, doi:10.1016/s0168-3659(97)00196-x.

87. Holgado, M.A.; Cózar-Bernal, M.J.; Salas, S.; Arias, J.L.; Alvarez-Fuentes, J.; Fernández-Arévalo, M. Protein-Loaded PLGA Microparticles Engineered by Flow Focusing: Physicochemical Characterization and Protein Detection by Reversed-Phase HPLC. Int. J. Pharm. 2009, 380, 147–154, doi:10.1016/j.ijpharm.2009.07.017.

USC UNIVERSIDADE DE SANTIAGO DE COMPOSTELA

88. Chakravarthi, S.S.; Robinson, D.H. Enhanced Cellular Association of Paclitaxel Delivered in Chitosan-PLGA Particles. Int. J. Pharm. 2011, 409, 111–120, doi:10.1016/j.ijpharm.2011.02.034.

89. Dillen, K.; Vandervoort, J.; Van den Mooter, G.; Ludwig, A. Evaluation of Ciprofloxacin-Loaded Eudragit RS100 or RL100/PLGA Nanoparticles. Int. J. Pharm. 2006, 314, 72–82, doi:10.1016/j.ijpharm.2006.01.041.

90. Bozkir, A.; Saka, O.M. Formulation and Investigation of 5-FU Nanoparticles with Factorial Design-Based Studies. Il Farm. 2005, 60, 840–846, doi:10.1016/j.farmac.2005.06.016.

91. Saw, C.L.L.; Heng, P.W.S.; Liew, C.V. Chick Chorioallantoic Membrane as an In Situ Biological Membrane for Pharmaceutical Formulation Development: A Review. Drug Dev. Ind. Pharm. 2008, 34, 1168–1177, doi:10.1080/03639040801974295.

92. Vargas, A.; Zeisser-Labouèbe, M.; Lange, N.; Gurny, R.; Delie, F. The Chick Embryo and Its Chorioallantoic Membrane (CAM) for the in vivo Evaluation of Drug Delivery Systems. Adv. Drug Deliv. Rev. 2007, 59, 1162–1176, doi:10.1016/j.addr.2007.04.019.

93. Schoubben, A.; Blasi, P.; Marenzoni, M.L.; Barberini, L.; Giovagnoli, S.; Cirotto, C.; Ricci, M. Capreomycin Supergenerics for Pulmonary Tuberculosis Treatment: Preparation, in vitro, and in vivo Characterization. Eur. J. Pharm. Biopharm. 2013, 83, 388–395, doi:10.1016/j.ejpb.2012.11.005.

94. Kean, T.; Thanou, M. Biodegradation, Biodistribution and Toxicity of Chitosan. Adv. Drug Deliv. Rev. 2010, 62, 3–11, doi:10.1016/j.addr.2009.09.004.

95. Luaces-Rodríguez, A.; Touriño-Peralba, R.; Alonso Rodríguez, I.; García-Otero, X.; González-Barcia, M.; Rodríguez-Ares, MT.; Martínez-Pérez, L.; Aguiar, P.; Gómez-Lado, N.; Silva-Rodríguez, J.; et al. Preclinical Characterization and Clinical Evaluation of Tacrolimus Eye Drops. Eur. J. Pharm. Sci. Off. J. Eur. Fed. Pharm. Sci. 2018, 120, doi:10.1016/j.ejps.2018.04.038.

USC
UNIVERSIDADE DE SANTIAGO DE COMPOSTELA

USC
UNIVERSIDADE
DE SANTIAGO
DE COMPOSTELA

Chapter 4.

Design, optimization, and in vitro characterization of idebenone-loaded PLGA microspheres for LHON treatment

USC
UNIVERSIDADE
DE SANTIAGO
DE COMPOSTELA

USC
UNIVERSIDADE
DE SANTIAGO
DE COMPOSTELA

Chapter 4

Design, optimization, and *in vitro* characterization of idebenone-loaded PLGA microspheres for LHON treatment

Rubén Varela-Fernández[1,2], Carlos Bendicho-Lavilla[1], Manuel Martin-Pastor[3], Rocío Herrero Vanrell[4], María Isabel Lema-Gesto[2], Miguel González-Barcia[3], and Francisco Javier Otero-Espinar[1]

1. Department of Pharmacology, Pharmacy and Pharmaceutical Technology. University of Santiago de Compostela (USC). Campus vida. Santiago de Compostela. Zip Code: 15782. Spain. francisco.otero@usc.es.
2. Clinical Neurosciences Group. University Clinical Hospital, Health Research Institute of Santiago de Compostela (IDIS). Travesía da Choupana s/n Santiago de Compostela. Zip Code: 15706. Spain. mariaisabel.lema@usc.es.
3. Magnetic Resonance Unit. Infrastructure Supporting Network of Research and Technological Development. University of Santiago de Compostela (USC). Campus vida. Santiago de Compostela. Zip Code: 15782. Spain. manuel.martin@usc.es
4. Innoftal Research Group (UCM 920415), Department of Pharmaceutics and Food Technology, Faculty of Pharmacy, Complutense University, Madrid. Zip Code: 28040. Spain. rociohv@farm.ucm.es
5. Clinical Pharmacology Group. University Clinical Hospital, Health Research Institute of Santiago de Compostela (IDIS). Travesía da Choupana s/n Santiago de Compostela. Zip Code: 15706. Spain. miguel.gonzalez.barcia@sergas.es.

Int J Pharm. 2022 Mar 25;616:121504. doi: 10.1016/j.ijpharm.2022.121504. Epub 2022 Feb 2. PMID: 35121045

INTRODUCTION

Leber's Hereditary Optic Neuropathy (LHON) is a hereditary mitochondrial neurodegenerative disease, characterized by retinal ganglion cells (RGCs) degeneration, accompanied by an optic nerve functionality progressive loss (1). The disease's etiology is unknown, although all cases presented a maternal hereditary pattern, based on the presence of mitochondrial DNA point mutations. These mutations change the coding process of the mitochondrial transport chain's complex I, causing a decreased ATP synthesis, high oxidative stress levels, and damaged glutamate transport, actions that lead to RGCs dysfunction and, consequently, to apoptotic cell death.

USC UNIVERSIDADE DE SANTIAGO DE COMPOSTELA

The interval between the RGC dysfunction and the cell irreversible damage may be considered as a chance where vision might be repaired by regularizing the mitochondrial function. Currently, the LHON treatment options remain limited. New generation CoQ10 analogs were

developed with the purpose of increasing the pharmacophore bioavailability and maximizing its therapeutic potential (2). Idebenone is a short-chain benzoquinone and an enzyme NADPH quinone oxidoreductase cofactor, endowed with a powerful antioxidant and inhibitory lipid peroxidation action, being able to protect cell membranes and mitochondria from oxidative damage. A few years ago (2015), idebenone was commercialized under the brand name of Raxone® (Santhera Pharmaceuticals, Pratteln, Switzerland), an orally administrated pharmaceutical form (film-coated tablets). It was administrated at high doses (900 mg/day for 24 weeks) for LHON treatment with low efficacy and great changeability because of the strain to reach active concentrations at the retinal level (2). Nowadays, there is no available commercialized medicine for this disease.

In recent years, technological advancements have given rise to different novel drug delivery systems (DDS) into marketable distribution. Biodegradable polymer-based carriers may be currently considered as controlled and site-specific DDS for a predetermined period, ranging from hours to months (3).

Currently, there are few commercial formulations specifically intended for the treatment of retinal or posterior segment diseases (4). Formulations such as Vitrasert®, Retisert®, Ozurdex®, Eylea®, Jetrea® or Lluvien® can be mentioned, among others. Most of them are commercialized as non-biodegradable or biodegradable intraocular implants or intravitreal solutions. Implants have the advantage of their prolonged drug release but microparticles can be intraocular delivered by a simple injection, and their composition and morphological properties can markedly influence their *in vivo* behavior, including drug release. Microencapsulation is known as one of the main drug-coating processes, leading to the obtention of free-flowing micrometric particles (MPs) with a 1-1000 μm range size, enabling the drug stabilization and protection from the environment (4). Among them, microspheres (MSs) were further introduced as new controlled DDS, being spherical particles with monolithic structure, where the drug is incorporated into the polymeric matrix. These systems show high selectivity for the target tissue and a controlled-and-sustained release ratio coupling, as well as high biocompatibility and bioavailability, minimizing possible side effects (3).

Oil-in-water (O/W) emulsion/solvent evaporation is the most commonly used method due to its ease and chance of preparing MPs with particular and tunable features. This technique is mainly grounded on the obtention of a simple oil-in-water emulsion (O/W), where the active substance and the polymer are included into the oil phase. The emulsification is made by adding the

USC UNIVERSIDADE DE SANTIAGO

organic phase into the external aqueous phase, which contains the surfactant to avoid caking or coalescence processes. The organic solvent is subsequently evaporated at room temperature, leading to the manufacture of drug-loaded MPs that can be collected by filtration (6).

Biodegradable polymers are of major awareness in microencapsulation procedures due to their easy removal from the body as non-toxic metabolites through innate hydrolysis reactions of ester bonds, by contact with biological or artificial fluids. A few biodegradable synthetic polymers, particularly linear polyesters such as poly (lactic-co-glycolic acid) (PLGA), approved by the Food and Drug Administration (FDA) for human use, are of prime interest in the design of carrier-based DDS. These polymers are usually soluble in organic solvents (7), including dichloromethane, ethyl acetate, chloroform, acetone or tetrahydrofuran, among others.

PLGA is a thermoplastic aliphatic polyester (8) that shows many of the ideal properties of a microscale DDS. It provides a long-term delivery of the encapsulated drug and it degrades into biocompatible products that are further excreted by the normal physiological pathways (9). PLGA also eases the MSs features customization (size, distribution size, surface, and charge, among others). Despite that, the hydrophobicity of the polymer straightly correlates with the drug ocular activity (10).

PLGA microspheres can be an excellent candidate to prepare idebenone-loaded DDS for the LHON treatment due to the drug physicochemical properties (Mw 338.4 g/mol, LogP 4.3, and poor aqueous solubility 0.00747 mg/mL), as well as the ease of obtaining biodegradable microspheres of adequate size for intravitreal administration.

The aim of this chapter was to investigate novel intravitreal approaches for an idebenone controlled and sustained release as a new alternative LHON treatment to diminish the need for systemic drug administration or minimize the frequency of required ocular injections. The present work describes the design and development of idebenone-loaded PLGA MSs by the oil-in-water emulsion/evaporation technique, as well as the physicochemical characterization. The appropriateness of idebenone-loaded PLGA MSs formulations to control and maintain the idebenone release was also performed by acquiring a reliable preclinical basis through *in vitro* and *ex vivo* assays.

USC
UNIVERSIDADE
DE SANTIAGO
DE COMPOSTELA

MATERIALS

Resomer® RG 502 (Mw: 10000 Da; lactide:glycolide = 50:50) (CAS number: 26161-42-2), Resomer® RG 502H (Mw: 17000 Da; lactide:glycolide = 50:50) (CAS number: 26780-50-7), Resomer® RG 503 (Mw: 24000 Da; lactide:glycolide = 50:50) (CAS number: 26161-42-4), and Resomer® RG 503 H (Mw: 38000 Da; lactide:glycolide = 50:50) (CAS number: 31213-75-9) were purchased from Evonik (Essen, Germany). Idebenone (CAS number: M0021480) was provided by Acofarma® (Terrasa, Barcelona). Polyvinyl alcohol (PVA) (CAS Number: 9002-89-5) was acquired from Sigma-Aldrich (St Louis, USA). Dichloromethane (CAS number: 75-09-2) was purchased from Labkem Labware SL (Vilassar de Dalt, Barcelona). Franz diffusion cells were bought from Viadriafoc (Madrid, Spain). All other chemical reagents were of analytical grade.

EXPERIMENTAL METHODS

1. Idebenone-loaded PLGA microspheres: preparation procedure

Idebenone-loaded PLGA MSs were prepared by an oil-in-water (O/W) emulsion/solvent evaporation technique, based on a method developed in combination with the UCM 920415 research group (11–13), with minor modifications. Briefly, both phases were firstly prepared; the oil phase was composed of dichloromethane (DCM) (5 mL), idebenone (40 mg) and the polymer (400 mg), while aqueous phase was composed of a PVA solution (1% w/v) (15 mL). The maturation medium was also prepared, being a 0.1% (w/v) PVA aqueous solution (50 mL). The inner phase was prepared by dissolving both components (polymer and drug) into the organic solvent through a vortex stirring (Vortex® Genius 3, VWR International) (Germany) until complete dissolution. The aqueous phase was then slowly added to the organic one, and a mechanic homogenization process (Ultra-Turrax T25, IKA® Laboratories) (Staufen, Germany) was applied to create the O/W emulsion under 8000 rpm for 30 seconds (in an ice bath to avoid DCM evaporation). The resultant emulsion was later added to the maturation medium for 3 hours, in an incubation bath at 40 °C under magnetic stirring (100 rpm) to ease the organic solvent evaporation. MSs were then collected by filtration through a 25 µm nylon sieve (first filtration step) and a 10 µm nylon filter (second filtration step) respectively, to select the desired size interval. The resulting MSs were thrice washed, filtered, and subsequently vacuum-dried for a 24-h period. In order to point out, the entire process was carried out under no aseptic

USC DE SANTIAGO DE COMPOSTELA

conditions. Asepsis is a fundamental factor in intraocular/periocular controlled DDS, so the sterilization process was conducted as a final step.

2. Microspheres physicochemical characterization

2.1. Mean particle size, particle size distribution, and surface charge

The mean particle size and particle size distribution were measured by two different methods: (I) imaging analysis as a previous control method, and (II) dynamic light scattering (DLS), being the confirmation method for both parameters.

In the imaging analysis method, MSs samples were fixed in a slide for the shape, surface, and size optical observation. Image subsets were defined and analyzed by using an Olympus BX60/SC100 optical microscope and an Olympus CellSens Entry software, respectively. A specific rule set was established as a way to standardize the measurement process. All formulations were analyzed in triplicate.

The MSs average diameter, size distribution, and ζ potential were also analyzed by dynamic light scattering (DLS) by means of two different particle sizers. The particle´s average size and size distributions were determined by using a Malvern® Mastesizer micro laser diffraction particle sizer, with an internal sampler, a measured beam obscuration above 12.0% and a residual value below 0.3%. MSs' ζ potential values were obtained through a Malvern® Zetasizer ZS instrument, using folded capillary cells.

The resulting data were processed by using a combination of Malvern Mastersizer/Zetasizer and GraphPad® Prism software. Prior to measurement, samples were dispersed in Milli-Q® water and ultrasonicated for 10 seconds to promote the sample's homogenization. Results were analyzed by a one-way ANOVA analysis and a Student's t-like test, for the different formulations. A Tukey's multiple comparison test was also employed to assess the presence of statistically significant changes among the prepared formulations.

The size distribution was also evaluated by obtaining the *span* value, a dimensionless measure of the particle's size distribution. DLS particle sizer's measurement range and resolution were adjusted according to the type of sample, varying from 2-60%, based on the tube opening diameter, depending on the MSs size.

The *span* value may indicate MSs distribution size considering $d_{0.1}$, $d_{0.5}$ and $d_{0.9}$ results from different MSs formulations. The larger the *span* value, the wider the particle size interval in the

USC UNIVERSIDADE DE SANTIAGO

powder; the lower the *span* value, the narrower the particle size range. A span value of 0 would indicate a monodisperse particle size distribution. Mathematically, the *span* value may be calculated as presented, through the following equation (equation 1):

$$span = \frac{d_{0.9} - d_{0.1}}{d_{0.5}} \qquad (equation\ 1)$$

Where 90% of the particles show a diameter inferior to $d_{0.9}$ value, 10% of the particles less than $d_{0.1}$ value and 50% of the particles below $d_{0.5}$ value. The diffraction particle sizer may obtain an absolute value related to the number of particles per unit of volume for the different size intervals. The resulting data may support the initial distribution size values obtained from the DLS analysis.

2.2. Morphological evaluation

The MSs external morphology was assessed by scanning electron microscopy (SEM), after the vacuum-drying process. MSs were included on an adhesive metal plate and sheltered by sputter-coating with iridium particles. Samples were further observed under different magnifications with an analytical scanning electron microscope.

2.3. Production yield (PY)

MPs were recovered and subsequently weighted at the end of the preparation process. The PY of each batch was obtained by dividing the MSs weight (after filtration and drying) by the total amount of the components used in the formulation process (14), as presented (equation 2):

$$PY\ (\%) = \frac{MSs\ weight}{Total\ amount\ of\ components\ in\ the\ formulation} \cdot 100 \quad (equation\ 2)$$

Likewise, a standardization value was established after taking 9 randomized samples from different batches for each formulation to guarantee the resulting data and as a way to confirm the preparation method's reproducibility. Results were processed by a two-way ANOVA analysis to simultaneously study two different variables. A Tukey's multiple comparisons test

USC UNIVERSIDADE DE SANTIAGO

was also applied to assess the existence of statistically significant differences among the prepared formulations.

2.4. Encapsulation Efficiency (EE) and Loading Capacity (LC)

EE and LC of MSs were measured by UV-Visible spectrophotometry at a 279.0 nm wavelength. EE (%) was calculated by both direct and indirect methods (determination of encapsulated drug and free drug, respectively), in order to verify that the low solubility of the drug did not interfere with its determination by either method. Data were further processed by the following mathematical equation (equation 3)):

$$EE\ (\%) = \frac{Total\ amount\ of\ drug - Encapsulated\ drug}{Total\ amount\ of\ drug} \cdot 100 \quad (equation\ 3)$$

LC values were obtained by a centrifugation technique, trailed by the free-drug measurement by UV-Vis spectrophotometry, after polymer precipitation (15,16). Briefly, 20 mg of MSs samples were dissolved into 2.5 mL dichloromethane, followed by a mechanic stirring process (Vortex®, VWR International) (Germany) to promote the polymer dissolution. Later, 5 mL of methanol were appended, and samples were subsequently vortexed for 1 min to foster polymer precipitation. Samples were then centrifuged (5000 rpm, 10 min) and the supernatant was subsequently collected. Idebenone was finally determined by UV-Vis spectrophotometry (λ = 279 nm). This procedure was repeated using 9 randomized batches for each formulation. Loading capacity was then calculated with the following mathematical equation (equation 4):

$$LC\ (\%) = \frac{Weight\ of\ released\ drug\ from\ the\ MSs}{MSs\ Weight} \cdot 100 \quad (equation\ 4)$$

Results were processed by a two-way ANOVA analysis to simultaneously study two different variables. A Tukey's multiple comparisons test was also applied to assess the existence of statistically significant differences among the prepared formulations.

USC UNIVERSIDADE DE SANTIAGO DE COMPOSTELA

2.5. Optimization of microspheres preparation procedure

Based on the MSs elaboration procedure, different key parameters were further modified in order to achieve the optimum values for the preparation process. Certainly, a factorial design was previously established, where different drug:polymer ratios (1:1 w/w to 1:10 w/w) and aqueous phase concentrations (0.5% to 2%) (see Table 1) were tested and subsequently assessed in terms of PY, EE and LC of the resulting MSs. It must be considered that only one parameter was modified during the elaboration process, keeping the other key factors constant. All experiments were performed in triplicate.

Table 1. Specifications of the factorial design for the MSs optimization procedure.

Drug:Polymer Ratio (w/w)	PVA (%) (w/v)
1:1	0.5
	1
	2
1:5	0.5
	1
	2
1:10	0.5
	1
	2

2.6. Effect of the polymer characteristics

The idebenone-loaded MSs prepared with Resomer® RG 502 and 503, which are characterized by esterified carboxyl end groups, and Resomer® RG 502H and 503H, which have shown free carboxyl end groups, were compared to assess the effect of the carboxyl end groups of the different PLGA polymers on the resulting MSs size. According to Cegnar et al. (2004) (17), an increase in the polymer's hydrophilic properties having free carboxyl end groups leads to a reduction of the solubility in methylene chloride and, therefore, a reduction of the MSs size.

USC DE SANTIAGO DE COMPOSTELA

MSs particle size may be additionally disturbed by the molecular weight (Mw) and the inherent viscosity of the polymer (see polymer details in Table 2). An increase in the Mw and the inherent viscosity may cause an upsurge in the viscosity of the internal phase, leading to a bigger MSs size, as a tougher shearing force for emulsion droplets' disturbance is needed (18,19).

Table 2. Physical characteristics of the different PLGA polymers employed in the present study.

Resomer	Feed Ratio	Mw (KDa)	Inherent viscosity (dL/g)	Form	Termination	Acid number (mg KOH/ g PLGA)
502	50:50	7 - 17	0.16 – 0.24	Amorphous	Ester	≤ 1
502H	50:50	7 - 17	0.16 – 0.24	Amorphous	Acid	> 6
503	50:50	24 - 38	0.32-0.44	Amorphous	Ester	≤ 1
503H	50:50	24 - 38	0.32-0.44	Amorphous	Acid	> 3

2.7. Effect of the drug:polymer ratio and PVA concentration

Three different drug:polymer ratios (1:1, 1:5, and 1:10) and three different PVA concentrations (0.5% w/v, 1% w/v, and 2% w/v) for each drug:polymer ratio were tested. Regarding the drug:polymer ratio assessment, it must be considered that all formulations were prepared following the same procedure, using different drug:polymer ratios, as previously presented in Table 1. The drug:polymer ratio was modified by maintaining the amount of polymer, surfactant, and phases proportions constant in all formulations, and changing the amount of drug.

Additionally, PVA concentration in the dispersant phase is also a key parameter for the MSs particle size. In the present study, predefined concentration values of PVA (see details in Table 1) were assessed to determine its influence on the MSs physicochemical characterization during the elaboration process. The presence of PVA promotes the emulsion droplets steadiness by diminishing the interfacial tension, avoiding MSs aggregation or coalescence phenomena (20,21).

USC UNIVERSIDADE DE SANTIAGO DE COMPOSTELA

3. *In vitro* release study

The idebenone release rate from MSs was determined by UV-Visible spectrophotometry, where vertical diffusion cells were employed as holding structures. The preparation and performance of the assay, as well as the sampling and analysis of the results, were detailed previously (22). To point out, vertical diffusion cells contained two chambers, a donor and a receptor chamber, both separated by a dialysis membrane of defined pore size (14000 Da). Once mounted, 2 mL of simulated vitreous humor (0.1% w/v agar and 0.5% w/v hyaluronic acid aqueous solution) was added to the donor chamber followed by 1 mL of the idebenone-loaded MSs formulation (C_{MSs} = 25 mg/mL, C_{IDB}=2.5 mg/mL), while the receptor chamber was filled with ocular buffer (PBS) (v = 7 mL). 1 mL of an idebenone suspension (C_{IDB} = 2.5 mg/mL) was added to the donor chamber instead of the microparticle formulation as a means of obtaining control data. The assay was run for a 50-day period, under controlled environmental conditions (100rpm and 37°C), and each formulation was tested in triplicate. Idebenone amount was measured using UV-Vis spectrophotometry at a 279.0 nm wavelength. Analytic validation was previously obtained by our group and exhibited linearity (R = 0.999) over a concentration interval of 0.19 – 250 µg/mL, 96.3% accuracy (1.85% RSD), of a 100.2% RSD intra-day precision and LOD and LOQ values of 0.3906 µg/mL and 0.7812 µg/mL, respectively. The resulting data proved that standard solutions remained stable for up to a week, protected from light exposure.

One-way ANOVA analysis was employed to determine time/group interactions among the MSs batches. A Tukey-Kramer Multiple Comparison Post-Test was run to establish the resemblance or variations concerning release profiles of selected formulations for cases where a significant interaction was found. Regression analysis of the *in vitro* release profiles was performed, and different mathematical models were fitted to formulation's release data by means of the GraphPad Prism® software.

4. Stability studies

Stability studies involve a complex set of procedures that are of prime interest to evaluate efficacy, quality, and safety of drug-loaded pharmaceutical forms. Stability assessment is also considered a major focus of attention to carry out drug shelf-life prediction and determine the optimum storage conditions.

USC UNIVERSIDADE DE SANTIAGO DE COMPOSTELA

4.1. Stability to storage

The stability-to-storage study was established according to the ICH guidelines (23), with negligible changes. MSs were placed in screw-capped, amber-colored glass containers (5 mL capacity) and stored at three different temperature conditions (4 ± 2°C, 25 ± 2°C, and 37 ± 2°C) for a three-month period. Stability was assessed through drug content uniformity. Drug content assay (n = 3 per batch) was carried out by weighing 20 mg of idebenone-loaded MSs, following the same procedure that has been applied for LC (%) determination. Drug content was finally estimated by UV-Vis spectrophotometry at a 279 nm wavelength.

4.2. Stability to pH

The physical evaluation of the pH-dependent MSs stability was carried out on freshly prepared formulations. The methodology of this procedure was based on the suspension of 100 mg idebenone-loaded MSs in 5 mL of Milli-Q® water at different predetermined pH values (from 2 to 12) (Hanna® HI5522, Hanna Instruments®, Spain). Samples were then kept refrigerated (T = 4°C ± 2°C) for 24 hours to be subsequently centrifuged at 5000 rpm for 10 minutes. Sink conditions were ensured for the accomplishment of the test. Finally, the determination of the free idebenone concentration in the solution was carried out at a 279 nm wavelength to verify the existence of MSs collapse or breakage phenomena with the consequent release of the drug into the medium. Each formulation was tested in triplicate for all set pH values.

4.3. Stability to ionic strength

The physical evaluation of the ionic strength-dependent MSs stability was carried out on freshly prepared formulations. The methodology of this procedure was based on the suspension of 100 mg idebenone-loaded MSs in 5 mL of NaCl aqueous solutions with different predetermined ionic strength values (from 0.2 M to 2 M). Samples were then kept refrigerated (T = 4 ± 2°C) for 24 hours to be subsequently centrifuged at 5000 rpm for 10 minutes. Sink conditions were ensured for the accomplishment of the test. Finally, the determination of the free idebenone concentration in the solution was carried out at a 279 nm wavelength to verify the existence of MSs collapse or breakage phenomena with the consequent release of the drug into the medium. Each formulation was tested in triplicate for all set ionic strength values.

USC UNIVERSIDADE DE SANTIAGO DE COMPOSTELA

5. Moisture content

The natural moisture content is an essential test for polymeric MSs, being defined as the ratio of the water weight compared to the weight of the solid materials in a certain mass of the formulation. Moisture content is assessed to ensure the quality of the formulations and to demonstrate that no significant stability changes occur during storage by hydrolysis of the components. Its determination was carried out by weight difference. For each formulation, 20mg MSs were placed on an aluminum plate and dried at 105°C until constant weight to completely guarantee water evaporation from the samples. The mass loss percentage was calculated as moisture content, where measurements were carried out in triplicate. Certainly, moisture content was mathematically estimated by using the following equation (equation 5):

$$Moisture\ content\ (\%) = \frac{Initial\ MSs\ weight - Final\ MSs\ weight}{Initial\ MSs\ weight} \cdot 100 \quad (equation\ 5)$$

6. Solid State Nuclear Magnetic Resonance (ss-NMR)

Solid NMR spectra of the idebenone-loaded PLGA formulations were obtained at 298°K in a NEO-750 spectrometer (750 MHz proton frequency), equipped with a Varian T3 solid triple resonance probe 1H/X/Y with a zirconia rotor (3.2 mm outer diameter and a 22 µL effective sample capacity – approx. 30 mg of the powder sample -). The probe was adjusted to the Bruker spectrometer by an A2B conversion kit (Revolution NMR, LLC) and TopSpin® 4.0 software was used as the spectrometer control. All the NMR spectra were treated by using the MestreNova® software v14.0 (Mestrelab® Research Inc., Spain). Carbon chemical changes were referenced to the carbon methylene signal of solid adamantane at 28.92 ppm. Proton chemical shifts were externally referenced to one of the methylene protons of solid glycine (resonance: 4.1 ppm). The assignment of ^{13}C resonances of idebenone and PLGA was based on the predictions made with the ChemDraw® v14.0 software (Perkin-Elmer, Inc) for the covalent structures.

Direct polarization 1D ^{13}C-PARIS-xy spectrum of each sample was measured at MAS 20 kHz following the procedure previously described by Purusottam et al. (24), with slight changes. During the inter-scan relaxation delay right before the ^{13}C excitation pulse, a train of 25 µs and 12.5 kHz field strength PARIS-xy pulses were applied to introduce modulation sidebands at

half the rotation rate causing the ^{13}C enhancement. The total duration of the PARIS-xy irradiation was 3 s. The ^{13}C excitation pulse had a tilt angle of 90 degrees and was applied with a 63.1 kHz B1 field strength. Heteronuclear decoupling throughout FID acquisition was carried out by the SPINAL-64 with a 79.4 kHz proton field strength. A 1 s inter-scan relaxation delay (d_1) and 512 scans were applied to finally obtained the spectrum.

Cross polarization 1D ^{13}C-CP-MAS spectrum of each sample ("hC.cp" sequence of the Bruker library) was acquired at MAS 20 kHz with 1000 scans and a 2.5 s inter-scan delay (d_1). Cross-polarization was operated for 2 ms with a 63.1 kHz constant carbon field strength, the power on the ^{1}H nucleus was linearly ramped from 70 to 100% with a 48.1 kHz peak field strength. Heteronuclear decoupling during the FID acquisition was performed by the Spinal-64 with a 79.4 kHz proton field strength.

7. Differential Scanning Calorimetry (DSC) and thermogravimetry analysis (TGA)

DSC is one of the most widespread thermal analysis procedures in powder characterization. Fusion, desolvation, recrystallization, decomposition or vitreous transition processes may be determined by this analysis technique (25,26). Possible interactions between idebenone and the polymers were studied by DSC, which was carried out by means of a TA Instruments® Q1000 DSC/TGA/IR analyzer (Madrid, Spain), calibrated with indium. 10 mg MSs were weighed and placed into sealed aluminum plates. DSC curves were obtained by a 10°C/min scanning rate, conducted through a temperature interval that went from 0 to 150 °C at a 10°C/min heating rate, in a liquid nitrogen environment, using a 50 mL/min flow rate. Each formulation was tested in triplicate.

Thermal gravimetry analysis is one of the main useful methods for the determination of the presence/absence of residual solvents in formulations prepared by the emulsion/solvent evaporation method. The schedule of the procedure is similar to that described for the DSC analysis. Briefly, approximately 10mg MSs were loaded into aluminum plates and heated from 0°C to 150°C at a heating rate of 10 °C/min by using a TA Instruments® Q1000 DSC/TGA/IR analyzer (Madrid, Spain). Each formulation was tested in triplicate.

USC
DE SANTIAGO
DE COMPOSTELA

8. Fourier-transformed infrared spectroscopy (FTIR) analysis

Infrared absorption spectroscopy (IR) is the method used to determine the molecule structures with infrared-radiation absorption characteristics according to their molecular vibration. FTIR assay was carried out to determine the MSs structural characterization. Certainly, MSs samples

were scanned through the IR interval, ranging from 400 to 4000 cm^{-1}, using a 4 cm^{-1} resolution and dry air as a background blank to stabilize the FTIR system (GladiATR™, Varian Pike Technologies). The spectra of each sample were recorded at a 64 scans/min speed, obtaining 4084 different points, and resulting data were collected in transmittance values (%) and processed through the *Resolutions Pro* software. Each formulation was tested in triplicate.

9. X-Ray diffractometry analysis

X-ray diffraction is one of the most commonly used methods in the study of solid materials, although it has also demonstrated a relevant application in the analysis of disordered states of matter. At present, this technique is moving towards the analysis of structured samples in submicron dimensions and towards the structural analysis of non-solid systems, by conducting a wide variety of studies including, not only qualitative and quantitative analysis of materials, but also microtextural, crystallinity, nonhomogeneous deformation analysis or phase change analysis, among others.

The X-ray diffractometry study was carried out following the ISO 9001: 2015 standard normative in terms of reception, sample management and analysis using monocrystalline, crystalline powder, and X-ray fluorescence techniques. All samples were kept at room temperature, in vials, waiting to be measured. The obtaining and handling of the materials to be analyzed was carried out by using latex gloves, with an agate mortar for spraying / homogenizing the physical samples.

MSs crystalline structure was analyzed by wide-angle X (WAX) ray powder diffraction in an X-ray diffractometer (Philips X'Pert, USA), operated with a PW170 control unit, a PW1820/00 vertical goniometer, and an Enraf Nonius FR590 generator, locating and assigning the most significant mathematical values of the peaks of the present diffractograms. Samples were scanned from a Cu- Kα source, monochromated with a graphite monochromator (λ = 1.5406 Å), at 40 kV and 30mA, using 2θ from 2° to 50° at a scan rate of 0.04°·min^{-1}. Samples were rotated during the analysis to obtain the most optimal peak profiles for the diffractograms, as well as to minimize the effect of the preferred orientation. It also must be considered that samples were deposited in oriented glass bases (Si-511 plate) to avoid background noise caused by a vitreous support. The mathematical analysis of the diffractograms was carried out by using the HighScore Plus® 3.0d software.

USC UNIVERSIDADE DE SANTIAGO

10. Mercury intrusion porosimetry (MIP) assay

The porosity, also known as void fraction, of polymeric MSs is a critical factor influencing the release kinetics of encapsulated active substances (21,27,28). Several approaches in the porosimetry determination of particulate DDS are grounded on previously established procedures used in other scientific fields (29). MIP is one of the most common and informative methods based on the pore size and distribution measurements. Furthermore, MIP presents certified reference material and standard measurement protocols (30).

Porosity measurements were made by mercury intrusion porosimetry, using a Micromeritics Autopore IV mercury porosimeter (Norcross, GA, USA), equipped with a 3-mL capacity penetrometer and a 0.004 to 172.4 MPa analysis pressure interval, leading to the acquisition of "Pore volume vs Pressure" data (31). The procedure's schedule was based on weighing 200 mg idebenone-loaded MSs, that were subsequently added to a glass penetrometer, appropriate for powder samples. Then, the penetrometer was closed, and preparations were formerly included into the porosimeter, using a 0.004 MPa filling pressure for testing. Total intrusion volume, total pore area, and porosity were recorded. Porosity was calculated by two different methods: (I) as the quotient of pore volume to total MPs volume, and (II) as the quotient of bulk density and apparent density as presented (equation 6):

$$Porosity\ (\%) = 1 - \frac{bulk\ density}{apparent\ density} \cdot 100 \quad (equation\ 6)$$

Mercury intrusion into each formulation was also analyzed by means of the Washburn equation (equation 7) to estimate the pore diameter distribution, and resulting data were recorded on the PoreXpert™ software.

$$Washburn\ equation: \quad D = -\frac{4\gamma}{P} \cdot \cos\theta \qquad (equation\ 7)$$

where D represents the pore diameter, γ refers to the surface tension of Hg at 20°C, P embodies the applied pressure, and θ denotes the contact angle between Hg and the powder, which is assumed to be 130° (32).

Pore volume values were described as the amount of volume per gram (cm^3/g) and obtained by using polymer density and sample weight of the porosimetry sample. Total MSs volume was measured as the sum of the pore volume and the polymer volume (33).

11. Syringeability and injectability studies

Syringeability and injectability are two important features in the preclinical evaluation of MSs formulations for intraocular dosage forms. The former denotes the ease of passage of a formulation to easily traverse a needle from an appropriate container prior to a syringe system, while the latter alludes to the passage of the MSs suspension throughout the injection process (34)**. S**uitably syringeability and injectability properties guarantee the right dose of MSs to be intraocularly administered.

Special care must be taken when preparing homogenous particle dispersion of MSs formulations intended to be injected as a conventional suspension in clinical practice. Buffer solutions, such as pH 7.4 Balanced Saline Solutions (BSS) or Phosphate Balanced Solutions (PBS), are mainly used as delivery vehicles due to their biocompatibility, transparency, ability to rapidly dilute in the intraocular fluids, and easy removal from the eye. Syringeability and injectability studies of MSs suspensions enable to establish the optimal characteristics of the intraocular needles (size and length) by calculating the needed force to inject a predetermined volume of the formulation. A 12 N force over 10 seconds was set as the maximum ejection force, being appropriate for proper intraocular injection.

Sample's preparation procedure was based on the elaboration of 1% (w/v) MSs suspensions by sonication (10% intensity for 10 s; Sonopuls® LS 40/HG 40 2000.2 series) (Berlin, Germany), where MSs were incorporated into a 0.1% (w/v) PVA aqueous solution. Once prepared, MSs suspensions were included in 5 mL syringes, equipped with different types of needles (21G, 27G, and 30G), in order to compare them for an appropriate administration (35). Ejection and aspiration forces were respectively obtained by using a universal testing machine (Shimadzu® AGS-X Series, Kyoto, Japan), managed through a specific software (Trapezium®). Established injectability and syringeability conditions were as presented in Table 3. All the samples were tested in triplicate for all the different syringe/needle systems.

USC DE SANTIAGO DE COMPOSTELA

Table 3. Injectability and syringeability conditions for MSs formulations test.

Condition	Parameter	Injectability conditions	Syringeability conditions
System	Assay mode	Simple	Simple
	Assay type	Compression	Traction
	Force polarity	Compression	Compression
	Force sense	Downwards	Upwards
Sensor	Force scale	1000 N	1000 N
	Displacement	500 mm	500 mm
Assay	Action	Force	Force
	Control	Displacement	Displacement
	Sampling	10 seg/sample	10 seg/sample
	Breakage sensitivity	10%	10%
	Sensor	Displacement	Displacement
Sample	Material	-	-
	Shape	Cylinder	Cylinder
	Dimensions	Diameter and height	Diameter and height
Data	Maximum force	-	-

12. Ocular irritancy and toxicity analysis of microspheres

12.1. Hen`s egg test on the chorioallantoic membrane (HET-CAM)

The general test for substance irritation and corrosion is based on the rabbit eye test settled by Draize et al. (36) and has turn into the universal and traditional assay for acute eye irritation and corrosion. Nevertheless, its cruelty gave way to several authorized alternative tests, showing potential as screens for ocular irritancy, such as the HET-CAM test (37).

USC DE SANTIAGO DE COMPOSTELA

In the HET-CAM test, three different phenomena are assessed (hemorrhage, lysis, and coagulation). The protocol was improved from the method formerly explained by Spielmann and Liebsch (38), with negligible changes. The preparation and performance of the assay, as well as the image sampling were previously detailed (22). The evaluation of the key parameters over a 5 min period was carried out by means of an Olympus SZ61TR Stereomicroscope and an Olympus CellSens Entry® software. Imaging analysis and processing were also carried out as detailed in previous works (22). Each formulation was tested in triplicate.

13. Statistical analysis

All tests were performed, at least, in triplicate and obtained data were included as average values and their standard deviations. Likewise, if needed, statistical significance was calculated and included in the result's paragraph. Additional data analysis procedures may be applied for specific parameters. Different specific software was used to analyze all the collected data.

RESULTS AND DISCUSSION

1. Microsphere's preparation

The emulsion/solvent evaporation technique is a commonly employed methodology for microencapsulation to prolong and control the drug release from the DDS. In the present work, an O/W emulsion/solvent evaporation methodology was used to efficaciously entrap a hydrophobic drug (idebenone) into polymeric MSs, according to the component's data previously mentioned (see details in Table 1). First, idebenone was dissolved into a polymer organic solution and subsequently emulsified with a PVA aqueous solution. Polyvinyl alcohol (PVA) acts as an emulsifying agent (20,21) and presents unique characteristics, making it ideal for controlled drug delivery. It provides control of the MPs mechanical properties, degradation rate changes, and immune response with negligible toxicity (22). After the organic solvent evaporation, polymer precipitation occurred and MPs solidified, entrapping the drug in its matrix. After vacuum-drying, all idebenone-loaded PLGA MSs showed a free-flowing powder aspect and orange color. In order to point out, idebenone-loaded PLGA MSs were named as 502 MSs, 502H MSs, 503 MSs, and 503H MSs, depending on the PLGA physical characteristics (see details in Table 2).

USC UNIVERSIDADE DE SANTIAGO DE COMPOSTELA

2. Microsphere's optimization procedure

The optimization procedure for the MSs preparation was carried out to obtain the optimal parameters for the final formulations, according to the factorial design previously described (see details in methods section 3). Table 4 includes the data for the PY, EE, and LC values for all the formulations tested during the optimization procedure. All formulations showed suitable PY, EE, and LC values. These data were supported by the idebenone low aqueous solubility, which provides high drug entrapment into polymeric MSs, as well as the drug:polymer proportion employed in the elaboration procedure.

The particle size and size distribution were similar for all the formulations due to the time fitting during the mechanic homogenization process to obtain the highest production yield for the different polymers. Those parameters also seemed to be influenced by the Mw and the inherent viscosity of the polymer. Thus, smaller particles would be obtained with Resomer® 502 and 502H compared with Resomer® 503 and 503H for the same mechanical homogenization procedure, possibly due to the slightly physicochemical differences of the polymer properties. All the MSs batches were assessed in terms of PY and found to be in the range of 50 - 90% (see Table 4). Despite all, these production yield values might be underestimated due to the manual manufacturing procedure and might be related to the handling loss throughout the processing steps, including polymer stickiness to the glass container, mechanic homogenization time or MSs loss during the washing step, among others. Nevertheless, the resulting data were analyzed by one-way ANOVA, Brown-Forsythe's, Bartlett's, and Tukey's tests and no-statistically significance was observed ($p < 0.05$) among all formulations.

The resulting data may also indicate that the particle size may be influenced by the Mw and the inherent viscosity of the polymer. Formulations prepared with Resomer® RG 502 or 502H (lower Mw and poorer inherent viscosity) were compared with formulations prepared with Resomer® 503 or 503H, with higher molecular weight and inherent viscosity, and a particle size increase would be observed during the preparation procedure. Nevertheless, the procedure schedule's times were adjusted for the different polymers to maximize the PY of the idebenone-loaded MSs. Thus, the resulting data were analyzed by one-way ANOVA, Brown-Forsythe's, Bartlett's and Tukey's tests, and no-statistically significance was observed ($p < 0.05$) among all the formulations.

USC UNIVERSIDADE DE SANTIAGO DE COMPOSTELA

Regarding idebenone-loaded PLGA MSs, two key parameters were also studied: (I) the PVA concentration in the external medium, and (II) the drug:polymer ratio. An increase in the PVA

concentration (from 0.5% to 2% (w/v)) did not produce a noteworthy modification in EE values ($p > 0.05$), but in the LC values ($p < 0.05$). It is expected that higher PVA concentrations in the dispersant medium enable a steadier emulsion's formation, preventing drug migration to the external phase in addition to increase the LC values (39,40). Nevertheless, when the ratio of polymer increases (1:5 and 1:10), the PVA concentration barely affects LC or even decrease.

The effect of ester (more hydrophobic) and carboxyl (more hydrophilic) end groups of the PLGA on the drug LC was also assessed. The dominant force between the drug and the polymer may be usually a hydrophobic interaction, since hydrophobic polymers with ester end groups improve the obtention of higher EE and LC values for hydrophobic drugs. Nevertheless, in this specific case, no significant differences were observed between the four different PLGA polymers used.

Table 4. Physicochemical characterization of idebenone-loaded PLGA MSs. Production yield (PY), encapsulation efficiency (EE), and loading capacity (LC) are presented for all the tested conditions of the optimization procedure.

Formulation	Drug:Polymer Ratio	PVA (%)	PY (%)	EE (%)	LC (%)
502 MSs	1:1	0.5	54.56 ± 5.85%	98.21% ± 0.17%	60.95% ± 8.65%
		1	62.10 ± 5.50%	98.22% ± 0.10%	67.50% ± 5.85%
		2	78.10 ± 10.91%	97.65% ± 0.32%	71.01% ± 5.03%
	1:5	0.5	88.50 ± 0.88%	93.15% ± 0.45%	26.42% ± 3.51%
		1	85.62 ± 7.12%	93.55% ± 0.81%	35.48% ± 3.41%
		2	80.88 ± 4.93%	90.90% ± 0.86%	16.22% ± 2.58%
	1:10	0.5	87.89 ± 1.13%	85.64% ± 0.65%	21.62% ± 3.20%
		1	87.37% ± 2.30%	87.59% ± 0.78%	22.05% ± 2.52%
		2	86.96% ± 0.65%	87.00% ± 0.58%	18.88% ± 4.03%
502H MSs	1:1	0.5	85.68% ± 1.95%	97.79% ± 0.33%	60.95% ± 8.89%
		1	88.73% ± 0.62%	97.58% ± 0.46%	67.47% ± 3.56%
		2	85.28% ± 4.05%	97.50% ± 0.35%	71.42% ± 6.22%

USC UNIVERSIDADE DE SANTIAGO DE COMPOSTELA

		0.5	76.14% ± 0.54%	91.56% ± 0.82%	26.41% ± 2.83%
	1:5	1	83.94% ± 2.14%	92.18% ± 1.12%	35.31% ± 2.24%
		2	84.53% ± 2.85%	93.59% ± 0.36%	16.28% ± 3.62%
		0.5	83.61% ± 2.94%	86.85% ± 0.36%	21.12% ± 2.55%
	1:10	1	86.32% ± 0.86%	88.65% ± 1.32%	22.09% ± 1.46%
		2	80.60% ± 2.37%	84.69% ± 1.80%	22.21% ± 1.33%
503 MSs		0.5	80.38% ± 4.31%	97.25% ± 0.20%	68.63% ± 5.38%
	1:1	1	77.47% ± 3.55%	97.99% ± 0.12%	72.32% ± 6.40%
		2	81.59% ± 1.08%	97.34% ± 0.14%	71.39% ± 4.72%
		0.5	87.91% ± 1.56%	91.93% ± 0.28%	28.60% ± 1.73%
	1:5	1	87.57% ± 1.13%	93.79% ± 0.20%	38.36% ± 6.88%
		2	84.74% ± 4.19%	88.21% ± 0.24%	23.48% ± 2.62%
		0.5	80.87% ± 1.80%	85.79% ± 2.04%	15.64% ± 3.01%
	1:10	1	83.64% ± 5.47%	88.40% ± 2.33%	17.01% ± 2.93%
		2	87.16 ± 1.28%	88.85% ± 0.55%	14.01% ± 1.51%
503H MSs		0.5	84.68% ± 1.64%	97.82% ± 0.89%	66.56% ± 5.93%
	1:1	1	87.98% ± 3.02%	98.02% ± 0.36%	69.44% ± 4.33%
		2	90.77% ± 3.05%	97.56% ± 0.10%	92.63% ± 7.56%
		0.5	79.76% ± 10.31%	92.70% ± 0.75%	28.79% ± 4.94%
	1:5	1	83.54% ± 3.35%	93.65% ± 0.75%	26.49% ± 1.74%
		2	84.70% ± 5.07%	93.04% ± 1.05%	18.17% ± 1.60%
		0.5	87.53% ± 1.66%	88.31% ± 0.41%	18.48% ± 2.43%
	1:10	1	85.68% ± 3.29%	89.20% ± 0.61%	13.94% ± 1.14%
		2	90.10% ± 0.59%	87.31% ± 0.65%	14.50% ± 1.72%

USC UNIVERSIDADE DE SANTIAGO DE COMPOSTELA

Based on these results, just one formulation prepared with each of the different polymers was carefully chosen. Certainly, the final formulation specifications are presented in Table 5. The rest of the characterization assays would be subsequently performed in these formulations.

Table 5. Final idebenone-loaded MSs formulations.

Formula	Polymer	Drug:Polymer Ratio	PVA (w/v)
F1	Resomer® RG 502	1:10	1
F2	Resomer® RG 502H	1:10	1
F3	Resomer® RG 503	1:10	1
F4	Resomer® RG 503H	1:10	1

3. Microspheres physicochemical characterization

3.1. Mean particle size, particle size distribution, and surface charge

Granulometric assays were performed for determining particle size and size distribution of the idebenone-loaded PLGA MSs. A predefined size interval makes MSs suitable for its intravitreal administration through a 30G needle, these being supported by previous studies (41,42). Furthermore, different sieves and filters (from 10 to 25 µm) were used during the filtration process to preestablish the desired size interval.

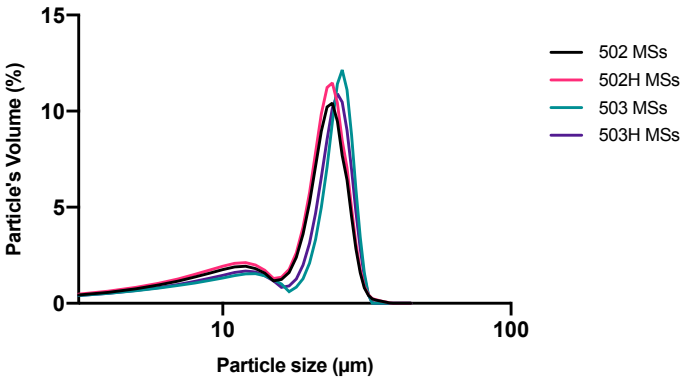


Figure 1. Size distribution of selected idebenone-loaded PLGA MSs.

USC UNIVERSIDADE DE SANTIAGO DE COMPOSTELA

Distribution size measurements may confirm that the preestablished filtration process is adequate for the obtention of an appropriate MSs size interval, as presented in Figure 1. Likewise, size distribution was assessed through the span value estimation, as shown in Table 6. All the resulting span values also confirm a closely-monodisperse size distribution.

Table 6. Distribution size characterization by span value of the PLGA MSs.

Formulation	$d_{0.1}$	$d_{0.5}$	$d_{0.9}$	Span
502 MSs	1.58 ± 0.05	9.42 ± 0.56	19.41 ± 4.49	1.87 ± 0.34
502H MSs	1.72 ± 0.02	10.40 ± 0.60	19.47 ± 1.34	1.71 ± 0.07
503 MSs	1.92 ± 0.01	13.06 ± 0.05	23.20 ± 0.09	1.63 ± 0.01
503H MSs	1.80 ± 0.03	11.67 ± 0.33	22.18 ± 0.87	1.75 ± 0.02

The particle size and size distribution were similar for all the formulations due to the time fitting during the mechanic homogenization process to obtain the highest production yield possible. Those parameters also seemed to be influenced by the Mw and the inherent viscosity of the polymer. Nevertheless, the resulting data were evaluated by a one-way ANOVA analysis and not statistically significance was observed ($p > 0.05$).

The MSs superficial charge was obtained by the ζ potential determination. All formulations show an appropriate negative surface charge, as presented in Figure 2. As per the Derjaguin, Landau, Verwey, and Overbeek (DLVO) electrostatic theory, this negatively charged net suggests that the formulations are stable over time because of the Brownian motion and the negative repulsive forces, desirable to prevent particle aggregation (43). Besides, this negativity might be attributed to PVA adsorption onto the MSs surface, functional group changes on the particle surface, or ionization of the PLGA carboxylic groups (44).

USC UNIVERSIDADE DE SANTIAGO DE COMPOSTELA

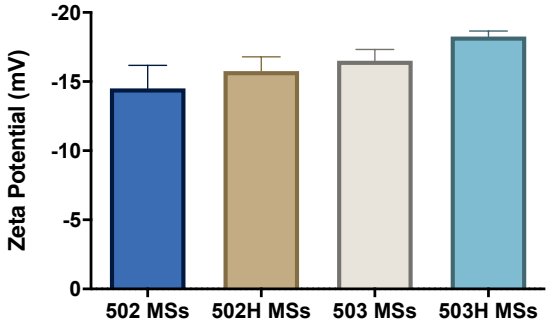


Figure 2. Surface charge values of selected idebenone-loaded PLGA MSs.

One-way ANOVA analysis was submitted, and no statistically significant differences ($p > 0.05$) were observed among the different formulations (F value = 8.057, P-value = 0.0579, Geisser-Greenhouse's epsilon = 0.3677). A Tukey's multiple comparison test was subsequently carried out, and no differences were spotted among formulations, except for 502H and 503H formulations, possibly due to test experimental conditions.

3.2. Morphology evaluation

The morphological evaluation through an optical microscopy was performed to relate the size and shape of the MSs. The microscopy images show spherical particles with a presumed internal granulation, observing uniformity in terms of morphology among the different types of polymers (see Figure 3).

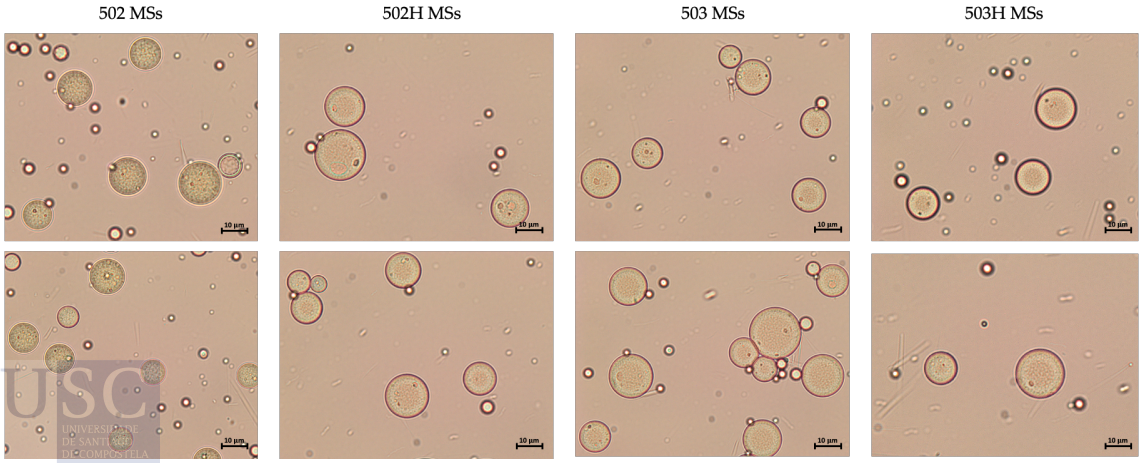


Figure 3. Optical microscopy images of idebenone-loaded PLGA-based microspheres.

SEM evaluation was also performed to analyze the MSs shape and surface, considering that the MSs morphological characterization may also correlate particle size and surface characteristics with the rest of pharmacokinetic parameters. SEM observation demonstrated reliable results with previous optical observation, where the MSs size distribution was narrow and adequate for intravitreal administration due to the selected size interval (see Figure 4). The resulting idebenone-loaded PLGA MSs were without pores, as can be seen in SEM images. Images reveal the methylene chloride complete removal during the elaboration process.

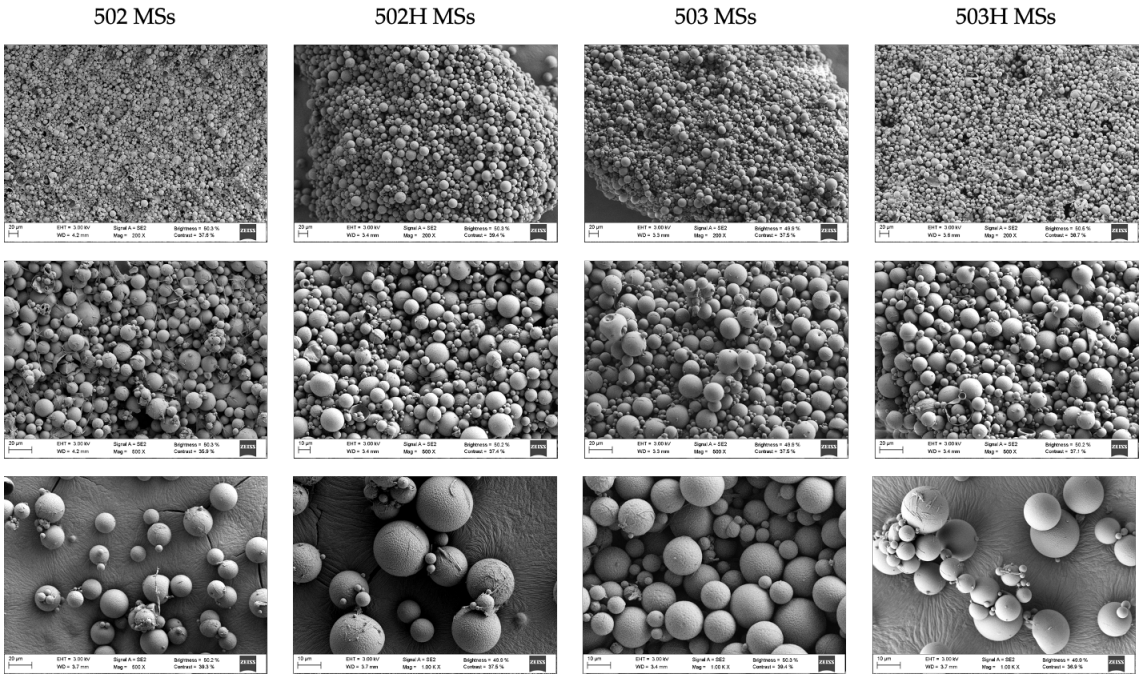


Figure 4. SEM images of idebenone-loaded PLGA-based microspheres.

The surface analysis demonstrated that blank and idebenone-loaded MSs were free flowing, with a diameter of 18.07 ± 4.13 μm, and revealed a spherical shape and relatively smooth surface, with micropores at high magnification, probably due to the slow release of dichloromethane. Furthermore, no detrimental effects were observed due to the drug loading.

3.3. Production yield (PY), Encapsulation Efficiency (EE), and Loading Capacity (LC)

USC UNIVERSIDADE DE SANTIAGO DE COMPOSTELA

Table 7 shows the results for PY, EE, and LC of idebenone-loaded PLGA MSs. All MSs batches showed suitable PY, EE, and LC values for the applied preparation procedure.

One of the main benefits of the O/W emulsion/solvent evaporation procedure was the chance of preparing MSs with high PY values (over 80%) for all the selected formulations (see Table 7). Furthermore, a decrease in the polymer's inherent viscosity may cause a reduction of the amount of adhered-to-container polymer and, thus, increases the production yield values. Final formulations were compared by a two-way ANOVA analysis, observing no statistically significant differences among the different formulations ($p > 0.05$).

The EE determination proved that the idebenone-loaded preparation process was reproducible and effective, with values above 85% in all formulations (see Table 7). The EE results were consistent for both the direct and indirect methods, and there were no significant differences between the two types of measurement. LC values ranged from 10 to 25% and, considering that a 1:10 drug:polymer ratio was employed, the resulting values are in line with expectations. These data are supported by the idebenone low aqueous solubility, which provides high drug entrapment into polymeric MSs, as well as the drug:polymer proportion used in the elaboration process.

Table 7. Encapsulation efficiency (EE) and loading capacity (LC) values of the selected idebenone-loaded PLGA MSs.

Formulation	PY (%)	EE (%)	LC (%)
502 MSs	87.37 ± 2.30	87.59 ± 0.78	22.05 ± 2.52
502H MSs	86.32 ± 0.86	88.65 ± 1.32	22.09 ± 1.46
503 MSs	83.64 ± 5.47	88.40 ± 2.33	17.01 ± 2.93
503H MSs	85.68 ± 3.29	89.20 ± 0.61	13.94 ± 1.14

A two-way ANOVA analysis was further submitted to the data to assess the presence or absence of differences among all formulations. The results show no statistically significant differences ($p > 0.05$) in terms of PY, EE, and LC.

USC
DE SANTIAGO
DE COMPOSTELA

4. *In vitro* release study

Different mechanisms may be involved in the encapsulated drug release from PLGA MSs, where diffusion and biopolymer erosion are the main ones (45,46). The diffusion rate is dependent upon drug diffusivity and partition coefficients (47), although drug physicochemical

properties, such as molecular size, hydrophilicity, and surface charge must be also taken into account (47).

Likewise, hydrophobic drugs may hamper water diffusion into MSs as well as reducing the polymer degradation rate (27,45). Hence, the effects of the encapsulated drug may be considered into the microparticulate systems' design due to its influence on the release mechanisms underlying biopolymer degradation (45).

The two leading mechanisms involving drug delivery from PLGA MSs are mainly diffusion and polymer erosion (46). Generally, drug release from PLGA MSs arises into different stages. Firstly, a quick reduction in the polymer's Mw but a slight mass loss is observed while, in the subsequent stage, the contrary phenomenon happens, supporting the fact that PLGA degradation from MSs comprises mixed mechanisms, where drug delivery is primarily buttressed by diffusion processes rather than polymer degradation (48). Nevertheless, none of the different MSs formulations prepared in the present work have shown the initial burst release phase, leading to a more slow, stable, and constant release from the beginning of the *in vitro* release study.

PLGA polymers are typical bulk-eroding biopolymers where water readily infiltrates into their matrix, leading to pore formation into the MSs structure, where degradation processes take place (49). Upcoming research relies on achieving a better enlightening of this knowledge gap regarding the design of microparticulate systems (48), which may potentially be included into formulations encompassing heterogeneous release-profile biopolymers (50).

Drug release profiles from polymeric MSs were described to be harshly conditioned by PLGA properties (size, molecular weight, lactide:glycolide proportion or surface thermodynamics, among others), and by the mechanisms involved in the release process (51,52). In the present study, idebenone release from PLGA MSs seems to follow a monophasic pattern, characterized by a prolonged, uniform, and controlled release phase along the studied interval. Such idebenone release profile might be associated with polymer degradation processes, from drug diffusion through the matrix or even both simultaneously (19,53). The *in vitro* release profiles of the idebenone-loaded MSs formulations are shown in Figure 5.

USC
UNIVERSIDADE
DE SANTIAGO
DE COMPOSTELA

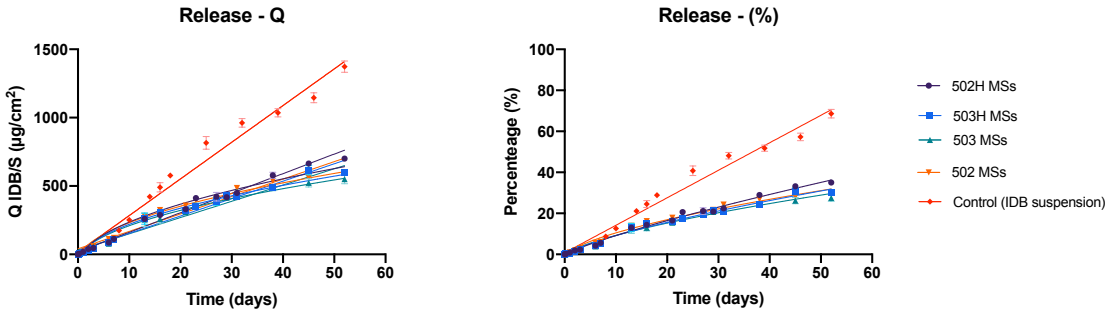


Figure 5. *In vitro* release study of idebenone-loaded PLGA MSs. The pharmacokinetic profile of the idebenone-loaded PLGA MSs was compared with an idebenone aqueous suspension containing the same amount of drug.

Very low dissolution kinetics of the idebenone suspension was observed. The drug apparent thermodynamic solubility in PBS and simulated vitreous humor was 1.303 ± 0.002 and 1.304 ± 0.005 µg/mL respectively. These values indicate that *no sink* conditions were followed during the experiment and so the low dissolution rate observed in IDB suspension is mainly due to the saturation of the release media caused by the low drug solubility.

Experimentally, a modified release of idebenone from the microparticles is observed, reaching about 25% over a 50-day period. This may be due to the concurrence of several factors simultaneously. Firstly, the microparticle formulation was included into simulated vitreous humor, a medium that mimics the physicochemical characteristics of physiological vitreous humor, being a medium of high viscosity, thus reducing the drug diffusion rate. In addition, the donor chamber was not subject to agitation (only in the receptor chamber to facilitate the renewal of the medium) in order to mimic, as closely as possible, the physiological state in the eye, as compared to an *in vitro* medium with a high rate of renewal. Therefore, it has been possible to obtain idebenone-loaded microparticles with a sustained and prolonged release, allowing the achievement of static and uniform drug levels at the site of action.

5. Stability studies

5.1. Stability to storage

USC
DE SANTIAGO
DE COMPOSTELA

Previous studies showed that PLGA MSs might be associated with aggregates formation at higher temperatures (55). Nevertheless, no aforementioned behavior was observed in the tested formulations, and stability studies were performed as previously established. The results for the short-term stability study showed that all formulations did not suffer major changes during the

studied period (see Figure 6). Negligible changes during the stability study by drug content uniformity may be linked to interferences from the polymer metabolites. Therefore, the idebenone entrapment into PLGA MSs did not modify the drug's native structure. Besides, orange physical appearance was preserved during the entire assay, as well as positive injectability and syringeability test results, supporting the free-flowing behavior of the formulations.

A two-way ANOVA was additionally submitted, and no statistically significant differences ($p > 0.05$) were found among formulations for the same storage conditions during the studied period. Thus, all formulations were stable over the studied time interval.

USC
UNIVERSIDADE DE SANTIAGO DE COMPOSTELA

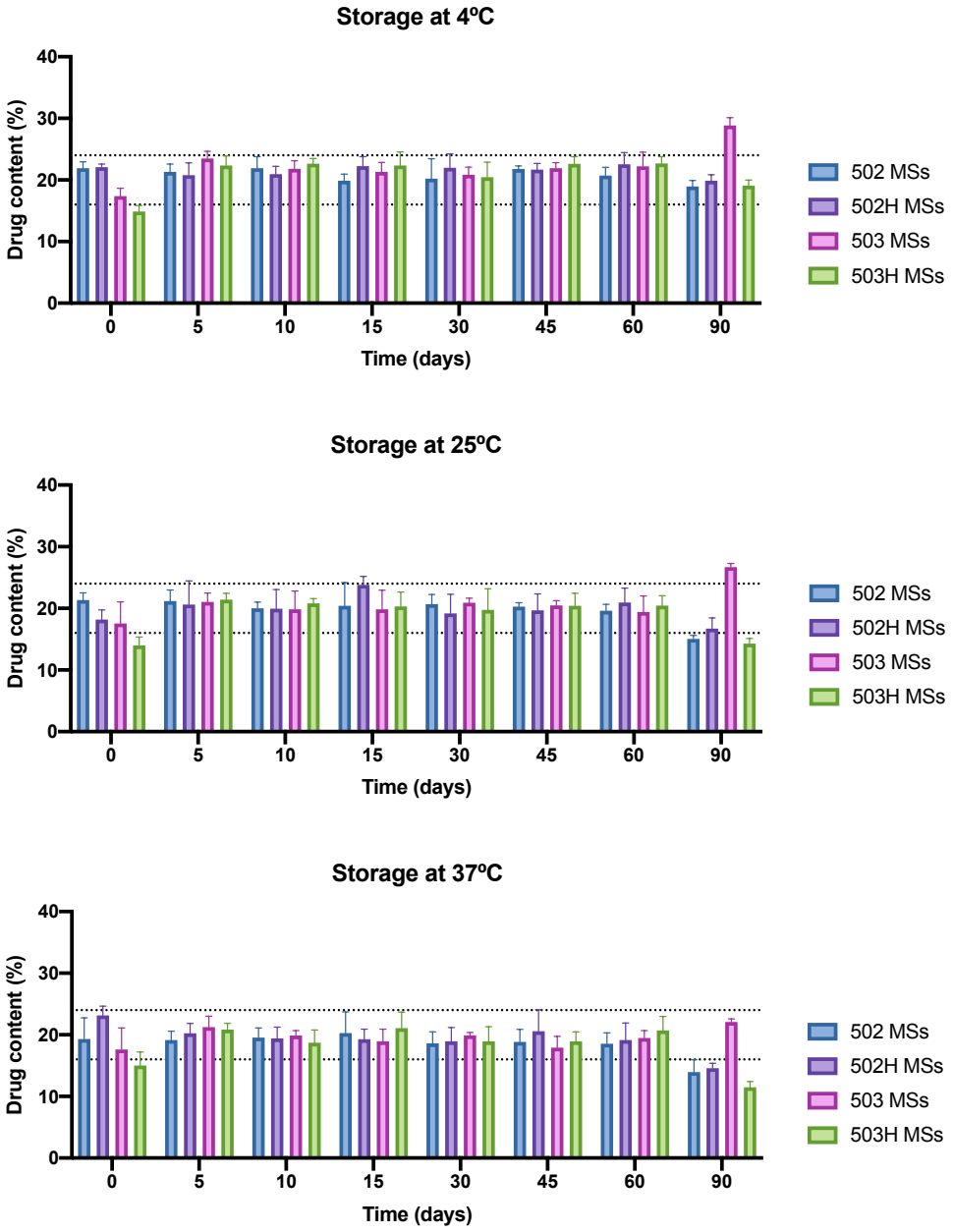


Figure 6. Resulting data of the stability to storage study at three different temperature conditions for the tested MSs formulations.

5.2. Stability to pH

Extreme pH conditions of the media may be generally used to achieve a quicker drug release rate from the microparticulate systems due to changes in the release mechanism involved. Stability-to-pH changes were evaluated through the MSs uniformity content by UV-Vis spectrophotometry, as presented in previous sections. Physical characteristics of the formulations were carefully examined for changes in appearance, color, and

clumping/aggregation behavior. The possibility of any MSs collapse or breakage was also assessed by optical microscopy.

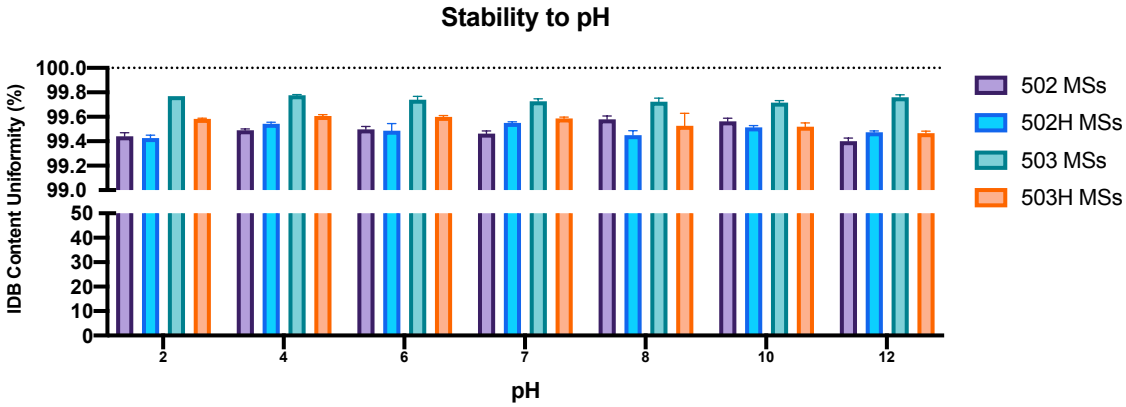


Figure 7. Idebenone content uniformity (%) values during the stability-to-pH study.

Figure 7 displays the resulting data for the stability-to-pH study of idebenone-loaded PLGA MSs. The hydrophobic nature of the idebenone would prevent its diffusion to the surrounding medium, thus enhancing its entrapment into the PLGA MSs, and protecting the drug from degradation phenomena. In addition, no changes in physical appearance, color or aggregation behavior were observed during the study.

A two-way ANOVA was also applied, and no statistically significant differences ($p > 0.05$) were observed along the studied period. Thus, all formulations were stable against variations over the studied pH interval.

5.3. Stability to ionic strength

Extreme ionic strength conditions of the media may be usually used to achieve a quicker drug release rate from the microparticulate systems due to changes in the release mechanism involved. Stability-to-ionic-strength changes were evaluated through MSs uniformity content by UV-Vis spectrophotometry, as presented in previous sections. Physical characteristics of the formulations were carefully examined for changes in appearance, color, and clumping/aggregation behavior. The possibility of any MSs collapse or breakage was also assessed by optical microscopy.

USC DE COMPOSTELA

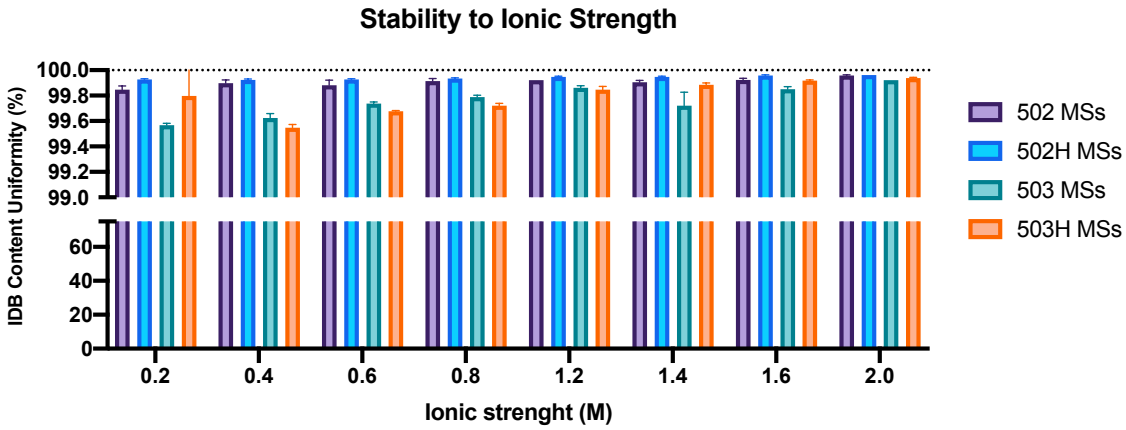


Figure 8. Idebenone content uniformity (%) values during the stability-to-ionic-strength study.

Figure 8 displays the resulting data for the stability-to-ionic-strength study of the idebenone-loaded PLGA MSs. The stability of the idebenone-loaded MSs suspension was maintained constant regardless of the ionic strength increase in the media. The hydrophobic nature of the idebenone would prevent its diffusion to the surrounding medium, thus improving its entrapment into the PLGA MSs and protecting the drug from the degradation phenomena.

A two-way ANOVA was then submitted, and no statistically significant differences ($p > 0.05$) were found along the studied interval. Thus, all formulations were stable against ionic strength variations over the studied time interval.

6. Moisture content

Moisture content assay may assess the MSs stability due to the fact that high moisture content may lead to particle agglomeration phenomena, lessening the MSs stability and increasing the interparticle cohesion and degradation processes of the formulation components (56,57). The moisture content of MSs should be under 10% weight of the entire formulation to guarantee the drug stability over time (58).

In the present assay, idebenone-loaded PLGA MSs moisture content ranged from 3.97 ± 2.21% to 4.89 ± 0.91%, lower enough to assure the long-term stability of the formulations, avoiding drug degradation (see Table 9). Furthermore, results may correlate with polymer properties, where the more hydrophilic it is, the more water content it will have.

USC
DE SANTIAGO
DE COMPOSTELA

Table 9. Data of the moisture content (%) for the selected MSs formulations.

Formulation	Moisture content (%)
502 MSs	4.89 ± 0.91
502H MSs	4.02 ± 1.47
503 MSs	3.97 ± 2.21
503H MSs	4.49 ± 1.11

7. Solid-State Nuclear Magnetic Resonance (ss-NMR)

Nuclear Magnetic Resonance Spectroscopy (NMR) allows the study of almost any element (isotope) of the periodic table. Molecular information is obtained by means of NMR spectra. There is a huge variety of types of NMR spectra and each of them is sensitive to one type of molecular information (covalent or chemical bond structure, spatial proximity between atoms, molecular translational scattering, rotational scattering, ...).

Solid state NMR allows the study of physical and chemical properties of samples in crystalline or amorphous state. Applications include the determination of molecular structure, intermolecular packing in amorphous solids, material properties (e.g., flexibility, fragility, ...), the evolution of materials, and the study of heterogeneous samples.

Phase separation and heterogeneity in solid formulations of polymers and drugs are relevant for their applications, especially as drug delivery systems (59). Even in formulations prepared with the same composition, subtle effects of the protocol of preparation, viscosity, pH or molecular weight may lead to differences in crystallinity as well as the formation of heterogeneous phases with differences in the molecular mobility of the components.

Phase separation and molecular mobility can be studied by ss-NMR methods (59–61). In this work, phase separation and mobility of the idebenone-loaded PLGA microparticles were studied by the comparison of two different types of ss-NMR ^{13}C spectra. The former is based on the direct-polarization ^{13}C-PARISxy spectrum (24), while the second one is grounded in the ^{13}C-CPMAS spectrum, related to the cross-polarization phenomenon (62,63). Both types of ss-NMR ^{13}C spectra have shown high sensitivity to sample heterogeneity and phase formation due to the fact that the signal intensity is affected by the degree of molecular flexibility/rigidity that experiences each carbon site.

The ^{13}C-PARISxy spectrum emphasizes the ^{13}C resonances intensity in a semi-fluid phase characterized by fast molecular mobility and long proton transversal relaxation times. The ^{13}C-CPMAS-spectrum signals are generated by a ^{1}H-^{13}C dipolar interaction during the cross-polarization period of the experiment (62,63). Since the dipolar interaction is attenuated or vanished for molecules that experience fast liquid-like molecular mobility, the ^{13}C-CPMAS emphasizes signals in a rigid environment characterized by relative short transversal relaxation times. Based in these principles, the comparison of ^{13}C-CPMAS and ^{13}C-PARISxy spectra of the solid formulations was employed to characterize the microparticles in terms of the formation of heterogeneous phases and differences of molecular mobility.

The ^{13}C-CPMAS and ^{13}C-PARISxy spectra of the 503 MSs formulation are shown in Figure 9. The PLGA component is the only visible in the ^{13}C-CPMAS spectrum (see Figure 9a), and its signals appear with considerable broadness, a typical condition of a rigid but disordered polymorphic state. Interestingly, the situation is the opposite in the ^{13}C-PARIS-xy spectrum (see Figure 9b); the signals of idebenone dominate the spectrum and appear as narrow peaks more typical of a fluid or semi-liquid state while the PLGA peaks are barely observed in Figure 9b despite the fact that is the main component in this sample. Overall, these results denote a different phase for PLGA and idebenone in this sample, the later component showing high mobility entrapped into the PLGA nanocavities. The analysis of the ^{13}C-CPMAS and ^{13}C-PARISxy spectra of the 502 MSs and 503H formulations (see supplementary Figures 1 and 2) has reached similar conclusions regarding sample heterogeneity as those seen above for the 503 MSs formulation.

The ^{13}C-CPMAS and ^{13}C-PARIS spectrum of formulation 502H MSs are given in Figure 10 and represents a different situation compared to the other three formulations. The ^{13}C-CPMAS spectrum (see Figure 10a) shows the idebenone and PLGA signals with good signal:noise ratio. In concordance, the intensity of the idebenone signals in the ^{13}C-PARISxy spectrum (see Figure 10b) is substantially diminished compared to the analogue spectrum of 503 MSs formulation (see Figure 9b). Overall, these results denote that PLGA and idebenone in the 502H MSs formulation are both in a rather homogeneous and relatively more rigid environment compared to the other three formulations. Besides that, the high mobility of idebenone in the polymeric environment detected for the other formulations has been considerably reduced.

The ss-NMR results obtained for the four microparticle formulations are in good agreement with those obtained herein by the X-ray diffractometry, DSC, and TGA analyses that showed

USC UNIVERSIDADE DE SANTIAGO

the idebenone amorphization in the MSs formulations. Solid state-NMR also provided positive information related to the phase heterogeneity in the polymeric microparticles, in particular for 502 MSs, 503 MSs, and 503H MSs formulations and, in a lower extension, for the 502H MSs formulation.

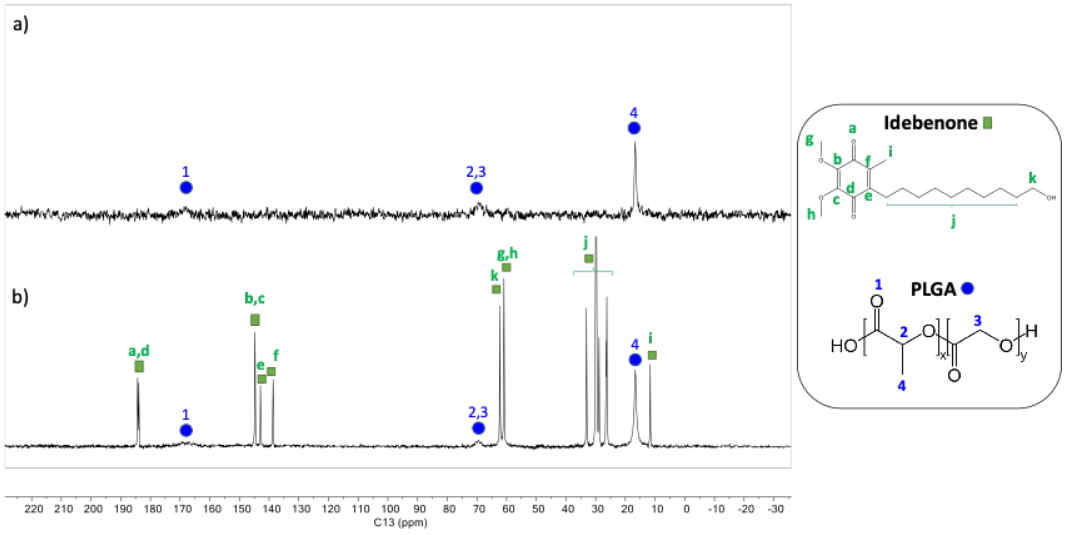


Figure 9. Solid state NMR spectra of formulation 503 MSs. a) 1D ^{13}C-CPMAS and b) 1D ^{13}C-PARISxy. The structures are shown on the right with the letters and number codes used to identify the atoms.

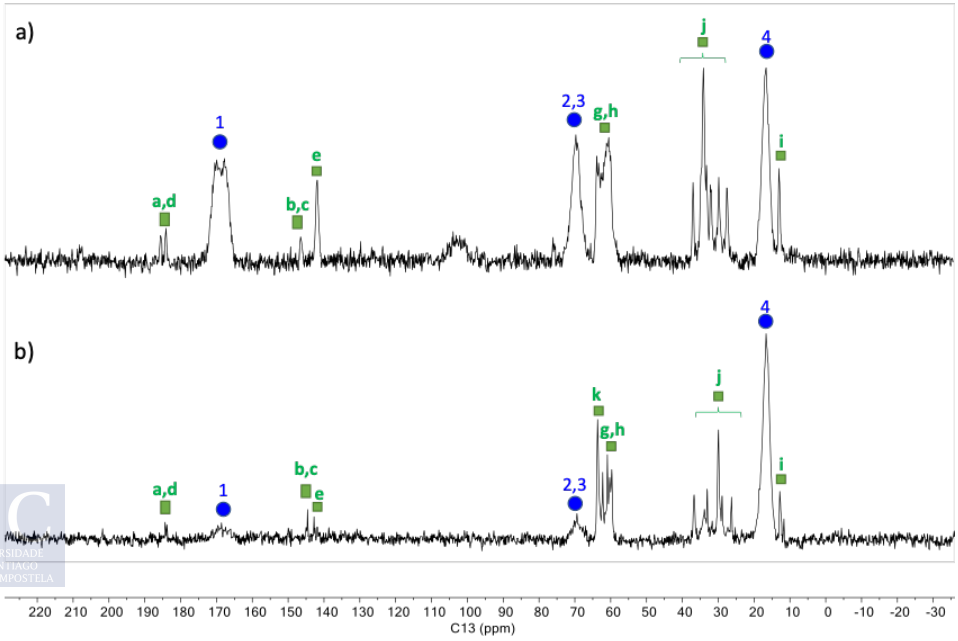


Figure 10. Solid state NMR spectra of formulation 502H MSs. a) 1D 13C-CPMAS and b) 1D 13C-PARISxy. The letters and number codes used to identify the atoms are given in Figure 9.

Despite the 3-month storage study, the 502, 503, and 503H MSs (1:10 polymer: drug ratio) were stored over a 12-month period inside a cabinet at room temperature (17–25°C) in the absence of light prior to a new ss-NMR analysis. The ^{13}C-CPMAS and ^{13}C-PARIS spectra of these formulations (see Supplementary Figures 3 and 4) did not show significant changes after the storage period, indicating that no major changes have occurred in their microparticulate solid structure.

8. Differential Scanning Calorimetry (DSC) and Thermogravimetry analysis (TGA)

DSC curves of idebenone-loaded PLGA MSs were measured to determine the existence of interactions, if any, between the PLGA and the idebenone within the polymer network of the MSs (see Figure 11).

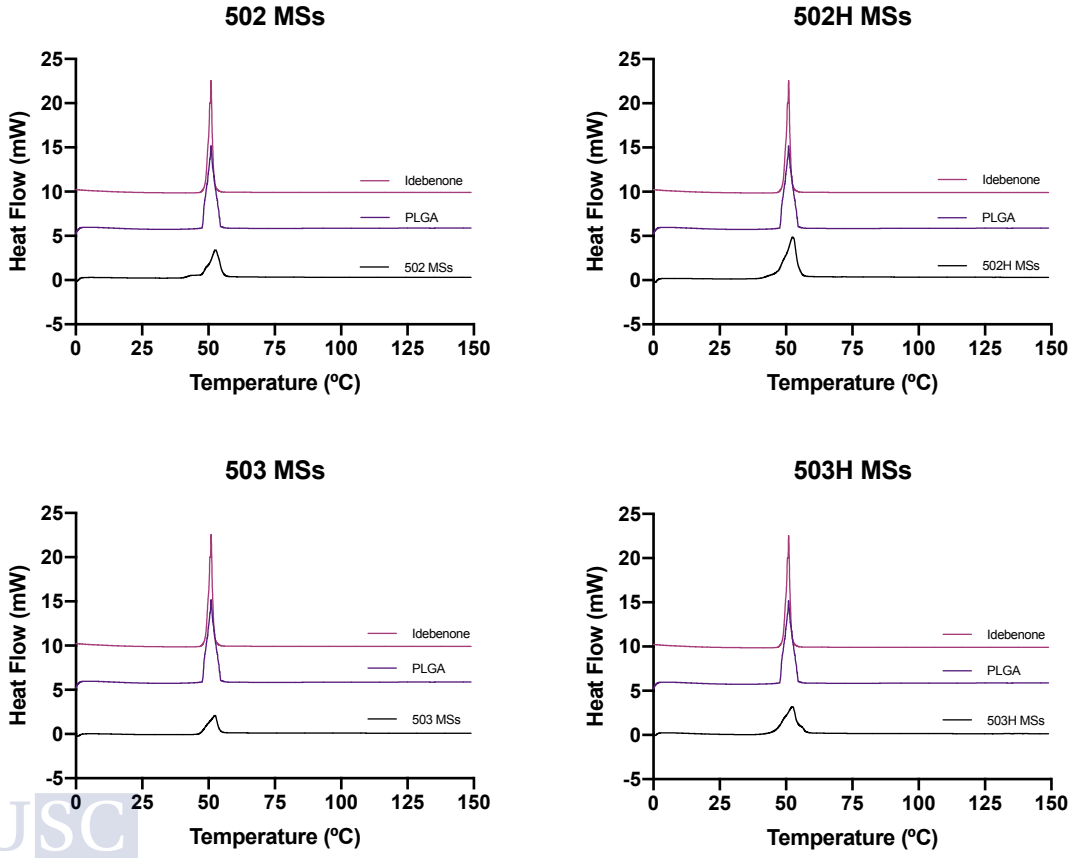


Figure 11. Differential Scanning Calorimetry (DSC) traces of idebenone-loaded PLGA MSs.

USC UNIVERSIDADE DE SANTIAGO DE COMPOSTELA

The DSC curves of idebenone-loaded MSs showed a melting point similar to the transition temperature of PLGA polymers (42 - 46°C). No detectable melting endotherm pattern was found for idebenone, possibly due to a masking phenomenon, by exhibiting a melting temperature similar to that of polymers (52 – 55°C). Furthermore, no detection was found in terms of drug state into the PLGA-based microspheres based on endothermal point measurement, where molecular dispersion or solid solution states might not be distinguished from the resulting data. Thus, results suggest that both idebenone and PLGA maintained their characteristics into the final MSs formulations. From the MSs thermal analysis, it can be concluded that the idebenone existed in amorphous or disordered crystalline form into the PLGA polymer matrix after the MSs preparation, which may have a noticeable therapeutic importance as it could lead to an enhanced biological activity.

The analysis of TGA/IR results of microspheres showed that weigh changes were not produced during the temperature ramp and no dichloromethane residues were detected by the IR analyzer associated with the TGA equipment. Consequently, no residues of the solvent used in microsphere fabrication were detected.

9. Fourier-transformed infrared spectroscopy (FTIR)

FTIR spectroscopy analysis was used to confirm the absence of no chemical interaction between the drug and the polymer. The FTIR spectra of idebenone, the different PLGA polymers, and the idebenone-loaded PLGA MSs are shown in Figure 12. Idebenone showed its main bands at 3568, 2921, 2846, 1650, and 1610 cm^{-1}, corresponding to the O-H, C-H, C=O, and C=C stretching vibrations. PLGA samples showed their major bands at 2900-3000, and 1752 cm^{-1}, agreeing with the C-H and C=O stretching bands. FTIR spectra of the MSs samples confirmed the absence of chemical interactions among the components of the formulation whereby confirming the chemical compatibility between the drug and the polymer by maintaining the integrity of main peaks. Idebenone characteristic peaks indicated no major shifts, matching the formulation spectrum. Thus, the resulting spectra demonstrated the compatibility between the idebenone and all PLGA tested polymers.

FTIR spectra of formulations 502, 503, and 503H MSs (see Supplementary Figure 5) after a 12-month storage period did not show significant changes in the main bands of the drug and polymer. These results indicate that no changes in the chemical structure of drug or polymer

USC UNIVERSIDADE DE SANTIAGO

have occurred, maintaining the compatibility between the idebenone and PLGA throughout the storage period.

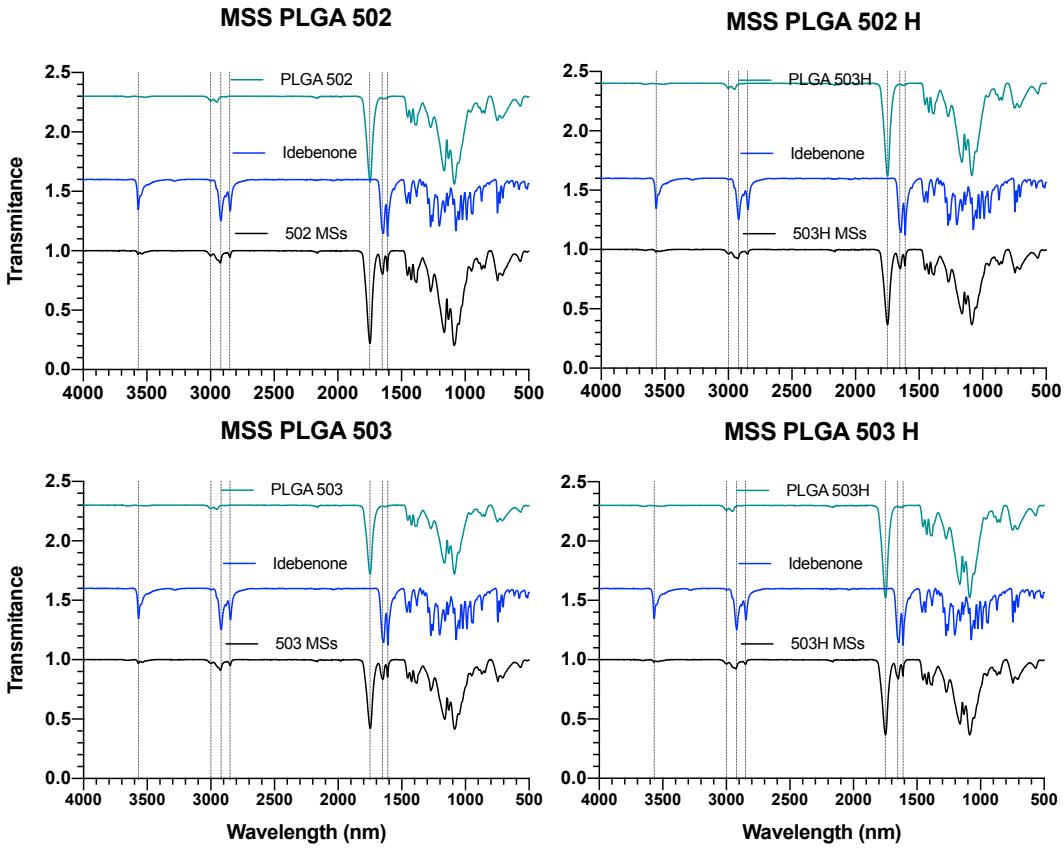


Figure 12. FTIR results for the components and the selected MSs formulations. Two different transformations ($Y = 2Y_0 + 1$ and $Y = 4Y_0 + 1$) were respectively applied on PLGA and idebenone graph representations to promote the complete observation and comparison of the resulting data.

10. X-Ray diffractometry analysis

All idebenone-loaded MSs formulations were characterized by X-ray diffraction studies. The physical state of the MSs components was also determined before the preparation of the formulations. The X-ray diffractograms for the MSs components and final formulations are shown in Figure 13.

The analysis by X-ray diffraction demonstrated the presence of many diffraction bands in the drug's powder sample, as well as for PLGA polymers, reflecting their characteristic crystalline properties. Idebenone remains in its amorphous state, randomly and rather homogenously distributed throughout the PLGA matrix, possibly due to low drug loading in the MSs.

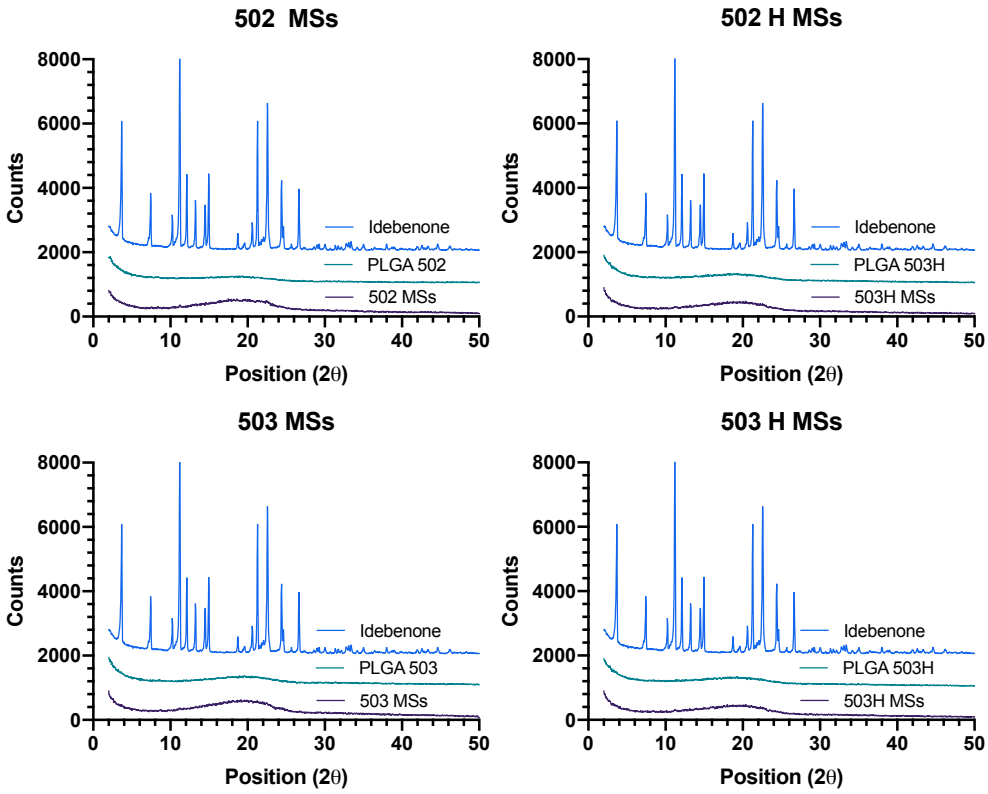


Figure 13. X-Ray diffractometry results for the components and the selected MSs formulations. Two different transformations ($Y = 1000Y_0 + 1$ and $Y = 2000Y_0 + 1$) were respectively applied on PLGA and idebenone graph representations to promote the complete observation and comparison of the resulting data.

After 12 months of storage at room temperature (see Supplementary Figure 6), peaks corresponding to idebenone crystalline state are observed in 502 MSs samples, indicating that a small proportion of the drug is recrystallizing in the MSs matrix. On the contrary, no changes in the amorphous structure of IDB were observed in the 503 and 503H MSs samples.

The differences observed might be attributed to the different molecular weights of the polymers. Resomer® 502 has a molecular weight distribution between 7000 and 17000 Da, while Resomer® 503 and 503H present a molecular weight distribution between 21000 and 38000 Da. Resomer® 502 provides a less compact and viscous MSs matrix (probably due to its low molecular weight) that allows the drug diffusion and migration, promoting the formation of crystallization nuclei. On the other hand, the higher molecular weight of Resomer® 503 and 503H hinder the drug diffusion and migration processes, inhibiting the crystalline growth of the

USC UNIVERSIDADE DE SANTIAGO DE COMPOSTELA

drug. The X-ray and NMR results indicate that these MSs maintained their stable structure throughout the storage period.

11. Mercury intrusion porosimetry

Mercury intrusion porosimetry allows the empty spaces quantification among MSs (inter-MSs porous volume), as well as the pore volume in the MSs microstructure (intra-MSs porous volume). Pore volume distribution of the idebenone-loaded PLGA MSs is shown in Figure 14. As observed, the cumulative pore distribution of 502H MSs shows the presence of a significant pore population ranging from 5 to 100 µm, representing the 20% of the pore population; hence, this interparticular space value may be associated with the formation of vaults and voids caused by the particle aggregation of the in the porosimeter probe. A main pore distribution with a 1-5 µm mean size is also observed in all MSs formulations, representing the common interparticular spaces. No significant pore distribution was observed for lower values, suggesting that all microparticulate formulations showed low microporosity.

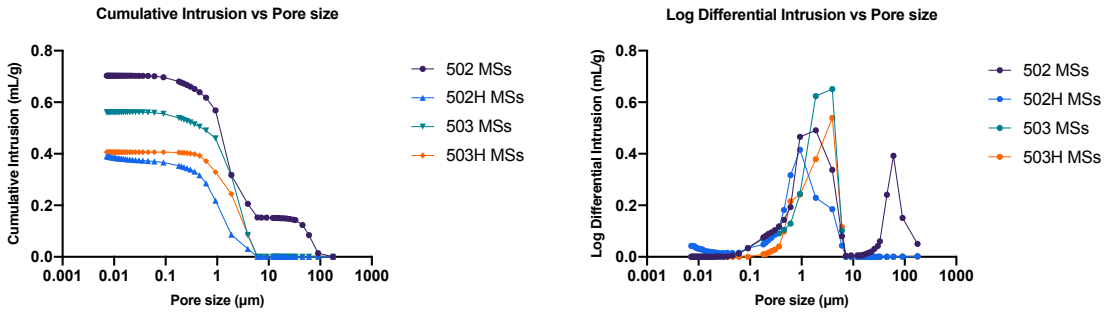


Figure 14. Resulting data of mercury intrusion porosimetry studies for the different idebenone-loaded MSs formulations. All data were fitted to a log-normal distribution.

12. Syringeability and injectability studies

Syringeability and injectability of MSs formulations are key-product parameters of intraocular DDS, where a formulation should be delivered by a syringe and easily pass through a needle. Since it is well recognized that kinematic viscosity of a formulation deeply influences its ejection from the syringe/needle system, the syringeability and injectability of the resulting MSs formulations were automatically evaluated by a panel test created with a universal testing

USC
UNIVERSIDADE DE SANTIAGO DE COMPOSTELA

machine. In addition, as the needle gauge might influence the patient's comfort and compliance, different needle consistency was also assessed (see Table 10 for needle specifications).

Table 10. Specifications of the different needles used during the syringeability and injectability assays.

Needle gauge	Inner diameter (mm)	Length (mm)
18	1.020	38
21	0.710	32
27	0.361	13
30	0.250	10

All predefined subsets were favorable in terms of MSs formulation's injection into air, independently of the needle diameter or length (see Table 10). The ease of injection into air was acceptable for the formulations tested. The results of injectability and syringeability revealed neither partial nor complete blockage of the MSs suspension flow (see details in Figure 15). Thus, resulting MSs are appropriate for intraocular injection through a 30G needle.

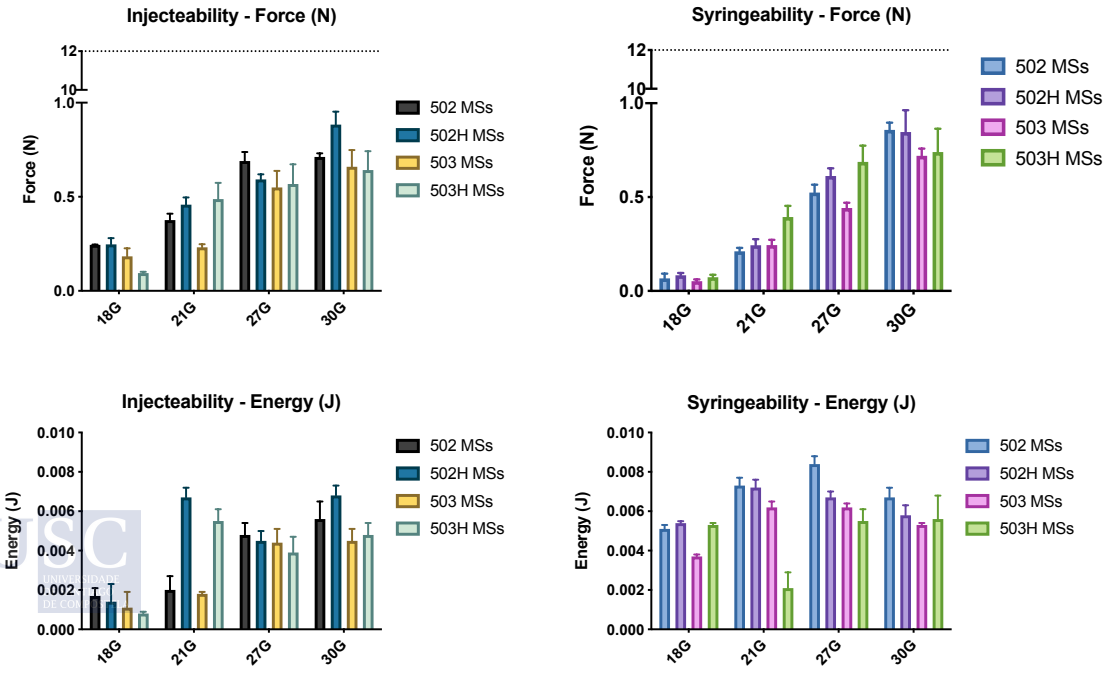


Figure 15. Injectability and syringeability results for the selected MSs formulations.

13. Ocular irritancy and toxicity analysis

The CAM is a no innervated complete tissue containing a complex structure of blood vessels (arteries, veins, and capillaries), being a well-developed vascularization organotypic model and an easy-to-study alternative strategy for ocular irritancy and toxicity, since it responds to damage with a complete inflammatory process, similar to that produced in the retinal tissue. Idebenone-loaded MSs cytotoxicity was assessed, and results were compared with those obtained for the negative (PBS) and positive (ethanol) control formulations, respectively. All MSs formulations demonstrate no cytotoxicity effects (Irritation Score = 0), comparing them with control formulations (see Figure 16). Nevertheless, it will be necessary to perform future studies in animal models to evaluate the long-term toxicity of the MSs formulations, since these systems are intended for long periods of time into the vitreous chamber.

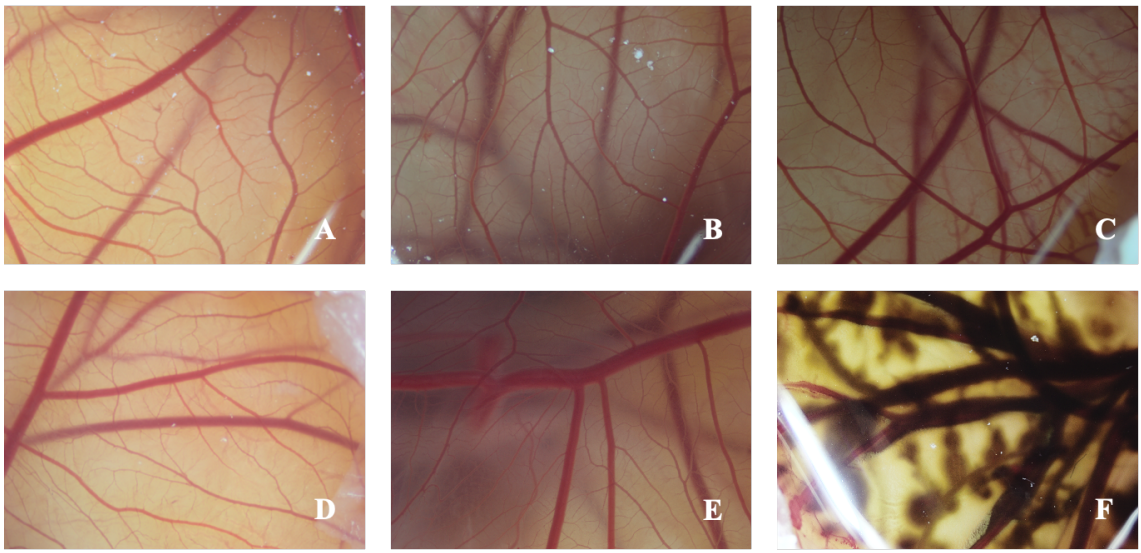


Figure 16. HET-CAM results for the idebenone-loaded PLGA MSs formulations. (A) 502 MSs, (B) 502H MSs, (C) 503 MSs, (D) 503H MSs, (E) PBS (negative control), and (F) Ethanol (positive control).

CONCLUSION

In the past decade, significant advancement has been made on addressing several concerns related to drug encapsulation into microparticulate systems, including low drug entrapment, formulation's instability, and appropriate control of drug release from the PLGA-based systems. Furthermore, an important need for innovation in the design and development of

efficient procedures for controlling the parameters that affect encapsulation efficiency, loading capacity, and release profiles is needed, as a way to enlighten the design and development of a new-generation controlled-release DDS (64). PLGA MSs are one of the most attractive novel DDS due to their biodegradability, ease of administration, and controlled release properties over a long-term period.

MSs formulations were prepared and physicochemically characterized in order to create a solid preclinical basis from which conduct *in vivo* studies. Idebenone was successfully loaded into PLGA MSs by an O/W simple emulsion/solvent evaporation technique, with adequate physicochemical characteristics. A 10 – 25 μm interval particle size and a surface potential of -17.13 ± 1.65 mV were obtained for all the idebenone-loaded PLGA MSs. The adopted method also favored the formation of smooth, regular, and spherical MSs with the optimal particle size interval for intravitreal administration through a 30G needle. Idebenone was evenly distributed into the MSs matrix, associated with the drug physicochemical properties.

Analogously, a controlled and sustained idebenone release was achieved from all MSs formulations, confirming their use as potential DDS for long-term intravitreal administration. All MSs formulations also demonstrated good stability to storage for a 3-month period, as well as no idebenone uniformity content changes were observed along the studied pH interval. Same behavior was observed for the ionic strength interval in terms of idebenone uniformity content. These stability results were also supported by the moisture content analysis, reinforcing *in vitro* characterization data of these formulations. Resulting data showed that all PLGA MSs may be considered as potential carriers for hydrophobic drug's-controlled release. However, *in vivo* assays with idebenone-loaded PLGA MSs should be considered in the future to assess its clinical application.

In the present work, different idebenone-loaded PLGA MSs formulations were proposed as the first pharmacological alternative based on microparticulate systems for the LHON treatment intended for intravitreal administration. This was reinforced by wide *in vitro* and *ex vivo* characterization studies. A preclinical coherent basis was accomplished as an alternative to LHON treatment, a pathology with no therapeutic alternatives so far. In addition, the versatility of these systems would enable the inclusion of new drugs intended for intravitreal administration according to the patient needs and characteristics, as a new method of partial personalization treatment strategies.

USC UNIVERSIDADE DE SANTIAGO

REFERENCES

1. Behbehani R. Clinical approach to optic neuropathies. Clin Ophthalmol Auckl NZ. 2007 Sep;1(3):233–46.
2. Newman NJ, Biousse V. Hereditary optic neuropathies. Eye Lond Engl. 2004 Nov;18(11):1144–60.
3. Langer R. Drug delivery and targeting. Nature. 1998 Apr 30;392(6679 Suppl):5–10.
4. Gattani YS. Floating multiparticulate drug delivery systems: An overview. IJPBS. 1.
5. Kumari S, Nagpal M, Aggarwal G, Jain UK, Sharma P. Microparticles drug delivery system: A review. World J Pharm Pharm Sci. 5(03):24.
6. Saez V, Hernández JR, Peniche C. Las microesferas como sistemas de liberación controlada de péptidos y proteínas. :10.
7. Jain RA. The manufacturing techniques of various drug loaded biodegradable poly(lactide-co-glycolide) (PLGA) devices. Biomaterials. 2000 Dec;21(23):2475–90.
8. Garvin K, Feschuk C. Polylactide-polyglycolide antibiotic implants. Clin Orthop. 2005 Aug;(437):105–10.
9. Karataş A, Sonakin O, Kiliçarslan M, Baykara T. Poly (epsilon-caprolactone) microparticles containing Levobunolol HCl prepared by a multiple emulsion (W/O/W) solvent evaporation technique: effects of some formulation parameters on microparticle characteristics. J Microencapsul. 2009 Feb;26(1):63–74.
10. Esteban-Pérez S, Bravo-Osuna I, Andrés-Guerrero V, Molina-Martínez IT, Herrero-Vanrell R. Trojan Microparticles Potential for Ophthalmic Drug Delivery. Curr Med Chem. 2019 05;
11. Bravo-Osuna I, Andrés-Guerrero V, Arranz-Romera A, Esteban-Pérez S, Molina-Martínez IT, Herrero-Vanrell R. Microspheres as intraocular therapeutic tools in chronic diseases of the optic nerve and retina. Adv Drug Deliv Rev. 2018 15;126:127–44.
12. Fernández-Sánchez L, Bravo-Osuna I, Lax P, Arranz-Romera A, Maneu V, Esteban-Pérez S, et al. Controlled delivery of tauroursodeoxycholic acid from biodegradable microspheres slows retinal degeneration and vision loss in P23H rats. PloS One. 2017;12(5):e0177998.
13. Leonardi D, Salomón CJ, Lamas MC, Olivieri AC. Development of novel formulations for Chagas' disease: Optimization of benznidazole chitosan microparticles based on artificial neural networks. Int J Pharm. 2009 Feb 9;367(1–2):140–7.

USC DE COMPOSTELA

14. Mello VA de, Ricci-Júnior E. Encapsulation of naproxen in nanostructured system: structural characterization and in vitro release studies. Quím Nova. 2011;34(6):933–9.

15. Guerreiro LH, Da Silva D, Ricci-Junior E, Girard-Dias W, Mascarenhas CM, Sola-Penna M, et al. Polymeric particles for the controlled release of human amylin. Colloids Surf B Biointerfaces. 2012 Jun 1;94:101–6.

16. Cegnar M, Kos J, Kristl J. Cystatin incorporated in poly(lactide-co-glycolide) nanoparticles: development and fundamental studies on preservation of its activity. Eur J Pharm Sci Off J Eur Fed Pharm Sci. 2004 Aug;22(5):357–64.

17. Freitas S, Merkle HP, Gander B. Microencapsulation by solvent extraction/evaporation: reviewing the state of the art of microsphere preparation process technology. J Control Release Off J Control Release Soc. 2005 Feb 2;102(2):313–32.

18. Mittal G, Sahana DK, Bhardwaj V, Ravi Kumar MNV. Estradiol loaded PLGA nanoparticles for oral administration: effect of polymer molecular weight and copolymer composition on release behavior in vitro and in vivo. J Control Release Off J Control Release Soc. 2007 May 14;119(1):77–85.

19. Freitas S, Merkle HP, Gander B. Microencapsulation by solvent extraction/evaporation: reviewing the state of the art of microsphere preparation process technology. J Control Release Off J Control Release Soc. 2005 Feb 2;102(2):313–32.

20. Mao S, Xu J, Cai C, Germershaus O, Schaper A, Kissel T. Effect of WOW process parameters on morphology and burst release of FITC-dextran loaded PLGA microspheres. Int J Pharm. 2007 Apr 4;334(1–2):137–48.

21. Varela-Fernández R, García-Otero X, Díaz-Tomé V, Regueiro U, López-López M, González-Barcia M, et al. Design, Optimization, and Characterization of Lactoferrin-Loaded Chitosan/TPP and Chitosan/Sulfobutylether-β-cyclodextrin Nanoparticles as a Pharmacological Alternative for Keratoconus Treatment. ACS Appl Mater Interfaces. 2021 Jan 27;13(3):3559–75.

22. Q 1 A (R2) Stability Testing of new Drug Substances and Products. 2006;20.

23. Purusottam RN, Bodenhausen G, Tekely P. Quantitative one- and two-dimensional 13C spectra of microcrystalline proteins with enhanced intensity. J Biomol NMR. 2013 Sep;57(1):11–9.

24. Clas N, Dalton N, Hancock N. Differential scanning calorimetry: applications in drug development. Pharm Sci Technol Today. 1999 Aug;2(8):311–20.

USC UNIVERSIDADE DE SANTIAGO

25. Verdonck E, Schaap K, Thomas LC. A discussion of the principles and applications of Modulated Temperature DSC (MTDSC). Int J Pharm. 1999 Dec 1;192(1):3–20.

26. Klose D, Siepmann F, Elkharraz K, Krenzlin S, Siepmann J. How porosity and size affect the drug release mechanisms from PLGA-based microparticles. Int J Pharm. 2006 May 18;314(2):198–206.

27. Vysloužil J, Doležel P, Kejdušová M, Mašková E, Mašek J, Lukáč R, et al. Influence of different formulations and process parameters during the preparation of drug-loaded PLGA microspheres evaluated by multivariate data analysis. Acta Pharm Zagreb Croat. 2014 Dec;64(4):403–17.

28. Volfkovich Y, Sakars A, Volinsky AA. Application of the standard porosimetry method for nanomaterials. In 2005.

29. Espinal L. Porosity and Its Measurement. 2013 Sep 17 (cited 2019 Dec 16); Available from: https://www.nist.gov/publications/porosity-and-its-measurement

30. Andhariya JV, Choi S, Wang Y, Zou Y, Burgess DJ, Shen J. Accelerated in vitro release testing method for naltrexone loaded PLGA microspheres. Int J Pharm. 2017 Mar 30;520(1–2):79–85.

31. Washburn EW. Note on a Method of Determining the Distribution of Pore Sizes in a Porous Material. Proc Natl Acad Sci U S A. 1921 Apr;7(4):115–6.

32. Reinhold SE, Schwendeman SP. Effect of Polymer Porosity on Aqueous Self-Healing Encapsulation of Proteins in PLGA Microspheres. Macromol Biosci. 2013 Dec;13(12):1700–10.

33. Cilurzo F, Selmin F, Minghetti P, Adami M, Bertoni E, Lauria S, et al. Injectability Evaluation: An Open Issue. AAPS PharmSciTech. 2011 May 7;12(2):604–9.

34. Xie X, Yang Y, Chi Q, Li Z, Zhang H, Li Y, et al. Controlled Release of Dutasteride from Biodegradable Microspheres: In vitro and In vivo Studies. PLOS ONE. 2014 Dec 26;9(12):e114835.

35. Wallig MA, Haschek WM, Rousseaux CG, Bolon B, editors. Chapter 22 - Special Senses. In: Fundamentals of Toxicologic Pathology (Third Edition) (Internet). Academic Press; 2018 (cited 2020 Mar 16). p. 673–747. Available from: http://www.sciencedirect.com/science/article/pii/B9780128098417000228

36. Luepke NP. Hen's egg chorioallantoic membrane test for irritation potential. Food Chem Toxicol Int J Publ Br Ind Biol Res Assoc. 1985 Feb;23(2):287–91.

USC UNIVERSIDADE DE SANTIAGO

37. Spielmann H, Kalweit S, Liebsch M, Wirnsberger T, Gerner I, Bertram-Neis E, et al. Validation study of alternatives to the Draize eye irritation test in Germany: Cytotoxicity testing and HET-CAM test with 136 industrial chemicals. Toxicol Vitro Int J Publ Assoc BIBRA. 1993 Jul;7(4):505–10.

38. Yang YY, Chung TS, Ng NP. Morphology, drug distribution, and in vitro release profiles of biodegradable polymeric microspheres containing protein fabricated by double-emulsion solvent extraction/evaporation method. Biomaterials. 2001 Feb;22(3):231–41.

39. Mao S, Xu J, Cai C, Germershaus O, Schaper A, Kissel T. Effect of WOW process parameters on morphology and burst release of FITC-dextran loaded PLGA microspheres. Int J Pharm. 2007 Apr 4;334(1–2):137–48.

40. Herrero-Vanrell R, Bravo-Osuna I, Andrés-Guerrero V, Vicario-de-la-Torre M, Molina-Martínez IT. The potential of using biodegradable microspheres in retinal diseases and other intraocular pathologies. Prog Retin Eye Res. 2014 Sep;42:27–43.

41. Martínez-Sancho C, Herrero-Vanrell R, Negro S. Optimisation of aciclovir poly(D,L-lactide-co-glycolide) microspheres for intravitreal administration using a factorial design study. Int J Pharm. 2004 Apr 1;273(1–2):45–56.

42. Soni A, Gadad A, Dandagi P, Mastiholimath V. Simvastatin-loaded PLGA nanoparticles for improved oral bioavailability and sustained release: Effect of formulation variables. Asian J Pharm AJP Free Full Text Artic Asian J Pharm (Internet). 2014 Aug 27 (cited 2020 Jun 8);5(2). Available from: https://www.asiapharmaceutics.info/index.php/ajp/article/view/87

43. Budhian A, Siegel SJ, Winey KI. Haloperidol-loaded PLGA nanoparticles: systematic study of particle size and drug content. Int J Pharm. 2007 May 24;336(2):367–75.

44. Siegel SJ, Kahn JB, Metzger K, Winey KI, Werner K, Dan N. Effect of drug type on the degradation rate of PLGA matrices. Eur J Pharm Biopharm Off J Arbeitsgemeinschaft Pharm Verfahrenstechnik EV. 2006 Nov;64(3):287–93.

45. Kamaly N, Yameen B, Wu J, Farokhzad OC. Degradable Controlled-Release Polymers and Polymeric Nanoparticles: Mechanisms of Controlling Drug Release. Chem Rev. 2016 Feb 24;116(4):2602–63.

46. Swarbrick J, Hillery AM, Lloyd AW, Corporation E. Drug delivery and targeting for pharmacists and pharmaceutical scientists (Internet). London : Taylor & Francis; 2001 (cited 2020 Mar 13). Available from: https://trove.nla.gov.au/version/46527386

USC UNIVERSIDADE DE SANTIAGO

47. Engineer C, Parikh J, Raval A. Hydrolytic Degradation Behavior of 50/50 Poly Lactide-co-Glycolide from Drug Eluting Stents. :8.

48. Varde NK, Pack DW. Microspheres for controlled release drug delivery. Expert Opin Biol Ther. 2004 Jan;4(1):35–51.

49. Feng S, Lu F, Wang Y, Suo J. Comparison of the degradation and release behaviors of poly(lactide-co-glycolide)–methoxypoly(ethylene glycol) microspheres prepared with single- and double-emulsion evaporation methods. J Appl Polym Sci (Internet). 2015 (cited 2020 Mar 13);132(19). Available from: https://onlinelibrary.wiley.com/doi/abs/10.1002/app.41943

50. Luan X, Bodmeier R. Influence of the poly(lactide-co-glycolide) type on the leuprolide release from in situ forming microparticle systems. J Control Release Off J Control Release Soc. 2006 Jan 10;110(2):266–72.

51. Sahana DK, Mittal G, Bhardwaj V, Kumar MNVR. PLGA Nanoparticles for Oral Delivery of Hydrophobic Drugs: Influence of Organic Solvent on Nanoparticle Formation and Release Behavior In vitro and In vivo Using Estradiol as a Model Drug. J Pharm Sci. 2008 Apr 1;97(4):1530–42.

52. Holgado MA, Cózar-Bernal MJ, Salas S, Arias JL, Alvarez-Fuentes J, Fernández-Arévalo M. Protein-loaded PLGA microparticles engineered by flow focusing: physicochemical characterization and protein detection by reversed-phase HPLC. Int J Pharm. 2009 Oct 1;380(1–2):147–54.

53. Wada R, Hyon S-H, Ikada Y. Kinetics of diffusion-mediated drug release enhanced by matrix degradation. J Controlled Release. 1995 Nov 1;37(1):151–60.

54. De S, Robinson DH. Particle size and temperature effect on the physical stability of PLGA nanospheres and microspheres containing Bodipy. AAPS PharmSciTech. 2004 Sep 13;5(4):18–24.

55. Zhang WF, Chen XG, Li PW, Liu CS, He QZ. Preparation and Characterization of Carboxymethyl Chitosan and β-Cyclodextrin Microspheres by Spray Drying. Dry Technol. 2007 Dec 28;26(1):108–15.

56. El-Sherbiny IM, Smyth HDC. Controlled Release Pulmonary Administration of Curcumin Using Swellable Biocompatible Microparticles. Mol Pharm. 2012 Feb 6;9(2):269–80.

57. Sander C, Madsen KD, Hyrup B, Nielsen HM, Rantanen J, Jacobsen J. Characterization of spray dried bioadhesive metformin microparticles for oromucosal administration. Eur J

USC UNIVERSIDADE DE SANTIAGO DE COMPOSTELA

Pharm Biopharm Off J Arbeitsgemeinschaft Pharm Verfahrenstechnik EV. 2013 Nov;85(3 Pt A):682–8.

58. Duan P, Lamm MS, Yang F, Xu W, Skomski D, Su Y, et al. Quantifying Molecular Mixing and Heterogeneity in Pharmaceutical Dispersions at Sub-100 nm Resolution by Spin Diffusion NMR. Mol Pharm. 2020 Sep 8;17(9):3567–80.

59. Courtier-Murias D, Farooq H, Masoom H, Botana A, Soong R, Longstaffe JG, et al. Comprehensive multiphase NMR spectroscopy: basic experimental approaches to differentiate phases in heterogeneous samples. J Magn Reson San Diego Calif 1997. 2012 Apr;217:61–76.

60. Nasu M, Nemoto T, Mimura H, Sako K. Development of qualitative and quantitative analysis methods in pharmaceutical application with new selective signal excitation methods for 13 C solid-state nuclear magnetic resonance using 1 H T1rho relaxation time. J Pharm Sci. 2013 Jan;102(1):154–61.

61. Fu R, Hu J, Cross TA. Towards quantitative measurements in solid-state CPMAS NMR: A Lee-Goldburg frequency modulated cross-polarization scheme. J Magn Reson San Diego Calif 1997. 2004 May;168(1):8–17.

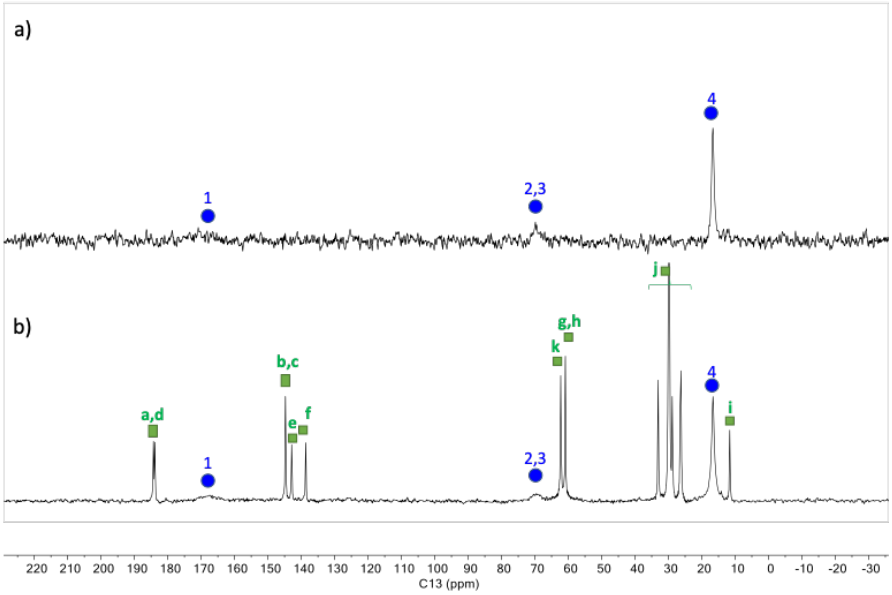
62. Lange A, Scholz I, Manolikas T, Ernst M, Meier BH. Low-power cross polarization in fast magic-angle spinning NMR experiments. Chem Phys Lett. 2009 Jan;468(1–3):100–5.

63. Draheim C, de Crécy F, Hansen S, Collnot E-M, Lehr C-M. A Design of Experiment Study of Nanoprecipitation and Nano Spray Drying as Processes to Prepare PLGA Nano- and Microparticles with Defined Sizes and Size Distributions. Pharm Res. 2015 Aug;32(8):2609–24.

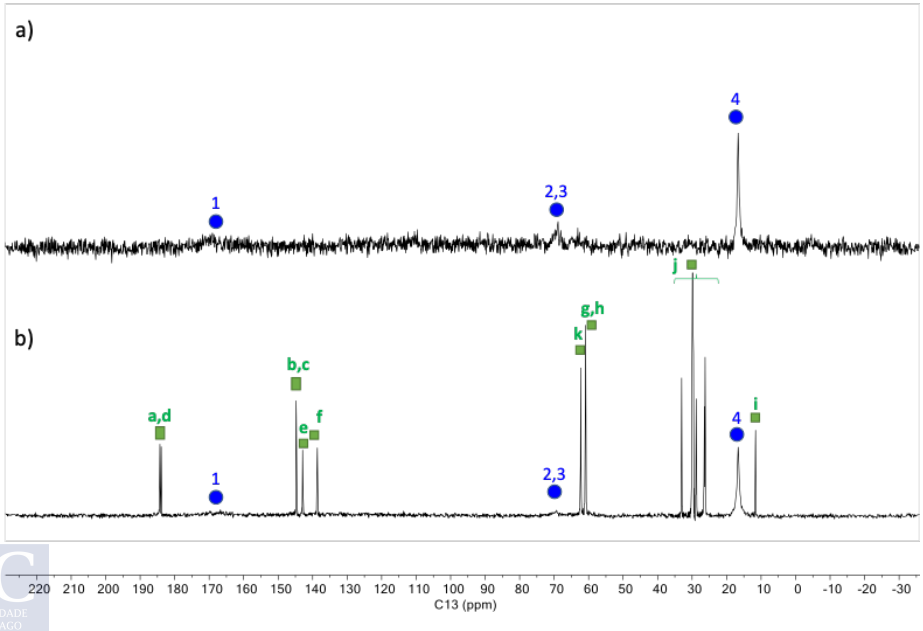
USC
UNIVERSIDADE DE SANTIAGO DE COMPOSTELA

SUPPLEMENTARY INFORMATION

1. Supplementary figures ss-NMR



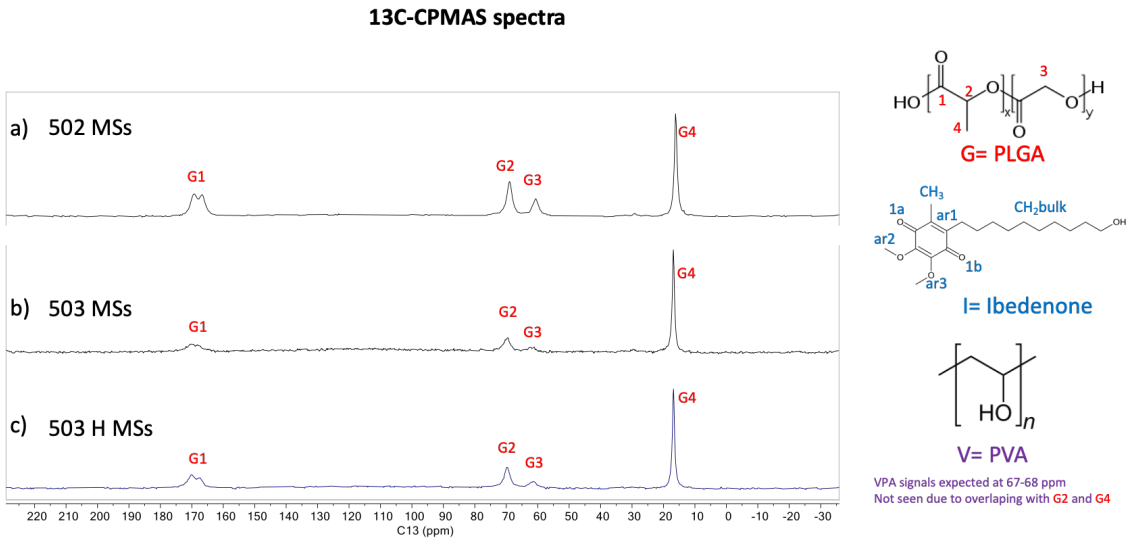
Supplementary Figure 1. Solid state NMR spectra of formulation 502 MSs. a) 1D 13C-CPMAS and b) 1D 13C-PARISxy. The letters and number codes used to identify the atoms are given in Figure 9.



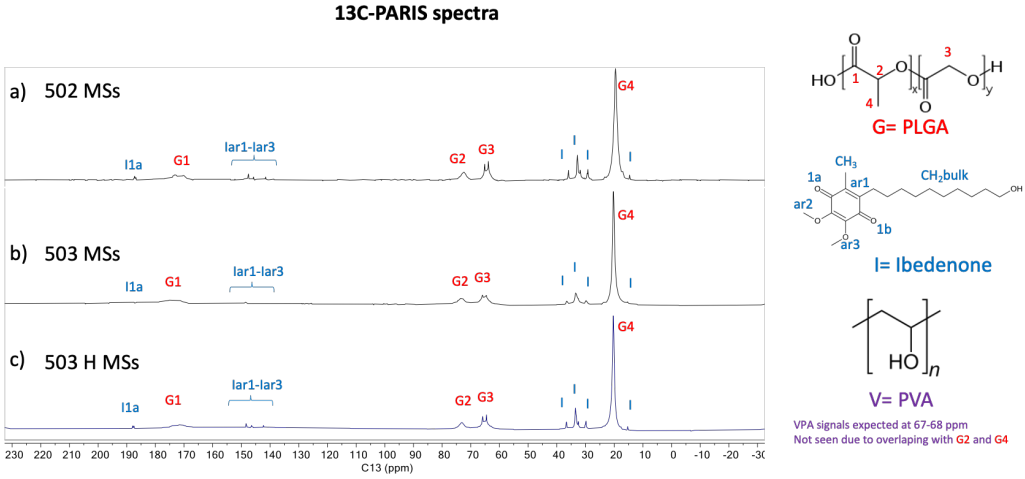
USC UNIVERSIDADE DE SANTIAGO DE COMPOSTELA

Supplementary Figure 2. Solid state NMR spectra of formulation 503H MSs. a) 1D 13C-CPMAS and b) 1D 13C-PARISxy. The letters and number codes used to identify the atoms are given in **Figure 9**.

2. Supplementary figures MSs stability

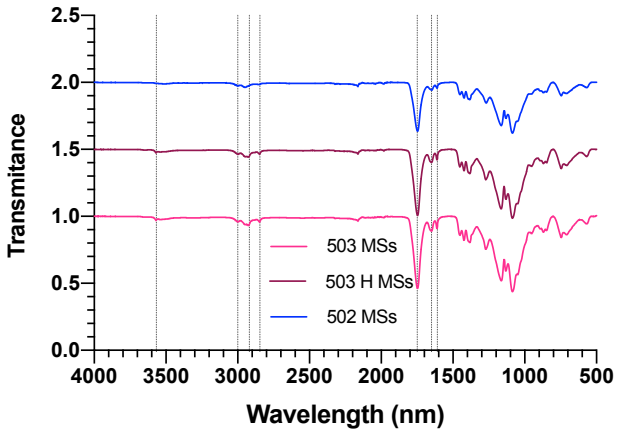


Supplementary Figure 3. 1D ^{13}C-CPMAS solid NMR spectra of 502 MSs, 503MSs, and 503H MSs after a 12-month period of storage at room temperature (17-25ºC) in the absence of light.

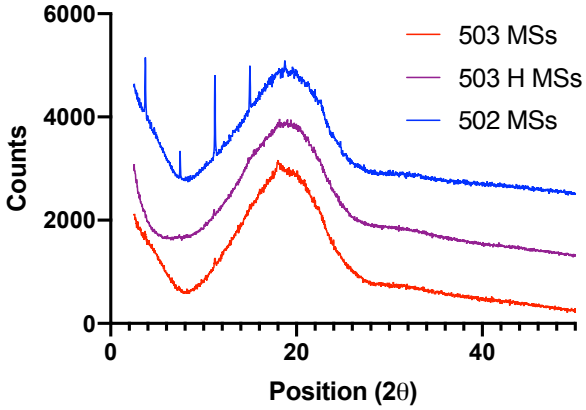


Supplementary Figure 4. 1D ^{13}C-PARISxy solid NMR spectra of 502 MSs, 503MSs, and 503H MSs after a 12-month period of storage at room temperature (17-25ºC) in the absence of light.

USC UNIVERSIDADE DE SANTIAGO DE COMPOSTELA



Supplementary Figure 5. FTIR spectra of 502 MSs, 503MSs, and 503 H MSs after a 12-month period of storage at room temperature (17-25ºC) in the absence of light.



Supplementary Figure 5. X-Ray diffractometry spectra of 502 MSs, 503MSs, and 503 H MSs after a 12-month period of storage at room temperature (17-25ºC) in the absence of light.

USC
UNIVERSIDADE DE SANTIAGO DE COMPOSTELA

Chapter 5.

Design, development, and characterization of an idebenone-loaded poly-ε-caprolactone intravitreal implant as a new therapeutic approach for LHON treatment

USC
UNIVERSIDADE DE SANTIAGO DE COMPOSTELA

USC
UNIVERSIDADE
DE SANTIAGO
DE COMPOSTELA

Chapter 5

Design, development, and characterization of an idebenone-loaded poly-ε-caprolactone intravitreal implant as a new therapeutic approach for LHON treatment

Rubén Varela-Fernández1,2, María Isabel Lema-Gesto2, Miguel González-Barcia3 and Francisco Javier Otero-Espinar1

1. Department of Pharmacology, Pharmacy and Pharmaceutical Technology. University of Santiago de Compostela (USC). Campus vida. Santiago de Compostela. Zip Code: 15782. Spain. francisco.otero@usc.es.
2. Clinical Neurosciences Group. University Clinical Hospital, Health Research Institute of Santiago de Compostela (IDIS). Travesía da Choupana s/n Santiago de Compostela. Zip Code: 15706. Spain. mariaisabel.lema@usc.es.
3. Clinical Pharmacology Group. University Clinical Hospital, Health Research Institute of Santiago de Compostela (IDIS). Travesía da Choupana s/n Santiago de Compostela. Zip Code: 15706. Spain. miguel.gonzalez.barcia@sergas.es.

Eur J Pharm Biopharm. 2021 Nov;168:195-207. doi: 10.1016/j.ejpb.2021.09.001. Epub 2021 Sep 7. PMID: 34500025

INTRODUCTION

Chronic retinal disorders account for 84% of visual damage worldwide (1). Leber's Hereditary Optic Neuropathy (LHON) is a hereditary mitochondrial neurodegenerative disease of the posterior segment of the eye, characterized by a progressive degeneration of the optic nerve as a result of a functional anergy of the retinal ganglion cells (RGCs) (2). Its etiology remains unclear, although high oxidative stress levels due to different DNA point mutations in the coding process of the mitochondrial NADH dehydrogenase complex appear to be the main trigger of the dysfunction and subsequent apoptosis of the RGCs cells.

The interval between RGCs dysfunction and cell apoptosis may be contemplated as a chance to restore vision by normalizing mitochondrial respiratory chain functionality. Presently, there are no effective LHON treatment options. Idebenone, a new generation CoQ10 analogue (3), is a short-chain benzoquinone with a potent antioxidant activity, being able to protect cell membranes and mitochondria from the action of the reactive oxygen species (ROS), as well as

retard lipid peroxidation, thus minimizing oxidative stress processes (4,5). Nevertheless, its low water solubility and the lack of an appropriate drug delivery system (DDS) limit its clinical application (6). In 2015, Raxone®, an idebenone film-coated tablet formulation (900 mg/day for 24 weeks), was commercialized as a new LHON treatment (7). Nevertheless, its low effectiveness, high interindividual variability, and high occurrence of systemic adverse effects seemed to be the main drawbacks of this treatment, due to the difficulty in obtaining sustained effective concentrations in the target tissue (3).

The therapeutic options remain limited to the use of topical ophthalmic or systemic drug delivery (8). Topical ophthalmic administration is a commonly used and non-invasive route, although a high dosage frequency is required, leading to a patient's adherence-to-treatment reduction (9,10). Likewise, systemic administration of drugs intended for the treatment of ocular posterior segment diseases is associated with high incidence of side effects (11,12).

Extended levels of the drug at the action site may improve treatment's efficacy, minimizing associated side effects. Long-acting injections and implants present several benefits in comparison to conventional administration routes (13). Certainly, long-acting DDS may lead to drug stable levels that are preserved within the therapeutic interval for a long time (14,15), improving the drug pharmacokinetic and pharmacodynamic profiles and, subsequently, the therapeutic response (16,17). Furthermore, the versatility of long-acting injections and implants may show these systems as appropriate DDS both for systemic and local drug delivery (18). Attached to this, less frequent administration may result in a patient's compliance enhancement and significant economic savings for the healthcare systems. Nevertheless, maintaining drug's constant concentration levels is a tough challenge (17,19,20). Ideally, the drug's concentration at the target site should remain constant within the boundaries of the therapeutic interval. Long-acting injections and implants show a combination of prolonged and controlled drug release and elimination profiles, resulting in a drug constant concentration at the site of interest (21). Even so, pharmacodynamic response may be affected by several parameters, changing drug's maximum concentration and the overall treatment duration (22,23).

An extensive selection of long-acting DDS was designed and developed in the past few decades. Nevertheless, the design of these systems requires an extensive knowledge of the system, as well as the drug pharmacokinetic and pharmacodynamic properties in order to guarantee an effective and predictable drug behavior, aside from the understanding of the foreign body

USC UNIVERSIDADE DE SANTIAGO

response (24,25). Injection-site biological characteristics that are involved in drug transport and uptake must also be considered.

Implant's local injection or implantation was reported to overcome several drawbacks of repeated topical ophthalmic or systemic administration, leading to prolonged drug levels into specific target sites within the therapeutic interval (26,27). Nevertheless, invasive administration procedures and fibrous encapsulation created by the foreign body response are the major drawback of its administration. The implant administration for long-term drug delivery may give rise to the formation of fibrous capsules because of a large foreign body reaction, causing undesirable effects in terms of drug release (28).

A major improvement has been seen in the past few years due to the polymer technology development, especially in the field of high-biocompatibility polymers. Nowadays, biodegradable polymers are characteristically attractive for drug delivery applications due to two possible key features: (I) sustained release profile, which may be reached when erosion is the main polymer degradation process, and (II) biodegradability, which leads to a complete polymer erosion, preventing the need for an ulterior removal procedure of the long-acting DDS at the end of the delivery lifetime.

Poly-ε-caprolactone (PCL) is an extensively studied synthetic polymer approved by the Food and Drug Administration (FDA) for ocular controlled drug delivery (29,30), due to its customizable physical and mechanical properties, as well as biocompatibility, biodegradability, and non-toxicity (31,32).

The purpose of the present chapter was based on the design, development, and physicochemical characterization of a biodegradable drug-loaded poly-ε-caprolactone implant that may provide flexibility in the choice of the active substance and controlled release for a long period; for this purpose, idebenone was employed as a model drug. A preclinical consistent base was obtained by means of the determination and assessment of the physicochemical, mechanical, and thermal properties, as well as the stability, cytotoxicity, and *in vitro* release. Additional studies were carried out to complete this preclinical background.

MATERIALS

USC UNIVERSIDADE DE SANTIAGO DE COMPOSTELA

Poly-ε-caprolactone (Mw: 45 KDa) was bought from Polusciences (Warrington, UK). Idebenone was provided by Acofarma® (Terrasa, Barcelona). Dichloromethane was purchased from Labkem Labware SL (Vilassar de Dalt, Barcelona). Dialysis cellulose membranes were

bought from Sigma Aldrich (St. Louis, Missouri). Additional substances and reagents might be used throughout the present work, being of the highest analytical grade.

EXPERIMENTAL METHODS

1. Preparation of idebenone-loaded PCL implants

Idebenone-loaded long-term implants were prepared by a homogenization/extrusion/solvent evaporation method. All components (poly-ε-caprolactone and idebenone) were physically premixed in three different proportions (1:1, 1:5, and 1:10 drug:polymer ratio) using a mechanic homogenizer (Ultra-Turrax T25, IKA® Laboratories, Staufen, Germany), until complete homogenization of the resulting powder. Organic solvent (dichloromethane) was then added into the mixture until the dissolution process was completed, under magnetic stirring (500 rpm) and at room temperature (25 ± 2°C). The resulting mixture was included into a 5 mL syringe, loaded with a 22G needle, and subsequently manually extruded into defined-size capillary tubes (0.8 mm diameter). Mixture-loaded tubes were then included into a vacuum-drying oven at room temperature for 24h to promote organic solvent evaporation, with a predefined staggered pressure decrease. Idebenone-loaded implants were finally obtained and stored into a desiccator for further analysis.

2. Physicochemical characterization of implants

2.1. Size, size distribution, and weight uniformity

Size and distribution size of idebenone-loaded PCL implants are critical parameters to consider for intravitreal delivery to the eye by conditioning the type and method of administration. Implant diameter measurements were carried out by using a digital caliper (RS Pro Electronic Digital Caliper, Madrid, Spain), while the weight data of the implants were obtained by means of the use of an analytical scale (Denver Instrument APX-200, USA), to obtain the final physical dimensions of the implants, as well as assess the preparation procedure's reproducibility.

USC UNIVERSIDADE DE SANTIAGO DE COMPOSTELA

2.2. Morphology evaluation

The implant's internal and external morphology as well as its microstructure were assessed by macroscopic observation, prior to the scanning electron microscopy (SEM) analysis, after a drying process. The macroscopic analysis of the implants was carried out by depositing the sample on a slide and subsequent observation by an electronic magnifying glass/camera system (Olympus® SZ-CTV/Olympus® SC100) in order to assess the external and internal structure of the resulting implants and verify the shape uniformity during the manufacturing process.
SEM analyses were further executed by implant deposition on a metal plate, attached to an appropriate adhesive tape, prior to the morphology examination, under different magnifications. Samples were incorporated as longitudinal and transversal cuts to observe both the external and internal morphology of the implants. Each batch was assessed in triplicate.

2.3. Production yield (PY, %)

The production yield (PY) (%) of each formulation was obtained by using a mathematical equation, dividing implant's weight after drying by the total amount of the components used in the formulation process, as follows (equation 1):

$$PY\ (\%) = \frac{Implant's\ weight}{Total\ amount\ of\ components\ in\ the\ formulation} \cdot 100 \quad Equation\ 1$$

Likewise, a standardization value was established after taking 10 randomized samples from different batches for each formulation to guarantee the elaboration process.

2.4. Encapsulation Efficiency (EE, %)

Encapsulation Efficiency (EE) of implants was determined by a centrifugation method, followed by the free-drug quantification by UV-Vis spectrophotometry, after polymer precipitation (33,34). Briefly, implants were dissolved into 2.5 mL of methylene chloride, followed by a mechanic stirring process (Vortex®, VWR International, Germany) to promote polymer dissolution. 6 mL methanol were then added and subsequently vortexed to foster polymer precipitation. Samples were later centrifuged (5000 rpm, 5 min), supernatant was subsequently collected and idebenone amount was determined at a 279 nm wavelength. This

procedure was repeated using 10 randomized batches for each formulation. EE was finally estimated by the following mathematical equation (equation 2):

$$EE\ (\%) = \frac{Amount\ of\ released\ drug\ from\ the\ implant}{Total\ amount\ of\ drug} \cdot 100 \quad Equation\ 2$$

2.5. Loading Capacity (LC, %)

Loading Capacity (LC) of implants was determined by a centrifugation method followed by the free-drug granulometric analysis (Denver Instrument APX-200, USA), after polymer precipitation (33,34). Briefly, implants were dissolved into 2.5 mL of methylene chloride, followed by a mechanic stirring process (Vortex®, VWR International, Germany) to promote polymer dissolution. 6 mL methanol were then added and subsequently vortexed to foster polymer precipitation. Samples were then centrifuged (5000 rpm, 5 min) and supernatant was subsequently collected, conducted to evaporation to obtain the resulting powder, which would correspond to the total amount of free drug released from the implant. This procedure was repeated using 10 randomized batches for each formulation. Loading capacity was then estimated by the following mathematical equation (equation 3):

$$LC\ (\%) = \frac{Weight\ of\ released\ drug\ from\ the\ implant}{Implant\ weight} \cdot 100 \quad Equation\ 3$$

3. Mechanical properties: tensile and elongation at break studies

Tensile strength and elongation at break are commonly used studies to obtain mechanical properties of solid materials (35). These parameters were determined by using an Autograph Table-TOP Precision Universal Tester (Shimadzu® AGS-X Series, Kyoto, Japan). The length (L_0) and the diameter of each implant were gauged, and surface area was estimated prior to the assay. Each implant was subjected to a controlled tension increase (0.5 mm/min speed) until mechanical failure, where tension force and distance changes (ΔL) were recorded during the entire process. Samples were gripped by the Precision Universal Tester at the two ends. It is imperative to validate that the sample is tightly grasped without slippage or breakdown

phenomena from the holding segments. Tensile strength (equation 4) and elongation at break (equation 5) were subsequently calculated as presented:

$$Tensile\ strength\ (MPa) = \frac{Force\ at\ break}{Area\ of\ cross\ section} \qquad Equation\ 4$$

$$Elongation\ at\ break\ (\%) = \frac{\Delta L}{L_0} \cdot 100 \qquad Equation\ 5$$

At predetermined times (0, 1, 7, 15, 30, 60, 120, 240, and 360 days), three implants from each batch were extracted from their respective media, dried to remove the excess of water, and mechanical properties were then assessed. Each measurement was performed in triplicate.

4. Friability test

The abrasion resistance of the idebenone-loaded PCL implants was evaluated through a friability test. Ten implants from each batch were randomly selected, weighed, and then included in a friabilator (Campbell Electronics Friabilator FTA-20, Mumbai, India). Each batch was test in triplicate. A predefined test sequence was established, based on a 100-rpm constant speed for 5 minutes at room temperature (25 ± 2°C). After this time, implants were weighed again, and the friability was calculated as presented (see equation 6). A friability percentage of ≤ 1% was established as the optimal value.

$$F\ (\%) = \frac{Initial\ weight - Final\ weight}{Initial\ weight} \cdot 100 \qquad Equation\ 6$$

5. Differential Scanning Calorimetry (DSC) and Thermogravimetry analysis (TGA)

Possible interactions between idebenone and PCL were studied by DSC, which was performed using a TA Instruments® Q1000 DSC/TGA/IR analyzer, standardized with indium. Samples (10 mg) were weighed and placed in sealed aluminum capsules. DSC curves were obtained by a 10°C/min scanning rate, conducted through a 0 to 150 °C temperature range, in a nitrogen environment, using a 50 mL/min flow rate. Each formulation was tested in triplicate.

USC UNIVERSIDADE DE SANTIAGO DE COMPOSTELA

Thermal stability of the implant components as well as the determination of the presence/absence of residual solvents in the formulations were assessed by thermogravimetry analysis (36). The procedure was similar to that described for the DSC analysis. Briefly, each implant loaded into a hermetic aluminum plate and heated from 0 to 150°C at a heating rate of 10°C/min by using a TA Instruments® Q1000 DSC/TGA/IR analyzer (Madrid, Spain). Each batch was tested in triplicate to confirm the presence or absence of dichloromethane in the final formulations, used as a solvent to solubilize the components prior the implant extrusion.

6. Fourier-Transformed Infrared Spectroscopy (FTIR)

FTIR assay was performed to determine implant's structural characterization. Certainly, samples were scanned through the IR interval, ranging from 400 to 4000 cm^{-1}, using a 4 cm^{-1} resolution and dry air as a background blank to stabilize the FTIR system (GladiATR™, Varian Pike Technologies). 64 scans/min were applied to each sample, obtaining 4084 different points, and resulting data were collected in transmittance values (%) and processed through the Resolutions Pro® software.

7. X-Ray diffractometry analysis

X-ray diffraction is a widely used technique in the study of solid materials, although it has also demonstrated an important application in the analysis of disordered states of matter. At present, this technique is moving towards the analysis of structured samples in submicron dimensions and towards the structural analysis of non-solid systems, by conducting a wide variety of studies including, not only qualitative and quantitative analysis of materials, but also microtextural, crystallinity, non-homogeneous deformation analysis, and phase change analysis, among others.

The X-ray diffractometry study was carried out following the ISO 9001:2015 standard normative in terms of reception, sample management, and analysis using monocrystalline, crystalline powder and X-ray fluorescence techniques. All samples were kept at room temperature, in vials, waiting to be measured. The material's handling was carried out with an agate mortar for spraying/homogenizing the physical samples.

Implant's crystalline structure was examined by wide-angle X ray powder diffraction (WAX) in an X-ray diffractometer (Philips X'Pert, USA), operated with a PW170 control unit, a PW1820/00 vertical goniometer, and a Enraf Nonius FR590 generator, locating and assigning the most significant mathematical values of the peaks of the diffractograms present. Samples

were scanned from a Cu- Kα source, monochromated with a graphite monochromator (λ = 1.5406 Å), at 40 kV and 30mA, using 2θ from 2° to 50° at a scan rate of 0.04°·min^{-1}. Samples were rotated during the analysis to obtain the most optimal peak profiles for the diffractograms, as well as to minimize the effect of the preferred orientation. It also must be taken into account that samples were deposited in oriented glass bases (Si-511 plate) to avoid background noise caused by a vitreous support. The mathematical analysis of the diffractograms was carried out by using the HighScore Plus® 3.0d software.

8. *In vitro* release study

The dialysis method is frequently employed to quantity drug release from DDS. In this process, two spaces are physically divided by a dialysis membrane (diffusion surface 0.784 cm^2), as previously explained (37), making a proper system to evaluate the drug delivery pattern from a variety of DDS (38–40).

The idebenone release rate from implants was obtained by UV-Visible spectrophotometry, by means of Franz diffusion cells. The receiving compartment was filled with 6 mL PBS, while donating compartment was filled with 3 mL of synthetic vitreous humor (VH). Two different compositions of synthetic VH were employed in order to simulate the physiological VH composition, these being: VH-A, containing an 0.1% (w/v) agar and 0.5% (w/v) hyaluronic acid, and VH-B, composed of an 0.1% (w/v) agar and 0.4% (w/v) hyaluronic acid. One implant (l = 5 mm and d = 0.8 mm) was then added to the donor chamber and Franz cells were then positioned in an orbital shaker at 100 rpm and 37°C for the whole study. At prearranged intervals, 1 mL from the receiving compartment was taken, and an equal volume of fresh PBS solution was then added to it to preserve sink conditions during the entire assay. The assay was run for a one-year period, and each formulation was tested in triplicate. Idebenone concentrations were measured by UV-Vis spectrophotometry (λ = 279.0 nm). Analytic validation was previously made by our group and showed linearity (R = 0.999) over a concentration interval of 1.5625– 250 mg/mL, 96.3% accuracy, of a 98.6% relative standard deviation (RSD) intra-day precision, and limit of detection (LOD) and limit of quantification (LOQ) values of 0.7813 mg/mL and 1.5625 mg/mL, respectively (data not published).

USC UNIVERSIDADE DE SANTIAGO DE COMPOSTELA

9. Water uptake, mass loss, and mass remaining studies

The erosion study of the implants was carried out in line with the *in vitro* release study, over a one-year period. Water uptake, mass loss, and mass remaining were gravimetrically assessed by using a granulometric scale (Denver Instrument APX-200, USA).

Freshly prepared implants were screened, and subsequently placed into amber vials containing 5 mL PBS (pH 7.4). All implants were accurately weighted prior to the immersion in the medium (initial weight). The extraction and renewal of the medium was performed at the same time as for the *in vitro* release study of the implants in order to maintain the sink conditions and allow the drug release from implants. Thirty implants from each batch were studied (l = 5 mm, d = 0.8 mm), using three different batches randomly chosen.

At predetermined times (0, 1, 7, 15, 30, 60, 120, 240, and 360 days), three implants from each batch were extracted from their respective media and weighted (wet weight). A drying process was then applied to remove the excess of water and weighted again until constant weight by using a vacuum oven (Heraeus RVT360, Gemini® BV, Apeldoorn, The Netherlands) (dry weight), at room temperature. The volume of water absorbed, and the quantity of polymer eroded were calculated and expressed as percentage. Each sample was separately immersed into the release medium and subsequently taken out; dried implants were later completely dried (dry weight). Water uptake (equation 7), mass loss (equation 8), and mass remaining (equation 9) values were then estimated as presented:

$$Water\ uptake\ (\%) = \frac{Wet\ weight - Dry\ weight}{Dry\ weight} \cdot 100 \qquad Equation\ 7$$

$$Mass\ loss\ (\%) = \frac{Initial\ weight - Dry\ weight}{Initial\ weight} \cdot 100 \qquad Equation\ 8$$

$$Mass\ remaining\ (\%) = \frac{Dry\ weight}{Initial\ weight} \cdot 100 \qquad Equation\ 9$$

USC UNIVERSIDADE DE SANTIAGO

The implants morphology was also assessed by scanning electron microscopy (SEM) analysis over time, as previously described (see methods section 2.2.), to determine the existence or absence of morphological changes along the studied period.

10. Stability studies

10.1. Stability to storage

Implants were placed in screw-capped glass containers and stored at three temperature subsets, these being: (I) 4 ± 2°C, (II) 25 ± 2°C, and (III) 37 ± 2°C for a six-month period. Stability was assessed through drug content uniformity, where zero-time samples were used as controls.

Drug content assay (n = 3 per batch) was carried out by weighting each implant, following the same procedure that has been applied for the LC (%) determination. Drug content was finally determined by UV-Vis spectrophotometry at a 279 nm wavelength. Each formulation was also macroscopically assessed in search of physical state changes (color and consistency).

10.2. Stability under physiological conditions

10.2.1. Stability to pH

The physical evaluation of the pH-dependent implant stability was carried out on freshly prepared formulations. The methodology of this procedure was based on the suspension of each implant (n = 3 per batch) in 5 mL of Milli-Q® water at different predetermined pH values (from 2 to 12) (Hanna® HI5522, Hanna Instruments®, Spain), previously adjusted by means of a HCl or a NaOH aqueous solutions, as necessary. Samples were then kept refrigerated (T = 4 ± 2°C) for 24 hours so as to be subsequently centrifuged at 5000 rpm for 10 minutes. Finally, the determination of the free idebenone concentration in the solution was carried out at a 279 nm wavelength in order to verify the existence of implant collapse or breakage phenomena with the consequent drug release into the medium. Each formulation was tested in triplicate for all set pH values.

10.2.2. Stability to ionic strength

The physical evaluation of the ionic-strength-dependent implant stability was performed on freshly prepared formulations. The methodology of this procedure was based on the suspension of each implant (n = 3 per batch) in 5 mL of NaCl aqueous solutions with different predetermined ionic strength values (from 0.2M to 2M). Samples were then kept refrigerated (T = 4 ± 2°C) for 24 hours so as to be subsequently centrifuged at 5000 rpm for 10 minutes.

USC UNIVERSIDADE DE SANTIAGO

Finally, the determination of the free idebenone concentration in the solution was carried out at a 279 nm wavelength in order to verify the existence of implant collapse or breakage phenomena with the consequent drug release into the medium. Each formulation was tested in triplicate for all set ionic strength values.

11. Injectability of implants

Injectability is a key parameter in the preclinical evaluation of implants for intravitreal administration. This factor alludes to the performance of the implant during injection (41). Suitably injectability properties guarantee an appropriate implant's intraocular administration.

Injectability studies of implants enable to establish the optimal characteristics of the intravitreal needles (size and length), by calculating the needed force to inject a predetermined formulation. Suitably injectability properties guarantee an accurate procedure for the implant to be intraocularly administered. A 12N force over 10s was set as the maximum ejection force, being suitable for a proper intraocular injection (42).

The implant preparation procedure was based on the preparation of a 5 mm x 0.8 mm implant, whose dimensions were properly selected in order to accomplish the equipment requirements. Once prepared, implants were included in a syringe system, equipped with different types of needles (15G, 16G, and 17G), in order to compare them for an appropriate administration (43) (see details in Table 1).

Table 1. Specifications of the different needles used during the injectability assay.

Needle gauge	Inner diameter (mm)	Length (mm)
16	1.16	40
17	1.01	38
18	0.838	38

USC UNIVERSIDADE DE SANTIAGO DE COMPOSTELA

Ejection force values were respectively obtained by using an Autograph Table-TOP Precision Universal Tester (Shimadzu® AGS-X Series, Kyoto, Japan), managed through a specific

software (Trapezium®). Established injectability conditions were as presented in Table 2. All the samples were tested in triplicate for all the different syringe/needle systems.

Table 2. Injectability and syringeability test conditions for idebenone-loaded PCL intravitreal implants.

Condition	Parameter	Injectability specifications
System	Assay mode	Simple
	Assay type	Compression
	Force polarity	Compression
	Force sense	Downwards
Sensor	Force scale	1000 N
	Displacement	500 mm
Assay	Action	Force
	Control	Displacement
	Sampling	10 seg/sample
	Breakage sensitivity	10%
	Sensor	Displacement
Sample	Material	-
	Shape	Cylinder
	Dimensions	Diameter and height
Processed data	Maximum force	-

12. Cytotoxicity analysis

12.1. Hen's egg test on the chorioallantoic membrane (HET-CAM)

The HET-CAM assay, an alternative organotypic model to the standard Draize rabbit eye test, is commonly used for the assessment and quantification (irritation score (IS) determination) of

three potential undesired effects that may be caused by irritative compounds, these being hemorrhage, lysis, and coagulation (44), taking into account the Kalweit et al. criteria (45). All actions with eggs accomplished the standard guidelines for animal materials management.

The procedure was adjusted to the instructions formerly established by Spielmann and Liebsch (46), with minor changes. Briefly, fertilized eggs were incubated for nine days at 37 ± 0.5°C and 65 ± 5% RH, under automatic rotation (every 2 h) for the first eight days. On the last day, rotation was blocked, and the eggs were vertically positioned for the correct chorioallantoic membrane (CAM) location. A cavity was subsequently made on the end of the eggs, through which implant's incubation media (300 µL) were straightforwardly administered onto the CAM. To point out, the intravitreal implants were not directly placed onto the CAM, since an observation period of 5 minutes would be too short and insufficient to assess the effect that they would have on the membrane vascular system. However, the instillation of the solution in which the implants were immersed during the degradation process over time (at t = 360 days) was carried out in order to evaluate whether the implant degradation products could become irritating to the eye.

An Olympus SZ61TR Stereomicroscope and an Olympus CellSens Entry software were used for the aforementioned factors evaluation, along a 5 min period. Images were taken at the beginning and at the end of the test, and each duplicate was recorded along the study to determine potential undesired consequences (if required). These observations were individually taken into account and later merged to obtain the IS (if possible), which was employed to categorize the irritancy potential. A 1.8% (w/v) NaOH solution and a BSS solution were used as positive and negative control solutions respectively, as previously described (37). Each batch was evaluated in triplicate.

13. Statistical analysis

Pairs of groups were matched by carrying out one-tailed Student's t-test, while multiple group comparison analysis was performed by parametric or non-parametric analysis (if necessary) of variance, with a 95% significance level ($p < 0.05$), using the GraphPad Prism® v.8.00 software. All data were presented as a mean value with its standard deviation. Additional test (Tukey's, Bonferroni's or Dunnet's tests) might be employed for post-hoc contrast, if possible.

USC UNIVERSIDADE DE SANTIAGO

RESULTS AND DISCUSSION

1. Preparation and optimization of idebenone-loaded PCL implants

The idebenone-loaded PCL implants were successfully obtained by a homogenization/extrusion/solvent evaporation method. The preparation method enabled the drug inclusion inside the polymer matrix, favored by the drug physicochemical properties, mainly by its hydrophobicity. Certainly, the versatility of hydrophobic polymers permits the elaboration of intravitreal administration implants with a variety of shapes or sizes (29,31). Firstly, premixed implant components were dissolved by an organic solvent, included into a syringe/needle system, and extruded into capillary molds prior to the solvent evaporation. After placing in a vacuum chamber, evaporation led to a polymer precipitation phenomenon and implants solidified, entrapping the drug in its matrix. After the vacuum-drying process, all idebenone-loaded PCL implants showed a cylindrical form and a uniform orange color.

Three different proportions (1:1, 1:5, and 1:10 drug:polymer ratio) were tested and 1:5 drug:polymer ratio was selected as the optimum quotient, discarding the other two tested drug:polymer ratios. Certainly, 1:1 drug:polymer ratio was rejected because the polymer plastic properties were compromised by the large amount of incorporated drug, increasing the breakage and fragility phenomena of the implants. On the other hand, 1:10 drug:polymer ratio was discarded because the drug:polymer proportion was too high, being associated to high variability in terms of idebenone content uniformity along the polymeric matrix.

2. Implant characterization

2.1. Mean size, size distribution, and weight uniformity

The idebenone-loaded PCL implants were extracted from the capillary molds after the vacuum-drying process and their size was subsequently adjusted to a 5 mm length. Afterwards, the diameter and weight of the resulting implants were determined by measuring 10 different implants randomly selected, and the study was carried out in triplicate. Resulting data showed a diameter interval of 0.0731 ± 0.0162 mm, as well as a weight interval ranging from 6.15 ± 0.41 mg.

USC UNIVERSIDADE DE SANTIAGO DE COMPOSTELA

2.2. Morphological evaluation

The evaluation of the implant morphology was firstly carried out by means of a batch macroscopic examination, prior to the SEM analysis. The macroscopic observation was performed as a preliminary analysis to confirm the existence of a shape uniformity of the resulting pharmaceutical form in order to verify the adequacy of the preparation method to the desired objective.

Macroscopic analysis of the samples allowed to conclude that the resulting idebenone-loaded PCL implants showed uniformity of shape and color, as well as a cylindrical appearance (see Figure 1). The implant surface could be assumed to be smooth and clean, with no adhered artifacts. The internal structure of the implants seems to follow the same pattern described.

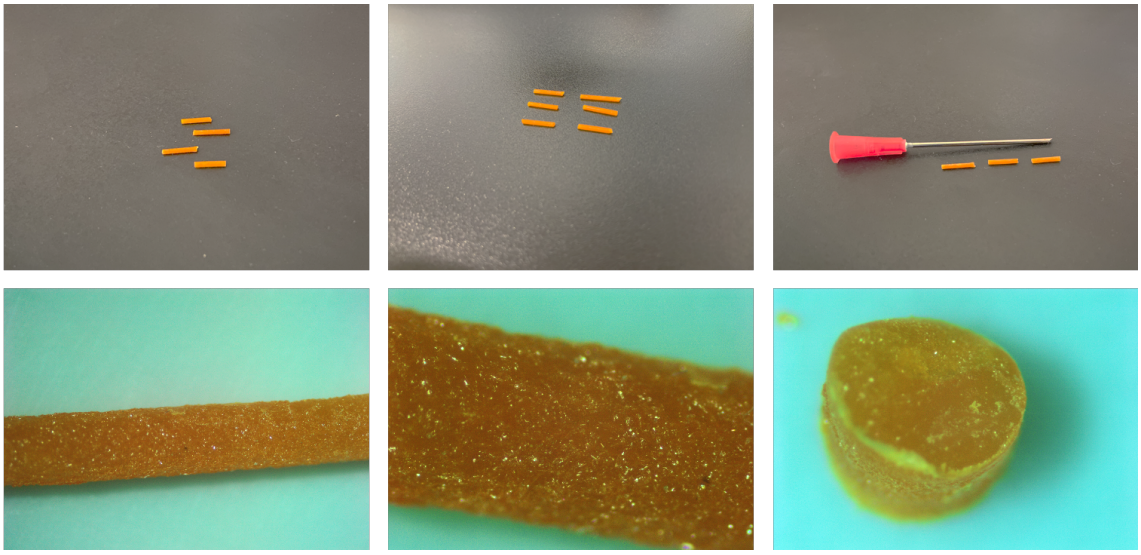


Figure 1. Macroscopic images of the idebenone-loaded PCL implants.

Morphological evaluation of the implants was also carried out in terms of shape and surface by a SEM assessment, taking into account that the implant morphological characterization may correlate surface characteristics with the pharmacokinetic behavior. All idebenone-loaded PCL implants prepared by a homogenization/extrusion/solvent evaporation method were without pores, and showed a uniform although not completely smooth surface, as it can be seen in SEM images (see Figure 2). In addition, the implant cross section showed a compact and consistent structure, ensuring the homogeneous drug distribution along its entire length. Images also reveal the methylene chloride complete removal during the elaboration process.

USC UNIVERSIDADE DE SANTIAGO DE COMPOSTELA

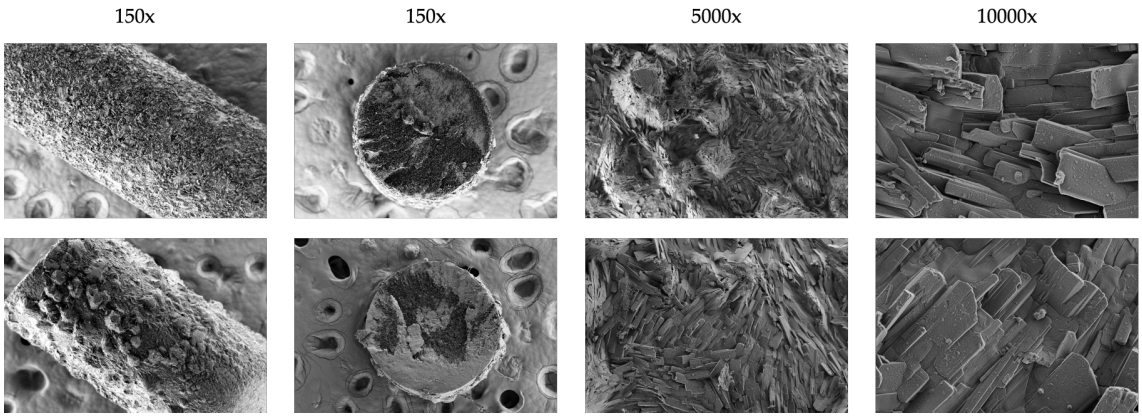


Figure 2. SEM images of idebenone-loaded PCL implants. The first-column images show the implant's longitudinal morphology. The second-column images show an implant cross-section, observing the implant internal structure. The last two columns show the polymer structure along the implant in more detail, at two different magnifications.

In order to point out, it seems that the implant surface shows a polymer stratification, this being supported by the polymer physicochemical characteristics, which highlights for its semi-crystalline aspect. Nevertheless, this appearance was not observed in the polymer internal structure. The main reason may strive to the fact that the drug is included into the internal polymer matrix, while the implant surface was mainly composed of a higher polymer concentration, acting as a coating film.

2.3. Production yield (PY), encapsulation efficiency (EE), and loading capacity (LC)

The homogenization/extrusion/solvent evaporation method is ideal for obtaining high production performance, encapsulation efficiency, and load capacity values. This is additionally enhanced by the hydrophobicity of petroleum-derived polymers (e.g., polycaprolactone) and the low water solubility of hydrophobic drugs such as idebenone, making them good candidates for the incorporation into intraocular polymeric implants. Figure 3 shows the results for production yield, encapsulation efficiency, and loading capacity of idebenone-loaded PCL implants. All formulations showed appropriate PY, EE and LC values for the preparation method.

USC UNIVERSIDADE DE SANTIAGO DE COMPOSTELA

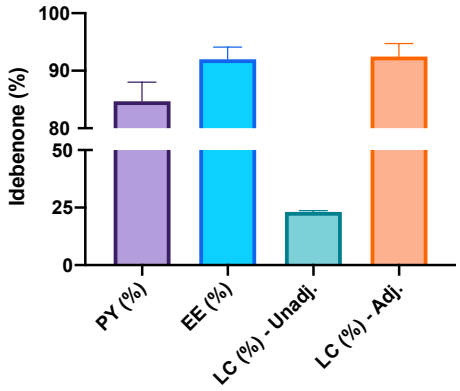


Figure 3. Production Yield (PY), Encapsulation Efficiency (EE), and Loading Capacity (LC) values (unadjusted and adjusted, respectively) for the idebenone-loaded PCL implants.

High PY values (almost 90%) were obtained, demonstrating the idea that the chosen preparation method is suitable, effective, and reproducible for the implant elaboration. Furthermore, the EE values were ranging from 90 to 95%, while LC values were around 20% but, considering that a 1:5 drug:polymer ratio was employed, the adjusted LC values varied from 90 to 95%, supporting the idea that the preparation process was reproducible and efficient. Resulting data are reinforced by the polycaprolactone hydrophobicity and the idebenone low aqueous solubility, providing high drug entrapment into polymeric matrix.

3. Mechanical properties: tensile strength and elongation at break

Figure 4 shows the tensile strength (MPa) and elongation at break (%) values for the idebenone-loaded PCL implants. In this context, it is possible to observe a slight decrease in both parameters over time, which may be associated with a progressive degradation process of the implant structure by the medium action in which implants were immersed. Taking into account the tensile strength data, it can be seen that, as the measurement time advances, the force gradually decreases. This phenomenon may be a result of the progressive degradation of the implant external structure, which ends in greater structural fragility. Nevertheless, the variability of the pressure values along the progressive determinations was minimal, supporting the fact that the drug was homogeneously dispersed along the polymer matrix.

A gradual reduction in elongation at break values was also observed as the trial time progressed. Resulting data proved that polymer matrix ductility gradually decreased over time. Even so, elongation at break values remained high and stable over almost the entire studied period, typical of a robust polymer structure, evidencing the PCL plastic deformation behavior. This is

supported by the low melting temperature (around 60°C) of this polymer, making implants relatively flexible at room temperature.

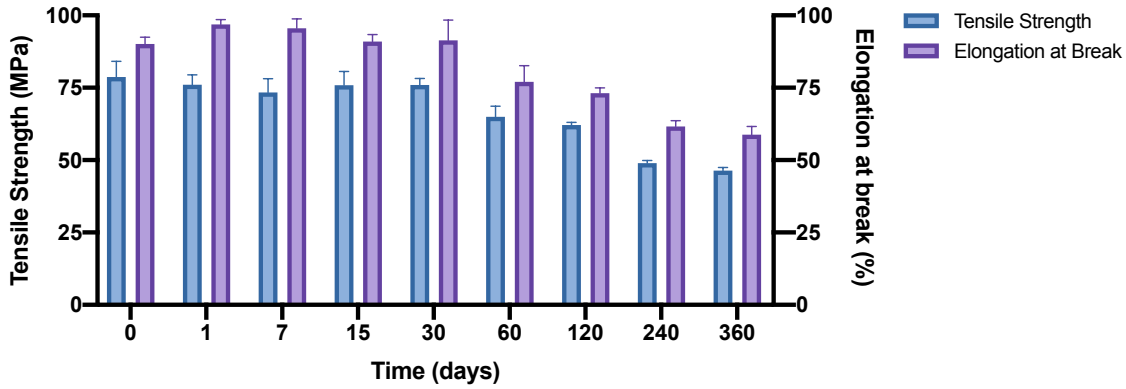


Figure 4. Tensile strength (MPa) and elongation at break (%) values for the idebenone-loaded PCL implants.

4. Friability test

Friability measuring of the idebenone-loaded PCL implants may tend to powder or fragment. This test is narrowly related to hardness properties, being designed to assess the implant ability to resist abrasion along the management process. Friability results were in the optimal range (0.90 ± 0.04%), suggesting that the final formulations show adequate resistance to abrasion or attrition processes.

5. Differential scanning calorimetry (DSC) and thermogravimetry analysis (TGA)

DSC and TGA curves of idebenone-loaded PCL implants were measured as a way to determine the existence of interactions between the polymer and the drug within the polymer net of this type of intravitreal implants and the determination of residual solvents.

Figure 5 shows the resulting DSC data for the idebenone-loaded PCL implants. As presented, the DSC trace showed a melting endotherm behavior at a T_{peak} of 65.39°C (T_{offset} 58.78°C, 5.85 J/g of melting enthalpy) that correspond to the PCL transition temperature (around 60°C). Besides, a slightly detectable melting point at a T_{peak} of 52.87°C (T_{offset} 52.40°C and 3.59 J/g of melting enthalpy) was early found for idebenone, by exhibiting a lower melting temperature (52 – 55°C).

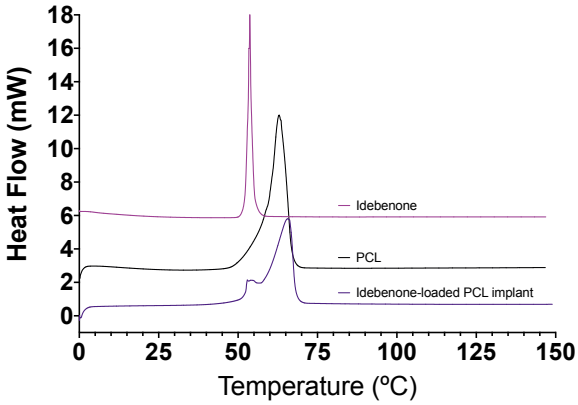
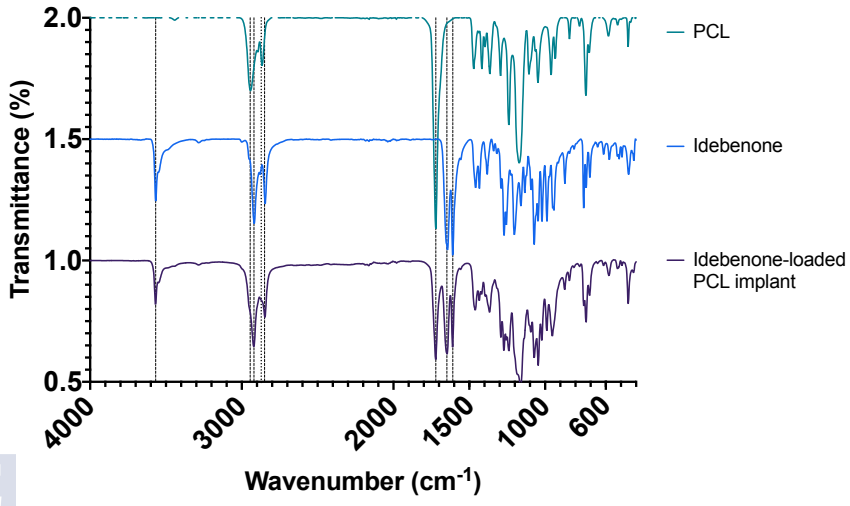


Figure 5. Differential Scanning Calorimetry (DSC) analysis of idebenone-loaded PCL implants.

TGA/IR analysis showed no change in the implant's weight due to the temperature increase, and no residues of the dichloromethane used in the implant fabrication were detected by the IR analyzer associated with the TGA equipment.

6. FTIR analysis

FTIR spectroscopy analysis was used to study possible chemical interactions between the drug and polymer. The FTIR spectra of idebenone, PCL, and idebenone-loaded PCL implants are shown in Figure 6.



USC
UNIVERSIDADE DE SANTIAGO

Figure 6. FTIR results for the components (idebenone and polycaprolactone) and the idebenone-loaded PCL implants.

The idebenone FTIR spectrum showed several characteristic bands for the O-H, C-H, C=O groups, and C=C ring, with stretching vibrations at 3568, 2920, 2850, 1648, and 1609 cm^{-1}, respectively. The PCL spectrum showed a doublet at 2945 and 2872 cm^{-1} due to the C-H stretching vibration of the methylene groups, as well as a characteristic single band that corresponded to the carbonyl group. Implants presented a mixture of the bands of both components, and no important changes were observed in the signals position. Thus, no interaction between idebenone and PCL was observed, where drug and polymer chemical structures were not modified during the preparation process.

7. X-Ray diffractometry analysis

The physical state of the idebenone-loaded implants and their components were characterized by X-ray diffraction studies. Figure 7 shows the idebenone-loaded PCL implant diffractograms, as well as the comparison with the drug (idebenone) and the pure polymer (PCL). The pure PCL and drug diffractograms show that both materials are in crystalline state. PCL diffractograms showed three main peaks at 21.4°, 22.0°, and 23.7° at 2θ, being characteristic of the polymeric crystalline structure and observed in the idebenone-loaded PCL implants. Idebenone showed numerous characteristic peaks in its crystalline structure between 22° and 50° at 2θ that remain in the implant diffractograms.

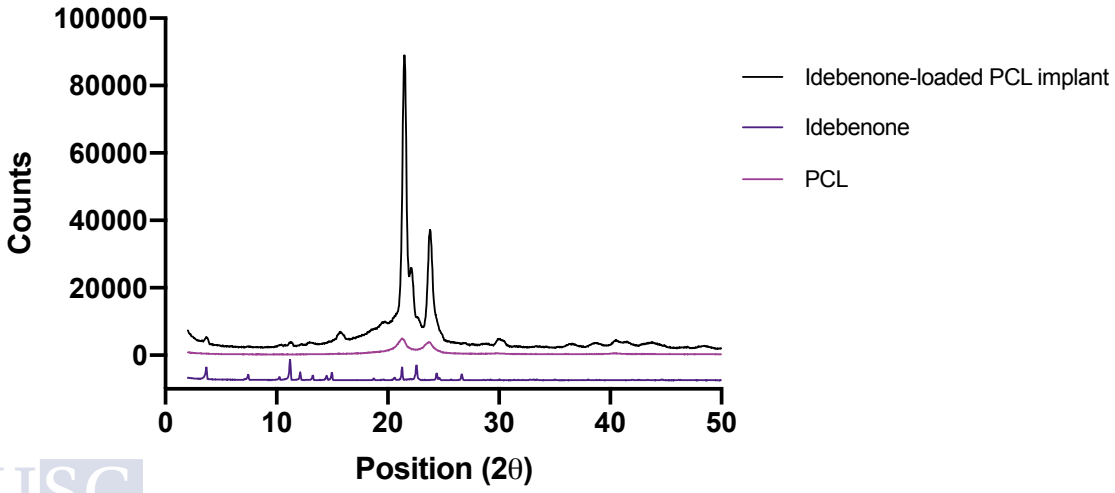


Figure 7. X-Ray diffractograms of idebenone-loaded PCL implants. Two different transformations (Y = -5000Y_0 + 1 and Y = 5000Y_0 + 1) were respectively applied on idebenone and polycaprolactone graph representations to promote the wide-ranging observation and comparison of the FTIR data.

8. Stability studies

8.1. Stability to storage

The stability-to-storage study of idebenone-loaded PCL implants was carried out by determining the drug content uniformity by maintaining samples at three different temperature sets for a 180-day period. Resulting data showed no major changes during the assay (see Figure 8). Insignificant changes in the drug content uniformity may be associated with interferences coming from the sensitivity of the quantification method. Thus, the idebenone entrapment into the PCL matrix was appropriate, providing drug stability and protection against variations in ambient temperature.

A two-way ANOVA was also conducted, and no statistically significant differences ($p > 0.05$) were detected among the three different storage conditions for the studied time. Thus, it can be concluded that idebenone-loaded PCL implants were stable over the considered interval.

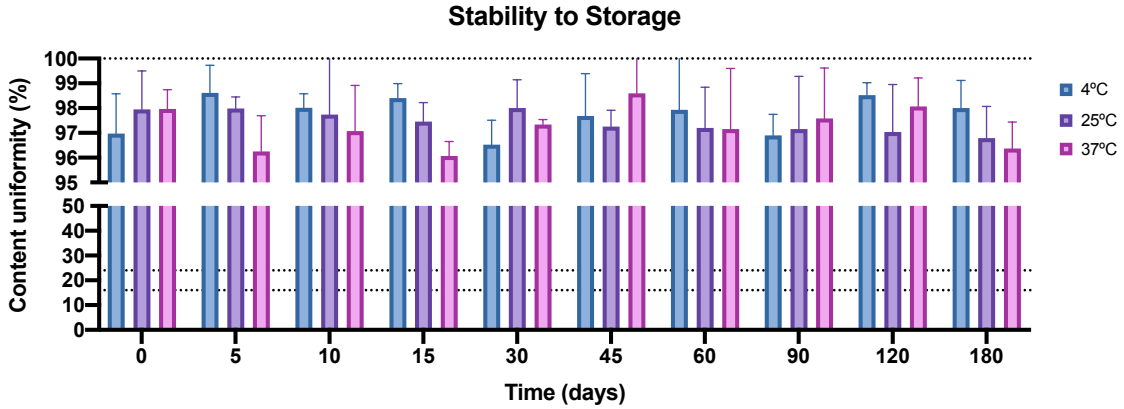


Figure 8. Idebenone content uniformity values (%) for idebenone-loaded PCL implants during the stability-to-storage study.

8.2. Stability to pH

Extreme pH conditions of the environment might lead to a faster drug release speed from the implants due to variations in the release mechanism. Stability-to-pH changes were assessed through idebenone uniformity content by UV-Vis spectrophotometry (279.0 nm wavelength), as explained in previous sections. Physical characteristics of the formulations were also evaluated for appearance color variations.

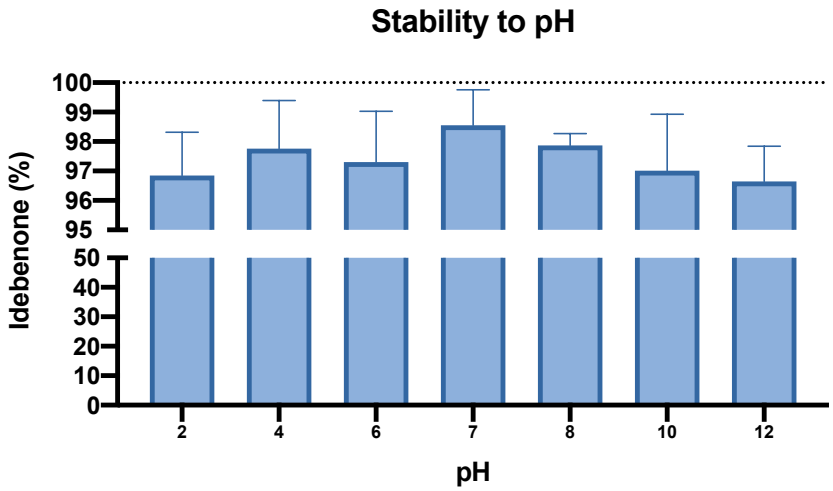


Figure 9. Idebenone content uniformity values (%) for idebenone-loaded PCL implants during the stability-to-pH study.

Figure 9 shows the stability-to-pH study data of idebenone-loaded PCL implants. The hydrophobic nature of the polycaprolactone and idebenone would generate a synergic effect, preventing the drug diffusion to the medium, thus enhancing the controlled delivery of idebenone from the PCL implants, as well as protecting the drug from degradation processes. Furthermore, no alterations in physical appearance or color were observed for the studied pH conditions. A two-way ANOVA was also applied, and no statistically significant differences ($p > 0.05$) were observed along the studied period. Henceforth, idebenone-loaded PCL implants were stable over the studied pH interval.

8.3. Stability to ionic strength

The medium's ionic strength value may promote a quicker drug release from the polymeric implants due to changes in the release mechanism. Stability-to-ionic-strength variations were assessed through idebenone uniformity content by UV-Vis spectrophotometry (279.0 nm wavelength), as described in previous sections. Physical characteristics of the formulations were also inspected for appearance or color changes.

USC
UNIVERSIDADE DE SANTIAGO DE COMPOSTELA

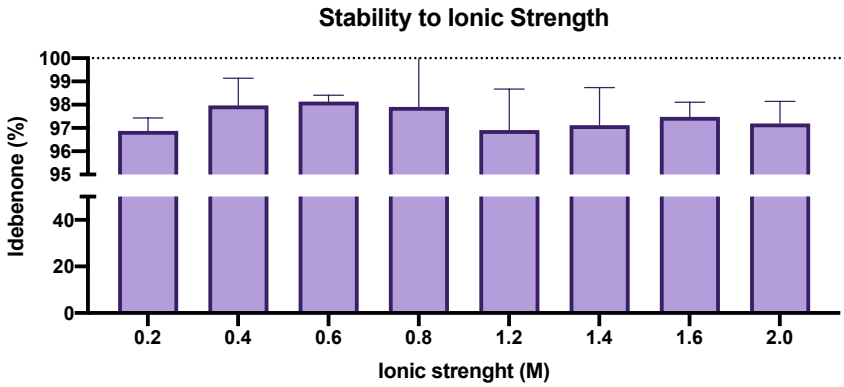


Figure 10. Idebenone content uniformity values (%) for idebenone-loaded PCL implants during the stability-to-ionic-strength study.

Figure 10 shows the resulting data for the idebenone-loaded PCL implants. The DDS stability was maintained unchanged regardless of the variations in the medium's ionic strength values. The hydrophobic characteristics of the drug and the polymer would prevent the fast release of idebenone from the PCL implants to the surrounding medium, as well as protecting the drug from degradation processes. A two-way ANOVA was also performed, and no statistically significant differences ($p > 0.05$) were observed along the studied interval, supporting the idea that idebenone-loaded PCL implants would be stable against ionic strength changes of the medium.

9. *In vitro* release study

The idebenone *in vitro* release profile from the PCL implants was reported to be conditioned by the polymer physicochemical characteristics, as well as by the release mechanisms behavior (i.e., drug desorption, polymer matrix erosion, and drug diffusion, which might even simultaneously happen) (47,48). The *in vitro* release profile for the idebenone-loaded PCL implants is shown in Figure 11. Idebenone release from PCL implants seems to follow a biphasic pattern, described by a faster preliminary release phase that lasts up to 120 days and a slower second phase that lasts beyond one year. As observed, the drug release from the implants shows a controlled release profile for at least one year, during which time only 65% of the drug was released, with approximately 35% remaining inside the polymer matrix. Such idebenone controlled release profile might be associated with a diffusion and degradation phenomena. The burst release might be related to the idebenone diffusion process from the implant surface (49),

USC DE SANTIAGO DE COMPOSTELA

while the controlled and sustained release phase might be regulated by polymer degradation and drug diffusion through the implant matrix or even both concurrently (50,51).

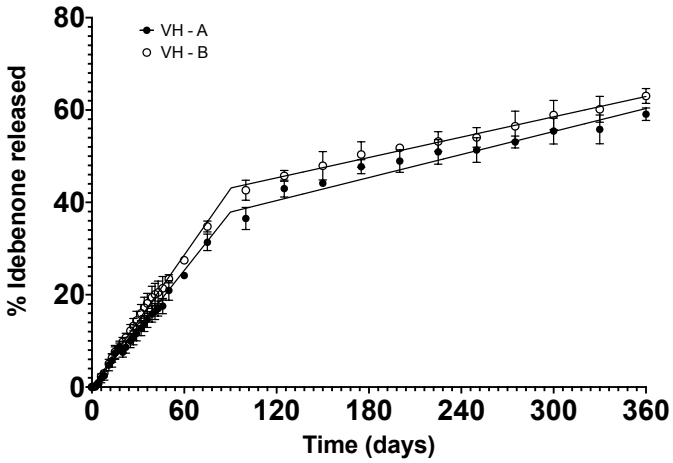


Figure 11. *In vitro* release study of idebenone-loaded PCL implants. The pharmacokinetic profile of the idebenone-loaded PCL was tested under two different synthetic vitreous humor compositions (VH-A, containing an 0.1% (w/v) agar and 0.5% (w/v) hyaluronic acid, and VH-B, composed of an 0.1% (w/v) agar and 0.4% (w/v) hyaluronic acid).

The initial release pattern of idebenone from the PCL implants (75-day period), the delivery followed a linear regression trend, while after 100 days, a greater stabilization was observed in terms of drug release, better adjusting to a non-linear kinetics. In order to point out, it is known that the vitreous cavity environment and the nature of the vitreous humor may condition the idebenone release from the PCL implants, generating a concentration gradient within the vitreous cavity (52,53). Based on these precedents, two different types of vitreous humor were used to perform the release study.

The resulting data of the idebenone cumulative delivery from the PCL implants were fitted to several kinetic models to establish the release behavior. Nevertheless, the greatest correlation data was obtained with a segmental linear regression model, proposing the polymer degradation as the leading release mechanism, combined with the drug diffusion from the implant itself (see details in Table 3).

USC
UNIVERSIDADE DE SANTIAGO DE COMPOSTELA

Table 3. Release data of idebenone-loaded PCL implants into a segmental linear regression.

Vitreous humor	Intercept X=0	First slope	T inflexion	Second slope	R^2

VH-A	0.28 ± 0.30	0.39 ± 0.01	108.3 ± 2.7	0.07 ± 0.01	0.9980
VH-B	0.26 ± 0.24	0.48 ± 0.01	90.5 ±1.6	0.07 ± 0.01	0.9990

In order to point out, Heitz et al (54) determined the idebenone pharmacokinetic behavior in plasma, aqueous, and vitreous humor after oral administration to a rat model. An estimation of the $t_{1/2}$ values from the results previously obtained by these authors was made, and resulting values of 0.035, 0.026, and 0.153 min^{-1} for plasm, aqueous and vitreous humor were found, respectively. Considering a mean value of 20 μL for vitreous humor in the rat model, it was possible to calculate the mean equilibrium concentration of idebenone into the vitreous humor using a linear monocompartimental model with a zero order (constant) drug incorporation rate. An equilibrium concentration of 1,2 μg/mL in the first initial 90 days and 0.2 μg/mL from the inflexion point (at 90 days) was obtained, with short times to reach the equilibrium concentration (< 1 h). These predicted values are higher than the idebenone concentrations observed by these authors following once daily administration of idebenone in the diet for 21 days with doses of 2000 mg/kg/day (approx. 14 ng/mL).

10. Implant's erosion study: water uptake, mass loss, and mass remaining

There are numerous key parameters that condition the implant's degradation rate, such as the molecular weight, the crystallinity, or the glass transition temperature, among others. Water uptake was proposed as a critical assay to modify the polymer degradation rate, by relating water absorption to the mass decrease of the implant matrix (polymer chain progressive breakage) (55).

Figure 12 shows the *in vitro* water uptake, mass loss, and mass remaining of the idebenone-loaded PCL implants. The water uptake and mass loss profiles revealed that the developed PCL implant exhibited a low degradation rate, related to the high percent of mass remaining in the implants at the 360-day endpoint. Resulting data showed almost no water uptake and weight loss over the first two months, possibly due to a decrease in the polymer molecular weight but without an implant significant mass loss, associated to a slow water penetration into the hydrophobic matrix. However, from the third month onwards, a greater water uptake and mass loss were observed, which might be attributed to a diffusion phenomenon of small polymer fragments that are detached from the implant matrix (56,57). The overall water uptake and

weight loss of the idebenone-loaded PCL implants were around 5% and 10% per year, respectively, suggesting that the drug release mechanism was mostly influenced by a combination of polymer erosion and drug diffusion from the implant matrix, as well as the hydrophobic nature of both components. Thus, a more robust correlation may be established between the drug release mechanism from the polymer matrix and changes in the structure/mass of the polymer over time. These results are in good arrangement with the resulting data obtained in the *in vitro* release assay.

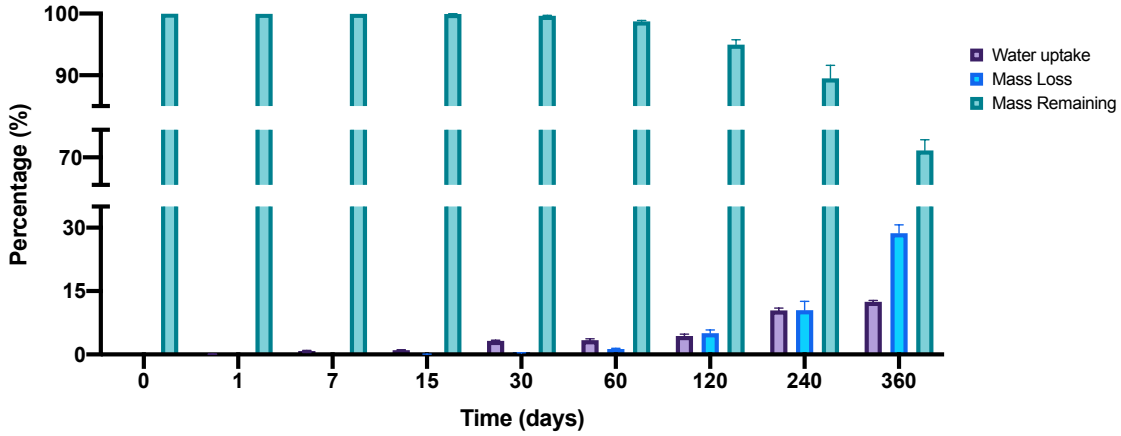


Figure 12. Erosion study of idebenone-loaded PCL implants. Water uptake, Mass Loss, and Mass Remaining data are presented as percentage.

The erosion study was also assessed by the examination of the surface erosion process of the implants. All the tested PCL implants showed comparable structural advancement over the studied period. Both the implant surface and the cross-section were dense and non-porous before the *in vitro* release test (see section 9). Moreover, PCL implants showed a homogeneously distributed crystalline structure along the surface at the beginning of the study. Nevertheless, changes in the external surface of the implants were observed throughout the studied period, especially after the 240-day determination, going from a defined crystalline structure to a more amorphous one (see Figure 13). The appearance of pores on the implant surface was also observed as the erosion process progressed, associated to the organic solvent evaporation process during the implant elaboration. However, the internal structure of the implants remained practically unchanged. These results suggest that idebenone was released by polymer erosion and gradual diffusion from the exterior to the interior of the PCL implant.

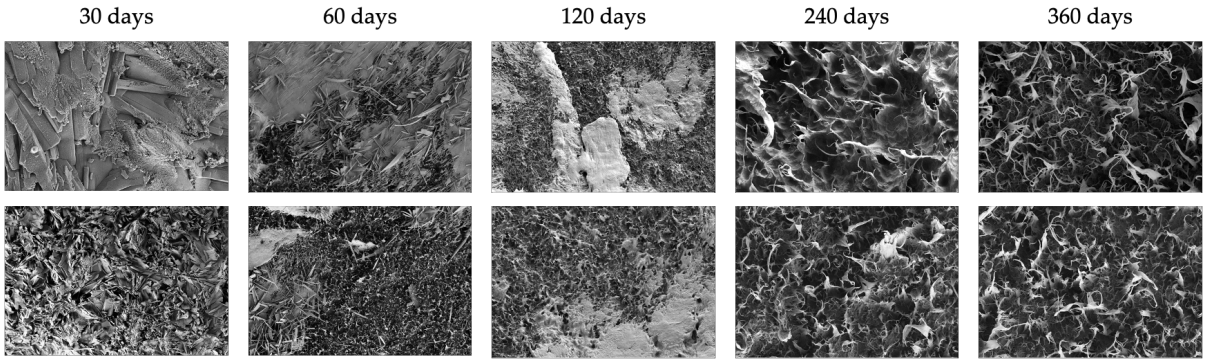


Figure 13. SEM images of idebenone-loaded PCL implants surface along the erosion study. PCL implant surface was assessed at predetermined time points under the same magnifications (5000x magnification), during the predefined study interval.

11. Injectability of implants

The injectability assessment constitutes a key-product routine factor of intraocular dosage forms, where the formulation should be delivered by passing through a needle-based system. The injectability of the resulting idebenone-loaded PCL implants was mechanically measured by the panel trial built for the universal tester. Furthermore, as the needle gauge might have a critical effect on the patient's comfort and compliance, different needles were tested (see Table 1 in methods section for needle specifications).

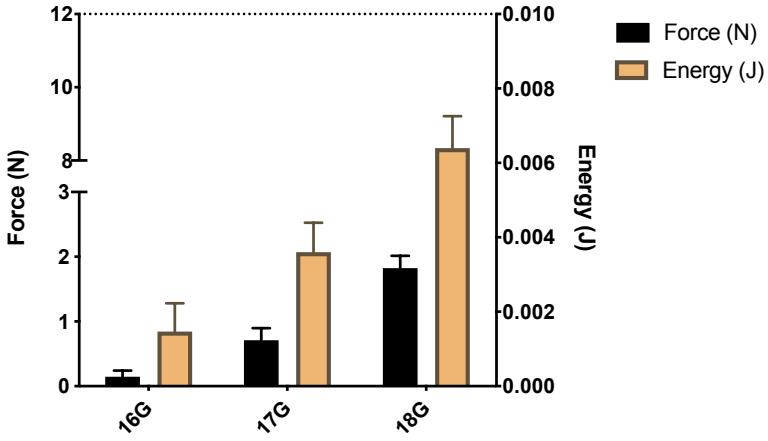


Figure 14. Injectability results for the idebenone-loaded PCL implants.

USC
UNIVERSIDADE DE SANTIAGO DE COMPOSTELA

All injectability values were appropriate in terms of injection into air, independently of needle diameter or length (see Figure 14). Nevertheless, the ease of injection into air was more acceptable for wider needle systems. The results of injectability also revealed neither partial nor complete blockage of the polymeric implants flow. Thus, idebenone-loaded PCL implants are suitable for intraocular injection through a 18G needle.

12. Cytotoxicity analysis

12.1. Hen's egg test on the chorioallantoic membrane (HET-CAM)

The HET-CAM test is commonly used to evaluate the short time cytotoxicity and biocompatibility of ocular formulations. Idebenone-loaded PCL implants were evaluated, and results were compared with those obtained for the negative and positive control formulations. These polymeric implants showed no cytotoxicity properties (Irritation Score = 0), in comparison with the control solutions (see Figure 15). These results are in good arrangement with formerly published works (58,59), validating that both components and implants are non-toxic and biocompatible. It will be necessary to develop future studies in animal models to evaluate the long-term toxicity of the implants, since implants will be in contact with ocular tissues during long periods of time.

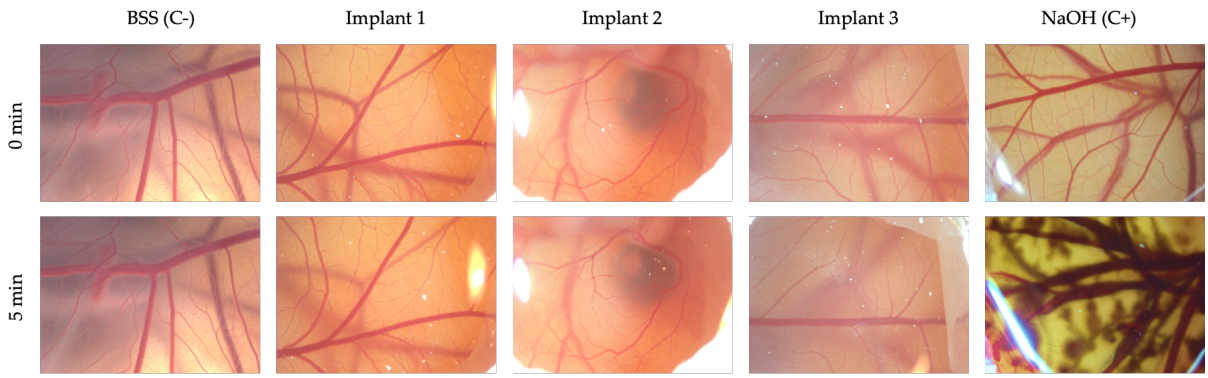


Figure 15. Images of CAM membranes after the administration of idebenone-loaded PCL intravitreal implant during the HET-CAM test, compared to the control solutions. (A) idebenone-loaded PCL intravitreal implant, (B) BSS (negative control), and (C) NaOH solution (positive control).

USC UNIVERSIDADE DE SANTIAGO DE COMPOSTELA

CONCLUSION

The treatment of posterior segment ocular diseases remains limited due to the drawbacks in achieving drug effective concentrations into the vitreous chamber through conventional administration routes, both local and systemic, considered as unproductive pathways (60). The development of biodegradable intravitreal-targeted DDS to the posterior segment of the eye may overcome most of these shortcomings of conventional pharmaceutical forms, as well as providing numerous advantages, including: (I) sustained and controlled drug release into the target tissue, (II) long-term vitreous concentration of the active substance, (III) frequency of administration reduction, (IV) minimization of side effects appearance, and (V) improvement in the patient's adherence to treatment and comfort, among others (61). Previous research on biodegradable polymers for implant development have been made, although a controlled and sustained drug release for more than six months has not been successfully achieved using biodegradable polymers (62–64).

In the present work, it is proposed, for the first time, a biodegradable long-acting intravitreal implant containing idebenone as a pharmacological alternative for the LHON treatment. PCL was selected as the matrix core compound due to its physicochemical properties, highlighting its extremely low hydrolysis rate of ester bonds and a type III erosion profile, leading to the progressive cleavage of the polymeric chains (65). A high tolerance by the retinal tissue, without inflammatory response or complications was also observed.

Idebenone-loaded PCL implants were successfully prepared by a homogenization/extrusion/solvent evaporation method. PCL implants showed uniformity of shape and color, as well as a cylindrical appearance, with no evidence of pores or channels, suggesting that drug diffusion is independent of the polymer degradation process. Idebenone release from PCL implants seemed to follow a biphasic pattern, described by a faster preliminary release phase and a slower second phase that lasts beyond one year. Furthermore, high production yield, encapsulation efficiency, and loading capacity values were obtained, as well as good mechanical properties. Appropriate physicochemical properties were achieved in terms of DSC/TGA, X-Ray, and FTIR, as well as adequate stability properties with regard to storage, pH, and ionic strength. Thus, its design and development were reinforced by an *in vitro* consistent preclinical base. Analogously, idebenone-loaded PCL implants showed appropriate physicochemical properties for intravitreal administration, controlling the idebenone release and guaranteeing the patient’s adherence-to-treatment.

USC
UNIVERSIDADE DE SANTIAGO DE COMPOSTELA

REFERENCES

1. Bourne RRA, Flaxman SR, Braithwaite T, Cicinelli MV, Das A, Jonas JB, et al. Magnitude, temporal trends, and projections of the global prevalence of blindness and distance and near vision impairment: a systematic review and meta-analysis. Lancet Glob Health. 2017 Sep;5(9):e888–97.
2. Behbehani R. Clinical approach to optic neuropathies. Clin Ophthalmol Auckl NZ. 2007 Sep;1(3):233–46.
3. Newman NJ, Biousse V. Hereditary optic neuropathies. Eye Lond Engl. 2004 Nov;18(11):1144–60.
4. Lyseng-Williamson KA. Idebenone: A Review in Leber's Hereditary Optic Neuropathy. Drugs. 2016 May;76(7):805–13.
5. Gillis JC, Benefield P, McTavish D. Idebenone. A review of its pharmacodynamic and pharmacokinetic properties, and therapeutic use in age-related cognitive disorders. Drugs Aging. 1994 Aug;5(2):133–52.
6. Bodmer M, Vankan P, Dreier M, Kutz KW, Drewe J. Pharmacokinetics and metabolism of idebenone in healthy male subjects. Eur J Clin Pharmacol. 2009 Jan 6;65(5):493.
7. European Medical Agency. Raxone® Technical Sheet (Internet). 2020. Available from: https://www.ema.europa.eu/en/documents/product-information/raxone-epar-product-information_en.pdf
8. Yellepeddi VK, Palakurthi S. Recent Advances in Topical Ocular Drug Delivery. J Ocul Pharmacol Ther Off J Assoc Ocul Pharmacol Ther. 2016 Mar;32(2):67–82.
9. Nordstrom BL, Friedman DS, Mozaffari E, Quigley HA, Walker AM. Persistence and adherence with topical glaucoma therapy. Am J Ophthalmol. 2005 Oct;140(4):598–606.
10. Reardon G, Kotak S, Schwartz GF. Objective assessment of compliance and persistence among patients treated for glaucoma and ocular hypertension: a systematic review. Patient Prefer Adherence. 2011;5:441–63.
11. Sleath B, Robin AL, Covert D, Byrd JE, Tudor G, Svarstad B. Patient-reported behavior and problems in using glaucoma medications. Ophthalmology. 2006 Mar;113(3):431–6.
12. Claxton AJ, Cramer J, Pierce C. A systematic review of the associations between dose regimens and medication compliance. Clin Ther. 2001 Aug;23(8):1296–310.

USC DE COMPOSTELA

13. Schneid TR. An in vitro analysis of a sustained release system for the treatment of denture stomatitis. Spec Care Dent Off Publ Am Assoc Hosp Dent Acad Dent Handicap Am Soc Geriatr Dent. 1992 Dec;12(6):245–50.

14. Wada R, Hyon SH, Nakamura T, Ikada Y. In vitro evaluation of sustained drug release from biodegradable elastomer. Pharm Res. 1991 Oct;8(10):1292–6.

15. D'Souza SS, DeLuca PP. Development of a dialysis in vitro release method for biodegradable microspheres. AAPS PharmSciTech. 2005 Jun;6(2):E323–8.

16. Waters LJ, Pavlakis E. In vitro controlled drug release from loaded microspheres--dose regulation through formulation. J Pharm Pharm Sci Publ Can Soc Pharm Sci Soc Can Sci Pharm. 2007;10(4):464–72.

17. Konsue N, Kirkpatrick J, Kuhnert N, King LJ, Ioannides C. Repeated oral administration modulates the pharmacokinetic behavior of the chemopreventive agent phenethyl isothiocyanate in rats. Mol Nutr Food Res. 2010 Mar;54(3):426–32.

18. Shi Y, Li LC. Current advances in sustained-release systems for parenteral drug delivery. Expert Opin Drug Deliv. 2005 Nov;2(6):1039–58.

19. Rainsford KD, Stetsko PI, Sirko SP, Debski S. Gastrointestinal mucosal injury following repeated daily oral administration of conventional formulations of indometacin and other non-steroidal anti-inflammatory drugs to pigs: a model for human gastrointestinal disease. J Pharm Pharmacol. 2003 May;55(5):661–8.

20. Hickey T, Kreutzer D, Burgess DJ, Moussy F. Dexamethasone/PLGA microspheres for continuous delivery of an anti-inflammatory drug for implantable medical devices. Biomaterials. 2002 Apr;23(7):1649–56.

21. Abrahamsson B, Alpsten M, Bake B, Jonsson UE, Eriksson-Lepkowska M, Larsson A. Drug absorption from nifedipine hydrophilic matrix extended-release (ER) tablet-comparison with an osmotic pump tablet and effect of food. J Control Release Off J Control Release Soc. 1998 Mar 31;52(3):301–10.

22. Gao P, Xu H, Ding P, Gao Q, Sun J, Chen D. Controlled release of huperzine A from biodegradable microspheres: In vitro and in vivo studies. Int J Pharm. 2007 Feb 7;330(1–2):1–5.

23. Bhardwaj U, Sura R, Papadimitrakopoulos F, Burgess DJ. Controlling acute inflammation with fast releasing dexamethasone-PLGA microsphere/pva hydrogel composites for implantable devices. J Diabetes Sci Technol. 2007 Jan;1(1):8–17.

USC UNIVERSIDADE DE SANTIAGO

24. Mh B, Rj D, Vs P. Use of in vitro and in vivo data in the design, development, and quality control of sustained-release decongestant dosage forms. Pharmacotherapy. 1994 Jul 1;14(4):430–7.

25. Zhang L, Parsons DL, Navarre C, Kompella UB. Development and in-vitro evaluation of sustained release poloxamer 407 (P407) gel formulations of ceftiofur. J Control Release Off J Control Release Soc. 2002 Dec 13;85(1–3):73–81.

26. Kälicke T, Schierholz J, Schlegel U, Frangen TM, Köller M, Printzen G, et al. Effect on infection resistance of a local antiseptic and antibiotic coating on osteosynthesis implants: an in vitro and in vivo study. J Orthop Res Off Publ Orthop Res Soc. 2006 Aug;24(8):1622–40.

27. Castro C, Evora C, Baro M, Soriano I, Sánchez E. Two-month ciprofloxacin implants for multibacterial bone infections. Eur J Pharm Biopharm Off J Arbeitsgemeinschaft Pharm Verfahrenstechnik EV. 2005 Aug;60(3):401–6.

28. Ratner BD. Reducing capsular thickness and enhancing angiogenesis around implant drug release systems. J Control Release Off J Control Release Soc. 2002 Jan 17;78(1–3):211–8.

29. Kimura H, Ogura Y. Biodegradable polymers for ocular drug delivery. Ophthalmol J Int Ophtalmol Int J Ophthalmol Z Augenheilkd. 2001 Jun;215(3):143–55.

30. Woodruff MA, Hutmacher DW. The return of a forgotten polymer—Polycaprolactone in the 21st century. Prog Polym Sci. 2010 Oct 1;35(10):1217–56.

31. Yasukawa T, Tabata Y, Kimura H, Ogura Y. Recent advances in intraocular drug delivery systems. Recent Pat Drug Deliv Formul. 2011 Jan;5(1):1–10.

32. Kim J, Kudisch M, Mudumba S, Asada H, Aya-Shibuya E, Bhisitkul RB, et al. Biocompatibility and Pharmacokinetic Analysis of an Intracameral Polycaprolactone Drug Delivery Implant for Glaucoma. Invest Ophthalmol Vis Sci. 2016 Aug 1;57(10):4341–6.

33. Mello VA de, Ricci-Júnior E. Encapsulation of naproxen in nanostructured system: structural characterization and in vitro release studies. Quím Nova. 2011;34(6):933–9.

34. Guerreiro LH, Da Silva D, Ricci-Junior E, Girard-Dias W, Mascarenhas CM, Sola-Penna M, et al. Polymeric particles for the controlled release of human amylin. Colloids Surf B Biointerfaces. 2012 Jun 1;94:101–6.

35. Siepmann J, Siegel RA, Rathbone MJ, editors. Fundamentals and Applications of Controlled Release Drug Delivery (Internet). Springer US; 2012 (cited 2020 Dec 23).

USC UNIVERSIDADE DE SANTIAGO

(Advances in Delivery Science and Technology). Available from: https://www.springer.com/gp/book/9781461408802

36. Mitragotri S, Lahann J. Materials for drug delivery: innovative solutions to address complex biological hurdles. Adv Mater Deerfield Beach Fla. 2012 Jul 24;24(28):3717–23.

37. Varela-Fernández R, García-Otero X, Díaz-Tomé V, Regueiro U, López-López M, González-Barcia M, et al. Design, Optimization, and Characterization of Lactoferrin-Loaded Chitosan/TPP and Chitosan/Sulfobutylether-β-cyclodextrin Nanoparticles as a Pharmacological Alternative for Keratoconus Treatment. ACS Appl Mater Interfaces. 2021 Jan 27;13(3):3559–75.

38. Muthu MS, Singh S. Poly (D, L-lactide) nanosuspensions of risperidone for parenteral delivery: formulation and in-vitro evaluation. Curr Drug Deliv. 2009 Jan;6(1):62–8.

39. Calvo P, Vila-Jato JL, Alonso MJ. Comparative in vitro evaluation of several colloidal systems, nanoparticles, nanocapsules, and nanoemulsions, as ocular drug carriers. J Pharm Sci. 1996 May;85(5):530–6.

40. Yan G-P, Zong R-F, Li L, Fu T, Liu F, Yu X-H. Anticancer drug-loaded nanospheres based on biodegradable amphiphilic ε-caprolactone and carbonate copolymers. Pharm Res. 2010 Dec;27(12):2743–52.

41. Cilurzo F, Selmin F, Minghetti P, Adami M, Bertoni E, Lauria S, et al. Injectability Evaluation: An Open Issue. AAPS PharmSciTech. 2011 May 7;12(2):604–9.

42. Varela-Fernández R, Díaz-Tomé V, Luaces-Rodríguez A, Conde-Penedo A, García-Otero X, Luzardo-Álvarez A, et al. Drug Delivery to the Posterior Segment of the Eye: Biopharmaceutic and Pharmacokinetic Considerations. Pharmaceutics. 2020 Mar 16;12(3).

43. Xie X, Yang Y, Chi Q, Li Z, Zhang H, Li Y, et al. Controlled Release of Dutasteride from Biodegradable Microspheres: In vitro and In vivo Studies. PLOS ONE. 2014 Dec 26;9(12):e114835.

44. Luepke NP. Hen's egg chorioallantoic membrane test for irritation potential. Food Chem Toxicol Int J Publ Br Ind Biol Res Assoc. 1985 Feb;23(2):287–91.

45. Kalweit S, Besoke R, Gerner I, Spielmann H. A national validation project of alternative methods to the Draize rabbit eye test. Toxicol Vitro Int J Publ Assoc BIBRA. 1990;4(4–5):702–6.

46. Spielmann H, Kalweit S, Liebsch M, Wirnsberger T, Gerner I, Bertram-Neis E, et al. Validation study of alternatives to the Draize eye irritation test in Germany: Cytotoxicity testing

USC UNIVERSIDADE DE SANTIAGO DE COMPOSTELA

and HET-CAM test with 136 industrial chemicals. Toxicol Vitro Int J Publ Assoc BIBRA. 1993 Jul;7(4):505–10.

47. Luan X, Bodmeier R. Influence of the poly(lactide-co-glycolide) type on the leuprolide release from in situ forming microparticle systems. J Control Release Off J Control Release Soc. 2006 Jan 10;110(2):266–72.

48. Sahana DK, Mittal G, Bhardwaj V, Kumar MNVR. PLGA Nanoparticles for Oral Delivery of Hydrophobic Drugs: Influence of Organic Solvent on Nanoparticle Formation and Release Behavior In vitro and In vivo Using Estradiol as a Model Drug. J Pharm Sci. 2008 Apr 1;97(4):1530–42.

49. Ibrahim MA, Ismail A, Fetouh MI, Göpferich A. Stability of insulin during the erosion of poly(lactic acid) and poly(lactic-co-glycolic acid) microspheres. J Control Release Off J Control Release Soc. 2005 Sep 2;106(3):241–52.

50. Mittal G, Sahana DK, Bhardwaj V, Ravi Kumar MNV. Estradiol loaded PLGA nanoparticles for oral administration: effect of polymer molecular weight and copolymer composition on release behavior in vitro and in vivo. J Control Release Off J Control Release Soc. 2007 May 14;119(1):77–85.

51. Holgado MA, Cózar-Bernal MJ, Salas S, Arias JL, Alvarez-Fuentes J, Fernández-Arévalo M. Protein-loaded PLGA microparticles engineered by flow focusing: physicochemical characterization and protein detection by reversed-phase HPLC. Int J Pharm. 2009 Oct 1;380(1–2):147–54.

52. Friedrich S, Cheng YL, Saville B. Finite element modeling of drug distribution in the vitreous humor of the rabbit eye. Ann Biomed Eng. 1997 Apr;25(2):303–14.

53. Tojo K, Isowaki A. Pharmacokinetic model for in vivo/in vitro correlation of intravitreal drug delivery. Adv Drug Deliv Rev. 2001 Oct 31;52(1):17–24.

54. Heitz FD, Erb M, Anklin C, Robay D, Pernet V, Gueven N. Idebenone protects against retinal damage and loss of vision in a mouse model of Leber's hereditary optic neuropathy. PloS One. 2012;7(9):e45182.

55. Rothen-Weinhold A, Besseghir K, Vuaridel E, Sublet E, Oudry N, Kubel F, et al. Injection-molding versus extrusion as manufacturing technique for the preparation of biodegradable implants. Eur J Pharm Biopharm Off J Arbeitsgemeinschaft Pharm Verfahrenstechnik EV. 1999 Sep;48(2):113–21.

USC UNIVERSIDADE DE SANTIAGO

56. Sinha VR, Bansal K, Kaushik R, Kumria R, Trehan A. Poly-epsilon-caprolactone microspheres and nanospheres: an overview. Int J Pharm. 2004 Jun 18;278(1):1–23.

57. Merkli A, Tabatabay C, Gurny R, Heller J. Biodegradable polymers for the controlled release of ocular drugs. Prog Polym Sci. 1998 Jan 1;23(3):563–80.

58. Ortiz R, Prados J, Melguizo C, Arias JL, Ruiz MA, Alvarez PJ, et al. 5-Fluorouracil-loaded poly(ε-caprolactone) nanoparticles combined with phage E gene therapy as a new strategy against colon cancer. Int J Nanomedicine. 2012;7:95–107.

59. Elmowafy M, Alruwaili NK, Shalaby K, Alharbi KS, Altowayan WM, Ahmad N, et al. Long-Acting Paliperidone Parenteral Formulations Based on Polycaprolactone Nanoparticles; the Influence of Stabilizer and Chitosan on In vitro Release, Protein Adsorption, and Cytotoxicity. Pharmaceutics. 2020 Feb 16;12(2).

60. Sheardown H, Saltzman WM. Novel Drug Delivery Systems for Posterior Segment Ocular Disease. In: Tombrain-Tink J, Barnstable CJ, editors. Ocular Angiogenesis: Diseases, Mechanisms, and Therapeutics (Internet). Totowa, NJ: Humana Press; 2006 (cited 2021 Apr 19). p. 393–408. (Opthalmology Research). Available from: https://doi.org/10.1007/978-1-59745-047-8_22

61. Kimura H, Ogura Y. Biodegradable polymers for ocular drug delivery. Ophthalmol J Int Ophtalmol Int J Ophthalmol Z Augenheilkd. 2001 Jun;215(3):143–55.

62. Yasukawa T, Ogura Y, Tabata Y, Kimura H, Wiedemann P, Honda Y. Drug delivery systems for vitreoretinal diseases. Prog Retin Eye Res. 2004 May;23(3):253–81.

63. Kunou N, Ogura Y, Yasukawa T, Kimura H, Miyamoto H, Honda Y, et al. Long-term sustained release of ganciclovir from biodegradable scleral implant for the treatment of cytomegalovirus retinitis. J Control Release Off J Control Release Soc. 2000 Aug 10;68(2):263–71.

64. Fialho SL, Rêgo MB, Siqueira RC, Jorge R, Haddad A, Rodrigues AL, et al. Safety and pharmacokinetics of an intravitreal biodegradable implant of dexamethasone acetate in rabbit eyes. Curr Eye Res. 2006 Jun;31(6):525–34.

65. Merkli A, Tabatabay C, Gurny R, Heller J. Biodegradable polymers for the controlled release of ocular drugs. Prog Polym Sci. 1998 Jan;23(3):563–80.

USC UNIVERSIDADE DE SANTIAGO DE COMPOSTELA

Conclusions

USC
UNIVERSIDADE
DE SANTIAGO
DE COMPOSTELA

USC
UNIVERSIDADE
DE SANTIAGO
DE COMPOSTELA

Conclusions

CONCLUSIONS

In the **first part** of this doctoral thesis, three different types of nanoparticles were successfully designed and developed, these being: (I) chitosan-based nanoparticles, where two different types were deeply studied, chitosan/TPP and chitosan/sulfobutylether-β-cyclodextrin nanoparticles, (II) nanostructured lipid carriers, and (III) PLGA nanoparticles, distinguishing two types of formulations, nanospheres and nanocapsules. All these formulations were loaded with lactoferrin as a target drug and proposed as pharmacological alternatives for the keratoconus treatment.

Stable and tunable-size nanoparticles were obtained by different preparation methods (ion gelation, double emulsion/solvent evaporation, and nanoprecipitation, respectively). All formulations showed appropriate average particle size, size distribution and ζ potential, as well as spherical and uniform shape. Similarly, they exhibited good stability to storage, pH, and ionic strength range. A controlled release of Lf was also proven, corroborating their use as possible DDS for hydrophilic drugs. Resulting data also confirmed their mucoadhesive properties, with no evidence of tissue cytotoxicity.

Analogously, all types of nanoparticles showed appropriate physicochemical properties suitable for topical ophthalmic administration, supporting the idea that they were retained in the corneal layer, prolonging the drug release time from the tissue itself, something that may guarantee the patient's adherence to the treatment, since a lower dosage frequency would be required. Furthermore, the versatility of these systems would allow including them in different pharmaceutical forms for ophthalmic administration based on the requirements and characteristics of the patient, as a new way to partially personalize and individualize the therapeutic strategy.

As overall conclusion, different nano-sized formulations were proposed, for the first time, as biodegradable nanocarriers for the delivery of lactoferrin, supported by extensive preclinical

USC UNIVERSIDADE DE SANTIAGO

studies in order to achieve a consistent base as the first pharmacological treatment for keratoconus as an alternative to current invasive clinical methods. This was supported by extensive *in vitro, ex vivo,* and *in vivo* characterization studies. A preclinical consistent basis was achieved for a potential pharmacological keratoconus treatment, as an alternative to the current invasive clinical methods, of palliative or supportive nature. Nevertheless, a better correlation with *in vivo* data should be profoundly explored in order to deeply understand the real potential of these nanocarriers as a topical ophthalmic alternative strategy for the prevention and treatment of keratoconus.

In the **second part** of this doctoral thesis, two different drug delivery systems were successfully designed and developed as new alternatives for the LHON treatment, these being: (I) idebenone-loaded PLGA MSs, and (II) idebenone-loaded PCL implants, both intended for intravitreal administration.

Idebenone was successfully loaded into PLGA MSs and PCL implants by two different preparation methods, an O/W simple emulsion/solvent and evaporation technique a homogenization/extrusion/solvent evaporation method, respectively. Both formulations were physicochemically characterized in order to create a consistent preclinical basis from which conduct *in vivo* studies. The adopted methods also favored the obtention of smooth, regular, and uniform formulations with the optimal size for intravitreal administration through a syringe/needle system. PLGA and PCL were selected as the matrix core compound due to their physicochemical properties, highlighting its low hydrolysis rate and erosion profile, where a high tolerance by the retinal tissue, without inflammatory response or complications was also observed.

Similarly, a controlled and sustained idebenone release was achieved from both formulations, confirming their use as potential drug delivery systems for long-term intravitreal administration. Furthermore, high production yield, encapsulation efficiency, and loading capacity values were obtained, as well as good mechanical properties. Appropriate physicochemical properties were achieved in terms of DSC/TGA, X-Ray, and FTIR, as well as adequate stability properties regarding storage, pH, and ionic strength changes. Resulting data showed that all formulations might be considered as potential carriers for hydrophobic drug's-controlled release. However, *in vivo* assays should be considered in the future to assess its clinical application.

USC UNIVERSIDADE DE SANTIAGO

To sum up, it is proposed, for the first time, two biodegradable long-acting intravitreal formulations containing idebenone as pharmacological alternatives for the LHON treatment, where a preclinical coherent basis was accomplished. The versatility of these systems would enable the inclusion of new drugs intended for intravitreal administration according to the patient needs and characteristics, as a new method of partial personalization treatment strategies.

CONCLUSIONES

En la **primera parte de esta tesis doctoral**, se diseñaron y desarrollaron con éxito tres tipos diferentes de nanopartículas, a saber: (I) nanopartículas basadas en quitosano, donde se estudiaron en profundidad dos tipos diferentes, nanopartículas de quitosano/TPP y quitosano/sulfobutiléter--ciclodextrina, (II) sistemas lipídicos nanoestructurados, y (III) nanopartículas de PLGA, distinguiendo dos tipos de formulaciones, nanoesferas y nanocápsulas. Todas estas formulaciones se cargaron con lactoferrina como fármaco diana y se propusieron como alternativas farmacológicas para el tratamiento del queratocono.

Se obtuvieron nanopartículas estables y de tamaño ajustable mediante diferentes métodos de preparación (gelificación iónica, doble emulsión/evaporación de disolventes y nanoprecipitación, respectivamente). Todas las formulaciones mostraron un tamaño medio de partícula, una distribución de tamaño y un potencial adecuados, además de forma esférica y uniforme. Asimismo, mostraron una buena estabilidad al almacenamiento, al pH y a la fuerza iónica. También se comprobó una liberación controlada de Lf, corroborando su uso como posibles sistemas de liberación de fármacos hidrofílicos. Los datos resultantes también confirmaron sus propiedades mucoadhesivas, sin evidencia de citotoxicidad tisular.

De igual modo, todos los tipos de nanopartículas mostraron propiedades fisicoquímicas adecuadas para su administración por vía tópica oftálmica, apoyando la idea de que quedaban retenidas en la capa corneal, prolongando el tiempo de liberación del fármaco desde el propio tejido, algo que puede garantizar la adherencia del paciente al tratamiento, ya que se requeriría una menor frecuencia de dosificación. Además, la versatilidad de estos sistemas permitiría incluirlos en diferentes formas farmacéuticas de administración oftálmica en función de los requerimientos y características del paciente, como una nueva forma de personalizar e individualizar la estrategia terapéutica.

USC
DE SANTIAGO
DE COMPOSTELA

Como conclusión general, se ha propuesto, por primera vez, diferentes formulaciones de tamaño nanométrico como nanotransportadores biodegradables para la administración de lactoferrina, apoyado en amplios estudios preclínicos con el fin de obtener una base preclínica sólida como el primer potencial tratamiento farmacológico del queratocono y como alternativa a los actuales métodos clínicos invasivos. Esto se ha visto apoyado por numerosos estudios de caracterización *in vitro*, *ex vivo* e *in vivo*. No obstante, debe explorarse en profundidad una mejor correlación con los datos *in vivo* para comprender el verdadero potencial de estos nanotransportadores.

En la **segunda parte de esta tesis doctoral**, se diseñaron y desarrollaron con éxito dos sistemas diferentes de administración de fármacos como nuevas alternativas para el tratamiento del LHON, siendo estos: (I) MSs de PLGA cargadas con idebenona, e (II) implantes de PCL cargados con idebenona, ambos destinados a la administración intravítrea.

La idebenona se ha cargado con éxito tanto en las MSs de PLGA y como en los implantes de PCL mediante dos métodos de preparación diferentes, una técnica de emulsión/evaporación de disolvente O/A y un método de homogeneización/extrusión/evaporación del disolvente, respectivamente. Ambas formulaciones se caracterizaron fisicoquímicamente para crear una base preclínica sólida a partir de la cual realizar estudios *in vivo*. Los métodos adoptados también han favorecido la obtención de formulaciones uniformes con el tamaño óptimo para la administración intravítrea a través de un sistema de jeringa/aguja. El PLGA y la PCL se seleccionaron como polímeros principales de la matriz debido a sus propiedades fisicoquímicas, destacando su baja tasa de hidrólisis y su perfil de erosión, donde también se observó una alta tolerancia por parte del tejido retiniano, sin respuesta inflamatoria ni complicaciones.

Asimismo, se ha logrado una liberación controlada y sostenida de idebenona a partir de ambas formulaciones, lo que confirma su uso como potenciales sistemas de liberación de fármacos para la administración intravítrea a largo plazo. Además, se han obtenido valores elevados de rendimiento de producción, eficiencia de encapsulación y capacidad de carga, así como buenas propiedades mecánicas. Ambos sistemas han mostrado propiedades fisicoquímicas adecuadas en términos de DSC/TGA, rayos X y FTIR, así como una estabilidad adecuada en relación con el almacenamiento, el pH y los cambios de fuerza iónica. Los datos resultantes mostraron que todas las formulaciones podrían considerarse como potenciales sistemas para la liberación

USC UNIVERSIDADE DE SANTIAGO

controlada de fármacos. Sin embargo, habría que considerar la posibilidad de realizar ensayos *in vivo* para evaluar su potencial aplicación clínica.

USC
UNIVERSIDADE
DE SANTIAGO
DE COMPOSTELA

USC
UNIVERSIDADE
DE SANTIAGO
DE COMPOSTELA

Appendix

USC
UNIVERSIDADE
DE SANTIAGO
DE COMPOSTELA

USC
UNIVERSIDADE
DE SANTIAGO
DE COMPOSTELA

Appendix

APPENDIX

1. Conflict of interests

The doctoral student declares that there is no conflict of interest regarding the doctoral thesis.

2. Animal experiments

In the present thesis, male adult Sprague-Dawley rats with a 200-300 g average weight were used, supplied by the animal facility of the University of Santiago de Compostela (Santiago de Compostela, Spain). During the experiments, the animals were kept in individual cages with free access to food and water in a room under controlled temperature (22 ± 1°C) and humidity (60 ± 5%) and with day–night cycles regulated by artificial light (12/12 hours).

The animals were treated according to the guidelines for the care and use of laboratory animals. Animal experiments complied with the ARRIVE guidelines (Kilkenny C, Browne WJ, Cuthill IC, Emerson M, Altman DG. Improving bioscience research reporting: the ARRIVE guidelines for reporting animal research. PLoS Biol. 2010 Jun 29;8(6):e1000412.). Experiments were performed at the Research Imaging Unit (UNIME) of the Health Research Institute of Santiago de Compostela (IDIS) (REGA number: ES1507802928 01).

Experiments were approved by the Consellería de Medio Rural da Xunta de Galicia (15010/2019/005) and were authorized by the Animal Research Committee of the Health Research Institute of Santiago de Compostela (IDIS). They followed the Spanish and European Union (EU) regulations for animal experimentation (86/609/CEE, 2003/ 65/CE, 2010/63/EU, and RD53/2013).

USC DE SANTIAGO DE COMPOSTELA

3. Funding

This project has been awarded grant from the Spanish Ministry of Economy and Competitiveness (Instituto de Salud Carlos III: PI18/00159), and partially supported by the Spanish Ministry of Science, Innovation and Universities (RTI2018-099597-B-100).

The doctoral student acknowledges the financial support of the FIDIS (Health Research Institute of Santiago de Compostela Foundation).

4. Articles derived from this thesis

1. **Varela-Fernández, R.**, García-Otero, X., Díaz-Tomé, V., Regueiro, U., López-López, M., González-Barcia, M., Lema, M. I., & Otero-Espinar, F. J. (2021). Design, Optimization, and Characterization of Lactoferrin-Loaded Chitosan/TPP and Chitosan/Sulfobutylether-β-cyclodextrin Nanoparticles as a Pharmacological Alternative for Keratoconus Treatment. ACS applied materials & interfaces, 13(3), 3559–3575. https://doi.org/10.1021/acsami.0c18926

   Journal Impact Factor (2021): 9.44

   Contribution: Rubén Varela Fernández contributed to the elaboration of the article and carried out the entire experimental analysis, as well as writing the original draft preparation, as well as being responsible for the writing review and editing of the manuscript.

   Rights and permissions: Permission is granted for author's request in both print and electronic formats, and translations (https://s100.copyright.com/AppDispatchServlet).

   → Corresponds to **Chapter 1**

2. **Varela-Fernández, R.**, García-Otero, X., Díaz-Tomé, V., Regueiro, U., López-López, M., González-Barcia, M., Isabel Lema, M., & Javier Otero-Espinar, F. (2022). Lactoferrin-loaded nanostructured lipid carriers (NLCs) as a new formulation for optimized ocular drug delivery. European journal of pharmaceutics and biopharmaceutics: official journal of Arbeitsgemeinschaft fur Pharmazeutische Verfahrenstechnik e.V, S0939-6411(22)00031-5. Advance online publication. https://doi.org/10.1016/j.ejpb.2022.02.010

   Journal Impact Factor (2021): 5.46

   Contribution: Rubén Varela Fernández contributed to the elaboration of the article and carried out the entire experimental analysis, as well as writing the original draft preparation, as well as being responsible for the writing review and editing of the manuscript.

USC DE SANTIAGO DE COMPOSTELA

Rights and permissions: Permission is granted for author's request in both print and electronic formats, and translations. This is an open access article distributed under the terms of the Creative Commons CC-BY license, which permits unrestricted use, distribution, and reproduction in any medium, provided the original work is properly cited. (https://s100.copyright.com/AppDispatchServlet?publisherName=ELS&contentID=S0939641122000315&orderBeanReset=true).

→ Corresponds to **Chapter 2**

3. **Varela-Fernández, R.**; García-Otero, X.; Díaz-Tomé, V.; Regueiro, U.; López-López, M.; González-Barcia, M.; Isabel Lema, M.; Otero-Espinar, F.J. Mucoadhesive PLGA Nanospheres and Nanocapsules for Lactoferrin Controlled Ocular Delivery. Pharmaceutics 2022, 14, 799. https://doi.org/10.3390/pharmaceutics14040799

   Journal Impact Factor (2021): 6.29

   Contribution: Rubén Varela Fernández contributed to the elaboration of the article and carried out the entire experimental analysis, as well as writing the original draft preparation, as well as being responsible for the writing review and editing of the manuscript.

   Rights and permissions: Permission is granted for author's request in both print and electronic formats, and translations. This is an open access article distributed under the Creative Commons Attribution License which permits unrestricted use, distribution, and reproduction in any medium (https://www.mdpi.com/1999-4923/14/4/799).

   → Corresponds to **Chapter 3**

4. **Varela-Fernández, R.**, Bendicho-Lavilla, C., Martin-Pastor, M., Herrero Vanrell, R., Lema-Gesto, M. I., González-Barcia, M., & Otero-Espinar, F. J. (2022). Design, optimization, and in vitro characterization of idebenone-loaded PLGA microspheres for LHON treatment. International journal of pharmaceutics, 616, 121504. Advance online publication. https://doi.org/10.1016/j.ijpharm.2022.121504

   Journal Impact Factor (2021): 6.27

Contribution: Rubén Varela Fernández contributed to the elaboration of the article and carried out the entire experimental analysis, as well as writing the original draft preparation, as well as being responsible for the writing review and editing of the manuscript.

Rights and permissions: Permission is granted for author's request in both print and electronic formats, and translations. This article is available under the Creative Commons CC-BY-NC-ND license and permits non-commercial use of the work as published, without adaptation or alteration provided the work is fully attributed (https://s100.copyright.com/AppDispatchServlet?publisherName=ELS&contentID=S0378517322000576&orderBeanReset=true).

→ Corresponds to **Chapter 4**

5. **Varela-Fernández, R.**, Lema-Gesto, M. I., González-Barcia, M., & Otero-Espinar, F. J. (2021). Design, development, and characterization of an idebenone-loaded poly-ε-caprolactone intravitreal implant as a new therapeutic approach for LHON treatment. European journal of pharmaceutics and biopharmaceutics: official journal of Arbeitsgemeinschaft fur Pharmazeutische Verfahrenstechnik e.V, 168, 195–207. https://doi.org/10.1016/j.ejpb.2021.09.001

   Journal Impact Factor (2021): 5.46

   Contribution: Rubén Varela Fernández contributed to the elaboration of the article and carried out the entire experimental analysis, as well as writing the original draft preparation, as well as being responsible for the writing review and editing of the manuscript.

   Rights and permissions: Permission is granted for author's request in both print and electronic formats, and translations. This article is available under the Creative Commons CC-BY-NC-ND license and permits non-commercial use of the work as published, without adaptation or alteration provided the work is fully attributed (https://s100.copyright.com/AppDispatchServlet?publisherName=ELS&contentID=S0939641121002332&orderBeanReset=true).

   → Corresponds to **Chapter 5**

USC
UNIVERSIDADE
DE SANTIAGO
DE COMPOSTELA

USC
UNIVERSIDADE
DE SANTIAGO
DE COMPOSTELA

USC
UNIVERSIDADE
DE SANTIAGO
DE COMPOSTELA





In the present thesis, the research, development, and characterization processes of controlled drug delivery systems intended for the treatment of two different ocular pathologies were described. Firstly, different types of lactoferrin-loaded nanoparticles intended for topical ophthalmic administration were developed and proposed as the first pharmacological alternative for the Keratoconus (KC) treatment. On the other hand, idebenone-loaded polymeric implants and microparticles were designed and proposed as new therapeutic strategies for the treatment of Leber's Hereditary Optic Neuropathy (LHON).